



**The Skin and Barrier Function
in Radiation
and Chemical Exposures**

Eyman Rashdan

**Submitted in Fulfilment of the Requirements for the Degree of Doctor of
Philosophy in the Institute of Cellular Medicine, Newcastle University**

2017

Abstract

Sunscreens provide protection against ultraviolet radiation (UV), UVB and more recently UVA rays. The active ingredients within sunscreen formulations can broadly be divided into either the chemical absorbers or physical filters. Titanium dioxide (TiO₂), a commonly used physical filter compound, has been shown to exhibit size dependent reactivity properties when primary particles are within the nano-range (one or more dimensions being within 1-100nm in size). Such effects are suspected to contribute to the disruption of the skins barrier function following topical application. The ability of solar UV to induce skin cancer and photoageing effects is well recognised. The effect of the infrared (IR) and the visible light (VIS) components of solar radiation on skin and their interaction with UV is however lesser known. Skin fibroblast and keratinocyte cells in monolayer were exposed to physiologically relevant doses of solar light. Biomarkers of damage including reactive oxygen species (ROS) generation, mitochondrial DNA (mtDNA) and nuclear DNA (nDNA) damage were assessed. Further to this the apparent toxicological effects of TiO₂ on skin cells were investigated through the assessment of cell viability, ROS generation, and nDNA damage in the form of double strand breaks. The effect of TiO₂ on the perturbation of skin barrier function was also investigated by measuring the percutaneous absorption of a marker compound radiolabelled (1-methyl ¹⁴C) caffeine through human skin. Absorption studies were carried out in the presence or absence of TiO₂ plus or minus solar UV.

Data obtained within this thesis indicate that the individual action of IR, VIS or UV alone have marginal effects on the level of biomarkers of damage detected. When applied simultaneously, complete solar light was found to produce a synergistic effect significantly greater than the cellular stress responses detected from the individual components. Similarly, blocking the UVB and a portion of the UVA rays from complete solar light appeared to reduce the level of ROS generation, albeit the synergistic action of solar light could still be observed. Sunscreens, both commercially relevant formulations and TiO₂ dispersions, were found to provide protection against solar light exposures in vitro. When assessed under cell culture conditions TiO₂ was seen to induce significant ROS generation and nDNA damage following the application of solar UV. No effects of TiO₂ were however detected when the absorption

of the marker compound was assessed. The data presented suggest a further need for broad spectrum protection within sunscreen formulations. Furthermore although the work identifies potential harmful effects arising from the TiO₂ compound, the human skin explants assessed in the study were able to maintain a natural skin barrier function following exposure to TiO₂ plus or minus solar UV.

Dedication

This work is dedicated to my father, for all his support which has inspired me throughout my studies, and to my mother for bringing true meaning and happiness to my life.

Acknowledgments

The project described within this PhD thesis was supported by The National Institute for Health Research (NIHR) and Public Health England (PHE).

I would firstly like to thank my primary supervisor Prof. Mark Birch-Machin for his tremendous support and guidance throughout the project, and for giving me the opportunity to work under his supervision. I would like to thank my supervisor Dr Simon Wilkinson for his guidance and expert input into the project, and my PHE supervisor Dr Simon Bouffler for his great hospitality and for making the collaborative work possible. I would also like to express my gratitude to Dr Graham Holliman and Dr Ken Raj for their kind support and guidance during my time at PHE.

I would like to acknowledge Mr David Rawlings (Regional Medical Physics Department) for his expert guidance and input during the project. I would also like to thank Dr Alex Laude and Ms Carol Todd for their technical expertise and help during my PhD. I would like to thank both previous and current members of the MBM team, Dr Sarah Jayne Boulton, Dr Anne Oyewole and Dr Jennifer Latimer for their guidance during the first year of the project, and thank Dr Laura Hudson, Dr Amy Bowman, Ms Rebecca Hannah, Dr Khimara Naidoo, Ms Catherine Bonne, and MJ. Jackson for making the MBM group an incredible working team. I have had the most amazing support from both family and friends, thank you all for being there throughout both the challenging and happy moments.

Declaration

This thesis is submitted to the degree of Doctor of Philosophy at Newcastle University. The research in this thesis was performed in the Department of Dermatological Sciences and Medical toxicology at the Institute of Cellular Medicine, under the supervision of Prof. Mark Birch-Machin, Dr Simon Wilkinson and Dr Simon Bouffler. Collaborative work has also been undertaken at PHE Centre for Radiation, Chemical and Environmental Hazards. The work presented is my own unless stated otherwise in the text. I certify that none of the material in this thesis has been submitted previously by myself for a degree or any other qualification at this or any other university.

Table of Contents

Abstract	2
Dedication	4
Acknowledgments	5
Declaration	6
Table of contents.....	7
List of Figures.....	16
List of Tables.....	24
List of Abbreviations.....	25
Chapter 1- Introduction.....	32
1 Background.....	33
1.1 Skin structure and funtion	33
1.1.1 Epidermal structure and function	34
1.1.2 Dermal structure and function	37
1.2 Percutaneous absorption	37
1.3 Electromagnetic spectrum.....	40
1.3.1 Solar spectrum.....	41
1.3.2 Measurement of solar exposure	44
1.4 Effects of solar radiation on skin	45
1.4.1 Effects of UV on skin	45
1.4.1.1 Molecular damage.....	46
1.4.1.2 Skin cancer.....	46
1.4.1.3 Photo-ageing	48
1.4.1.4 Beneficial effects of UV exposure	48
1.4.2 Effects of IR on skin	49
1.4.3 Effects of VIS on skin	51

1.5 Mitochondria	52
1.5.1 mtDNA	53
1.5.2 mtDNA damage	55
1.5.3 mtDNA as a biomarker	56
1.6 ROS and ageing	57
1.7 Skins natural defence mechanisms	58
1.8 Sunscreens	61
1.9 Nanomaterials	62
1.10 Titanium dioxide (TiO ₂)	63
1.10.1 TiO ₂ in sunscreens	65
1.10.2 Regulations on nano TiO ₂ use in sunscreens.....	67
1.10.3 Considerations for nano TiO ₂ assessment.....	68
1.11 Project overview	70
1.12 Overall Aims.....	72
Chapter 2-Materials and Methods.....	73
2 General methods.....	74
2.1 Cell culture	74
2.1.1 Primary tissue samples	74
2.1.1.1 Tissue processing.....	74
2.1.1.2 Primary keratinocytes.....	75
2.1.1.3 Differentiated primary keratinocytes.....	75
2.1.1.4 Primary fibroblasts	75
2.1.2 HaCaT and HDFn cells lines.....	76
2.1.3 Long term storage of cells	76
2.2 Cell viability.....	77
2.2.1 MTS assay	77
2.2.2 RT-Glo	77

2.3 ROS Detection	78
2.3.1 ROS-Glo assay - cellular ROS generation	78
2.3.2 ROS-Glo assay -acellular ROS generation	78
2.3.3 DCFDA - cellular ROS generation	78
2.3.4 DCFDA – acellular ROS generation	79
2.4 Real time-QPCR.....	79
2.4.1 Cell treatment.....	79
2.4.2 DNA extraction and NanoDrop measurements	79
2.4.3 83bp mtDNA fragment QPCR analysis - mtDNA copy number	80
2.4.4 1Kb mtDNA fragment QPCR analysis.....	82
2.4.5 11Kb mtDNA fragment QPCR analysis.....	83
2.5 Comet Assay	85
2.5.1 Cell treatment and harvesting.....	85
2.5.2 Slide and buffer preparation	85
2.5.3 Staining, visualisation and analysis.....	86
2.5.4 Enzyme modified comet assay (hOGG1)	86
2.6 Sunscreen protective effect against solar light	86
2.7 Solar light sources.....	87
2.7.1 Solar Simulator	87
2.7.2 Hydrosun lamp	88
2.8 Filters	88
2.8.1 IR/VIS Filter	89
2.8.2 IR and UV cut off filters	89
2.8.3 Glass and plastic (UVB blocking) filters.....	91
2.9 Calibration of UV Lamps	91
Chapter 3 – Solar Radiation Exposure Effects on Human Skin.....	94
3 Chapter Overview.....	95

3.1 Chapter aims:.....	97
3.2 Chapter specific methods	97
3.3 Results.....	97
3.3.1 Background data.....	97
3.3.2 Preliminary work and experimental optimisation	101
3.3.2.1 Calibration of UV sources	101
3.3.2.2 Temperature monitoring of the Solar Simulator and Hydrosun lamps	107
3.3.3 Determining the sublethal dose of complete solar light and IR.....	108
3.3.4 ROS generation in response to solar light exposure	112
3.3.4.1 Measurements of ROS generation using the DCFDA assay HDFn cell	112
3.3.4.2 Measurements of ROS generation using the ROS-Glo assay	112
3.3.4.3 Comparing HDFn and HaCat cell response to solar light	116
3.3.4.4 Assessing the effect of individual components of solar light and combinations on ROS generation in HDFn and HaCat cells	117
3.3.4.5 Assessing the effect of individual components of solar light and combinations on ROS generation in primary skin cells	123
3.3.4.6 Comparison of primary keratinocyte and HaCat cell response to solar light	125
3.3.5 mtDNA damage	127
3.3.5.1 mtDNA damage in HDFn cells following exposure to solar light.....	130
3.3.5.2 Assessing mtDNA copy numbers following exposure to solar light.....	130
3.3.5.3 Assessing mtDNA damage in primary skin cells following exposure to solar light	132
3.3.6 Assessing UV and IR preconditioning in HDFn cells	134
3.4 Discussion	135
3.4.1 Doses of complete solar light and IR assessed did not induce cytotoxicity..	135
3.4.4 Fibroblasts are more sensitive to longer wavelengths of solar light when compared to keratinocytes	144

3.4.5 Primary keratinocytes show signs of greater sensitivity when compared to HaCat cells	144
3.4.7 Treating cells with IR followed by UV has no effect on ROS generation	145
3.5 Summary of main findings:.....	148
Chapter 4 – Protection Against Solar Radiation Induced Damage in Human Skin	149
4 Chapter Overview	150
4.2 Chapter aims.....	153
4.3 Chapter specific methods	153
4.4 Results.....	154
4.4.1 ROS generation in skin cells following a reduction in the level of UV from complete solar light	154
4.4.1.1 ROS generation in HDFn and HaCat cells following exposure to solar light plus filters.....	154
4.4.1.2 ROS generation in primary skin cells following exposure to solar light plus filters	158
4.4.2 mtDNA damage in primary skin cells following exposure to solar UV plus filters	164
4.4.3 Comparison of primary cell response to the reduction in solar UV levels...	167
4.4.4 Protective effects of sunscreens against solar radiation exposure	169
4.4.5 mtDNA damage accumulation over time following exposure to intermittent doses of solar light	173
4.4.6 Comparison of mtDNA damage following exposure to intermittent and an equivalent single dose of solar light.....	176
4.4.7 Comparison of mtDNA damage following exposure to intermittent and an equivalent single dose of solar light -11Kb QPCR assay	177
4.4.8 mtDNA damage susceptibility	179
4.4.9 Assessing the level of mtDNA damage across the mtDNA genome following exposure to solar light	181
4.5 Discussion	182

4.5.1 Presence of a reduced amount of UV alongside IR and VIS leads to synergistic ROS generation in skin cells.....	182
4.5.2 No synergy in mtDNA damage levels was detected when a percentage of UVA was present alongside IR and VIS	183
4.5.3 Sunscreen formulations are able to provide cellular protection against mtDNA damage	184
4.5.4 Exposure to intermittent and single doses of solar light both lead to similar levels of mtDNA damage as demonstrated using the 11kb QPCR assay	185
4.5.5 mtDNA damage levels were seen to be similar across the regions of the genome assessed following exposure to solar light.....	185
4.6 Summary of main findings:.....	187
Chapter 5 – Assessing the Apparent Health Hazards of Nanoparticulate TiO ₂	189
5 Chapter overview	190
Chapter 5 - Section I.....	194
5.1 Chapter aims.....	195
5.2 Chapter specific methods	195
5.2.1 Dispersions and suspension characterisation	195
5.2.1.1 Reagents	195
5.2.1.2 TiO ₂ oil in water suspension	196
5.2.1.3 TiO ₂ working suspensions.....	196
5.2.1.4 Peak absorbance of TiO ₂	196
5.2.1.5 TiO ₂ stability in suspension.....	197
5.2.1.6 TiO ₂ particle sizing	197
5.2.2 TiO ₂ internalisation	198
5.2.4 Assessing the protective abilities of compounds (TiO ₂ and Parsol HS).....	198
5.2.4.1 Acellular experiments.....	198
5.2.4.2 Cellular experiments.....	198

5.3 Results.....	199
5.3.1. Characterisation of TiO ₂ suspensions	199
5.3.2 Cell viability assays for the assessment of TiO ₂ and positive control compounds (Tiron and Parsol HS)	207
5.3.3 Cellular TiO ₂ internalisation in HDFn cells.....	211
5.3.4 Genotoxicity.....	214
5.3.5 Protective effects of TiO ₂	218
5.3.6 ROS generation following exposure to TiO ₂ and Parsol HS sunscreen compounds	221
5.4 Discussion	234
5.4.2 No cell death was detected following exposure of HDFn cells to TiO ₂	236
5.4.3 TiO ₂ internalisation is suspected to have an effect on the level of cellular toxicity induced	240
5.4.4 TiO ₂ induces nDNA damage in HDFn cells with further significant levels of nDNA damage being detected following the photoactivation of TiO ₂	241
5.5 Summary of main findings:.....	245
Chapter 5 - Section II	246
5.6 Chapter aims:.....	247
5.7 Absorption studies- Franz cell model	247
5.7.1 Experimental design (donor chamber, receiver chamber and permeant compound)	248
5.7.2 Detection of the permeant compound	250
5.8 Chapter specific methods – section II.....	251
5.8.1 Franz-type diffusion cell skin processing.....	251
5.8.1.1 Dose preparation	251
5.8.1.2 Sampling	252
5.8.1.3 Mass balance	252
5.8.1.4 Tape stripping	252

5.8.1.5 Skin digest.....	253
5.8.1.6 Analysis	253
5.8.1.7 Statistical analysis.....	253
5.8.1.8 Mass balance terminology:	255
5.8.2 Cutaflex.....	255
5.8.3 Porcine skin preparation	256
5.9 Results.....	257
5.9.1 The effects of TiO ₂ compound on skin barrier function	257
5.9.2 Temperature and irradiance of the Cleo performance lamp	264
5.9.3 Ambient light measurement	265
5.9.4 The CutaFlex™ cell model for dermal absorption studies.....	265
5.10 Discussion	277
5.10.1 TiO ₂ is not absorbed beyond the skins superficial layer	277
5.10.2 TiO ₂ is suspected to act as a dermal absorption enhancer however this was not been found to be the case in human skin	279
5.10.3 Skin flexion.....	282
5.11 Summary of main findings:.....	283
Chapter 6 – Final Discussion	284
6.1 Main Conclusions.....	285
6.1.2 Sunscreens provide protection against solar light therefore reducing the risk of DNA damage, this finding is also relevant during exposure to suberythemal doses...287	
6.1.3 TiO ₂ exhibits interference properties and instability in suspension albeit, toxicity in HDFn cells was seen under the conditions assessed with relevant controls in place....288	
6.1.4 No perturbation in human skin barrier function was seen as a result of exposure to TiO ₂	289
6.2 Implications of the Study in the wider field	291
6.2.1 Solar exposure	291

6.2.2 Protection against solar exposure	292
6.2.3 Use of nano technology in sunscreen formulations.....	294
Chapter 7 - References	298
Appendix.....	330

List of Figures

Figure 1: Schematic representation of the basic human skin structure	33
Figure 2: Diagram showing the structure of the epidermal layer in human skin	36
Figure 3: Arrangement of lipid stacks in the stratum corneum	36
Figure 4: Schematic diagram representing the three levels of cutaneous absorption	38
Figure 5: Showing the “Brick and mortar” model of the stratum corneum structure and the transcellular and intercellular absorption routes.....	39
Figure 6: Illustrating the arrangement of the electromagnetic spectrum	41
Figure 7: Illustrating the components of the solar spectrum and the differential levels of absorption occurring through human skin.....	43
Figure 8: Illustration showing the structure of mitochondria.....	53
Figure 9: Illustration of the human mtDNA map.....	54
Figure 10: The positioning of UV-induced damage within human mtDNA.....	56
Figure 11: Examples of sunscreen active compounds and protective abilities	60
Figure 12: The effect of decreasing particle size on the surface area and properties of TiO ₂ .	63
Figure 13: The behaviour of TiO ₂ compounds in suspension.....	64
Figure 14: Showing examples of TiO ₂ concentrations found in a range of personal care products.....	65
Figure 15: The potential toxicological effect of TiO ₂ on cells.....	66
Figure 16: Issues raised regarding the use of nanoparticulate TiO ₂	66
Figure 17: Literature survey showing the percentage of papers assessing nanoparticle interference in spectroscopic based assays in 2010 and 2012	69
Figure 18: Location of the amplified 83bp region in the mtDNA genome.....	81
Figure 19: Schematic diagram showing the position of the 1Kb QPCR fragment primer pairs along the mtDNA.....	82
Figure 20: Positioning of the amplified 11Kb section along the mtDNA genome.....	84
Figure 21: Schott UG-11 bandpass optical glass filter UV transmitting filter.....	89
Figure 22: Showing spectral data for IR cut off filter.....	90
Figure 23: Showing spectral data for the UV blocking filter.....	91
Figure 24: Output of solar simulated light following the application of the various filters....	92

Figure 25: The irradiance data of the UV6, TL01, Arimed B and Cleo + glass lamps.....	94
Figure 26: Comet assay showing the appearance of normal and damaged cells.....	100
Figure 27: Complete solar light and solar UV induced nDNA damage in primary keratinocyte and fibroblast cells.....	100
Figure 28: Showing the calibration readings for the Newport Solar Simulator	102
Figure 29: Showing the calibration readings for the Newport Solar Simulator with the plastic UVB blocking filter	103
Figure 30: Showing the calibration readings for the Newport Solar Simulator with the glass UVB blocking filter.....	105
Figure 31: Spectral irradiance and effective irradiance of the Newport Solar Simulator plus filters.....	107
Figure 32: Temperature under the Solar Simulator.....	108
Figure 33: Temperature under the Hydrosun lamp.....	109
Figure 34: Effect of complete solar simulated light, and IR exposure on primary fibroblast cell viability.....	110
Figure 35: Effect of complete solar simulated light and IR exposure on primary keratinocyte cell viability	110
Figure 36: Effect of complete solar simulated light and IR exposure on HDFn cell viability ..	111
Figure 37: ROS generation in HDFn cells following exposure to solar simulated light.....	113
Figure 38: ROS generation in HDFn cells following exposure to solar simulated light.....	115
Figure 39: HDFn cell dose response following the application of complete solar light and solar UV.....	116
Figure 40: ROS generation in HaCat cells following exposure to solar simulated light.....	117
Figure 41: Comparison of HDFn and HaCat cell response to solar light.....	118
Figure 42: ROS generation in HDFn and HaCat cells following exposure to solar UV.....	120
Figure 43: ROS generation in HDFn and HaCat cells following exposure to VIS.....	120
Figure 44: ROS generation in HDFn and HaCat cells following exposure to IR plus VIS.....	121
Figure 45: ROS generation in HDFn and HaCat cells following exposure to UV plus VIS.....	122
Figure 46: Summary of cellular ROS generation response in HDFn and HaCat cells following exposure to solar light dosing conditions.....	123

Figure 47: ROS generation in primary fibroblast, keratinocyte and differentiated keratinocyte cells following exposure to VIS	123
Figure 48: ROS generation in primary fibroblast, keratinocyte and differentiated keratinocyte cells following exposure to solar UV.....	123
Figure 49: ROS generation in primary fibroblast, keratinocyte and differentiated keratinocyte cells following exposure to IR	124
Figure 50: ROS generation in primary fibroblast, keratinocyte and differentiated keratinocyte cells following exposure to UV plus VIS.....	124
Figure 51: ROS generation in primary fibroblast, keratinocyte and differentiated keratinocyte cells following exposure to IR plus VIS.....	125
Figure 52: ROS generation response in HaCat and primary keratinocyte cells following exposure to complete solar light.....	126
Figure 53: ROS generation comparison between primary keratinocyte and HaCat cells following exposure to UV plus VIS.....	126
Figure 54: ROS generation comparison between primary differentiated keratinocyte and HaCat cells following exposure to UV plus VIS.....	127
Figure 55: Showing a representative multicomponent plot.....	129
Figure 56: The principle of real-time QPCR.....	130
Figure 57: Showing a representative melt curve analysis.....	130
Figure 58: mtDNA damage in HDFn cells following exposure to solar UV and complete solar light	130
Figure 59: 83bp QPCR analysis showing mtDNA copy numbers in primary fibroblast cells following exposure to solar simulated light	131
Figure 60: 83bp QPCR analysis showing mtDNA levels in primary keratinocytes following exposure to solar simulated light.....	133
Figure 61: mtDNA damage in primary fibroblast, keratinocyte and differentiated keratinocyte cells following exposure to VIS.....	134
Figure 62: mtDNA damage in primary fibroblast, keratinocyte and differentiated keratinocyte cells following exposure to IR.....	134
Figure 63: mtDNA damage in primary fibroblast, keratinocyte and differentiated keratinocyte cells following exposure to IR plus VIS.....	135

Figure 64: mtDNA damage in primary fibroblast, keratinocyte and differentiated keratinocyte cells following exposure to UV plus VIS.....	135
Figure 65: ROS generation response in HDFn cells following exposure to UV and IR.....	136
Figure 66: Schematic diagram showing an example of the effect of ROS on cellular response in skin.....	140
Figure 67: ROS generation in HDFn cells following exposure to complete solar light with varying levels of UVA and UVB	155
Figure 68: ROS generation in HDFn cells following exposure to complete solar light with varying levels of UVA and UVB	156
Figure 69: ROS generation in HaCat cells following exposure to complete solar light with varying levels of UVA and UVB	156
Figure 70: ROS generation in HDFn cells following exposure to complete solar light plus glass or plastic filters.....	158
Figure 71: ROS generation in HaCat cells following exposure to complete solar light plus glass or plastic filters	157
Figure 72: ROS generation in primary keratinocytes following exposure to full spectrum solar simulated light with varying UVA and UVB levels	161
Figure 73: ROS generation in differentiated primary keratinocytes following exposure to full spectrum solar simulated light with varying UVA and UVB levels	162
Figure 74: ROS generation in differentiated primary fibroblasts following exposure to full spectrum solar simulated light with varying UVA and UVB levels	163
Figure 75: mtDNA damage in primary keratinocytes following exposure to full spectrum solar simulated light plus or minus plastic and glass filters	165
Figure 76: mtDNA damage levels in primary fibroblasts following exposure to full spectrum solar simulated light plus or minus the plastic and glass filters	166
Figure 77: mtDNA damage in differentiated primary keratinocytes following exposure to full spectrum solar simulated light plus or minus the plastic and glass filters.....	167
Figure 78: Comparison of ROS generation in primary fibroblast, keratinocyte and differentiated keratinocyte cells following exposure to full spectrum solar simulated light plus or minus the plastic and glass filters	168
Figure 79: Comparison of ROS generation in primary fibroblast, keratinocyte and differentiated keratinocyte cells following exposure to solar UV	169
Figure 80: Protective effects of sunscreen formulations - acellular.....	171

Figure 81: Protective effects of sunscreens against complete solar light induced mtDNA damage in HDFn cells	171
Figure 82: Protective effects of sunscreens against solar UV induced mtDNA damage in HDFn cells.	172
Figure 83: Protective effects of sunscreens against arimed B induced mtDNA damage in HDFn cells	172
Figure 84: Comparison of mtDNA damage levels in HDFn cells following exposure to different solar light sources and dosing conditions	173
Figure 85: Level of mtDNA damage accumulation over 4 days following exposure to single or intermittent doses of solar light.....	174
Figure 86: mtDNA damage in HDFn cells following exposure to intermittent and single doses of complete solar light.....	175
Figure 87: mtDNA damage in HDFn cells following exposure to either an intermittent dose single dose of complete solar UV	176
Figure 88: mtDNA damage in HDFn cells following exposure to either an intermittent or a single dose of arimed B	176
Figure 89: mtDNA damage in HDFn cells following exposure to either an intermittent or a single dose of complete solar light.....	177
Figure 90: Amplification regions of the 1kb and 11kb QPCR fragments.....	179
Figure 91: mtDNA damage detection using the 1Kb and 11kb fragments following single and intermittent dose exposure to solar light	178
Figure 92: Standard curve assessing the linear range amplified by the 1kb primer pairs	180
Figure 93: mtDNA damage level in HDFn cells following exposure to complete of solar light	181
Figure 94: Level of mtDNA damage detection across different regions of the mitochondrial genome.....	182
Figure 95: Outline of method used to creat TiO ₂ working suspensions	197
Figure 96: Absorbance profile of TiO ₂ suspensions at different concentrations	202
Figure 97: Comparison of TiO ₂ settling with and without the addition of 10% FCS to DMEM	202
Figure 98: Absorbance analysis of TiO ₂ in DMEM plus 10% FCS illustrating TiO ₂ settling levels over 72h.....	203
Figure 99: Absorbance analysis of TiO ₂ in PBS illustrating TiO ₂ settling levels over 72h.....	205

Figure 100: Effect of sonication on TiO ₂ settling in PBS suspension	205
Figure 101: Assessing the average size of nano TiO ₂ particles in suspension.....	206
Figure 102: HDFn cell viability following exposure to Tiron	209
Figure 103: HDFn cell viability following exposure to Parsol HS	209
Figure 104: HDFn cell viability following exposure to TiO ₂	210
Figure 105: HDFn cell viability following exposure to TiO ₂	210
Figure 106: Showing internalization in NIH 3T3 fibroblasts following exposure to uncoated TiO ₂ nanoparticles (15µg/cm ²).	212
Figure 107: TEM image of human fibroblast cell incubated with TiO ₂ nanoparticles (0.4 mg/ml) for two days.....	213
Figure 108: Showing representative images of potential TiO ₂ internalisation by HDFn cells following exposure to TiO ₂	214
Figure 109: Comet assay control conditions.....	216
Figure 110: nDNA damage following exposure of HDFn cells to TiO ₂ +/- complete solar simulated light.	216
Figure 111: Enzyme modified (hOGG1) comet assay control conditions	217
Figure 112: nDNA damage detection following exposure of HDFn cells to TiO ₂ +/- complete solar simulated light- enzyme modified assay.	218
Figure 113: Protective effects of TiO ₂ suspensions- acellular	219
Figure 114: Protective effects of Parsol HS in solution- acellular	220
Figure 115: TiO ₂ protective effects against complete solar light induced ROS generation in HDFn cells.	220
Figure 116: TiO ₂ acellular ROS generation following exposure to solar light sources	223
Figure 117: Parsol HS acellular ROS generation following exposure to solar light sources ...	224
Figure 118: Assessing the protective effect of TiO ₂ on HDFn cells following exposure to Cleo performance + glass	225
Figure 119: Assessing the protective effect of TiO ₂ on HDFn cells following exposure to TL01	226
Figure 120: Assessing the protective effect of TiO ₂ on HDFn cells following exposure to UV6	227
Figure 121: Assessing the protective effect of Parsol HS on HDFn cells following exposure to Cleo performance + glass	228

Figure 122: Assessing the protective effect of Parsol HS on HDFn cells following exposure to TL01	229
Figure 123: Assessing the protective effect of Parsol HS on HDFn cells following exposure to UV6	230
Figure 124: TiO ₂ acellular ROS generation following exposure to Cleo performance + glass.....	231
Figure 125: ROS generation in HDFn cells following exposure to TiO ₂ +/- Cleo performance	233
Figure 126: ROS generation in HaCat cells following exposure to TiO ₂ +/- Cleo performance	233
Figure 127: Photograph of a Franz type diffusion cell	248
Figure 128: Showing the structure of radiolabelled carbon-14 caffeine.....	251
Figure 129: Outline of percutaneous absorption study methodology using the Franz-type diffusion cell.....	255
Figure 130: Cumulative absorption of radiolabelled caffeine through human skin plus or minus 5mg/ml TiO ₂	258
Figure 131: Mass balance showing the distribution of radiolabelled caffeine through human skin plus or minus 5mg/ml TiO ₂	259
Figure 132: Cumulative absorption of radiolabelled caffeine through human skin plus or minus 50µg/ml TiO ₂	260
Figure 133: Mass balance showing the distribution of radiolabelled caffeine through human skin plus or minus 50µg/ml TiO ₂	261
Figure 134: Cumulative absorption of radiolabelled caffeine through human skin exposed to 1mg/ml TiO ₂ plus or minus UVA.....	262
Figure 135: Mass balance showing the distribution of radiolabelled caffeine through human skin when exposed to 1mg/ml TiO ₂ plus or minus 1mg/ml TiO ₂	263
Figure 136: Temperature and irradiance readings of Cleo performance+ glass lamp over time	264
Figure 137: Ambient light measurements.....	265
Figure 138: In vitro diffusion cells used for percutaneous absorption studies - Franz-Type and CutaFlex™	267
Figure 139: Diffusion Cell experimental setup	268

Figure 140: Cumulative absorption of radiolabelled caffeine through porcine skin under static conditions plus or minus TiO ₂ (5mg/ml).....	269
Figure 141: Mass balance showing the distribution of radiolabelled caffeine through porcine skin plus or minus TiO ₂ (5mg/ml) - Static cells	270

List of Tables

Table 1: Description of the three skin layers (epidermis, dermis and subcutis).....	34
Table 2: The various components of solar light and effects on human skin.....	44
Table 3: Fitzpatrick scale of skin types with descriptions. Figure adapted from	59
Table 4: Primer sequences for the 83bp fragment QPCR assay.....	81
Table 5: Cycling conditions used for the 83bp QPCR assay	81
Table 6: Primer sequences for the 1Kb fragment QPCR assay.....	83
Table 7: Cycling conditions for the 1kb QPCR assay.....	83
Table 8: Primer pair sequences for the 11Kb fragment QPCR assay	84
Table 9: Cycling conditions for the 11Kb QPCR assay	85
Table 10: Summarising the percentage increase in ROS relative to unirradiated control following exposure of primary skin cells to solar light (2.16 SED).....	158
Table 11: QPCR efficiency for each primer pair and comparison with previous findings in the literature.....	180
Table 12: Showing examples of the range of TiO ₂ particles available	191
Table 13: Showing the total level of caffeine retrieval from each Franz-cells (radiolabelled caffeine plus or minus TiO ₂ (5mg/ml)).....	258
Table 14: Showing the total level of caffeine retrieval from each Franz-cells (radiolabelled caffeine plus.....	260
Table 15: Showing the total level of caffeine retrieval from each Franz-cells (radiolabelled caffeine plus 1mg/ml TiO ₂ (plus or minus UVA)).....	262
Table 16: Showing the total level of caffeine retrieval from the static Franz cells (radiolabelled caffeine plus or minus TiO ₂ (5mg/ml)).....	269
Table 17: Showing the total level of caffeine retrieval from static Franz cells (radiolabelled caffeine plus or minus TiO ₂ (5mg/ml)).....	271
Table 18: Showing the total level of radiolabelled caffeine retrieval from each Franz cell...	274
Table 19: Outlining the key difference observed between the static Franz cell and CutaFlex cell model	276

List of Abbreviations

Abs - Absorbance

ANOVA - Analysis of variance

ATP - Adenosine triphosphate

BCC - Basal cell carcinoma

BER- Base excisions repair

Bp - Base pair

BRL- Bunsen-Roscoe law

BSA - Bovine serum albumin

C - Celsius

CIE - Commission Internationale de l'Éclairage - (International Commission on Illumination)

Cm - Centimeters

CO₂ - Carbon dioxide

COX- Cytochrome C oxidase

CPD- Cyclobutane pyrimidine dimers

CT- Cycle threshold

Da - Daltons

DCFDA - 2',7' -dichlorofluorescein diacetate

dH₂O₂ - Deionised water

DMEM - Dulbecco's modified eagles medium

DMSO - Dimethylsulfoxide

DNA - Deoxyribonucleic acid

dNTP - Deoxyribonucleotide

DSB - Double strand breaks

ECM - Extracellular matrix

EDTA - Ethylenediaminetetraacetic acid

EGW - Environmental Working Group

ELISA - Enzyme-linked immunosorbent assay

EMEM - Eagle's minimum essential medium

ENO III - Endonuclease III

ESCODD - European Standards Committee on Oxidative DNA Damage

ETC - Electron transport chain

FCS - Fetal calf serum

FPG- Formamidopyrimidine DNA glyosylase

g - Grams

h - Hours

H₂O - Water

H₂O₂ - Hydrogen peroxide

HaCaT - High calcium and temperature immortalized keratinocyte cell line

HDFn - Human neonatal dermal fibroblast cell line

HKGS - Human keratinocyte growth supplement

HO -Hydroxyl radical

hOGG1 - human 8-oxoguanine DNA N-glycosylase 1

HPLC - High-performance liquid chromatography

HSE - Human skin equivalent

Hsp70 - Heat shock protein 70

IR - Infrared radiation

IRA - Infrared A

IRB - Infrared B

IRC - Infrared C

J - Joule

KDa - Kilodaton

Kp - Permeability coefficient

l - Litre

M - Meter

MAPK - Mitogen-activated protein kinases

MED - Minimal erythema dose

Mg - Milligrams

Min - Minutes

mJ - Millijoules

ml - Millilitres

mM - Millimolar

MMP- Matrix metalloproteinase

mtDNA -Mitochondrial DNA

MTS - [3-(4,5-dimethylthiazol-2-yl)-5-(3-carboxymethoxyphenyl)-2-(4 sulfophenyl)-2H-tetrazolium,
inner salt]

mW - Milliwatts

nDNA - Nuclear DNA

NER - Nucleotide excision repair

NF-kB- Nuclear factor-kappa B

ng - Nano grams

NIHR - National Institute for Health Research

NMF - Natural moisturising factor

NMSC - Non-melanoma skin cancers

NO- Nitric oxide

O₂⁻ - Superoxide radical

O₂ - Oxygen

OH - Origin of heavy strand replication

OL - Origin of light strand replication

ONOO - Peroxynitrite

OXPPOS - Oxidative phosphorylation

PBS - Phosphate buffered saline

PTFE - Polytetrafluoroethylene

PH - Promoter of heavy strand transcription

PHE - Public Health England

PL - Promoter of light strand transcription

PZC - Point of zero charge

qPCR - Quantitative real-time polymerase chain reaction

RNA - Ribonucleic acid

RNS- Reactive nitrogen species

ROS - Reactive oxygen species

RT- Room temperature

SC - Stratum corneum

SCC - Squamous cell carcinoma

SCCNFP - Scientific Committee on Cosmetic Products and Non-food products intended for Consumers

SCCP- Safety of Nanomaterials in cosmetic products

Sec - Seconds

SEM - Standard error of the mean

SED -Standard erythemat dose

SOD - Superoxide dismutase

SPF - Sun protection factor

SSB- Single strand breaks

TAE - Tris acetate ethylenediaminetetraacetic acid

TBS - Tris-buffered saline

TE - Trypsin ethylenediaminetetraacetic acid

TEM -Transmission electron microscopy

TGF- β - Transforming growth factor beta

TIMPS - Tissue inhibitors of metalloproteinases

TiO₂ - Titanium dioxide

UV - Ultraviolet radiation

UVA - Ultraviolet radiation A

UVB - Ultraviolet radiation B

UVC - Ultraviolet radiation C

VIS- Visible light

W - Watt

μ g - Micrograms

μ l - Micro litre

6-4 PP - Pyrimidine pyrimidone (6 4) photoproducts

8-OHdG - 8-hydroxydeoxyguanosine

Chapter 1- Introduction

1 Background

1.1 Skin structure and function

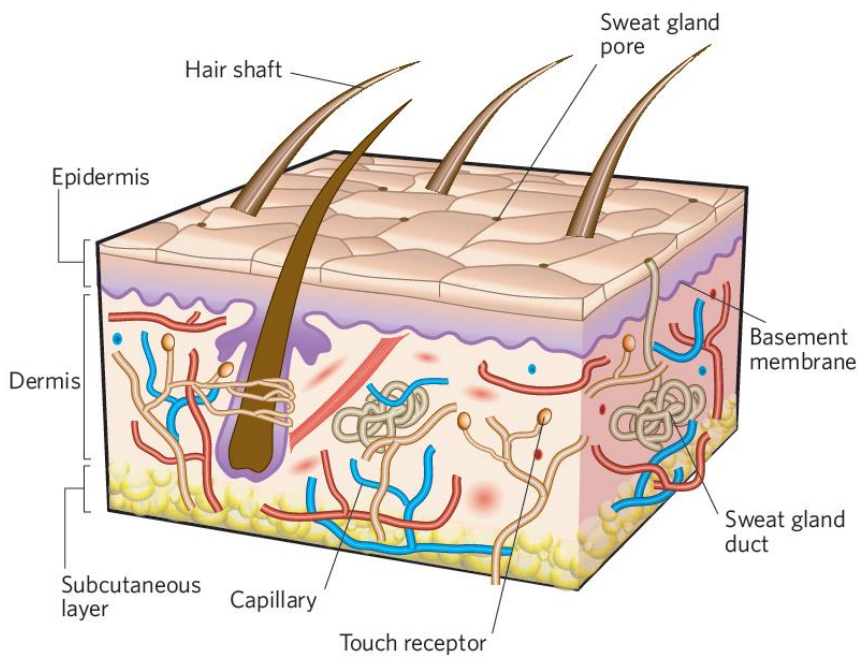


Figure 1: Schematic representation of the basic human skin structure (MacNeil, 2007)

The structure of skin (Figure 1) may be divided into three distinct layers known as the epidermis, dermis and subcutis (Table 1). Furthermore, the skin is seen to contain additional structures and appendages such as hair follicles, sebaceous glands and sweat glands as shown in Figure 1 (Peira et al., 2014 and Luigi Battaglia a, 2014).

Skin layer	Description
Epidermis	The outermost layer of the skin which is composed predominantly of keratinocytes. Other cells found include melanocytes, Langerhans and Merkel cells. The epidermis acts as the rate limiting skin layer for compound absorption (Gawkrodger, 2012).
Dermis	The middle layer of supportive connective tissue between the epidermis and the underlying subcutis with fibroblasts being the predominant cell type. Contains sweat glands, hair follicles, nerve cells, immune cells, blood vessels and lymph vessels (Gawkrodger, 2012).
Subcutis	A layer composed predominantly of loose connective tissue and fat beneath the dermis. This layer may also be referred to as the hypodermis (Gawkrodger, 2012).

Table 1: Description of the three skin layers (epidermis, dermis and subcutis)

1.1.1 Epidermal structure and function

Keratinocytes are the predominant cell type in the epidermal skin layer and are responsible for synthesising keratin. The epidermis is a stratified squamous epithelial layer and is the body's first contact with the external environment. It varies in thickness depending on body region, for example it has a thickness of 0.05mm on the eyelids and 0.8-1.5mm on the soles and palms of the feet and hands respectively (Chilcott, 2008). The epidermis is comprised of four main layers (Figure 2), namely the stratum corneum (SC) (horny layer), stratum granulosum (granular cell layer), stratum spinosum (spinous or prickle cell layer) and stratum basale (basal or germinativum cell layer) (Chilcott, 2008).

Keratinocytes are in a constant state of motion whereby the innermost cells escalate towards the skins surface as they mature. End stage differentiated keratinocytes are shed from the skin surface through desquamation, this vital process allows for the surface of the skin to be renewed on average every 4-6 weeks. Desquamation acts as a natural skin protective mechanism, as the loss of older more differentiated keratinocytes minimises the risk of diseases such as the development of skin cancers (Wilkinson, 2008).

The stratum basale is the innermost layer of the epidermis and is composed predominantly of dividing and non-dividing keratinocytes that are attached to the basement membrane via hemidesmosomes. As keratinocytes multiply and differentiate, they move from the basal layer towards a more superficial layer to form the stratum spinosum. Intercellular bridges known as desmosomes, connect neighbouring keratinocytes together to postpone the process of transition towards the surface. Maturing keratinocytes become flattened and anuclear as they move further up to form a layer known as the stratum granulosum, or the granular layer (aptly named due to the granular appearing cytoplasm). The granular layer contains immunologically active cells such as Langerhans, which act as antigen-presenting cells and play a significant role in the immune reactions of the skin (Wilkinson, 2008).

The SC is the outermost surface of the epidermis and consists of 10-30 layers of flattened hexagonal-shaped, non-viable cornified keratinocyte cells known as corneocytes. These are the final maturation products of keratinocytes. Each corneocyte is surrounded by a protein envelope filled with approximately 70% keratin proteins and 30% water (Wilkinson, 2008). The shape and orientation of the keratin proteins in corneocytes adds strength to the SC. Lipid bilayers or lamellae fill the extracellular space and covalently link neighbouring corneocytes together (Bouwstra and Ponc, 2006). Such compact arrangement contributes towards providing the skin's effective barrier function (Michaels et al., 1975). The "brick and mortar" analogy first described by Michaels et al., is often used to illustrate the SC structure. This model describes corneocytes as the bricks with the surrounding lipid layers acting as the mortar (Michaels et al., 1975).

Lipid constituents of the SC include sphingolipids, cholesterol and free fatty acids. Ceramide, a form of sphingolipid, is the main lipid responsible for water retention in the SC. Ceramide forms a stacked lipid structure that helps to minimise water and natural moisturising factor (NMF) loss from the skin surface. Healthy skin is found to contain around 30% water in the SC. Molecules such as salts, free amino acids, urea and lactic acid make up the NMF. This helps maintain the skin moisture due to the ability of such molecules to attract water. The specific arrangement of the lipid stacks remains an area of continued research, as there is uncertainty in the arrangement of the ceramide groups. A widely accepted model describes ceramide

groups as being arranged in a head to tail manner with heads being on the outer surface and tails on the inner similar to a phospholipid bilayer (Wilkinson, 2008) (Figure 3).

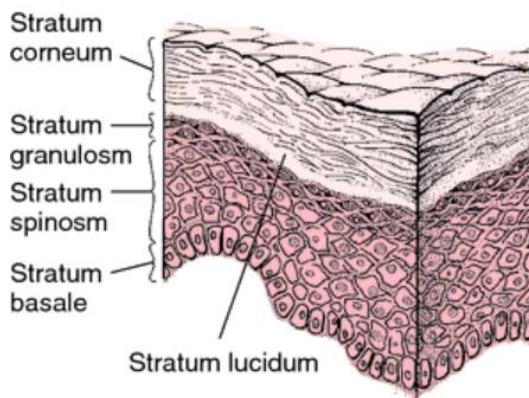


Figure 2: Diagram showing the structure of the epidermal layer in human skin (Dorland, 2007)

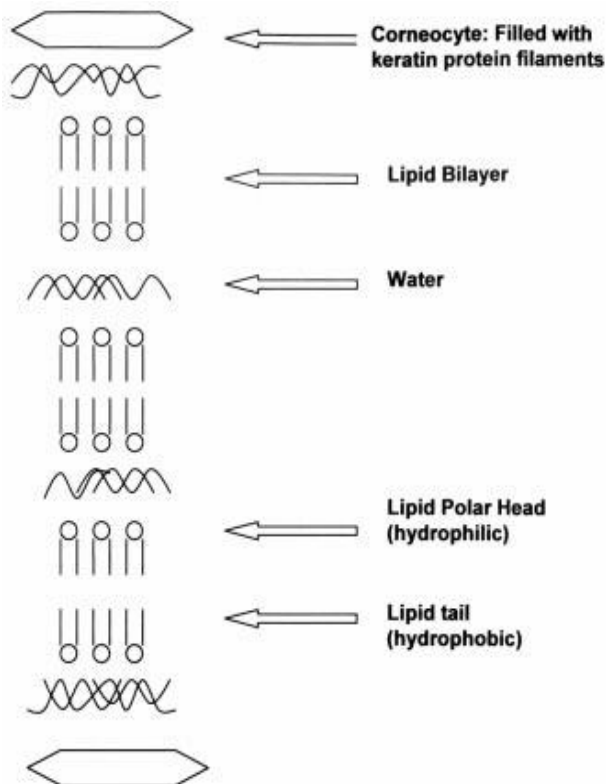


Figure 3: Arrangement of lipid stacks in the stratum corneum (Wilkinson, 2008)

1.1.2 Dermal structure and function

The dermis (Figure 1) is composed primarily of a network of fibrous, filamentous and amorphous connective tissue. This provides skin with the necessary flexibility, elasticity and strength to anchor and protect the associated neural and vascular tissues (Losquadro, 2017). The dermis contains fewer cells than the epidermal layer whilst also harbouring appendages such as hair follicles, sebaceous and sweat glands. Fibroblasts are the predominant cell type in the dermis, these cells synthesise collagen, elastin and other connective tissue. In addition to fibroblasts, dermal dendrocytes, mast cells, macrophages and lymphocytes can also be found in small numbers. The dermis contains an unstructured fibrous extracellular matrix that surrounds the epidermal appendages, neurovascular networks, sensory receptors and dermal cells. Interaction between the dermis and the epidermis occurs during development and enables the maintenance of the properties of both tissues (for example wound healing). The dermis, unlike the epidermis, does not undergo a series of differentiation steps (Wilkinson, 2008).

A vascular system exists in the dermis which is involved in processes such as heat exchange, immune response, repair, thermal regulation and nutrient exchange (Schaefer, 1996). This vascular network is divided into an upper papillary plexis and lower reticular plexis. The capillary system reaches the upper epidermal layer and capillary loops line the papillae, which is in contact with the epidermis. A lymphatic system is also present within the dermis, which functions to regulate the pressure from the interstitial fluid (Schaefer, 1996).

The subcutis anchors the dermis to the underlying muscle and bone structures. This layer consists of connective and adipose tissue with its functions including thermoregulation and systemic metabolism (Wilkinson, 2008).

1.2 Percutaneous absorption

The skin forms a tough protective layer in order to minimise the penetration of exogenous compounds. Healthy skin usually provides an effective barrier against pathogens due to factors such as low pH (4-7). The skin has a large surface area and a significant level of

enzymatic activity, albeit relatively low compared to other organs such as the liver. An exogenous compound is able to exert a biological effect when the compound or its metabolites reach a target site and are at a sufficient concentration for a certain amount of time. The dose of a substance is the amount of the compound over the weight of the body to which the compound is applied (Gulson et al., 2015). Furthermore, the frequency of exposure is also an important consideration (Bolzinger et al., 2012). The stratum corneum acts as an effective barrier to prevent topical compounds from permeating the skin and from coming into contact with viable cells.

Cosmetic products are designed to remain on the surface of the skin, substances which break this barrier may be classed as pharmaceuticals as they have the ability to exert biological effects on viable tissue. Cosmetic products containing bioactive substances which exhibit an effect on the skin are often referred to as cosmeceuticals (Yanti et al., 2017). Percutaneous or dermal absorption is governed by the basic laws of thermodynamics and occurs solely through the process of diffusion. This process may be subdivided into three main steps those being: 1) penetration (entry of a substance into a particular skin layer), 2) permeation (movement of a substance from one skin layer to another) and 3) resorption involving the uptake of the substance into the blood vasculature system (Figure 4) (Wilkinson, 2008). The thermodynamic activity of a molecule present in the vehicle is of greater importance than its absolute concentration (Moser et al., 2001).

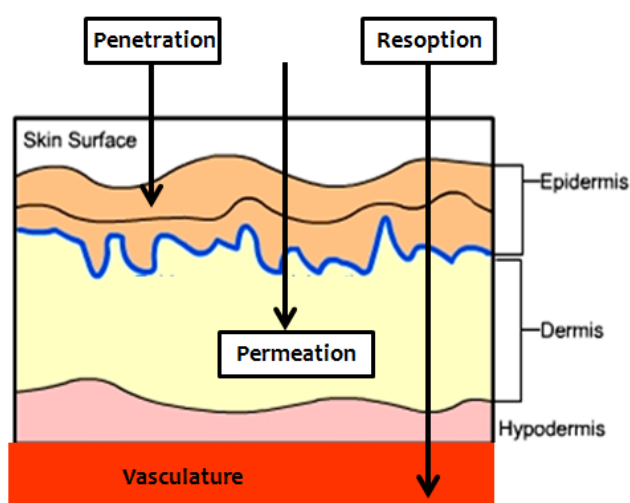


Figure 4: Schematic diagram representing the three levels of cutaneous absorption

Substances are generally thought to penetrate the skin surface through three main routes (Figure 5), namely the intracellular/transcellular route (involving movement of a substance through the cell), the extracellular/intercellular route (involving movement of a substance through the lipid matrix surrounding the cells) and the interfollicular route whereby substances move through appendages such as hair follicles (Wilkinson, 2008).

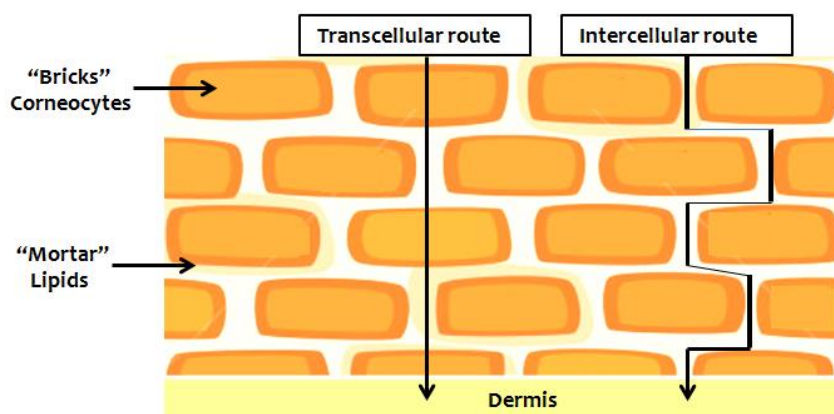


Figure 5: Showing the “Brick and mortar” model of the stratum corneum structure and the transcellular and intercellular absorption routes

The majority of dermal absorption occurs mainly through the intercellular route (Wilkinson, 2008). The interfollicular route is thought to have negligible effects on absorption due to the relatively low abundance of hair follicles in human skin (0.1-1%). It has however been suggested that hair follicles may provide a relevant route as well as a long term reservoir for topically applied compounds (Jatana and DeLouise, 2014). Regional differences in skin morphology exist such as the thickness and number of appendages, i.e. the number of hair follicles and sweat glands present. Differences in skin permeability have also been reported for different anatomical sites, the reasons for this are however unknown. For example, the forearm and palm show similar permeability (Marzulli, 1962) whereas the abdomen and dorsum show double the level of permeability relative to the forearm (Maibach et al., 1971).

In order to bypass the skin, a particle must have certain properties to facilitate passive diffusion. Size, shape, charge, form of deposition (solid, liquid, gas) lipophilicity, solubilisation, interaction with the delivery medium and surface reactivity are all properties that have a role in determining the level of absorption (Chilcott, 2008). Furthermore, other influencing factors

may include: concentration, temperature, humidity, occlusion, application site, skin condition, substance purity as well as age and gender of the skin sample (Larese Filon et al., 2015). The exposure scenario (length, dose and frequency of exposure) also has an influence on the level of absorption through the skin. Such variables complicate the predictability of the toxicological outcome of topically applied compounds. Substances must therefore be assessed as a case-by-case scenario. Substances such as titanium dioxide (TiO₂) in the nanoparticle form have added metrics that should also be considered during analysis. These include, size distribution, agglomeration/aggregation, crystallinity and type of surface coating (Larese Filon et al., 2015).

In order to bypass the skin barrier, a compound needs to have solubility in the solvent it is in, whilst also being sufficiently lipophilic so as to cross the lipid rich stratum corneum. The skin surface is rich in keratins, which have positive and negative charges; this along with the SC being lipophilic creates a barrier against charged compounds. A compound in the uncharged form can be 1-2 orders of magnitude more permeable across the SC when compared to the ionised compound form (L. Bartosova, 2012). It is largely accepted that substances ~500 Da (~2.5 nm diameter) cannot penetrate the SC in healthy intact skin (Bos and Meinardi, 2000). Cells making up the SC have an intercellular space of approximately 100nm³. This space may be widened by the topical application of various substances which act as penetration enhancers and disrupt the skin lipid membranes e.g. DMSO and ethanol (Lane, 2013; Bolzinger et al., 2012). The use of some ingredients found in the final cosmetic formulations may act to enhance dermal penetration. There have also been reports of sunscreen actives such as TiO₂ in the uncoated form affecting dermal absorption (Peira et al., 2014).

1.3 Electromagnetic spectrum

The electromagnetic spectrum is an arrangement of wavelengths that are divided into bands illustrating the differences in wavelength characteristics (Figure 6). The ordering is based on the different wavelengths or frequency of the radiation. Furthermore, classification of the electromagnetic spectrum is determined by the energy that the photons carry. Higher energy levels are seen with shorter wavelengths (Diffey, 2002).

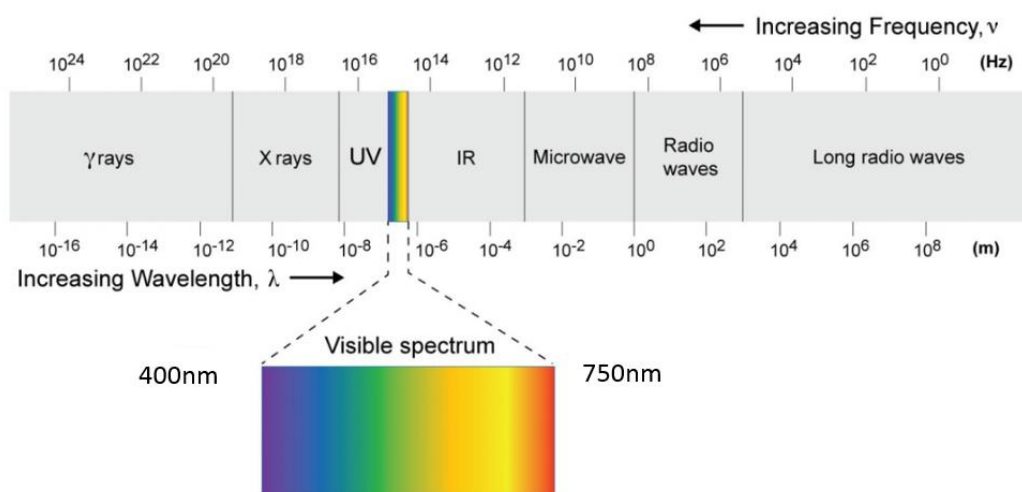


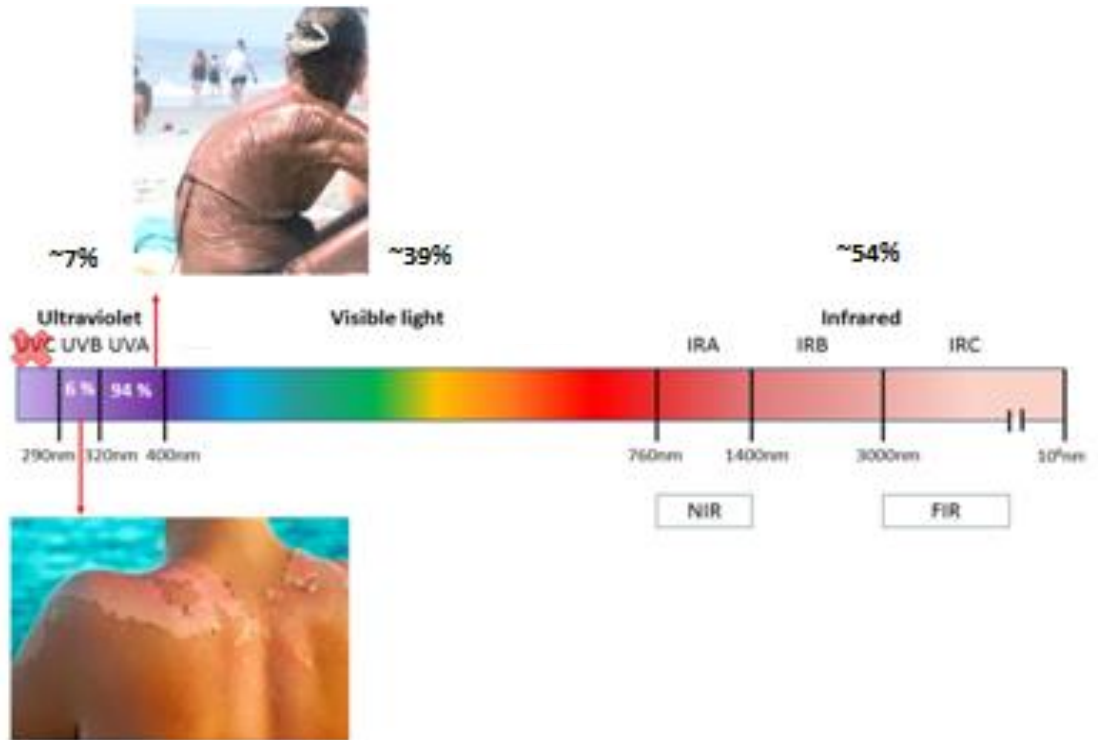
Figure 6: Illustrating the arrangement of the electromagnetic spectrum. Figure is adapted from (CHEM101-IntroductoryChemistry, 2017)

1.3.1 Solar spectrum

The solar spectrum can broadly be divided into three main bands, namely the ultraviolet radiation (UV), visible light (VIS) and infrared radiation (IR). The UV portion of the spectrum lies between the X ray and VIS regions and has a wavelength ranging from 100 to 400 nm. The band is further subdivided by wavelength into UVA (400-315nm), UVB (315-280 nm) and UVC (280-100 nm) (Diffey, 2002). Although UV only makes up approximately 7% of the spectrum, the UV component is recognised as the main wavelength in solar radiation which contributes to both changes in the skins appearance, as well as the increased risk of skin cancer development (Diffey, 2002; Kochevar IE, 2008; Birch-Machin et al., 2013b). Solar UV reaching the Earth's surface is comprised of approximately 6% UVB and 94% UVA (Figure 7). The proportion of solar light reaching the Earth's surface is dependent on multiple factors, including the atmospheric and environmental conditions, time of day, seasonal changes, and changes in altitude and latitude (Diffey, 2011). The short wavelengths of UVC are absorbed completely by the stratospheric ozone layer and are therefore less of a biological concern (Birch-Machin and Wilkinson, 2008). It is estimated that the atmosphere also absorbs approximately 90% of UVB, however a rise in the level of UV has been documented due to

depletion in the ozone layer. This has led to further concerns regarding the harmful effects of prolonged UV exposure (Bharath and Turner, 2009). As mentioned previously, shorter wavelengths of UV carry higher energy levels per photon and are therefore seen to elicit greater levels of damage to skin (Birch-Machin and Wilkinson, 2008). This effect can be seen clearly in the action spectrum of UV-induced erythematous effects whereby UVB is more effective at inducing erythema (skin reddening) relative to UVA. UVB is reported to be one thousand times more potent at inducing sunburn compared to UVA (Birch-Machin et al., 2013a). As shown in Figure 7 UVB however, does not travel deep into the skin and mainly exerts its effects on the superficial epidermal layer leading to the eventual burning effects observed (Rodrigues et al., 2017). In contrast UVA travels deeper into the dermal layer of skin affecting both the epidermal and dermal layers (Swalwell et al., 2012b). VIS (400-700nm) and IR (760-1mm) penetrate deep into the dermal layers of the skin as shown in Table 2 and Figure 7. VIS has been shown to cause various effects in the skin including erythema, reactive oxygen species (ROS) generation and pigmentation (Liebel et al., 2012; Randhawa et al., 2015). ROS is an umbrella term used to describe a series of highly reactive oxygen species that have unpaired valence electrons or unstable bonds. IR has also been shown to have effects on the skin (Naidoo and Birch-Machin, 2017), despite it having a lower energy level relative to UV. The IR waveband can further be subdivided into IRA (760-1440nm), IRB (1440-3000nm), and IRC (3000-1mm). IRA in particular, is seen to penetrate further into the skin when compared to UV where it has been reported to induce biological effects by increasing the generation of ROS and matrix metalloproteinase (MMP) expression, eventually contributing to the skin's overall ageing process (Maddodi et al., 2012). MMPs are a family of zinc-dependent endoproteases with a broad range of specificities which together are capable of degrading all extracellular matrix (ECM) components (Kim et al., 2005).

A



B

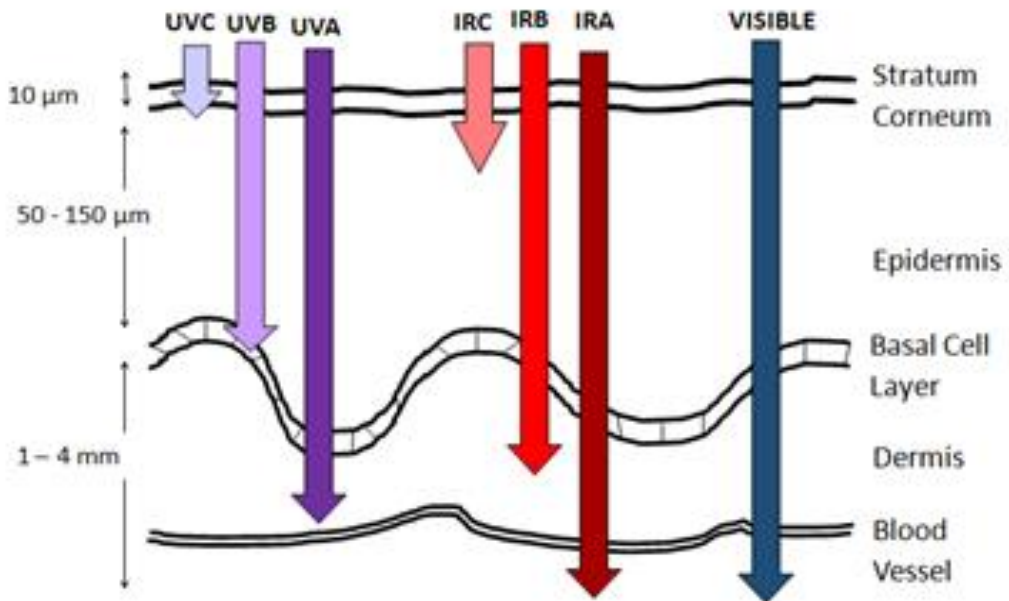


Figure 7: Illustrating the components of the solar spectrum and the differential levels of absorption occurring through human skin

UVA mainly leads to the ageing effects observed in skin whilst UVB induces sunburn (A). The different components of solar light are absorbed through the skin layers at different depths as illustrated in the diagram and are able to induce wavelength dependent mechanistic effects (B). This figure is adapted from (Barolet et al., 2016a) (A) and (J.Moan D.Brune, 2001; Kochevar IE, 2008) (B) respectively.

Source	Wavelength Range (nm)	Penetration Level	Effects on skin	Mechanism of effect
UVB	290-320	Epidermis	Reddening, blistering and burning, skin cancer, direct DNA damage	Vibrational energy
UVA	320-400	Dermis	Skin ageing, wrinkling, vascular and lymphatic damage, indirect DNA damage	ROS generation
VIS	400-700 (High energy VIS is 400-500nm)	Dermis to blood cells	Age-related macular degeneration by activating metalloproteinases to promote degradation of collagen and elastin, forming glycation wrinkles and premature ageing	ROS generation
IRA	760-1440	Epidermis, dermis, hypodermis	Photo ageing	ROS generation, cell signalling, collagen/elastin degradation
IRB	1440-3000	Epidermis, partially dermis	Heating effect	Vibrational energy
IRC	3000-10 ⁶	Epidermis only	Heating effect	Vibrational energy

Table 2: The various components of solar light and effects on human skin (Maddodi et al., 2012; Polefka et al., 2012)

1.3.2 Measurement of solar exposure

It is recommended that the emission of an irradiation source should be measured regularly to monitor the intensity as this is usually seen to decrease over time (Diffey et al., 1997). Spectroradiometry is the fundamental way to characterise the emissions (radiant energy or spectral irradiance) of a particular light source (Diffey, 2002). The radiant flux is the total power emitted by the source and the irradiance is the radiant flux per unit area. Radiant exposure may loosely be termed as the dose, and is the time integral of irradiance (Diffey, 2002). Irradiance and radiant exposure can be used in a simple calculation in order to determine the time of exposure to a particular source required to achieve a specific dose:

$$\text{Exposure time} = \text{Dose} [\text{mJ}/\text{cm}^2] / \text{Irradiance} [\text{mW}/\text{cm}^2]$$

Minimal Erythema Dose (MED) is often used as a measure of erythema radiation. However, this value is dependent on the skin type of an individual and therefore the dose of UV required to produce a minimal erythema response in a particular skin type will not be consistent

(Parrish and Jaenicke, 1981). Standard Erythema Dose (SED) is being increasingly used as it provides a standard number as opposed to the MED and therefore is independent of skin type. One SED is equivalent to an erythema effective dose of 100 J/m² (Utrillas et al., 2012).

Differences in skin pigmentation influence the sensitivity to UV, with the most sensitive persons being able to tolerate 1 SED before erythema is detected. More pigmented skin types for example Fitzpatrick scale type IV (see section 1.7.1) will tolerate between 8-10 SED before the occurrence of erythema (Wulf et al., 2010).

1.4 Effects of solar radiation on skin

UV is a form of electromagnetic energy originating mainly from the sun. Man-made sources also exist, such as those arising from tanning beds and welding torches. Solar radiation is polychromatic and the effects seen in skin are not only the result of the separate action of each wavelength, but also the result of the interaction of the numerous wavelengths (Cho et al., 2009; Birch-Machin et al., 2013b).

1.4.1 Effects of UV on skin

Exposure to UV exhibits beneficial as well as a number of deleterious effects. Intermittent UV exposure is beneficial for vitamin D production, particularly in skin containing lower pigmentation levels (Birch-Machin and Wilkinson, 2008). UV is recognised as being a mutagen and carcinogen, with exposure resulting in the formation of various DNA lesions. UVB affects the cohesive and mechanical integrity of corneocytes and has been reported to cause morphological changes in the SC lipid structure, leading to increased transepidermal water loss and decreased SC hydration. Skin dryness and chapping may lead to inflammation and an immune response in skin (Jatana and DeLouise, 2014). Other effects of UV include an increase in mean SC thickness vasodilatation (skin erythema) and leukocyte infiltration (Jatana and DeLouise, 2014).

UVA exposure is thought to be the main cause of photoageing, whereby the skin appears wrinkled, leathery, fragile and less able to carry out normal wound healing function. Ageing skin is usually accompanied by further changes such as thinning, an increase in SC dryness, dermal-epidermal junction flattening and lower sebaceous gland activity leading to lower levels of cell surface lipids. Such changes over time impact the skins ability to function as an effective barrier with UV exposure accelerating and amplifying the damage seen in the skin with age (Birch-Machin and Wilkinson, 2008).

1.4.1.1 Molecular damage

DNA acts as a chromophore primarily for UVB, absorbing four-fold more UVB than UVA (Maddodi et al., 2012). The direct absorption of UVB photons produces dimeric photoproducts and wide DNA damage, including protein-DNA crosslinks, thymine glycol and single strand DNA breaks (SSB). The most prevalent photoproducts are the cyclobutane pyrimidine dimers (CPDs) followed by the pyrimidine pyrimidone (6-4) photoproducts (6-4 PPs) (Ichihashi et al., 2003). This leads to the induction of characteristic UV-induced mutations commonly found within the p53 gene of UV-induced cancer cells (Melnikova and Ananthaswamy, 2005). Absorption of UVA and UVB by chromophores found within skin leads to the generation of ROS. An increase in ROS levels is able to induce oxidative stress, which may lead to cellular damage as a secondary effect of UV exposure. ROS induced damage includes the oxidation of DNA, proteins and lipids. One particular target is the DNA base guanine, which gives rise to 8-hydroxydeoxyguanosine (8-OHdG), a miscoding lesion leading to the G to T transversion (Birch-Machin and Swalwell, 2010).

1.4.1.2 Skin cancer

UV is a well-recognised carcinogen often being associated with the development of skin carcinomas. Skin cancer is generally categorised as being either a melanoma or non-melanoma form (Birch-Machin and Wilkinson, 2008). Melanoma is the more serious form of skin cancer which is initiated in the melanocytes found between the dermis and epidermis and is most often seen to develop from a nevi. According to Cancer Research UK, the risk of

melanoma is slightly more common in females than males and around half of the people diagnosed with melanoma in the UK each year are aged 65 and over. Although UV is the most common cause of melanoma there are other risk factors including skin type, hair and eye colour, number of moles, family history of melanoma and certain predisposing medical conditions such as a compromised immune system (Simões et al., 2015). Melanoma is the fifth most common cancer in the UK. Approximately 14,500 people are diagnosed annually with an average of 40 new cases being reported each day. Over the last decade, the number of people diagnosed with melanoma in the UK has increased by almost a half (Cancer Research UK, 2017).

Non-melanoma skin cancers are the less aggressive forms and are categorised into two main types, those being basal cell carcinoma (BCC) and squamous cell carcinoma (SCC). It is however possible for a non-melanoma skin cancer to be a mixture of both these types. BCC is the most common form, accounting for up to 75% of the non-melanoma skin cancers (Simões et al., 2015). BCC develop from basal cells found in the deepest layer of the epidermis and around the hair follicle. They are reported to develop mostly in areas of skin exposed to the sun including parts of the face such as the nose, forehead and cheeks (Simões et al., 2015). SCC generally grow faster than BCC. On average 20% of skin cancers are SCC, most of which develop in areas that have been exposed to the sun. These areas include parts of the head, neck, and on the back of hands and forearms. They may also develop in areas of the skin that have been burnt, scarred, or that have been ulcerated for a long period of time. BCCs do not often spread but if metastasis does occur it is usually in the deeper layers of the skin. In rare cases, they can spread to nearby lymph nodes and other organs causing secondary cancers (Cancer Research UK, 2017). Rare types of skin cancer make up 1% of the skin cancers diagnosed in the UK. These include Merkel cell carcinoma, Kaposi's sarcoma and T cell lymphoma of the skin (Cancer Research UK, 2017).

1.4.1.3 Photo-ageing

Skin ageing is influenced by both genetic (intrinsic) and environmental (extrinsic) factors. UV is thought to have a major influence on accelerating the ageing processes, this effect is termed photo-ageing (Maddodi et al., 2012). Other factors such as tobacco smoke, airborne particulate matter, malnutrition and other solar wavelengths such as IR are also thought to contribute to the skin ageing processes (Naidoo and Birch-Machin, 2017). IR (specifically IRA) has been linked to extrinsic ageing in human skin. Interestingly, photo-ageing develops differentially across different ethnic groups. For example, in Caucasian skin an initial wrinkling is seen whereas the Japanese primarily acquire small pigment spots known as lentigines (Maddodi et al., 2012). Both UVA and UVB contribute to photo-ageing, however alterations within the dermis seem to have the greatest contribution. This suggests that UVA plays a major role in photo-aged skin due to its ability to be absorbed in to the dermis (Hudson et al., 2016). Collagen and elastin are what provide structure and support in the dermal skin layer, however UVA and UVB can induce the expression of MMPs. UV has been reported to increase the expression of MMP-1 (degrades type I and III collagen) as well as the expression of MMP-9 (degrades collagen fragments further) and MMP-3 which degrades collagen IV. Together these factors result in the subsequent evident wrinkle formation (Kim et al., 2005). Furthermore, Sherratt et al., have found that UVB can directly alter the structure of isolated fibrillinmicrofibrils, which are fundamental in mediating tissue elasticity (Sherratt et al., 2010).

1.4.1.4 Beneficial effects of UV exposure

Although this investigation focuses on the deleterious effects of solar radiation, intermittent exposures are able to induce multiple beneficial effects. This includes the synthesis of vitamin D, stimulation of hormones that regulate circadian rhythm and mood, as well as the usefulness of UV in phototherapy (Polefka et al., 2012).

Vitamin D is an essential precursor of the steroid hormone 1, 25-dihydroxyvitamin D that is essential for calcium absorption and for bone development, growth and preservation. Vitamin D production occurs naturally in skin through the interaction of UVB with an intrinsically found skin cholesterol compound known as dehydrocholesterol (7-DHC). 7-DHC is converted into a

pre-vitamin which is then later spontaneously converted to vitamin D (Birch-Machin and Wilkinson, 2008). Although vitamin D is available within our diet from foods such as fish and eggs, they only contain small amounts and therefore our main source of vitamin D is from the sun. A reduced vitamin D intake can lead to detrimental bone conditions such as osteoporosis (Ebeling, 2014). The sun also has an effect on mood elevation, seasonal changes can be related to episodes of depression, a condition termed seasonal affective disorder (Ness et al., 1999). Phototherapy is also widely used for the treatment of a variety of skin disorders including psoriasis, mycosis fungoides, vitiligo, eczema, acne and atopic dermatitis (Matsumura and Ananthaswamy, 2004).

1.4.2 Effects of IR on skin

IR is a form of non-ionising radiation, which has lower energy than red light but more energy than microwaves. IR can be divided into IRA (760-3000nm), IRB (3000-30000nm) and IRC (30000-1mm) (Barolet et al., 2016b). The photon energy of electromagnetic radiation is related to the wavelength in an inverse manner. Radiation in the IRA range has an energy of 1.9×10^{-19} J/photon which is approximately one third of that associated with UVA/B radiation ($5.6-6.6 \times 10^{-19}$ J/photon) (Schieke et al., 2003).

Solar light provides the main natural source of IR. Artificial sources are used for therapy, for example in the treatment of rheumatoid arthritis. Photodynamic therapy is used in the treatment of dermatological conditions such as actinic keratosis and basal cell carcinoma (Hönigsmann, 2012). Additionally other artificial sources are increasingly being used for wellness and lifestyle purposes including their use in saunas, skin rejuvenation and fat reduction (Barolet et al., 2016b).

IRA is the largest single component of solar light (30%) and can pass deep into the skin layers reaching down into the subcutaneous tissue level. Approximately 65% of IRA will reach the dermis without causing substantial heating effects per photon of light (Schieke et al., 2003). Contrary to this, UVB does cause a marked increase in heat when absorbed by the epidermis

(Cho et al., 2009). An increase in skin temperature can activate heat shock factors resulting in some of the effects observed. Essentially ROS generation can be induced through temperature effects or an IR dose effect, these two factors can influence each other with IR being a direct effect and temperature being indirect. Physiological skin temperature is reported to be between 27.6-33.1°C, when in the sun this can go up to 40-45°C (Kleesz et al., 2012). Chronic exposure to heat leads to medical conditions such as erythema ab igne where reticular pigmentation and elastosis similar to that found in photoaged skin is seen (Cho et al., 2009).

Like UV, the amount of IR reaching an individual's skin is dependent on several factors such as the ozone layer, latitude, cloud coverage, clothing choice etc. There is no data available on human exposure to solar radiation during recreational activities perhaps due to the absence of personal dosimeter devices (Diffey and Cadars, 2016). Exposure to IR is therefore estimated from predictions of the time spent in the sun (in a horizontal or vertical stance) along with cloud cover and seeking shade. Diffey and Cadars estimate the maximum human exposure to IR at the surface of the Earth at noon during the summertime to be 250J/cm² and for many people just a few tens of J/cm² (Diffey and Cadars, 2016).

The effect that IR has on the skin ageing process has been described over two decades ago by (Kligman, 1982). The authors were the first to report that IR enhanced the UV induced skin damage in guinea pigs, which consequently led to further investigations into the effects of IR alone on skin. The molecular mechanisms behind this were then investigated (Holzer and Elmetts, 2010). IRA has been reported to enhance the process of wound healing both in vitro using human skin cells and in vivo using mouse studies (Schroeder and Krutmann, 2017). The mechanism of action of IR in human skin is thought to be through its absorption via chromophores and interaction with electron bonds (Karu, 2008).

IRA is absorbed by components of the mitochondrial respiratory chain, causing a disruption in mitochondrial electron flow which in turn increases mitochondrial ROS. This initiates a downstream signalling effect influencing nuclear gene expression. IRA causes generation of mitochondrial ROS, which induces increased transcription and translation of the MMP-1 gene

via activation of the MAPkinase ERK1/2 (Schroeder et al., 2008). Following IR exposure, there is no increase in the expression of tissue inhibitors of metalloproteinases (TIMPs) seen. The MAPkinases ERK 1/2 react to changes in the redox-status of the cells. IRA has been reported to activate ERK1/2 and p38 in dermal fibroblasts (Schroeder et al., 2008).

An increase in UV-induced MMP-1 expression is not associated with mitochondrial ROS levels (assuming this is more cytoplasmic) as mitochondrial targeted antioxidants have not been found to be effective. Human dermal fibroblasts have been reported to withstand IRA doses of up to 1200 J/cm². Gene regulatory effects have been reported to be observed at much lower doses 54-360J/cm² and increased levels of ROS detected after a treatment with 30J/cm². Such changes within the cells and extracellular matrix contribute significantly to photoageing due to collagen degradation and accumulation of abnormal elastic fibres. Experiments carried out by Kligman and others observed that IR irradiation enhances UV induced actinic skin damage and IR alone cause actinic skin damage similar to that found in UV exposed skin (Kligman, 1969;Schroeder et al., 2008).

Since 2006 sunscreens as well as other skin care products claiming protection against IR have been available. Marketing of IR protection products began in Europe and later appeared in countries across Asia as well as North and South America. One solution for protection against IRA would be to use IRA reflecting mineral pigments such as TiO₂ or zinc oxide (ZnO), however there is a lack of customer acceptance due to the viscous feel and white residue left on skin following application (Krasnikov et al., 2011). Antioxidants including N-acetylcysteine; MitoQ; ascorbic acid and flavonoids have been shown to be effective at protecting against IRA-induced ROS in vitro (Schroeder et al., 2010). A topical mix of antioxidants has been demonstrated to reduce IRA-induced MMP-1 expression by 60% (Schroeder et al., 2008).

1.4.3 Effects of VIS on skin

Despite making up 44% of the solar spectrum, the effects of VIS on human skin remains an area which is understudied. VIS is able to reach the deeper skin layers where it has been shown

to induce a number of effects. Skin can be subjected to VIS for substantial amounts of time throughout the day, cumulative exposure is speculated to be a contributing factor to the ageing process. Leibel et al., reported that irradiation of human skin equivalents with VIS produces ROS, proinflammatory cytokines and MMP-1 expression (Liebel et al., 2012). Further to this, VIS is thought to have both transient and long lasting pigmentation effects, with pigmentation lasting up to 8 weeks following exposure depending on the total dose of light (Randhawa et al., 2015).

Although the effects of VIS are regarded as being less substantial when compared to the effects of UV, VIS becomes relevant in VIS sensitivity diseases such as porphyria and solar urticaria, as well as other idiopathic photodermatoses, for example polymorphous light eruption (Lehmann and Schwarz, 2011). VIS is known to trigger reactions such as itching, stinging and burning in patients with the rare skin condition solar urticaria (also known as hives, weals or nettle rash). Patients who undergo photodynamic therapy treatments also become sensitive to VIS for a few days due to the accompanying topical medications (for example aminolevulinic acid and methylaminolevulinate), or for a few weeks due to systemic agents such as porfimer sodium (Wan and Lin, 2014). Sunscreens allowing for protection against VIS exist and are available upon prescription through the NHS. The Dundee reflectant sunscreen is a formulation prescribed for such conditions. This sunscreen is in the form of a tinted formulation designed to match the natural colour of the patients skin and contains ZnO and TiO₂ particles in larger microform, these particles are able to some extent reflect VIS (Dorser-Medicines, 2015).

1.5 Mitochondria

Mitochondria are membrane-bound organelles found within most eukaryote cells. The number, size and shape of the mitochondria may however vary. Mitochondria are typically described as oval shaped organelles of approximately 1µm in diameter and 3-4 µm in length (Scheffler, 2007). When stained and examined under light microscopy, mitochondria are seen to be threadlike active structures with reoccurring cycles of fission and fusion. Two membranes exist within mitochondria the outer and the inner, which separate the inter-

membrane compartment and the inner matrix compartment (Figure 8). The smooth outer membrane compartmentalises the organelle from the cytosol of the cell. The inner membrane is folded into the matrix in multiple invaginations known as cristae, which have the effect of increasing the surface area (Scheffler, 2007).

Mitochondria are often described as the powerhouse of the cell as their main function is to produce the majority of the cell's energy in the form of adenosine triphosphate (ATP), through the process of oxidative phosphorylation (OXPHOS) via the electron transport chain (ETC) (Birch-Machin, 2006). Another vital function of mitochondria is the key role they have in ROS production and apoptosis (Liesa et al., 2008). Damage induction in mtDNA may potentially disrupt the assembly of the ETC complexes, which can ultimately lead to the loss of the mitochondrial respiratory function. UV-induced mtDNA damage may lead to a dysfunction in the OXPHOS system. UV may also directly interfere with the ETC, this may further enhance the resulting deleterious effects observed (Dranka et al., 2011).

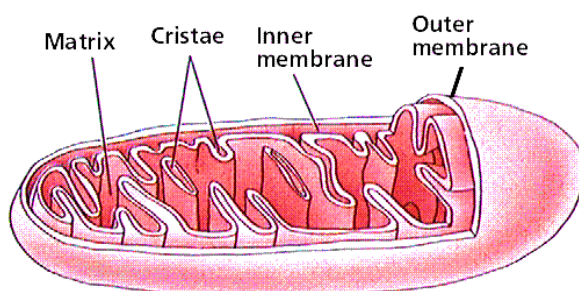


Figure 8: Illustration showing the structure of mitochondria

Mitochondria possess a double membrane with each of these membranes being a phospholipid bilayer with embedded proteins. The inner membrane forms folds known as cristae which envelopes the matrix (Purves, 1994).

1.5.1 mtDNA

mtDNA (Figure 9) can be found in multiple copies (usually 10^3 - 10^4 per cell) (Shadel GS, 1997) in a double stranded, closed, circular form that is 16,569-bp in length. mtDNA encodes for 13 essential polypeptides necessary for the complexes of the respiratory chain, as well as also encoding 22 for tRNAs and 2 rRNAs required for mitochondrial protein synthesis (Chinnery

and Schon, 2003; Birch-Machin, 2006). Additional proteins that are required by the mitochondria are encoded for by the nDNA and are then later imported. These proteins include the remaining subunits required for the respiratory chain, and those needed for mtDNA transcription, translation, replication, and for mitochondrial maintenance (Scheffler, 2007; Birch-Machin and Swalwell, 2010). Heteroplasmy typically exist within the mitochondrial genome whereby a mixture of both wild type and mutant mtDNA can exist (Birch-Machin, 2006). The performance of the cell is however not usually altered due to the mutations being recessive, and the detrimental effects created being compensated for by the wild type mtDNA. A threshold level however (usually 50-60% for deletions and 60-90% for point mutations) does exist, and in the event of the threshold being exceeded cellular dysfunction may then occur (Birch-Machin and Swalwell, 2010).

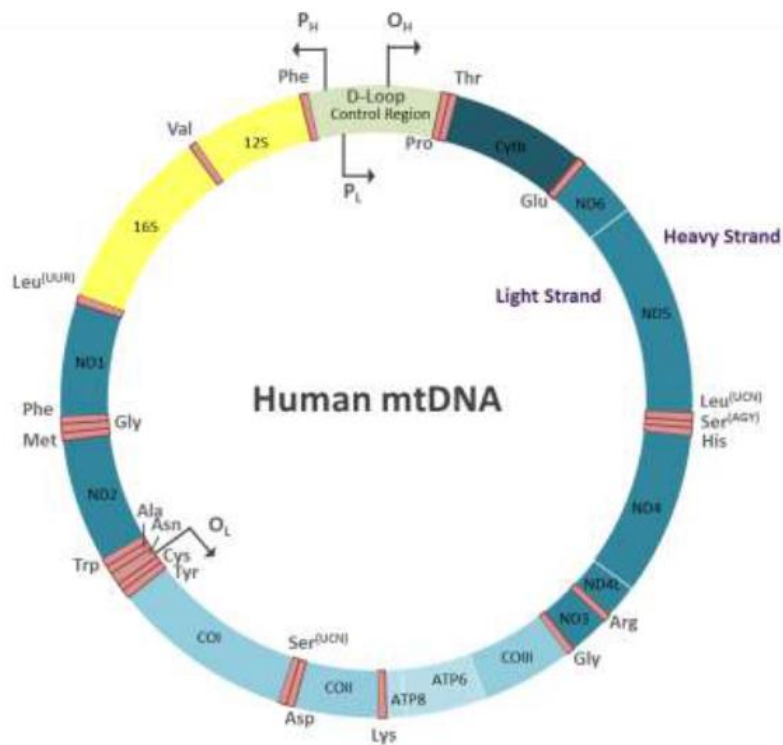


Figure 9: Illustration of the human mtDNA map

The mtDNA genome (16,569 bp) is present in multiple copies per cell and encodes 37 genes that are essential for the production of the components of the ETC (Birch-Machin and Swalwell, 2010)

1.5.2 mtDNA damage

Numerous mtDNA mutations that have been linked to mitochondrial disease have been described in the literature. Amongst these, there are several deletions and tandem mtDNA duplications which are associated with exposure to UV (Birch-Machin, 2006).

UV exposure results in the formation of SSB and double strand breaks (DSB) both of which have been found to contribute to the initiation and the progression of tumours (Helleday et al., 2007). ROS is the main initiator of SSB and DSB formation, as well as resulting in the production of lesions such as photoproducts, which may later contribute to the generation of DSBs post replication. This can lead to the loss of large amounts of genetic material (Helleday et al., 2007; Rastogi et al., 2010). Quantification of strand breaks can therefore provide a good indication of the integrity of the genome. SSB and DSB are more easily detected *in vitro* than deletions, which are often less prevalent and require a repeated pattern of UV exposure (Passos et al., 2007). Point mutations found within mtDNA have also been identified in numerous tumour types (Eshaghian et al., 2006). As reviewed by Birch-Machin et al. many mtDNA deletions have been found to be associated with UV exposure (Birch-Machin et al., 2010, Ray et al., 2000b; Krishnan and Birch-Machin, 2006). Of those identified in sun-exposed human skin, the major species have been the 4977 bp common deletion and a 3895 bp deletion (Figure 10) (Krishnan et al., 2004; Birch-Machin, 2006; Eshaghian et al., 2006). These mtDNA deletions can be induced in cultured human skin cells through repetitive sub-lethal dosing with UV, (Berneburg et al., 2004). A high frequency of tandem mtDNA duplications has also been reported in sun-exposed human skin (Krishnan and Birch-Machin, 2006). mtDNA lesions such as deletions and tandem duplications are seen to occur more frequently in skin which has been exposed to the sun for a prolonged period of time as opposed to skin which has received less sun-exposure (Krishnan et al., 2004; Harbottle et al., 2004). This is relevant in the context of skin cancer as NMSC are found to be more prevalent in body sites which are more exposed to solar light such as the neck, ears and face when compared to areas which are usually more covered, such as the back and chest region. mtDNA damage therefore serves as a potential biomarker for cumulative UV exposure in skin. It has been suggested that mtDNA damage may also provide a method of monitoring the long-term safety of clinical UV phototherapy regimes and possibly give an indication of the risk of skin cancer development early on (Birch-Machin and Swalwell, 2010).

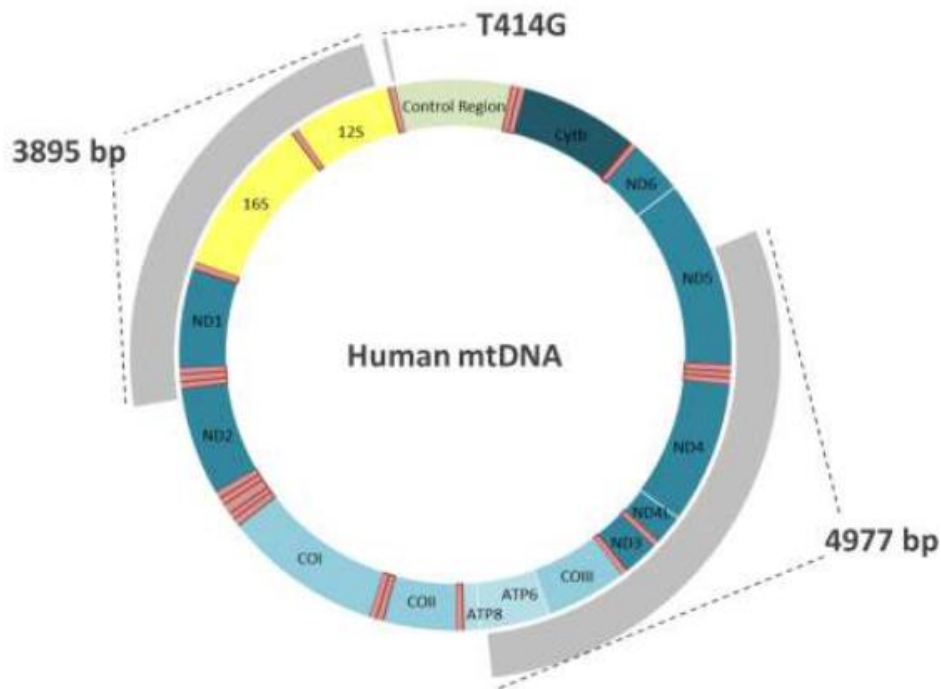


Figure 10: The positioning of UV-induced damage within human mtDNA

The most common markers of UV-induced mtDNA damage are illustrated along with the sections of mtDNA affected by the deletions (Birch-Machin et al., 2013b).

1.5.3 mtDNA as a biomarker

mtDNA has limited repair mechanisms when compared to nDNA and is therefore unable to repair UV-induced damage such as photoproducts. This limited ability to induce repair, coupled with the capacity to harbour mutated DNA without altering the cells function is what makes mtDNA a reliable biomarker of UV-induced damage (Birch-Machin and Swalwell, 2010).

Exposure of cells to UV leads to the production of ROS and reactive nitrogen species (RNS), which ultimately leads to mtDNA damage due to the close proximity of the respiratory chain to mtDNA. Mutations in the mtDNA genome can progressively lead to dysfunction in the respiratory chain and consequently lead to further production of ROS, resulting in further mtDNA damage. This phenomenon is termed the vicious cycle theory. An increase in the level of mtDNA mutations causes a deficiency in the respiratory chain. This leads to reduced energy production and ultimately tissue ageing (Shokolenko et al., 2009; Schroeder et al., 2008). The

vicious cycle theory remains a hypothesis, albeit, the argument can be strengthened by the research showing the increased incidence of mtDNA mutations in photo-aged skin (Birch-machin et al., 1998;Schroeder et al., 2008).

1.6 ROS and ageing

One of the most widely accepted theories of ageing is the free-radical theory proposed by Denham Harman during the mid-1950s. The theory suggests that age-related damage observed in an organism is the result of the endogenous free radicals created naturally within the aerobic organism (Harman, 1956). Intrinsic ageing is determined primarily by genetics and the body's ability to combat the accumulation of damage. Environmental effects such as UV exposure and lifestyle choices have a significant influence on the extrinsic ageing process (Naidoo and Birch-Machin, 2017).

As mentioned previously ROS is an umbrella term used to describe a series of highly reactive oxygen species that have unpaired valence electrons or unstable bonds. ROS may either exist as neutral molecules (e.g. H_2O_2) or as free radicals (e.g. superoxide anion). The term oxidative stress describes the numerous damaging effects resulting from an imbalance between ROS production and antioxidant defence mechanisms, leading to an overall increase in ROS (Pérez et al., 2009).

A large proportion of ROS is generated intracellularly from metabolic reactions such as cellular respiration. ROS may be produced by the action of enzymes such as NADPH oxidases, p450 cytochromes, xanthine oxidase and nitric oxide synthetase in macrophages and endothelial cells, as well as cellular structures such as peroxisomes. The vast majority of ROS (90%) is produced by the mitochondria as a result of oxidative phosphorylation during ATP production (Turrens, 2003;Patlevič et al., 2016).

Antioxidants are molecules that inhibit the oxidation of other molecules. They are the primary defence mechanism used by cells in order to lower ROS levels. Following increased oxidative

insult, cells are seen to up-regulate their defence mechanisms as a means of adaptation to restore oxidative balance. Enzymatic antioxidants such as catalase, peroxidase and superoxide dismutase are employed by the body as well as several non-enzymatic antioxidants such as vitamin A, C and E (Trifunovic and Larsson, 2008; Liochev, 2013).

1.7 Skins natural defence mechanisms

The skin has a number of natural protective mechanisms such as its compact structure, desquamation, detoxification, immune surveillance and melanin production. The viable skin layers have DNA repair mechanisms and the ability to counteract high levels of ROS generation (Madison, 2003). The biochemical composition and mechanical structure of skin makes it difficult for exogenous substances to bypass the SC layer as described in further detail in section 1.1.1. The SC is the rate-limiting step in dermal penetration, any substances that are absorbed through the skin eventually do so via the process of passive diffusion as skin primarily acts to block the entrance of exogenous compounds (Bolzinger et al., 2012).

Melanocytes determine the pigmentation level of the skin and are themselves a secondary cell type found amongst keratinocytes in the epidermal basal layer. The level of baseline pigmentation present within the skin, hair and eyes can be classified along the Fitzpatrick scale (Table 3). Skin initially responds to solar light through immediate tanning (usually 5-10 min following exposure) whereby hyperpigmentation is seen to occur (Maddodi et al., 2012). Existing melanocytes migrate to cover the nucleus of keratinocytes in the lower layers to form what is known as a nuclear cap, this protects genomic DNA from UV damage. This process is mainly UVA-dependent and occurs due to the oxidation and redistribution of pre-existing melanin and melanosomes, rather than increased melanin synthesis (Birch-Machin and Wilkinson, 2008). Delayed tanning involves the production of new melanocytes and occurs within two to three days following UV exposure (Birch-Machin and Wilkinson, 2008). The differences seen in skin pigmentation across populations are thought to have arisen through evolution as a means of providing UV protection balanced with the need for vitamin D synthesis. The greater the level of melanin present in the skin, the more difficult it becomes to synthesise vitamin D naturally within skin. Longer lasting pigmentation is seen with the delayed tanning process (up to weeks following exposure). Such pigmentation is associated

with both UVA and UVB with the delay being owed to the time taken to synthesise new melanin (Maddodi et al., 2012;Videira et al., 2013).

There are two distinct types of melanin, eumelanin (insoluble, black-brown in colour) and pheomelanin (soluble, red-yellow in colour). Eumelanin, along with its precursors, exhibit photo-protective abilities by acting as an antioxidant, thereby reducing ROS. Eumelanin is found at higher levels within darker skin. The levels of pheomelanin have been found to be consistently higher in lighter skin (Videira et al., 2013). There is evidence to suggest that melanin plays a dual role, not only as a photo-protector but also as a photosensitiser. As well as its UV-filtering and ROS scavenging abilities, melanin may increase the incidence of melanoma by an UVA-dependent mechanism. Our group has provided evidence of this by showing an increase in the level of damage of isolated mtDNA following UVA-irradiation in the presence of melanin (Swalwell et al., 2012b).







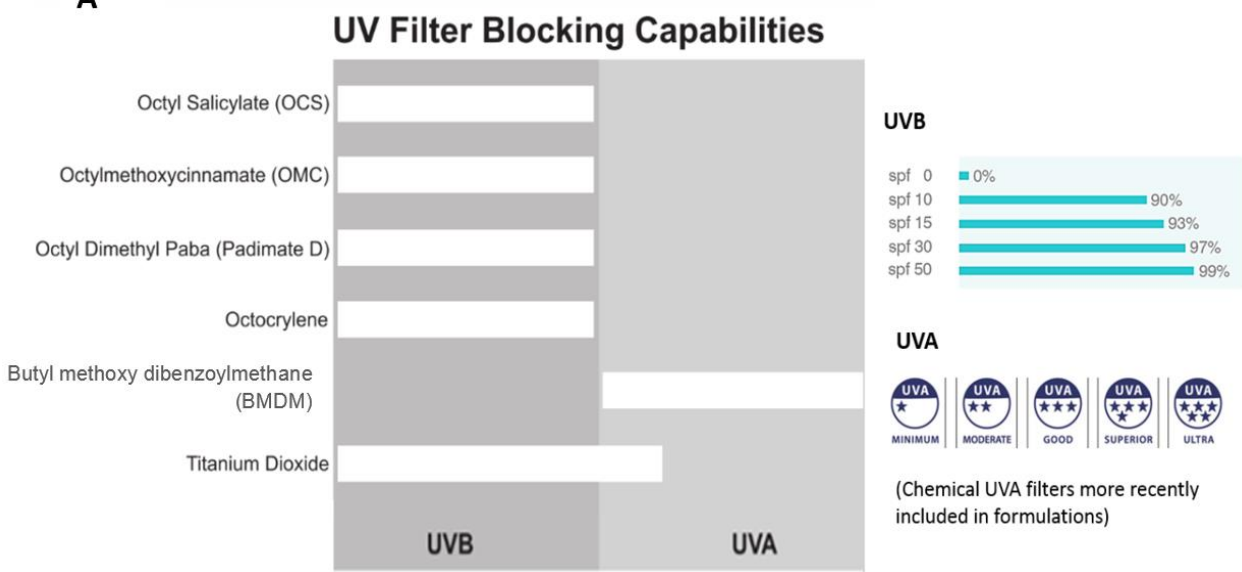
The Fitzpatrick Scale					
					
TYPE I Light, pale white Always burns, never tans	TYPE II White, fair Usually burns, tans with difficulty	TYPE III Medium, white to olive Sometimes mild burn, gradually tans to olive	TYPE IV Olive, moderate brown Rarely burns, tans with ease to a moderate brown	TYPE V Brown, dark brown Very rarely burns, tans very easily	TYPE VI Black, very dark brown to black Never burns, tans very easily, deeply pigmented

Table 3: Fitzpatrick scale of skin types with descriptions. Figure adapted from (Labban et al., 2017)

A



B

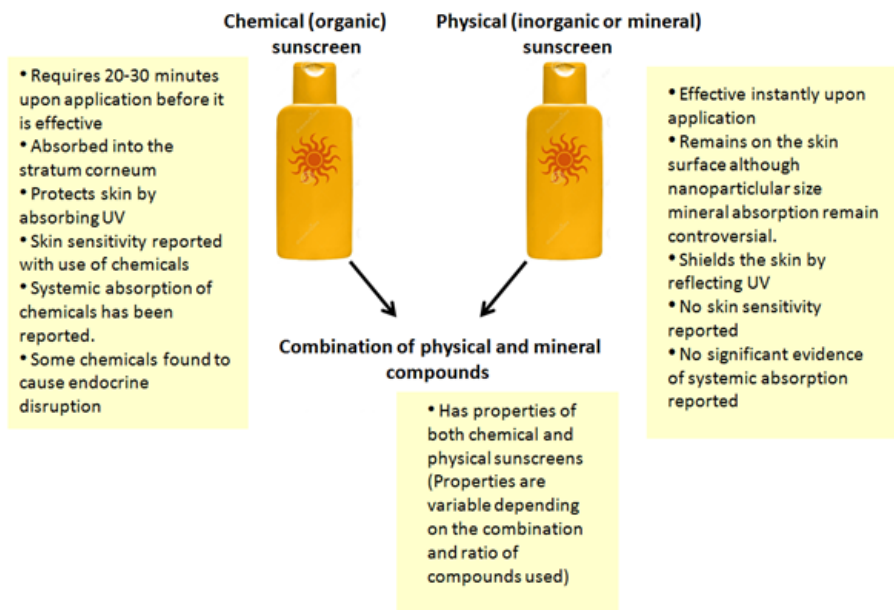


Figure 11: Examples of sunscreen active compounds and protective abilities

Examples of chemical and physical sunscreen actives are shown along with the UVA/UVB blocking efficiency. The UVB (SPF) and UVA protection labelling system is also displayed (A). Illustrates the properties associated with sunscreens containing chemical and/or physical sunscreen actives (B). Information has been adapted from (Latha et al., 2013) and (Skin Cancer Foundation, 2016).

1.8 Sunscreens

Although the sun is vital for life on Earth, prolonged exposure may be damaging to human skin and through the resulting deleterious effects as described previously. It is often advised to seek sun protection by covering the skin with clothing, applying sunscreen and limiting outdoor exposure.

Sunscreens are the most common form of sun protection used in western countries (Maslin, 2014). The active ingredients within the formulations may be categorised as being either chemical/organic (examples of which include PABA derivatives, salicylates, cinnamates, camphor derivatives) or physical/inorganic filters such as TiO_2 and ZnO with many formulations relying on the use of both (Burnett and Wang, 2011; Serpone et al., 2007; Kohl et al., 2011) (Figure 11). An “ideal” sunscreen formulation should provide adequate broad spectrum protection, no sensitisation and remain chemically and physically stable in sunlight (Huncharek and Kupelnick, 2002). Modern day sunscreens use primary (either physical and or chemical compounds) as well as secondary photoprotective substances such as antioxidants, DNA repair enzymes and osmolytes. Secondary photoprotective compounds are added to sunscreen formulations in order to enhance the disruption of the photochemical cascades triggered in skin following UV exposure. Many sunscreen formulations are enhanced with antioxidants such as vitamin C, E and polyphenols to help quench ROS production (Yarosh et al., 1999; Burke, 2011). According to the Environmental Working Group (EWG), chemical sunscreens usually contain filters made up of between two to six active ingredients. This includes ingredients such as avobenzene, oxybenzone, octinoxate, octocrylene, octisalate and homosalate (Gilbert et al., 2013). Despite chemically active compounds being the more widely used form of filter, there have been numerous reports of dermal absorption which has led to skin sensitisation reactions occurring amongst a proportion of consumers (Wong and Orton, 2011). Chemical sunscreens may act as endocrine disruptors and have also been found to be present in human breast milk (Janjua et al., 2008; Krause et al., 2012; Rodríguez et al., 2006). Mineral sunscreens are recommended as an alternative, particularly for sensitive skin types. The most commonly used compounds in mineral sunscreens, ZnO and TiO_2 have so far not been reported to cause contact allergies following application (Jatana and DeLouise, 2014).

The amount of protection offered by a sunscreen formulation against skin burning is measured by an entity known as the sun protection factor (SPF) this is indicative of the protection against UVB. The SPF is defined as the sun UV dose which produces 1 MED following application of sunscreen (2 mg/cm²) divided by the sun UV dose required to produce 1 MED on unprotected skin. A SPF of 10 for instance would filter out 90% of the UVB rays (Marks et al., 1995). However, the UV filtering ability however is non-linear, for example an SPF of 30 filters out 97% and SPF 50 filters 99% of the UVB (Figure 11).

Sunscreen use has also been suggested to have negative effects such as encouraging individuals to stay in the sun for longer periods of time, as the consumer is lead to believe that they are well protected. Furthermore, sunscreens are often not applied to the skin at the recommended amounts with for example body areas being missed. Interestingly, some case-control studies have even reported an increased risk of melanoma with sunscreen use most likely due to the reasons mentioned (Diffey, 2004).

1.9 Nanomaterials

The term nanoparticle has been loosely defined with the definition being ambiguous until more recently in 2011 when the European Commission published a report with the first official definition. This document states that a nanoparticle is “a natural, incidental or manufactured material containing particles, in an unbound state or as an aggregate or as an agglomerate and where, for 50% or more of the particles in the number size distribution, one or more external dimensions is in the size range of 1-100 nm”. Materials with one dimension below 100 nm have been termed as nanosheets, those with two <100nm are known as nanofibres and materials with three dimensions below 100nm are often referred to as nanoparticles (Stankovich, 2007;Teo et al., 2010;Auffan et al., 2009).

Nanomaterials may be synthetic or naturally occurring compounds and are either carbon based or created from metals and metal oxides. They are generally categorised into two main groups, the soluble and/or biodegradable group, and the insoluble group. In the context of

skin care products, soluble nanomaterials disintegrate into their molecular components after being applied on to the skin, examples of these include liposomes and nanoemulsions. Insoluble nanoparticles such as TiO_2 , quantum dots and fullerenes do not disintegrate following application (SCCP, 2013).

Being smaller in size nanomaterials exhibit properties which differ from the material in its original non-nanoform. Such changes in properties are due to the increase in surface area leading to increased reactivity (Figure 12) (Hongbo Shi, 2013b). It has been suggested that compounds in the nano range should be re-subjected to toxicological analysis regardless of the safety data available on the compound in bulk form (Jatana and DeLouise, 2014).

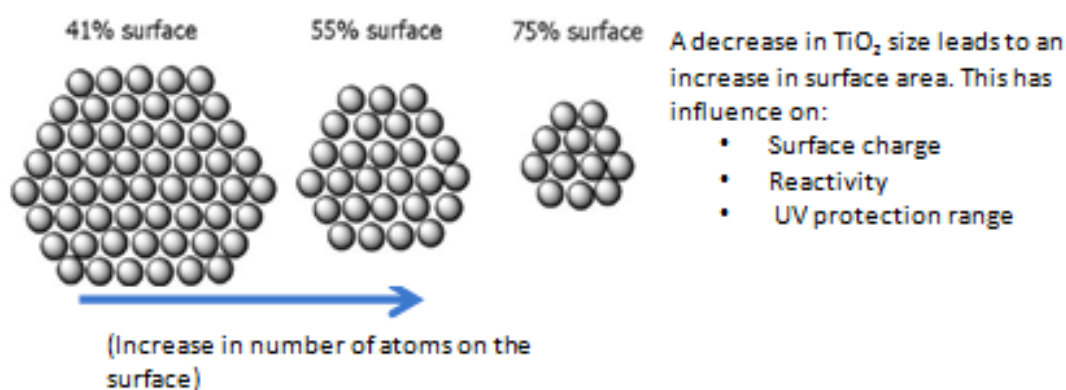


Figure 12: The effect of decreasing particle size on the surface area and properties of TiO_2
Figure adapted from (High School NanoScience, 2017)

1.10 Titanium dioxide (TiO_2)

TiO_2 is also known as titanium (IV) oxide, titanic acid anhydride, titanic anhydride, Ti white or titania. It is often found in a solid white powder form and occurs naturally in the Earth's crust. The average primary particle size ranges from 20-100 nm and is described as being either needle, lanceolate or spherical in shape. TiO_2 is an insoluble molecule which does not dissolve in water or organic solvents (SCCP, 2013). Primary TiO_2 particles often clump together to form

fairly stable agglomerates that are difficult to break apart. Such agglomerates may clump together further to form less stable aggregates (Figure 13). Large aggregates can be broken apart into smaller aggregates or agglomerates with greater ease as they are held together by weak Van Der Waal forces (Wang et al., 2010).

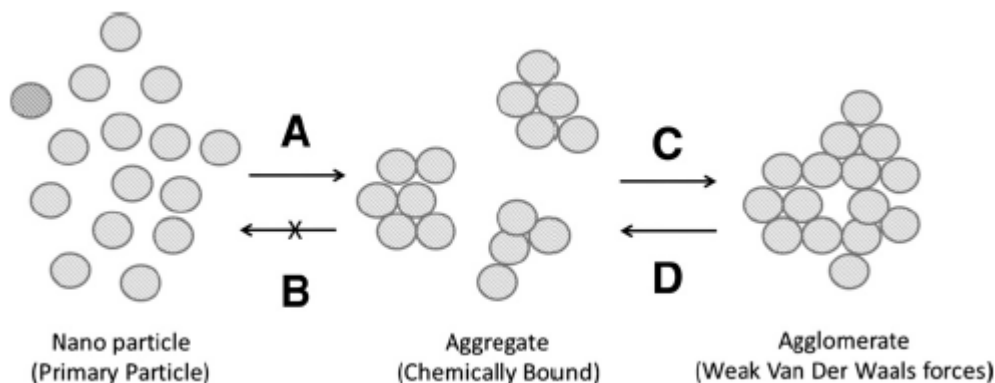


Figure 13: The behaviour of TiO₂ compounds in suspension

Aggregate formation from primary size nanoparticles and further agglomerate formation is shown (Wang et al., 2011)

Due to its useful electrical and optical properties TiO₂ is used extensively in industry for a range of diverse applications. Examples of the many uses of TiO₂ include the white pigment in paint (titanium white or pigment white 6), white food colorant (E171), self-cleaning surfaces, antibacterial materials, paper, plastic, medicines, electronics and personal care products (Jacobs et al., 2010b). As mentioned previously TiO₂ is used as one of the two main mineral or physical compound in sunscreens with the other being ZnO. Within a sunscreen formulation TiO₂ absorbs and to some degree reflects UV rays which may otherwise reach the underlying skin. It exists in one of three main crystalline forms, those being anatase, brookite and rutile. Anatase and rutile are the more commonly used forms in cosmetic products with rutile often being the preferred form as it has been reported to produce up to six times less ROS relative to anatase (SCCP, 2013).

1.10.1 TiO₂ in sunscreens

TiO₂ has been used in sunscreens since 1952 (FDA, 2000). It is known to provide wide spectrum protection against UVB, and to some degree UVA, whilst remaining chemically inert on the skin surface. Despite these benefits, mineral sunscreens containing microform TiO₂ have undesirable aesthetic effects due to their viscosity and white tint appearance (Skocaj et al., 2011).

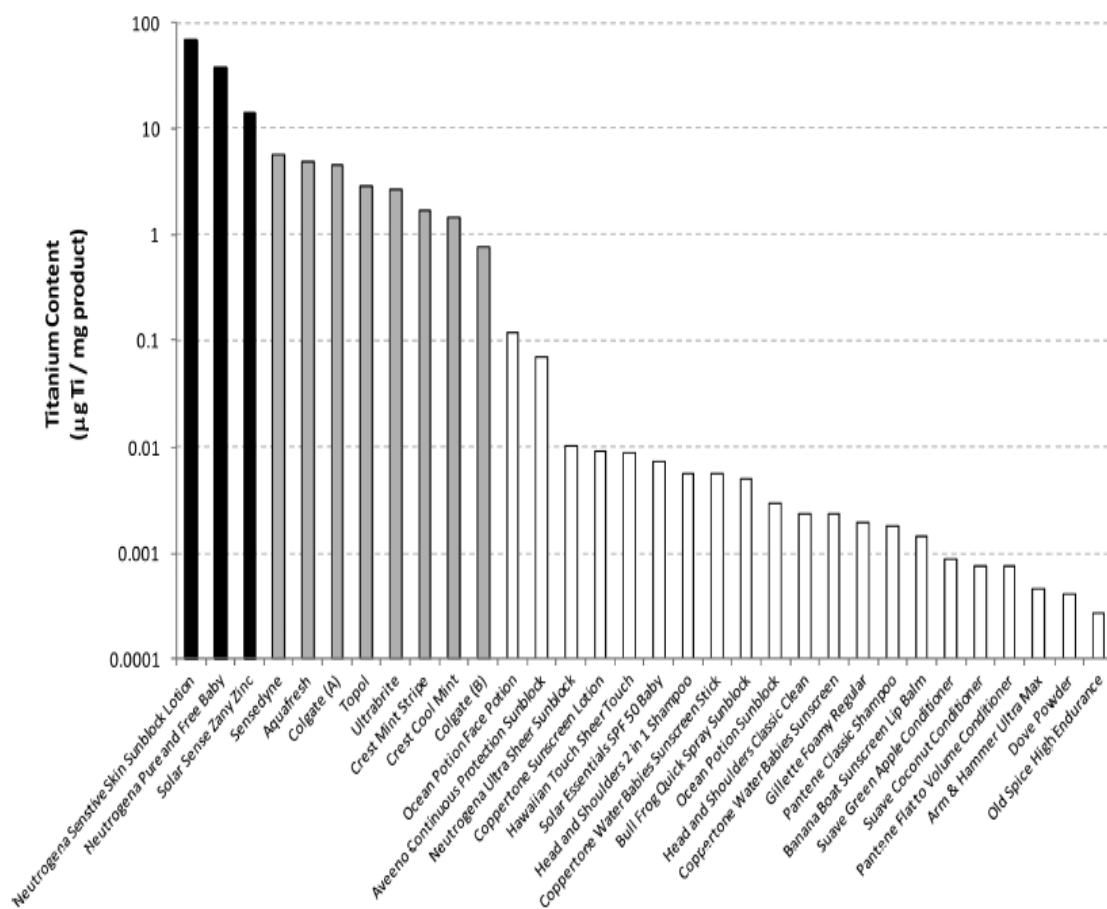


Figure 14: Showing examples of TiO₂ concentrations found in a range of personal care products (Weir et al., 2012a)

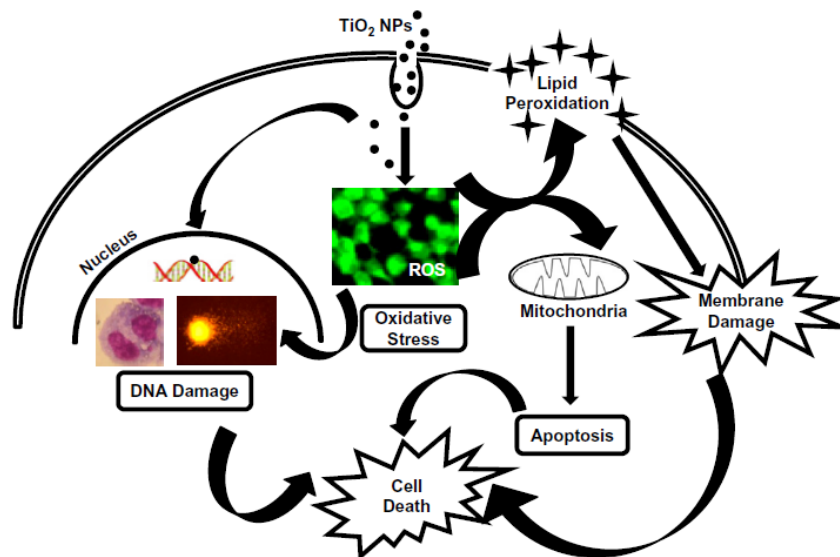


Figure 15: The potential toxicological effect of TiO₂ on cells

If internalised via endocytosis TiO₂ may induce ROS generation. The production of ROS may lead to nDNA damage, mtDNA, membrane damage, and lipid peroxidation along with other oxidative stress signalling responses. Significant amounts of damage may also induce an apoptotic response (Shukla et al., 2011b).

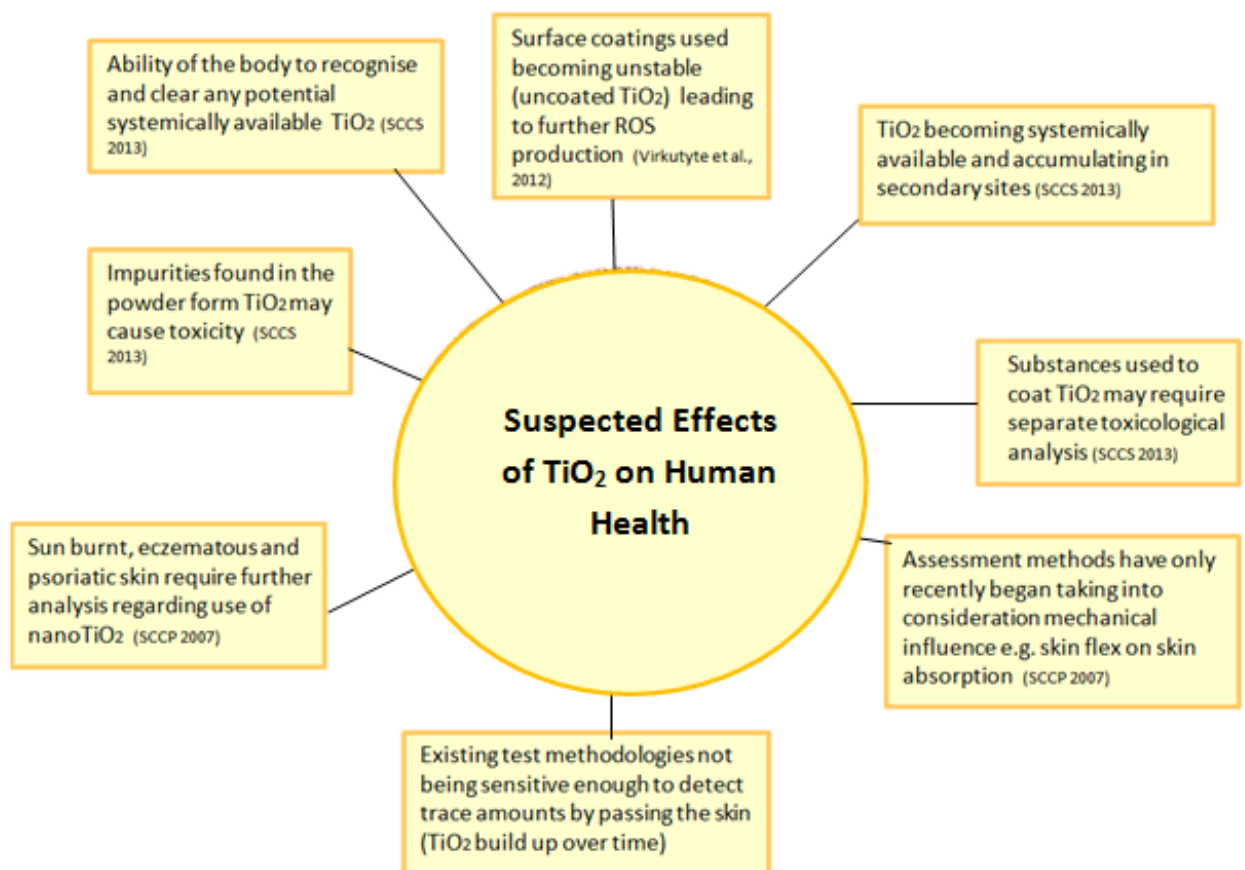


Figure 16: Issues raised regarding the use of nanoparticulate TiO₂

Information has been adapted from (SCCP, 2007a;SCCP, 2013 ;Ölschläger et al., 2009;Virkutyte et al., 2012)

As mentioned previously, VIS has a wavelength of \approx 400- 750nm and mineral particles with a diameter of 200-400 nm scatter VIS leading to a white appearance on the skin. Lack of aesthetic appeal has led to the commercial development of mineral sunscreens containing smaller nano sized TiO_2 particles in the early 1980s. Notably, there was an increase in the use of sunscreens containing nano TiO_2 in the 1990s. Being smaller than the wavelength of light, the particles become invisible to the naked eye when applied to the skin allowing for a transparent appearance. Typically particles with a size of 200nm and over (half the wavelength of light) appear opaque when applied to the skin (Nohynek et al., 2007). Smaller sized TiO_2 particles also give a greater level of SPF protection and a lower level UVA protection, sunscreen formulation manufacturers aim to achieve a balanced formulation (Wang and Tooley, 2011). The average TiO_2 particle size found in nano sunscreens is between 10-100nm with some sunscreens containing particle sizes ranging from 5-500nm. Weir et al., analysed the level of TiO_2 present in personal care products including 13 sunscreens. The authors found 1-10% TiO_2 by weight in samples tested (Figure 14) (Weir et al., 2012b). There have been concerns that if TiO_2 particles were to bypass the skin barrier they may cause deleterious effects in the viable skin layer. Such effects include an increase in oxidative stress, increased mtDNA damaged lipid peroxidation and cell death (Figure 15) (Brausch and Smith, 2009; Maynard, 2008,) Figure 16 illustrates some of the concerns which have been raised regarding the use of nano TiO_2 in sunscreens.

1.10.2 Regulations on nano TiO_2 use in sunscreens

Cosmetic products are highly regulated within the European Union (EU). They are classified as over the counter drugs in the US whilst in the EU they are considered to be cosmetic products (Nohynek et al., 2007). The Scientific Committee on Cosmetic Products and Non-food products intended for Consumers (SCCNFP) first issued an opinion on the safety of TiO_2 use in consumer products in October 2000 whereby it was deemed as safe for use as a UV-filter at a maximum concentration of 25%. Toxicological analysis studies employed however did not consider “nanoparticulate” sized TiO_2 differently to TiO_2 in the micronized form (SCCP, 2013). Materials in their nano form are however known to exhibit changed properties compared to the original parent compound. With this knowledge in mind the Safety of Nanomaterials in cosmetic products (SCCP) issued an opinion in 2007 (SCCP/1147/07) as follows: "The SCCNFP

opinion from 2000 (SCCNFP/0005/98) is on micro-crystalline preparations of TiO₂ and preparations of coarse particles. However, since this opinion, new scientific data on nano sized particles including TiO₂ has become available. Therefore, the SCCP considers it necessary to review the safety of nano sized TiO₂ in the light of recent information. Also, a safety assessment of nano sized TiO₂, taking into account abnormal skin conditions and the possible impact of mechanical effects on skin penetration needs to be undertaken" (SCCP, 2007a). Further to this the EU cosmetic regulation (1223/2009) has stated that from July 2013 all ingredients present as nanomaterials must be labeled on the package with the term 'nano' in brackets (EUCosmeticsLegislation, 2017).

1.10.3 Considerations for nano TiO₂ assessment

Nano materials require further consideration when assessing their toxicity profile compared to compounds in the original parent form. The discrepancy in findings reported within the literature may be due to the use of biochemical assays that can be affected by nano materials themselves (Ong et al., 2014). This has resulted in artefacts and subsequent incongruent estimations of toxicity. Such inconsistent findings make it difficult for regulators to establish guidelines and procedures for the use of nanomaterials.

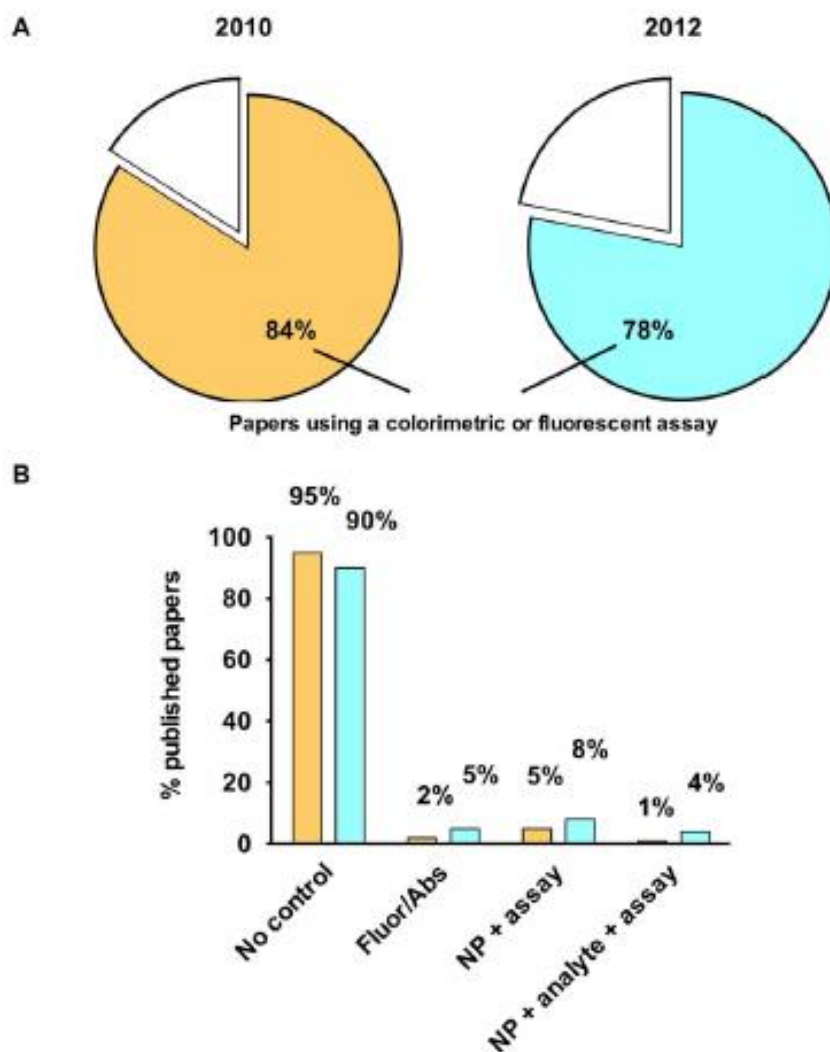


Figure 17: Literature survey showing the percentage of papers assessing nanoparticle interference in spectroscopic based assays in 2010 and 2012

Percentage of published papers that use a toxicity assay based on measurement of colorimetric or fluorescent change in either 2010 or 2012 (A). Showing the breakdown of the controls performed in papers using one of these assays (Note that the percentages do not add up to 100% due to overlap in papers performing more than one control) (B) (Ong et al., 2014).

Due to the unique physicochemical properties and increased reactivity, nanoparticles have a high potential to interfere with spectrophotometric and spectrofluorometric assays. Commonly used tests such as the lactate dehydrogenase (LDH) cytotoxicity assay, alamar blue, and tetrazolium based assays (e.g. MTS and MTT) are frequently reported to be affected by a range of different nanoparticles (Han et al., 2011;MacCormack et al., 2012). Nanoparticles can also bind to dyes (Casey et al., 2008) and proteins (Kane and Stroock, 2007;Stueker et al., 2014;Asuri et al., 2006) potentially altering their structure and/or function as well as leading

to changes in enzyme activity (Stueker et al., 2014;Asuri et al., 2006), fluorescence, and/or the absorbance characteristics of indicator molecules (Hedderman et al., 2004).

A literature survey indicated that 95% of papers from 2010 using biochemical techniques to assess nanotoxicity did not account for the potential interference of nanoparticles, and this number had not substantially improved in 2012 (Figure 17). The top 200 papers were selected from each year after searching for “nanoparticle toxicity assay” using the Google Scholar search engine (Ong et al., 2014). The authors recommend that more stringent controls are required for future studies to minimise the potential for nanoparticle interference and the associated aberrant results. Higher concentrations of nanoparticles (10 mg/l) have a higher chance of interfering with detection assays. The nanoparticle concentration should therefore be limited in the final sample. Ong et al., have suggested that it should be recognised that even with multiple washes and/or centrifugations nanoparticles could remain within cells or bound to membranes (Monteiro-Riviere et al., 2009). Furthermore, centrifugation may be counter productive if nanoparticles have bound to the assay components, as this could lead to the removal of dyes and/or proteins essential for accurate readings (Holder et al., 2012).

The regulatory guidance on the safety assessment of nanomaterials in cosmetics June 2012 has emphasised that optimisation of methodologies used for the assessment of nanoparticles is required. Newer emerging studies on nanotoxicity are beginning to take into consideration further factors such as skin flex and mechanical influences on dermal penetration (SCCP, 2007a). Such models may also be applied for the study of other compounds through skin as flexion is suspected to influence the level of absorption through skin (Gulson et al., 2015) as discussed further in chapter 5.

1.11 Project overview

Skin is the largest organ of the human body and is the first line of defence against external insults. It primarily functions to protect and to allow for a compartmentalised and controlled environment to be maintained within the body. The stratum corneum comprises the outermost layer, which provides the main barrier function through preventing or limiting the permeation and/or penetration of substances (Hongbo Shi, 2013a;Matteo Crosera et al.,

2009). Throughout the human life span skin is exposed to a vast array of stressors, those of which include chemical exposures (both natural and artificial), mechanical stresses and exposure to ionising and non-ionising radiation (Birch-Machin et al., 2013). Being the body's first line of defence, it is crucial to maintain a healthy skin barrier function as disturbances can have multiple deleterious consequences, for example increased water loss and a higher risk of infections.

Attitude towards solar radiation exposure in particular is an area of great public health interest, as the incidence of skin cancer is reported to be on the rise. This along with the increase in life expectancy has raised concerns (Skincancer.org, 2015). Prolonged UV exposure is a major cause of cell damage and as such has a significant effect on the progression of skin cancer and photo damage (Birch-Machin and Swalwell, 2010). It should however be noted that solar light exposure also exhibits beneficial effects when received in moderation.

Given the role of skin as a barrier to topically applied compounds as well as being the main source of vitamin D production, studying UV effects at low levels is important for understanding consequences to human health (Bolzinger et al., 2012; Madan and Levitt, 2014). Currently there is not much known about the interactions of the VIS, IR and UV components of the spectrum. There is also debate as to whether photoprotection in the UV region only is adequate for the prevention of damage in skin (Dupont et al., 2013). The effects of the components of solar light have been explored throughout this thesis with the aim of gaining a further understanding of their biological effects in human skin cell monolayers.

Sunscreen formulations containing mineral active ingredients such as TiO₂ are commonly used to minimise the level of skin damage caused as a result of solar light exposure. As mentioned previously, TiO₂ is a white powder utilised in cosmetic products for its ability to provide wide spectrum protection whilst remaining chemically inert (Nohynek et al., 2007). Investigations of smaller sized particle formulations containing nanoparticulate TiO₂ have recently increased as the larger micronized form has been shown to provide less effective UV protection alongside a poorer aesthetic appearance. Recent research has demonstrated that TiO₂ has particle size dependent photo activity which results in the generation of cell damaging ROS (Shi et al., 2013). Numerous in vivo and in vitro studies have been carried out to assess the

potential adverse effects of nanoparticulate TiO₂ use in cosmetic products. Findings however appear to be controversial and a full picture is yet to be understood (Ilves et al., 2014). A further aim of the work is to provide experimental evidence which would contribute towards the discussion regarding the use of nano sized TiO₂ particles in sunscreen formulations (Teeguarden et al., 2007).

1.12 Overall Aims

The aims of the thesis are as follows:

1. To further investigate the effects of solar radiation exposure on human skin through the measurement of biomarkers of damage.
2. To assess the effectiveness of sunscreen use in reducing the cellular damage response following exposure to solar light.
3. To investigate the apparent concerns regarding the use of nanoparticulate TiO₂ in sunscreen formulations.

Chapter 2-Materials and Methods

2 General methods

The methods presented in this chapter are described as general, and are applicable throughout this thesis. More chapter specific methods are presented within each results chapter as individual methods.

2.1 Cell culture

2.1.1 Primary tissue samples

Human primary skin cells were obtained following the processing of patient samples from the Urology Department at the Newcastle Freeman Hospital. Ethical approval was obtained by the Newcastle University Biobank. After obtaining informed consent, normally discarded healthy adult skin samples from patients undergoing a surgical procedure were used to derive and culture primary keratinocyte and fibroblast cells.

2.1.1.1 Tissue processing

Following surgical removal, surplus skin samples of various sizes (2-4cm²) from patients were placed in 10ml of keratinocyte growth medium (EpiLife) supplemented with 2% penicillin streptomycin amphotericin B (PSA) (Lonza biologics, Slough, UK) and were stored at 4°C for collection. Upon receipt, samples were stored at 4°C and processed on the same day. Prior to processing, skin samples were washed in phosphate buffered saline (PBS) supplemented with 2.5% PSA to remove any residual blood and placed in a petri-dish with PBS to keep moist. Utensils (forceps and scissors), which had previously been baked in an oven at 100°C overnight, were washed in 100% ethanol and flame sterilised. Forceps and scissors were used to remove excess dermal tissue, fat and blood vessels, which were discarded. The remaining sample was firmly scored with a scalpel every 5mm to achieve a “grid” effect allowing penetration of dispase II (Roche Diagnostics Ltd, Burgess Hill, UK). Tissue was added to PBS supplemented with 10% (V/V) PSA and 0.2% dispase II and stored at 4°C overnight. Dispase II is a protease produced in *Bacilluspolymyxa* which hydrolyses the N-terminal peptide bonds of

non-polar amino acid residues, which are found at a high frequency in collagen. This allows the separation of the epidermis from the dermis.

2.1.1.2 Primary keratinocytes

Following an overnight incubation, flamed utensils were used to remove the epidermis which was then placed into a universal containing 0.05% trypsin ethylene diamine tetraacetic acid (TE) (Lonza biologics, Slough, UK). This was incubated in a water bath set at 37°C for 5 min, shaking vigorously half way through to disaggregate keratinocytes. Fetal Calf Serum (FCS) neutralised TE and the sample was centrifuged at 3000g for 5 min to pellet the keratinocytes. The pellet was resuspended in Epilife (Life Technologies, Paisley, UK) supplemented with 1% PSA and 1% Human Keratinocyte Growth Supplement (HKGS) (Life Technologies, Paisley, UK) and placed into a 175cm² tissue culture flask. Culture medium was changed every two days to maximise keratinocyte growth until cells reached approximately 80% confluency. Cells were then passaged as required. All cells used for experiments within this project were passage 1-3. Whilst cells were growing to optimal confluency they were kept in an incubator set at 37°C, 5% carbon dioxide (CO₂) and 95% humidity. Epilife cell culture medium along with HKGS, provide a complete culture environment for primary keratinocytes.

2.1.1.3 Differentiated primary keratinocytes

Keratinocyte cells were grown as described in section 2.1.1.2 however cells were left to reach 100% confluency before carrying out a media change to epilife containing calcium (1.28µl of 1M calcium per ml epilife). After 5 days cells were considered differentiated and were ready for use in further experiments.

2.1.1.4 Primary fibroblasts

Fibroblasts cells were grown from the dermal layer of the peeled skin. Using a scalpel and flamed forceps 5-7 small pieces of dermis (approximately 0.5cm²) were cut and placed into a

new petri dish. Regions on the inside of the 75cm² flask were carefully lightly scored with a scalpel (5-7 cross-hatches). Dermal pieces were placed on top of the cross-hatch in the flask and a small drop of FCS was added on top of each piece of dermis before incubating at 37°C overnight. The following day 10ml complete DMEM (DMEM, FCS and PSA) was added. Complete DMEM media changes were carried out twice a week for two weeks – after week 1 fibroblasts can be seen to migrate out of the dermis. The pieces of dermis were removed on day 14 using a scalpel. The flask was then washed with PBS to remove excess media and 2ml trypsin added to the flask for 3-5 min. Once the fibroblasts were detached 12-15ml of complete DMEM was added and cells incubated at 37°C overnight. The next day the media was removed and 10ml of fresh complete DMEM was added. Cells were grown with media changes every other day until they were approximately 80% confluent, after which they were split into 2 x 175cm² flasks (P1).

2.1.2 HaCaT and HDFn cells lines

The immortalized human skin keratinocyte cell line (HaCaT) (Boukamp.P and Fusenig, 1988) and the human neonatal dermal fibroblast cell line (HDFn) (Invitrogen, UK), were maintained in Dulbecco's modified eagles medium (DMEM; Lonza, UK) containing 10% FCS (Lonza, UK) and penicillin; streptomycin (Lonza; UK), at 37 °C with 5% CO₂. The cells were passaged every 2-3 days (HaCat) or 5-6 days (HDFn), when they reached a confluency of 80-90%.

2.1.3 Long term storage of cells

For long term storage cells were trypsinised before re-suspending in DMEM and centrifuging at 1200 RPM for 5 min. The supernatant was later removed and cells were re-suspended in a solution of 10% dimethylsulphoxide (DMSO) diluted in FCS and transferred to 2 ml cryovials (Helena Biosciences, UK). Cells were then stored at -80 °C for short term and before long term storage in liquid nitrogen.

2.2 Cell viability

For cell viability assays (MTS and Real time-Glo™ (RT-Glo)) cells were seeded into a flat bottom 96 well plate (5×10^3 cells per well) and incubated overnight at 37°C. The culture medium was removed and replaced with the dosing compound in DMEM. Alternatively if cells were to receive a dose of UV, DMEM was replaced with PBS prior to dosing. Control (untreated cells) and blank (containing media only) received phenol red free DMEM alone. The detection and analysis methods on day 2 or 3 (depending on the incubation time of cells with the test compound) is described below for the MTS assay (section 2.2.1). The detection method for the RT-Glo assay is described in section 2.2.2. The data expressed relative to control was assessed in GraphPad Prism 5. Statistical significance was performed using a one-way analysis of variance (ANOVA) with Dunnett's correction, where $P < 0.05$ was considered significantly different from control (untreated). Replicates were averaged and the error bars represent the SEM of 3 independent experiments (unless otherwise stated).

2.2.1 MTS assay

For detection of cell viability using the MTS assay, 20µl of MTS (Promega, UK) was added to each well before being incubated in a humidified incubator (5% CO₂) at 37°C for 4h (in accordance to manufacturer's guidelines). Following incubation, the optical density of each well was measured at 490 nm using a plate reader (SpectraMax 250, Molecular Devices).

2.2.2 RT-Glo

The RT-Glo assay (Promega) involves the addition of NanoLuc® Enzyme (10µl) and MT Cell Viability Substrate (10µl) to each well of the 96 well white clear flat bottom culture plates (Greiner Bio-One) following a 70-90% cell confluence stage. The assay substrates are added at the same time as the dose medium allowing for fluorescence levels, proportional to the level of viable cells, to be monitored in real-time. A fluorometer (Tecan plate reader) was used to

measure the fluorescence levels at a wavelength of 530nm absorbance and emission of 590nm.

2.3 ROS Detection

2.3.1 ROS-Glo assay - cellular ROS generation

Cells were seeded at a density of 5×10^3 cells per well (96 well clear flat bottom white plates) (Greiner-Bio One). Culture media was replaced with 80 μ l PBS the following day. H₂O₂ substrate solution (20 μ l) was added to each well to give a 25 μ M H₂O₂ concentration in PBS. Cells were incubated with the substrate at 37°C for 4 h before the detection solution (50 μ l/well) was added along with 10 μ l/ml of D-cysteine and 10 μ l/ml signal enhancer. The detection solution was incubated for 20 min after which the plate was read using the Glo-Max luminometer with the Cell-titre Glo in built protocol (PMT activated). Menadione (20 μ M) was used as a positive experimental control.

2.3.2 ROS-Glo assay -acellular ROS generation

Experiments were carried acellularly in 96 well (clear flat bottom white plates) as described in section 2.3.1.

2.3.3 DCFDA - cellular ROS generation

Cells were cultured in 96 well (black solid flat bottom plates) (Greiner Bio-one) and dosed with the compound of interest and/or solar light. Following dosing a PBS wash was carried out and 2',7'-dichlorofluorescein diacetate (DCFDA) (10 μ g/ml) in PBS was applied to each well for a 20 min incubation period. DCFDA was removed followed by two PBS wash steps. Wells were later filled with 200 μ l PBS and fluorescence levels measured using the Tecan plate reader at an excitation of 488nm and an emission of 535nm.

2.3.4 DCFDA – acellular ROS generation

Experiments were carried acellularly in 96 well (clear flat bottom white plates) as described in section 2.3.3.

2.4 Real Time-QPCR

QPCR was carried out using the StepOnePlus™ machine (Applied Biosystems). Samples from each experiment were performed in triplicate for each condition. A positive control of known cycle threshold (CT) value was included with each reaction along with a negative control containing master mix only. Analysis was carried out using the StepOnePlus™ v2.3 software. The CT was manually adjusted to the linear range. The correct product sizes were assessed using the melt curve analysis.

2.4.1 Cell treatment

Cells were seeded in 60mm dishes at a density of 250,000 cells/dish. When at the required confluency cells were washed with PBS and irradiated in PBS. PBS was then replaced with 500µl trypsin for approx. 3 min after which cells were scraped, transferred to an eppendorf tube and spun at 1200rpm for 5 min. The supernatant was removed and the pellet was either frozen at -20°C or processed for DNA extraction (section 2.4.2).

2.4.2 DNA extraction and NanoDrop measurements

DNA extraction was carried out using a commercially available QiaAmp DNA mini kit (Qiagen). The cell pellet was resuspended in PBS to a final volume of 200µL. Proteinase K (20µl) along with Buffer AL (200µ) were added before pulse-vortexing for 15 sec and incubating at 56°C for 10 min on a heat block. Following incubation, 200µl ethanol (100%) was added and the sample pulse vortexed for 15 sec. The samples were transferred to a QIAamp Mini spin column and centrifuged at 8000 rpm for 1 min. The spin column was placed in a clean collection tube and the tube containing the filtrate was discarded. Buffer AW1 (500µl) was added and samples centrifuged at 8000 rpm for 1 minute. The spin column was placed in a clean collection tube

and the tube containing the filtrate discarded before adding Buffer AW2 (500µl) and centrifuging at 14,000 rpm for 3 min. The spin column was placed in a sterile eppendorf and the old collection tube containing the filtrate was discarded. The spin column was centrifuged at 14,000 rpm for 1 min and the collection tube containing any remaining filtrate discarded. DNA was eluted from the spin column by adding between 50-150µl Buffer AE (depending on the sample size) and incubating the samples at room temperature (RT) for 1 min. Centrifugation 8000 rpm for 1 min was carried out to elute the DNA and the spin column discarded.

The total DNA content in each sample was analysed using the NanoDrop ND-1000 spectrophotometer (Thermo Scientific). A volume of 1.5µl Buffer AE was used as a blank control. The blank was then removed using tissue lens and 1.5µl of each sample was assessed relative to the Buffer AE blank control. DNA quality was assessed based on the 260/280 and 260/230 NanoDrop absorbance ratio readings.

2.4.3 83bp mtDNA fragment QPCR analysis - mtDNA copy number

The mtDNA content was investigated using QPCR amplification of an 83bp section of the mitochondrial genome (Figure 18). QPCR was performed in 23 µl reactions containing 2µl of 5ng DNA sample (10ng total), 1µl of each primer, 12.5µl SYBR® Green JumpStart™ Taq Ready Mix™ and 8.5µl high grade PCR water. The primers used are in accordance with previously used sequences (Koch et al., 2001) (Table 4). The cycling conditions are displayed in Table 5. Analysis was performed on the StepOne PCR machine (Applied Biosystems, UK).

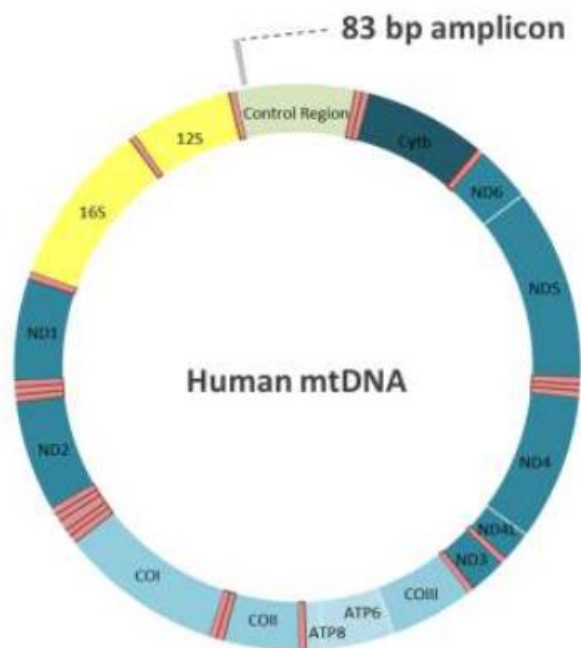


Figure 18: Location of the amplified 83bp region in the mtDNA genome (Koch et al., 2001).

Primer	Sequence	Size (bp)	Template
IS1 F	GAT TTG GGT ACC ACC CAA GTA TTG	83	16042-16124
IS2 R	AAT ATT CAT GGT GGC TGG CAG TA		

Table 4: Primer sequences for the 83bp fragment QPCR assay.

The primer sets specific for human mtDNA, with product sizes of 83bp are displayed. The base sequences from 5' to 3' are shown for the forward (F) and reverse (R) primers, as well as the exact product length (bp), and the nucleotide numbers (bp) which give the positions of the products to be amplified within the mtDNA.

Cycles	Temperature	Time
40	95°C	15 sec
40	60°C	1 min

Table 5: Cycling conditions used for the 83bp QPCR assay

2.4.4 1Kb mtDNA fragment QPCR analysis

The 1kb region QPCR reactions (Figure 19) were performed in 20 μ l reactions containing: 4 μ l of 3ng DNA sample, 0.5 μ l of each of the primer pairs (10 μ M), 5 μ l PCR grade water and 10 μ l of 2X sensiMix SYBR Hi-ROS Reagent (Bioline). The primer nucleotide sequences are in accordance with sequences described previously (Rothfuss et al., 2010) (Table 6). The cycling conditions are shown in Table 7

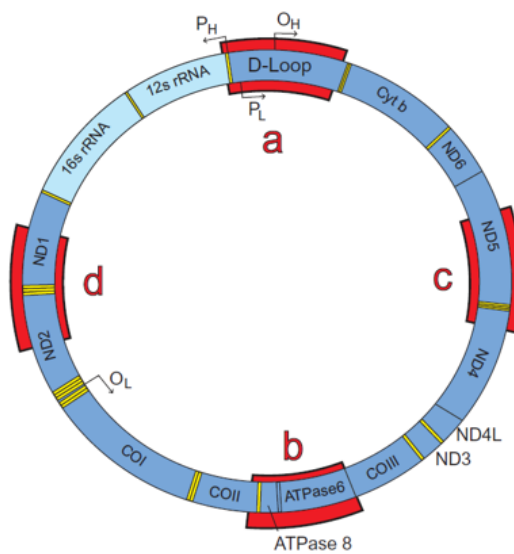


Figure 19: Schematic diagram showing the position of the 1Kb QPCR fragment primer pairs along the mtDNA. The four selected 1kb sized regions are shown as red sectors a–d. mtDNA position: chrM:16021+423 (a), chrM:8204+9203 (b), chrM:12050+13049 (c) and chrM:3962+4998 (d) (Rothfuss et al., 2010).

Primer	Sequence	Size (bp)	Template
AL4.F	CTGTTCTTTCATGGGGAAGC	972	chrM:16021 + 423
AS1.R	AAAGTGCATACCGCCAAAAG		
BL1.F	CATGCCCATCGTCCTAGAAT	1000	chrM:8204 + 9203
BL1.R	TGTTGTCGTGCAGGTAGAGG		
CL1.F	CACACGAGAAAACACCCTCA	1000	chrM:12050 + 13049
CL1.R	CTATGGCTGAGGGGAGTCAG		
DL1.F	CCCTTCGCCCTATTCTTCAT	1037	chrM:3962 + 4998
DL1.R	GCGTAGCTGGGTTTGGTTTA		

Table 6: Primer sequences for the 1Kb fragment QPCR assay

Cycles	Temperature	Time
1	95°C	10 min
40	95°C	15sec
	60°C	15sec
	72°C	55sec

Table 7: Cycling conditions for the 1kb QPCR assay

2.4.5 11Kb mtDNA fragment QPCR analysis

The 11Kb region QPCR reactions (Figure 20) were performed in 20µl reactions containing: 12.5µl PCR grade water, 2µl of Expand Long Template Buffer 2, with 27.5nM MgCl² (10x concentrated), 1µl PCR nucleotide mix (10nm dATP, dCTP, dGTP and dTT), 0.6µl of each primer, SYBR Green (5x concentrated; Tris-EDTA pH 8 diluent) ROX passive reference dye (50x

concentrated), Expand Long Template Enzyme Mix and 2µl of DNA (6ng/µl) The primer pair sequences were designed as described previously (Kleinle et al., 1997) (Table 8).Cycling conditions are displayed in Table 9.

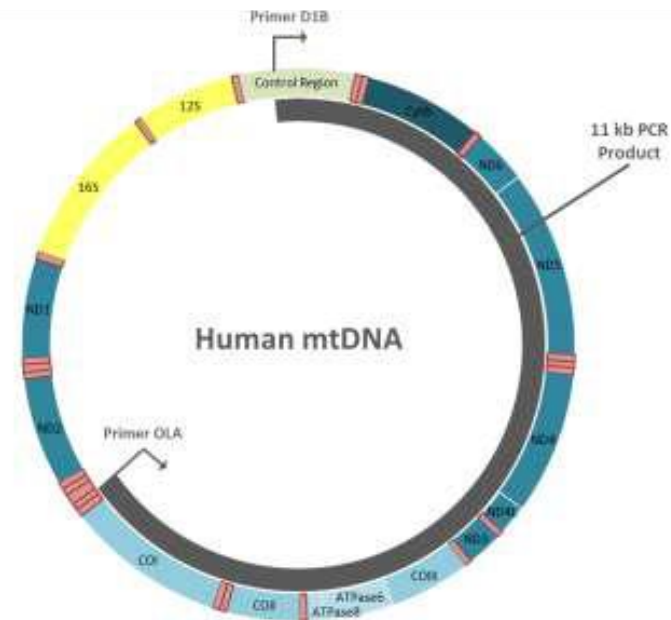


Figure 20: Positioning of the amplified 11Kb section along the mtDNA genome.

Primer	Sequence	Size (bp)	Template
D1B F	5'-ATG ATG TCT GTG TGG AAA GTG GCT GTG C-3'	11kb	(282-255)
OLA R	5'-GGG AGA AGC CCC GGC AGG TTT GAA GC-3'		(5756-5781)

Table 8: Primer pair sequences for the 11Kb fragment QPCR assay

Cycles	Temperature	Time	Notes
1	94°C	2 min	Polymerase activation
10	94°C	15sec	Denaturation
	60°C	30sec	Annealing
	72°C	9min	Extension
25	94°C	15sec	Denaturation
	60°C	30sec	Annealing
	68°C	8.5min (+10seconds per cycle)	Extension

Table 9: Cycling conditions for the 11Kb QPCR assay

2.5 Comet Assay

2.5.1 Cell treatment and harvesting

Cells were seeded (75,000 cells/per well) in a 24 well (clear flat bottom plate) overnight at 37°C. For HDFn and primary fibroblasts, complete DMEM was used. EpiLife plus HGKS was used for primary keratinocyte cells. For H₂O₂ control experiments cells were washed with PBS and treated with H₂O₂ diluted in serum free DMEM (HDFn and primary fibroblast cells) or HGKS free EpiLife media (primary keratinocytes) and cells harvested immediately. For TiO₂ treatments cells were washed with PBS prior to dosing with TiO₂ in complete DMEM and incubating for a 24h time period at 37°C. Following treatment cells were washed twice with PBS, trypsinised (100µl) and neutralised with 100µl complete DMEM. DNA damage was assessed in each sample using the comet assay, in accordance with the method of (Singh et al., 1988).

2.5.2 Slide and buffer preparation

Frosted microscope slides were pre-coated with 500µl of low melting point agarose (LMPA) (Scientific Laboratory Supplies, UK) (1% w/v in PBS) and allowed to dry at RT overnight. Slides were pre-cooled at 4°C before use with all procedures being carried out under red light. LMPA (1% w/v in PBS) (70µl) and harvested cells (70µl) were mixed before being added to the glass slides and covered with a cover slips. Once dry, the cover slips were gently removed and the

slides immersed in lysis buffer (2.5 M NaCl, 100mM EDTA pH 8, 10mM Tris pH 10, 1% Triton X-100 and 1% DMSO) the latter two reagents were added to the buffer prior to immediate use). Following cell lysis at 4°C (1h) slides were washed for 15 min in PBS before being transferred into an electrophoresis tank filled with chilled Alkali buffer (300mM NaOH, 200mM EDTA pH 8) and left for 30 min. After this time period, an electric current was applied (22 V; 0.5-0.7mA) for 30 min, after which the slides were removed, immersed in neutralising buffer (0.5 M Tris, pH 7.5) for 15 min and immediately washed in PBS.

2.5.3 Staining, visualisation and analysis

Following the final PBS wash, 500µl of SYBR Gold (Invitrogen, UK) (1:10,000 in Tris -EDTA buffer, pH 7.5 (10mM Tris and 1mM EDTA) was added to each slide. Slides were then left to dry (uncovered at RT) in the dark room overnight. Once dry, the slides were then rehydrated with distilled water and observed using a fluorescent microscope. Nucleoids were analysed using Comet assay IV software (Perceptive instruments, UK) in order to determine the mean tail length of each treatment. One hundred nucleotides chosen at random were measured per slide.

2.5.4 Enzyme modified comet assay (hOGG1)

Following the lysis step (2.5.2) 1µl hOGG1 enzyme (Trevigen) and 75µl reaction buffer was made up on ice. The enzyme mix (75 µl) was added to each sample area and slides placed in a humidity chamber before being incubated at 37°C for 30 min.

2.6 Sunscreen protective effect against solar light

Creams containing SPF were assessed, as well as a sham cream containing no SPF protection. Transpore Clear tape (3M, UK) was used as a surface to which cream was applied. A 5 cm² section of Transpore tape was adhered to the top of a cell Petri dish with lid removed. The cream was weighed for the required amount to cover a surface area. A concentration of

2 mg/cm² cream was applied to the top of the tape by finger using a disposable nitrile powder-free glove. Following irradiation with the relevant irradiation source, cells were collected and the total DNA was extracted. A 1kb QPCR assay was performed as described in section 2.4.4 to determine the level of mtDNA damage.

2.7 Solar light sources

2.7.1 Solar Simulator

Calibration of the Solar Simulator, accompanying filters and the Hydrosun lamp was carried out by the Newcastle Regional Medical Physics Department. A Newport solar simulator (Class ABA) containing a xenon arc lamp was used to provide controlled illumination approximating natural sunlight. According to the manufacturers the ABA system provides the highest spectral match performance (Class A) as defined by the most recent standards from the IEC, JIS and ASTM. The uniformity is Class B (based on the IEC testing protocols). The device uses a xenon lamp with associated optics designed to give a uniform downwardly directed beam. In particular this device is intended to be spectrally compliant with the COLIPA irradiance response curve with a specified time of 59s as the typical time to reach 1SED (=10mJ/cm² weighted) at maximum output power. The spectral irradiance and weighted irradiances of the Newport device were verified at the standard treatment distance. Three set-ups were tested – one being the standard (with only IR heat filter in place), the other with an additional UVB filter in place, the third with a sheet of window glass covering the detector (this is the same sheet that is currently used to filter the cell-solarium). The local broadband meter was calibrated on the basis of measurements made.

The photo-sensor contained within the monochromator was cooled to 15°C using a thermoelectric cooling device (Peltier cooling) and the input optic to the device was aligned with the treatment axis of the lamp and at the usual treatment distance (5mm from bench level). In order to do this the illuminating device was turned so that it no longer illuminated the bench and the input optic to the BENTHAM DMc150 could be positioned at the

appropriate point. Following initial warm up of the illuminator, a spectrum was acquired at a 1nm resolution from 250-320nm. Spectra were also acquired with the UVB filter in place (at two slightly different treatment distances) and with the window glass in place. At each part of the spectrum a sensitivity factor was applied resulting in a measure of absolute spectral irradiance in $\text{mW}/\text{cm}^2/\text{nm}$. Additional corrections were also made to determine a weighted irradiance according to CIE standard CIE S 007/E-1998 "Erythema Reference Action Spectrum and Standard Erythema Dose". Following this the NEWPORT device was returned to its normal orientation and stable readings taken using the local broadband meter with the sensor placed at bench level.

2.7.2 Hydrosun lamp

The Hydrosun® Irradiator 750 lamp reproduces a combination of the sun and the humid atmosphere. The emission lies in the IRA with wavelengths from 780 to 1400nm. The water filtering system prevents overheating effects. The energy output is measured prior to performing dosing experiments using a hand held hydrosun meter from which the dosing time is calculated. Water-filtered IRA is produced by special radiators, whose full spectrum of radiation of a halogen bulb is passed through a cuvette containing water, which absorbs or decreases the described undesired wavelengths of the IR (Hoffmann, 2009).

2.8 Filters

Bandpass filters allow all the light between the specified wavelengths to pass through whilst cut-off filters allow for the passage of all the light above the specified wavelength (Christiano and Fitzgerald, 2003).

2.8.1 IR/VIS Filter

The IR/VIS filter (UG11 Glass-Type) was purchased from UQG optics. This bandpass filter allows access of UV whilst blocking the IR and VIS regions as shown in Figure 18.

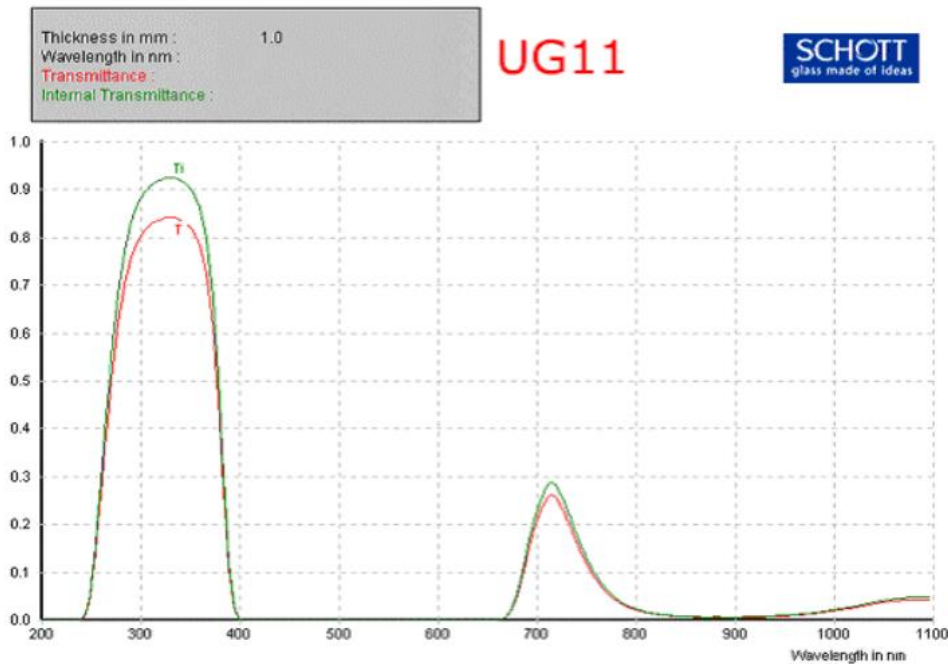


Figure 21: Schott UG-11 bandpass optical glass filter UV transmitting filter

Schott UG11 transmission data of linear internal transmittance spectral response curve and technical data. The filter transmits wavelengths between 250-400nm and a fraction of the wavelengths between approximately 670-800nm

2.8.2 IR and UV cut off filters

The IR cut-off and UV blocking filters used for the experiments were purchased from UQC Optics (Cambridge, UK). The IR cut-off filter allows for the simultaneous passage of UV and VIS (Figure 22) whilst the UV filter allows for a combination of IR and VIS to pass through (Figure 23). When both filters are overlaid and used in combination they allow for the passage of VIS wavelengths. A hand held radiophotometer was used to monitor the output from the UV sources.

IR CUT OFF FILTERS

MATERIAL: Float Glass Coated IRC-09
VIS. Transmission 420-620nm $T_{min} > 80\%$. $T_{avg} > 85\%$
SPECTRAL DATA: IR Reflection: 700-1000nm $T_{max} < 3\%$ 1000-1100nm $T_{max} < 5\%$
T50% at $645 \pm 10\text{nm}$
Broadband AR Coated both sides

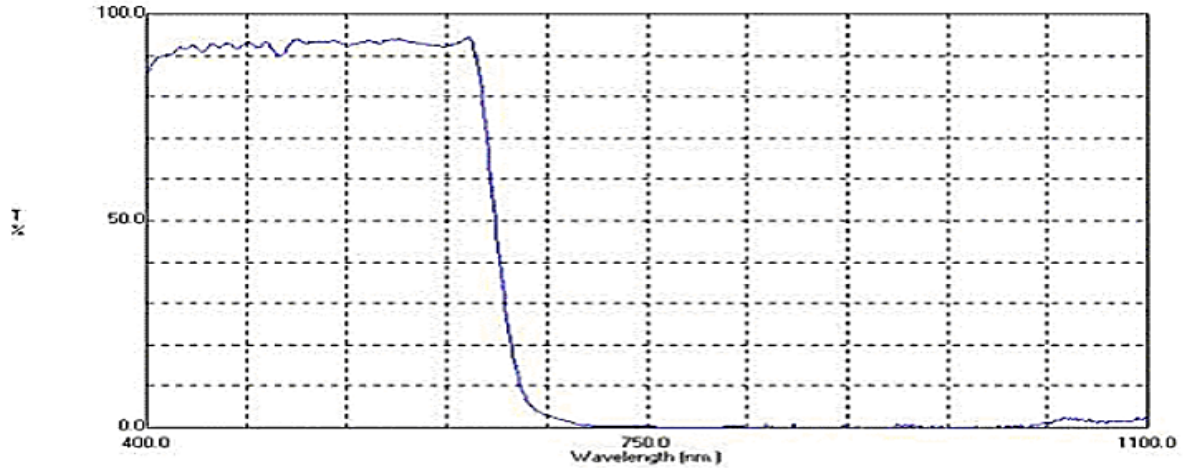


Figure 22: Showing spectral data for IR cut off filter
The filter is designed to block wavelengths of light beyond approximately 700nm

UV BLOCKING FILTERS

MATERIAL: Borosilicate "Borofloat" Dielectric Coated
VIS. Transmission 440-690nm avg $> 97\%$
UV Reflection: 300-400nm avg $< 1\%$
SPECTRAL DATA: Transmission 50% @ $410\text{nm} \pm 5\text{nm}$
AR Coated Both Sides

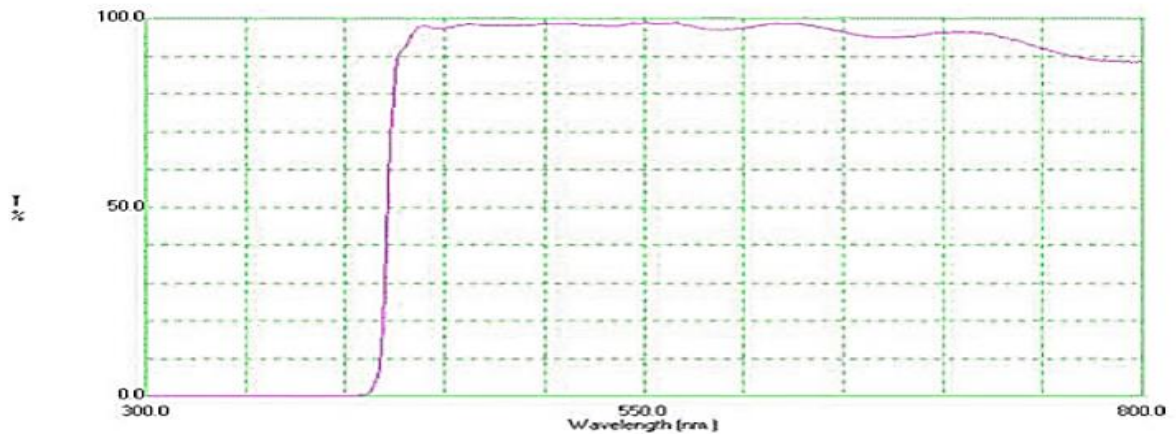


Figure 23: Showing spectral data for the UV blocking filter
The filter is designed to block wavelengths of light below approximately 400nm

2.8.3 Glass and plastic (UVB blocking) filters

Window glass and a plastic UVB filter were used to block the UVB component of complete solar light. In doing so the filters also reduce the level of UVA by 51% (glass) and 88% (plastic) whilst allowing for VIS and IR to pass through. Figure 24 shows a schematic diagram of the wavelengths passing through following the application of the filters (IR/VIS, IR, UV, IR+VIS, glass and plastic filters).

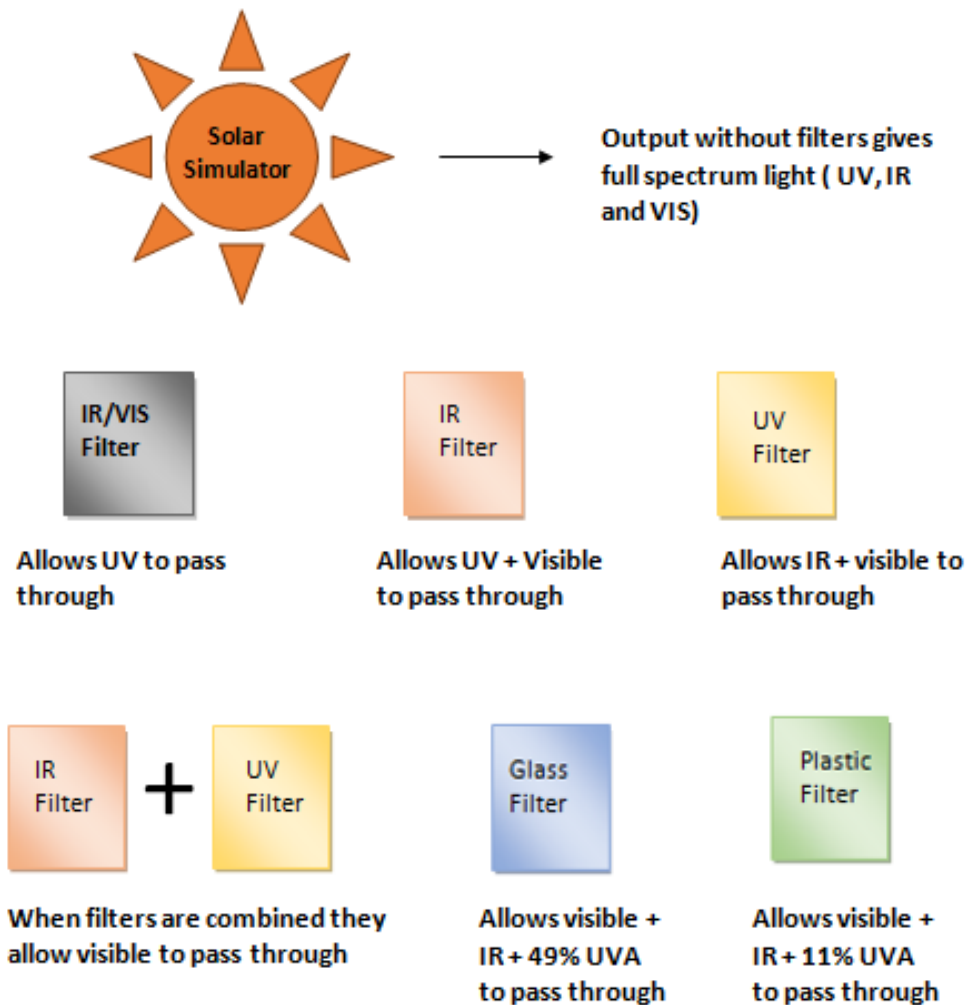


Figure 24: Output of solar simulated light following the application of the various filters

2.9 Calibration of UV Lamps

Calibration of the UV sources was carried out by the Regional Medical Physics Department. The spectral irradiance was measured for the following fluorescent lamps used in this thesis:

Philips TL 20W/01 RS (TL01), Helarium B1-12-40W (Arimed B), Waldmann F85/100W-UV6 (UV6), iSOLde Cleo performance 100W-R with a glass filter (Cleo + Filter). Measurements were taken at approximately 20 cm from the midpoint of a solarium containing four of each lamp and were taken from 250 to 400nm in steps of 1nm with a portable spectroradiometer (Bentham Instruments Ltd, Reading; model DMc150FC).

The monochromator was fixed with a bandwidth of 1nm and the wavelength calibration was achieved using a low-pressure mercury discharge lamp (253.7nm and 435.8 nm). Prior to calibration a spectral sensitivity calibration of the instrument was determined by reference to a calibrated deuterium spectral irradiance standard (National Physical Laboratory, UK (NPL 2003 irradiance scale). The input optic for two other meters (to be used to measure irradiance on a daily basis) was placed as close as possible to the input of the spectroradiometer and the reading on each radiometer was noted at the midpoint of the spectroradiometer scan. Correction factors were applied so the correct irradiance could be measured for the various meter/lamp combinations. Total UV (UVA, UVB and UVC) was calculated by integrating the spectral irradiance curve and the erythemally weighted irradiance was calculated by combining the spectral irradiance with the erythema action spectrum (CIE standard CIE S 007/E – 1998. Erythema Reference Action Spectra and Standard Erythema Dose). Prior to dosing experiments a hand held radiometer was used to monitor the output and calculate the required dose.

Summary results- UV6			Summary results - TL01			Summary results -Cleo + Glass			Summary results- Arimed B		
Irradiance	(mw / cm2)	%	Irradiance	(mw / cm2)	%	Irradiance	(mw / cm2)	%	Irradiance	(mw / cm2)	%
Total UV	1.453		Total UV	5.597		Total UV	4.900		Total UV	5.157	
UVC (250-280)	0.001	0.0	UVC (250-280)	0.001	0.0	UVC (250-280)	0.000	0.0	UVC (250-280)	0.000	0.0
UVB (280-315)	0.542	37.3	UVB (280-315)	4.386	78.4	UVB (280-315)	0.000	0.0	UVB (280-315)	0.196	3.8
UVB (290-320)	0.694	47.8	UVB (290-320)			UVB (290-320)	0.001	0.0	UVB (280-315)	0.196	3.8
UVA (315-400)	0.910	62.6	UVA (315-400)	1.210	21.6	UVA (315-400)	4.900	100.0	UVA (315-400)	4.960	96.2
Weighted	0.186		Weighted	0.323		Weighted	0.003		Weighted	0.029	
SED / min	1.116		SED / min	1.940		SED / min	0.016		SED / min	0.173	

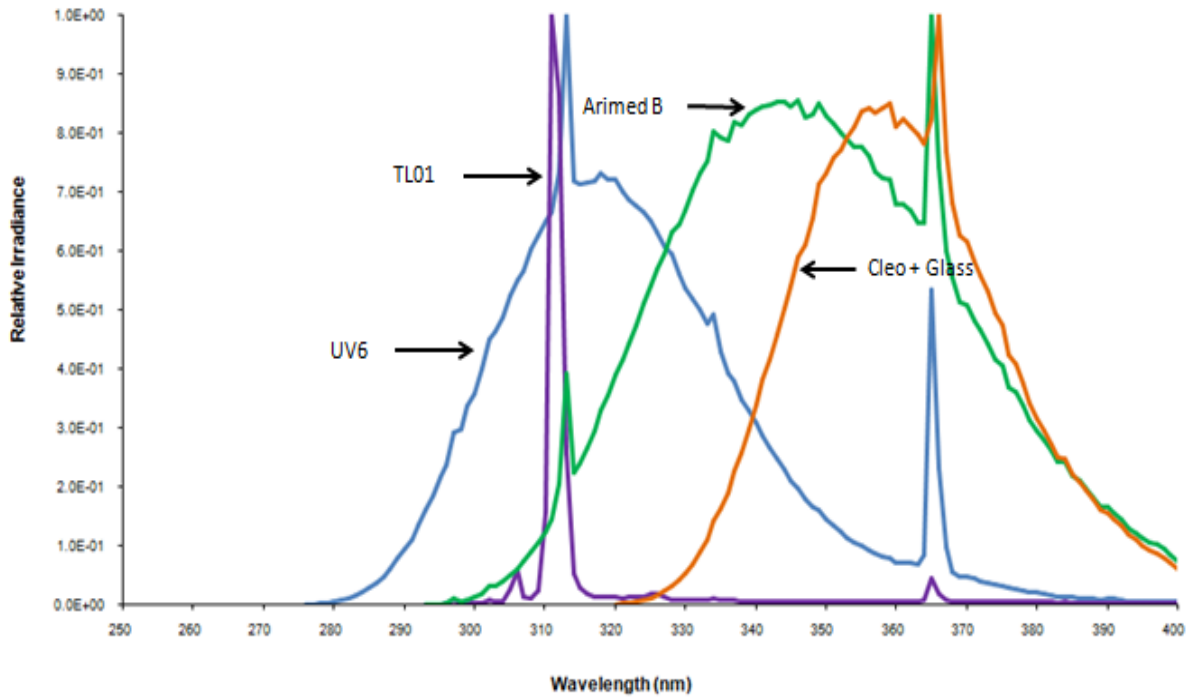


Figure 25: The irradiance data of the UV6, TL01, Arimed B and Cleo + glass lamps

This figure has been adapted from data obtained previously in the lab by Dr Jenifer Latimer and Dr James Lloyd

Chapter 3 – Solar Radiation Exposure

Effects on Human Skin

3 Chapter Overview

Solar radiation exposure from both natural and artificial sources is a fundamental area of public health interest. Our further understanding of the field of photobiology over the years has influenced the current advice available on sun exposure and protective strategies (Barolet et al., 2016a; Diffey and Cadars, 2016). This chapter focuses on the response of donor matched skin cells (primary fibroblast, keratinocyte, and differentiated keratinocyte cells) following exposure to solar radiation. Established cell line models (HDFn and HaCat cells) were also employed during further investigations.

The deleterious effects of UV have been well documented in the literature (Meinke et al., 2013). UV is known to have the ability to induce nDNA and mtDNA damage both directly via the absorption of UVB by DNA bases and indirectly via UVA mediated ROS generation (Brugè et al., 2014). As mentioned earlier in chapter 1, although UV is the more energetic wavelength it makes up approximately 7% of the solar spectrum (Birch-Machin et al., 2013a). The remaining portion consists of the longer wavelength IR and VIS bands, both of which have received less scientific attention until more recently (Diffey and Cadars, 2016). IR has been found to exhibit various biological effects, most notably the increase in MMP mRNA and protein expression levels eventually contributing to the ageing phenotype observed in skin (Barolet et al., 2016a). The effects reported in the literature do however seem to be variable depending on the dose and pattern of IR application as reviewed by Akhalaya et al., 2014. Similarly, the skins response to VIS is less well established. Recent evidence has suggested involvement of VIS in ROS generation as well as the skin tanning process particularly in darker skin types (Mahmoud et al., 2010). Depending on the geographical location and seasonal changes, members of the general population may be exposed to varying levels and intensities of solar radiation. Nevertheless the cumulative exposures and the behavioural attitudes towards solar light contribute to the overall health and appearance of skin over time (Dupont et al., 2013). Due to the named variables which exist (geographical location and attitudes towards solar exposure) the level of solar light received is not well defined (Sklar et al., 2013). Physiologically relevant doses of solar light components, in particular IR, have therefore been theorised in the literature (Diffey and Cadars, 2016; Sklar et al., 2013).

Work involving exposure to physiologically relevant doses of UV, IR and VIS is required in order to better understand the potential damaging effects of solar radiation on human skin. The interaction of all three components (UV, IR and VIS) as well as the effects of combinations of the wavebands warrants further investigation as currently little is known about this (Sklar et al., 2013). This chapter aims to assess the effects of the components of solar radiation on human skin cells. Furthermore, keratinocyte and fibroblast cells were compared for potential differences in response to solar light. Comparisons were also made between the cell line and primary cell data obtained.

The experimental model involved using skin cells cultured in monolayer. Controlled doses of solar light were applied, specifically a dose of 0.54 SED and 2.16 SED were used for experiments involving primary cells. Higher doses of solar light were used to investigate the effects in cell line. This was carried out to ensure that any biological effects observed were consistent over a range of higher doses and to assess whether a dose dependent response is present. Immediately following irradiation cells were assessed for biomarkers of damage. ROS generation was tested using the ROS-Glo and DCFDA methods as ROS is a well-established biomarker of cellular stress (Frijhoff et al., 2015). Further to this the level of mtDNA damage was assessed through a QPCR method using an 11kb fragment template. This method of damage detection has been developed in the lab and is used routinely for analysis. The level of mtDNA damage is a reliable biomarker of stress due to its close proximity to the main site of ROS generation (Birch-Machin et al., 2013a). The nDNA damage levels were also investigated in primary skin cells using the comet assay to measure double strand breaks as a further marker of solar light induced stress.

3.1 Chapter aims:

- Assess the radiation sources used for cellular dosing experiments with the aim of minimising any confounding factors such as heating effects and inaccurate inclusion/exclusion of wavelengths within the dose.
- Assess the sensitivity of the detection assays employed.
- Identify potential cytotoxic effects that may arise due to the doses of solar light used.
- Investigate the contribution of IR, UV and VIS on the level of cellular stress induction (ROS, mtDNA and nDNA damage) in skin cells following exposure to solar light.
- Assess the effect of priming cells with either IR or UV on cellular stress response
- Compare the response of dermal and epidermal cells to solar radiation both in primary and cell line cultures.

3.2 Chapter specific methods

Details of the methods used including cell culture techniques, cell viability, ROS generation (DCFDA and ROS-Glo method), solar light filters and calibration as well as the monitoring of temperature changes under the solar light source can be found in the general methods section (Chapter 2). The QPCR assay employing both the 83bp and 11kb fragment templates is also described in the general methods section along with details of the comet assay.

3.3 Results

3.3.1 Background data

Initial investigations into the effects of solar light on skin cells were carried out in the lab in collaboration with Croda International Plc (a global speciality chemicals company). Primary skin cells were either given a dose of complete solar light (UV, IR and VIS) or solar UV. Established biomarkers of damage were utilised to quantify the levels of cellular stress and damage inflicted by each of the dosing conditions described. The ROS-Glo assay that was used for investigating ROS levels assesses the amount of H₂O₂ generation. H₂O₂ is relatively more

stable when compared to other ROS species as it has the longest half-life, furthermore, many other ROS species are converted to H₂O₂, therefore it is thought to be a more reliable detection method (Alfadda and Sallam, 2012;Newsholme et al., 2012). Data for the ROS generation and mtDNA damage following exposure of primary skin cells to solar UV and complete solar light were carried out by Dr Laura Hudson and can be found in the appendix section (Appendix Figure 1.1 and 1.2 respectively). Both fibroblast and keratinocyte cells were seen to generate ROS in response to complete solar light. Fibroblasts however show a greater sensitivity as a 1.5 fold increase compared to control is seen at a dose equivalent to 2h. A 0.72 fold increase could be seen in keratinocyte cells assessed under the same conditions (Appendix Figure 1.1). Interestingly primary fibroblasts generated significantly more H₂O₂ in response to complete solar light exposure when compared to solar UV. This suggests that the IR and VIS components may be having a significant role in ROS generation. The findings also suggest that fibroblast cells are more sensitive to the longer wavelengths of light in comparison to keratinocytes whereby no significant difference in ROS can be seen between complete solar light and solar UV (Appendix Figure 1.1).

Data assessing the level of mtDNA was in support of the findings from the ROS-Glo assay. The response pattern in fibroblast and keratinocyte cells following exposure to complete solar light and solar UV was similar to that seen in the ROS response (Appendix Figure 1.2). The level of nDNA damage was investigated using the comet assay in order to further validate the findings. The comet assay also known as the single cell gel electrophoresis assay, is an established method used to quantify and visualise low levels of DNA damage. The method was first used by Rydberg (1975) whereby nDNA damage in individual cells was assessed (Fairbairn et al., 1995). The technique was further developed later on to enhance the sensitivity for detecting nDNA damage (Singh et al., 1988). The comet assay essentially enables the measurement of DNA fragments which have migrated away from the nucleus producing a tail (indicative of double strand breaks) under the influence of electrophoresis (Figure 26). Being negatively charged DNA migrates towards the anode (+) electrode. The length of the tail is proportional to the amount of DNA damage present, specifically the double strand breaks. Further modifications may be carried out using enzymes to uncover potential DNA damage, this is achieved by cleaving the lesions to create DSB that may then be detected through the comet assay (Fairbairn et al., 1995).

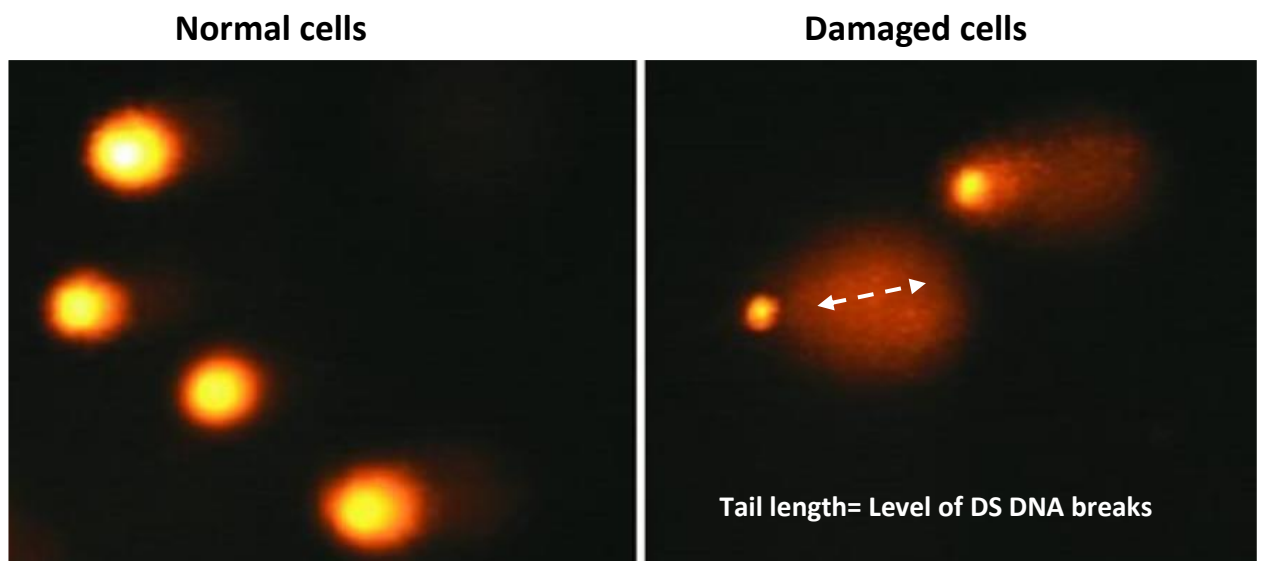


Figure 26: Comet assay showing the appearance of normal and damaged cells

Two representative images are shown for normal (control) cells (left) and damaged (treated) cells (right). Each fluorescent circle represents a nucleus from a single cell. The damaged cells are seen to have longer tail lengths and appear in the shape of “comets”. The tail length is indicative of the amount of DNA DSB.

Following the exposure of keratinocyte and fibroblast cells to complete solar light (2.16 SED), both cell types showed significant levels of nDNA damage with nDNA damage being greater in fibroblast cells (Figure 27). These data provide further evidence that the different cell types within the skin have differential sensitivities to components of solar light (UV, IR and VIS).

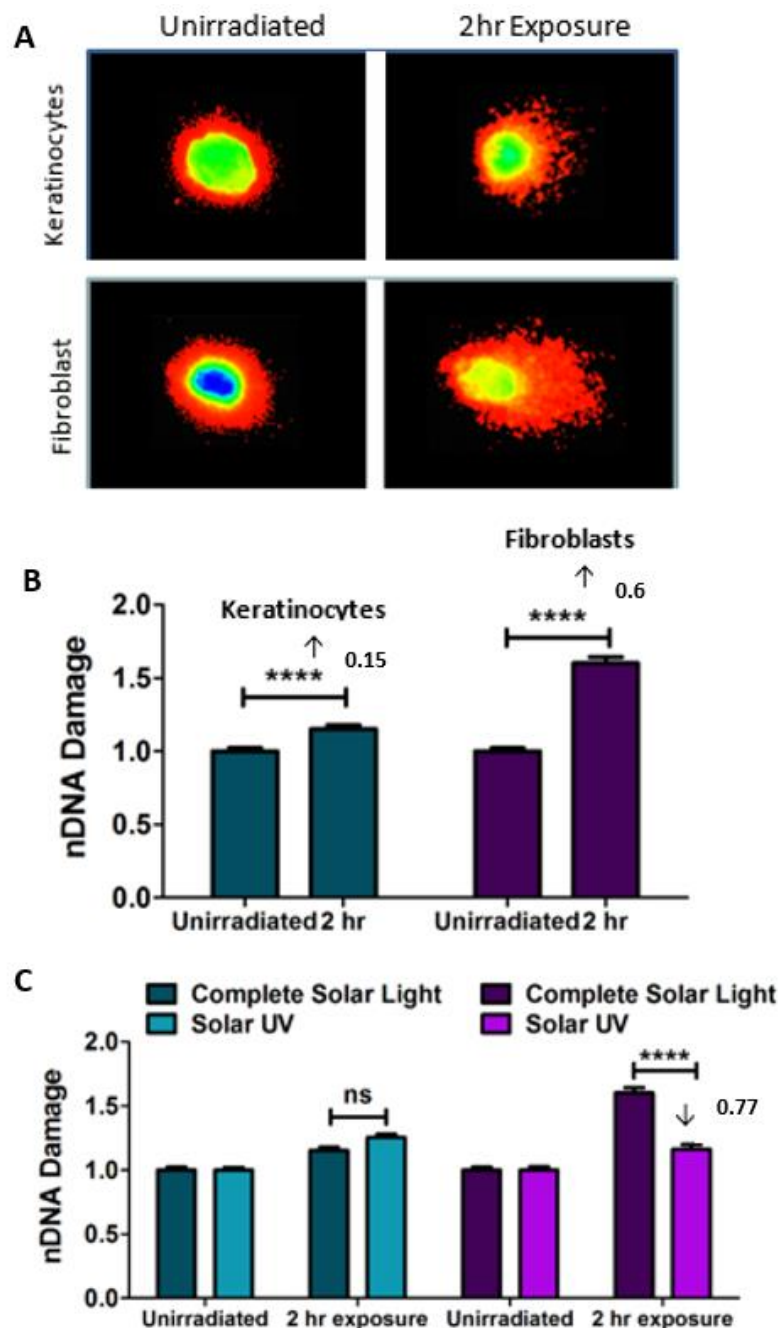


Figure 27: Complete solar light and solar UV induced nDNA damage in primary keratinocyte and fibroblast cells
 Representative images of nDNA damage from fibroblast and keratinocyte cells are shown following comet assay analysis. Each image represents the nDNA taken from a single cell following either unirradiated (control) or a 2hr (2.16 SED) exposure (A). Keratinocyte and fibroblast cells were treated with complete solar light at a 2hr dose (2.16 SED) or were unirradiated (control) (B). A 0.15 fold increase (keratinocytes) and 0.6 fold increase (fibroblasts) in nDNA damage can be seen suggesting a greater level of damage induction in fibroblast cells. A comparison between the effects of solar UV and complete solar light on nDNA damage in fibroblast and keratinocyte cells is shown (C). No significant difference between the dosing conditions can be seen in keratinocyte cells. A 0.77 fold reduction in nDNA damage is however seen in fibroblast cells following exposure to solar UV when compared to complete solar light. Statistical analysis was carried out using an unpaired T test with Welch's correction. Comet assays were carried out alongside Dr Laura Hudson. Results are represented as the mean value relative to the untreated control (error bars represent the SEM) N=3, N=3 respectively.

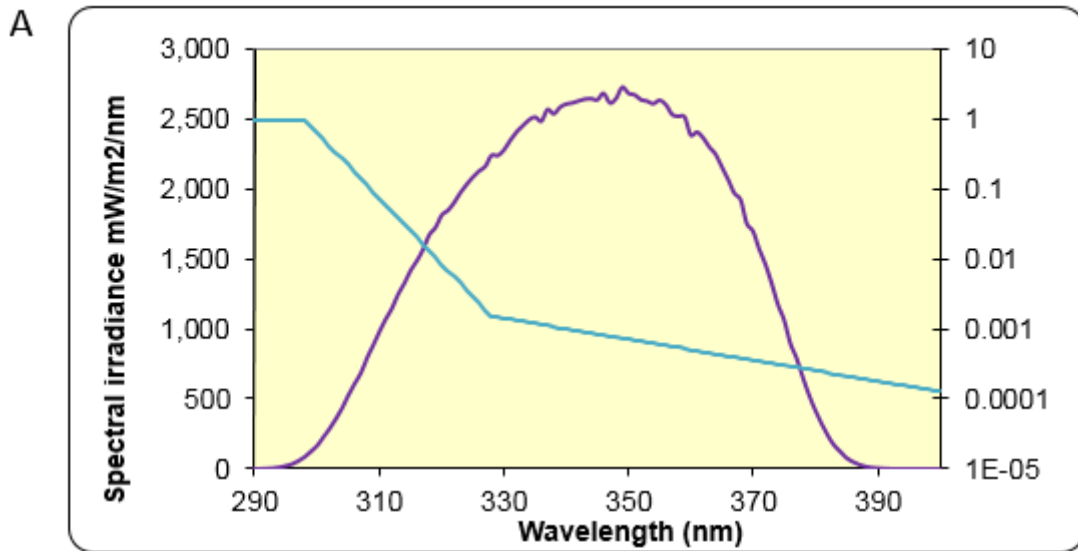
3.3.2 Preliminary work and experimental optimisation

3.3.2.1 Calibration of UV sources

The solar light dosing equipment within the lab are calibrated on a regular basis by the Regional Medical Physics Department (Newcastle Freeman Hospital). Calibration of the Newport Solar Simulator was an essential aspect for the project as it would ensure for controlled and accurate dosing to be achieved within each experiment. Being an artificial source of radiation, the solar simulator allows for more precise and reproducible doses of solar light to be applied.

The radiation emitted by a light source can be specified by determining the spectral output (Diffey, 2002). Measuring the radiation spectrum emitted uses a procedure known as spectroradiometry, this is the fundamental way to characterise the emissions (spectral irradiance). Spectroradiometry differs from radiometry (measurement of total radiant energy emitted by the source), and photometry (measurement of the VIS spectrums radiant energy (380-780 nm)) as it is more precise in its measurements of radiant energy by measuring the individual wavelengths of the source (Schneider and Young, 1998). This project utilises both spectroradiometry and radiometry. Once the spectral radiance of the individual sources is determined a hand held radiometer calibrated to the spectral reading was used on a more frequent basis to calculate the solar light dosage.

Work also involved assessing the biological effect of the individual components of solar light and components in combination. In order to achieve the desired wavelength emissions from the solar simulator a compatible IR cut-off and UV blocking filter were used. Glass and plastic filters were also utilised to allow for a reduction in the level of UV (section 2.8.2). The Newport Solar Simulator is designed to provide controlled doses of solar light (UVA, UVB, VIS and IR) in proportions similar to that found in natural sunlight (Newport). The proportion of UVA to UVB emissions were measured and confirmed to be within physiological range as a reading of 92.2% UVA and 7.8% UVB was recorded with no UVC being present (Figure 28).



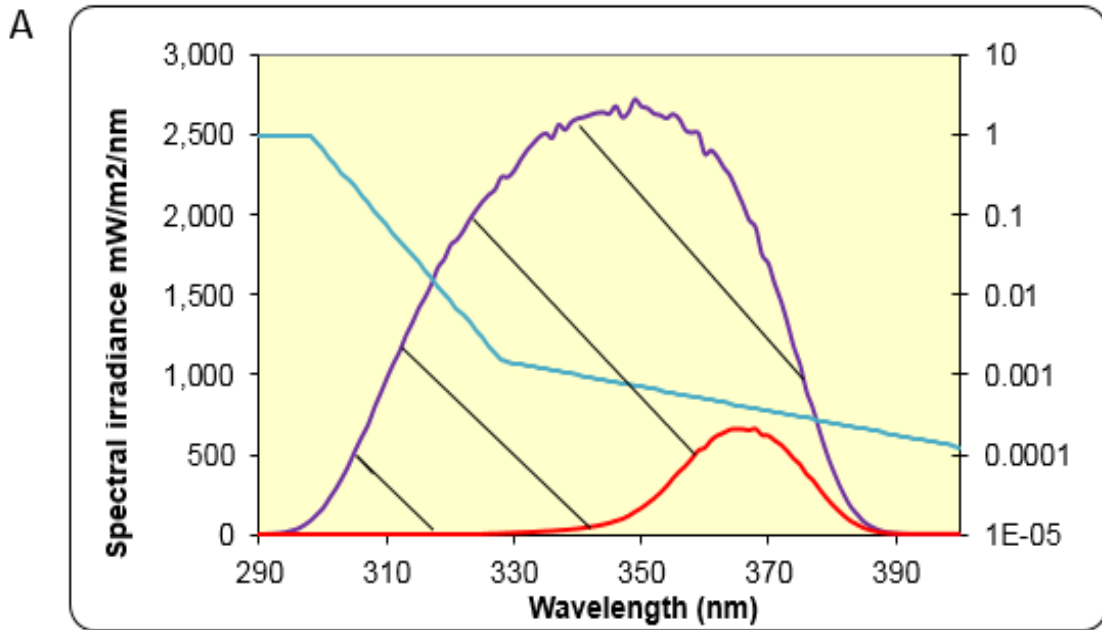
B

Measured Irradiance – IR/VIS blocking filter only			
Irradiance	(mw / cm ²)	%	Calibration factor
Total UV	15.079		1.263
UVC (250-280)	0.000	0.0	0.000
UVB (280-315)	1.182	7.8	0.099
UVA (315-400)	13.897	92.2	1.164
Weighted	0.199		0.017
SED / min	1.191		

Figure 28: Showing the calibration readings for the Newport Solar Simulator

The spectral irradiance of the Solar Simulator was measured with the presence of the IR/VIS blocking filter, the irradiance output is represented by the purple line (A). The output percentage of UVA to UVB is 7.8% and 92.2% respectively, no UVC was detected from the emission (B). The blue line represents the erythema dose. CIE standard weighting factors were used to determine the SED. The proportions of UV emitted simulate the levels that may be found in natural sunlight.

The plastic UVB filter (Figure 29) is able to provide complete protection against UVB and in doing so also reduces the output of UVA by 88.6%. Similarly the glass filter (Figure 30) is able to provide complete UVB protection whilst blocking less of the UVA as the glass material is more effective at allowing UVA rays to pass through with only 51% UVA being blocked.

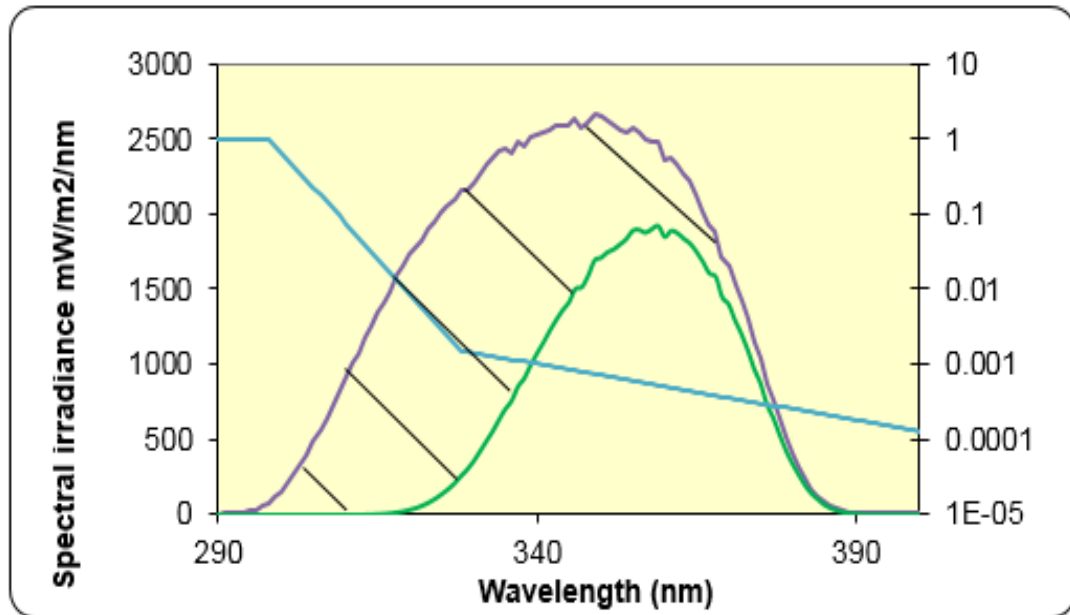


B

Measured irradiance – IR/VIS blocking filter with UVB filter				
Irradiance	(mw / cm2)	%	Cal factor	% error
Total UV	1.579		1.016	0.3
UVC (250-280)	0.000	0.0	0.000	
UVB (280-315)	0.000	0.0	0.000	
		99.99		
UVA (315-400)	1.579	9	1.016	0.3
Weighted	0.00071			
SED / min	0.0043			

Figure 29: Showing the calibration readings for the Newport Solar Simulator with the plastic UVB blocking filter
 The spectral irradiance of the Solar Simulator was measured in the presence of the IR/VIS blocking filter and the UVB filter. The irradiance output for the IR/VIS blocking filter with the UVB filter is represented by the red line, the IR/VIS blocking filter is also shown (purple) for comparison. The blue line represents the erythema dose. CIE standard weighting factors were used to determine the SED (A). The UVB filter reduces the output of UVA by 88.6% (A) as well as completely blocking UVB (B). The area under the red line represents the 11.4% of UVA passing through the UVB filter.

A



B

Measured irradiance – IR/Vis filter with window glass			
Irradiance	(mw / cm2)	%	Calibration factor
Total UV	6.818		
UVC (250-280)	0.000	0.0	
UVB (280-315)	0.001	0.0	
UVA (315-400)	6.818	99.99	
Weighted	0.00466		
SED / min	0.0280		

Figure 30: Showing the calibration readings for the Newport Solar Simulator with the glass UVB blocking filter

The spectral irradiance of the Solar Simulator was measured in the presence of the IR/VIS blocking filter and the window glass filter. The irradiance output for the IR/VIS blocking filter with the window glass filter is represented by the green line, the IR/VIS blocking filter is also shown (purple) for comparison. The blue line represents the erythema dose. CIE standard weighting factors were used to determine the SED (A). The window glass filter reduces the output of UVA by 51% (A) as well as completely blocking UVB (B). The area under the green line represents the 49% of UVA passing through the window glass filter.

The IR cut-off filter allows for a combination of UV and VIS rays to pass through whilst blocking the IR component of solar light. The UV blocking filter prevents UV from passing through allowing for a combination of IR and VIS to be emitted. Use of the IR cut-off and the UV blocking filter in combination allows for the passage of VIS from solar simulated light. Further details regarding the filters are presented in the general methods (Chapter 2, section 2.6).

When assessing the application of solar simulated light plus filters, a spectral irradiance curve was taken from 250nm up to 700nm and weighted according to the Commission Internationale de l'Éclairage/ International Commission on Illumination (CIE), erythema action spectrum. This works well in the UV region but is less proven in the VIS and IR regions since the CIE weighting is undefined beyond 400nm (Vanicek et al., 2000;Serrano et al., 2012). This gives two curves, both of which are shown within the graphs (Figure 31). The effective irradiance curve converges with the spectral irradiance curve at low wavelengths but is essentially displaced downwards by approximately 4 orders of magnitude within the VIS since the final point of the CIE curve (400nm) has been extrapolated across the whole of the VIS region. Integrating the effective irradiance curve across the whole range gives 0.034W/m^2 Based on a SED of 100J/m^2 this gives a time of 0.815h ($100/0.034=2934\text{sec}$) to achieve perceptible erythema (Figure 31). The irradiance ratio for the UV blocking filter compared to the combined filters (IR cut-off filter and UV blocking filter) is 1.14 or 14% more using the un-weighted data (Figure 31). The irradiance ratio for IR cut-off filter to the combined filters (IR cut-off filter and UV blocking filter) is 1.18 or 18% more using the un-weighted data (Figure 31). Using both the IR cut-off filter and the UV blocking filter, the time taken to achieve an equivalent of 1 SED VIS is 0.82h. To achieve an equivalent of 1 SED using the IR cut-off filter only (giving an output of UV plus VIS) takes 0.69h. Application of the UV blocking filter (giving an output of IR plus VIS) takes 0.72h to achieve a dose that would be equivalent to 1 SED.

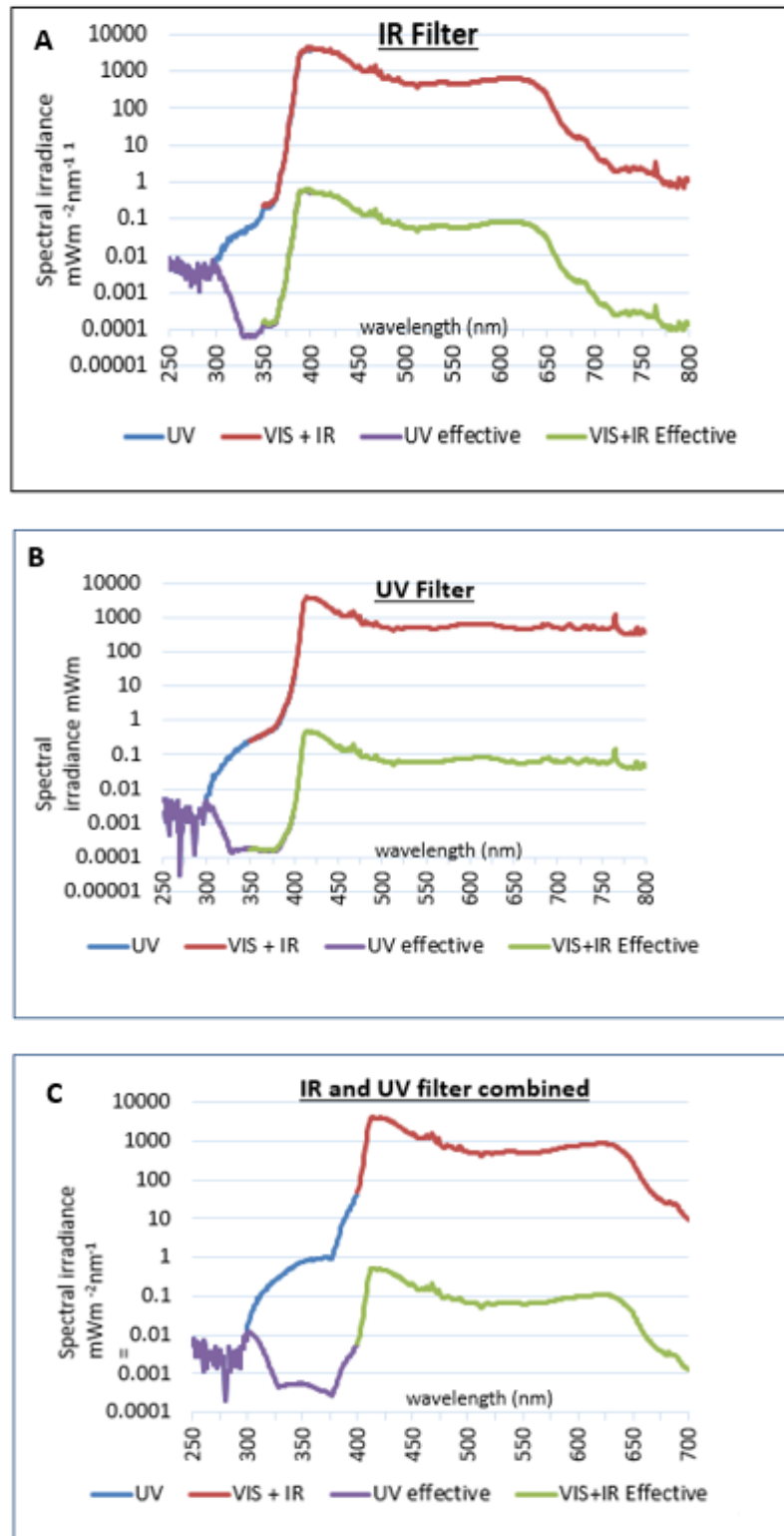


Figure 31: Spectral irradiance and effective irradiance of the Newport Solar Simulator plus filters

The Spectral irradiance and effective irradiance of the Solar Simulator were measured with blocking filters at bench height using the Bentham Spectroradiometer. The spectral irradiance was assessed following the application of the IR cut-off (A), UV blocking (B) both separately and in combination (C). This was carried out in order to make the output comparable to the known UV values. The time taken to reach a perceptible erythema (1 SED) with the IR filter is 0.62h compared to 0.72h with the UV filter. The time taken to reach 1 SED with both the UV and IR filters in place is 0.815h.

Following the calibration of the hand held Hydrosun meter, the output of the Hydrosun lamp was measured before each dosing experiment and the required doses calculated.

3.3.2.2 Temperature monitoring of the Solar Simulator and Hydrosun lamps

Temperature changes above physiological range have been reported to have an effect on cellular responses in both fibroblast and keratinocyte cells (Kim et al., 2005). Such effects may influence cellular response and act as confounding factors within experiments. For example an increase in temperature during IR exposure may trigger the generation of heat induced cellular ROS therefore masking the effects of IR only (Frank et al., 2004). To measure changes in temperature under the solar simulator (Figure 32) and Hydrosun lamps (Figure 33), a thermometer was placed under the irradiation sources at a distance similar to that at which the cells would be exposed to. Temperature changes were monitored over time using both a tin foil covered and exposed thermometer. No concerning heating effects were observed during the time span monitored as the temperature increases recorded were still within physiological range.

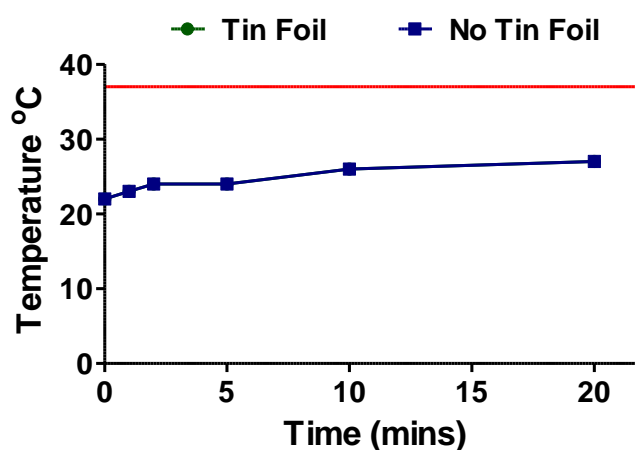


Figure 32: Temperature under the Solar Simulator

The temperature under the Solar Simulator was monitored using a thermometer at a distance of 19cm from the lamp (equivalent to the distance at which cells would be dosed). Readings were taken with the thermometer exposed or covered with tin foil. The red line represents 37°C (temperature at which cells were cultured). A minimum temperature of 22°C was recorded at time 0 and a maximum temperature of 27°C was recorded at 20 min.

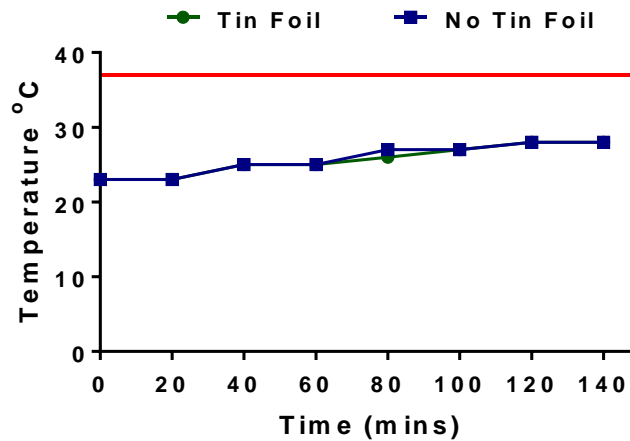


Figure 33: Temperature under the Hydrosun lamp

The temperature under the Hydrosun lamp was monitored using a thermometer at a distance of 35cm from the lamp (the distance at which cells would be dosed is approximately 50cm). Readings were taken with the thermometer either exposed or covered with tin foil. The red line represents 37°C (temperature at which cells were cultured). A minimum temperature of 23°C was recorded at time 0 and a maximum temperature of 28°C was recorded at 140 min. Measurements were taken alongside Dr Laura Hudson.

3.3.3 Determining the sublethal dose of complete solar light and IR

The MTS cell viability assay was used to assess the effect of complete solar light and IR on cell survival. Through personal contact a decision was made by experts at Croda to use a dose of solar light equivalent to 2h and a dose equivalent to 30min in the Mediterranean sun at noon during the summer months at the northern latitude of 30-35 degrees (Berneburg et al, 1999). Doses were suggested to be both physiological and commercially relevant. A wider range of doses were used during preliminary work carried out on cell lines as a proof of concept study. Such experiments were performed to assess whether the effects seen with solar light are consistent over a higher dose range. Using higher doses is also advantageous as there may be different sensitivity levels present between primary and cell line cells (Ölschläger et al., 2009; Kaur and Dufour, 2012). IR was also assessed at physiologically relevant doses (300-800J/cm²) with 300J/cm² estimated as being equivalent to 4h in the Mediterranean sun (Schroeder et al., 2010; Dupont et al., 2013). The cell viability assays for complete solar light in primary cells were carried out along with Dr Laura Hudson. Following the exposure of primary fibroblasts to complete solar light (2.16 SED) a 6% decrease in cell viability can be seen which is within an acceptable sublethal range (P<0.05) (Figure 34 A). No significant difference in cell viability relative to control was seen when primary fibroblasts were exposed to the

range of IR doses assessed (Figure 34 B). Similarly, primary keratinocyte cells did not show any significant difference in cell viability when exposed to doses of complete solar light or IR ($P < 0.05$). Greater levels of experimental variability were however noticed with primary keratinocytes (Figure 35 A and B). HDFn cells exposed to complete solar light were not affected by the doses assessed (Figure 36 A). No change in cell viability was seen when HDFn cells were dosed with IR (Figure 36 B).

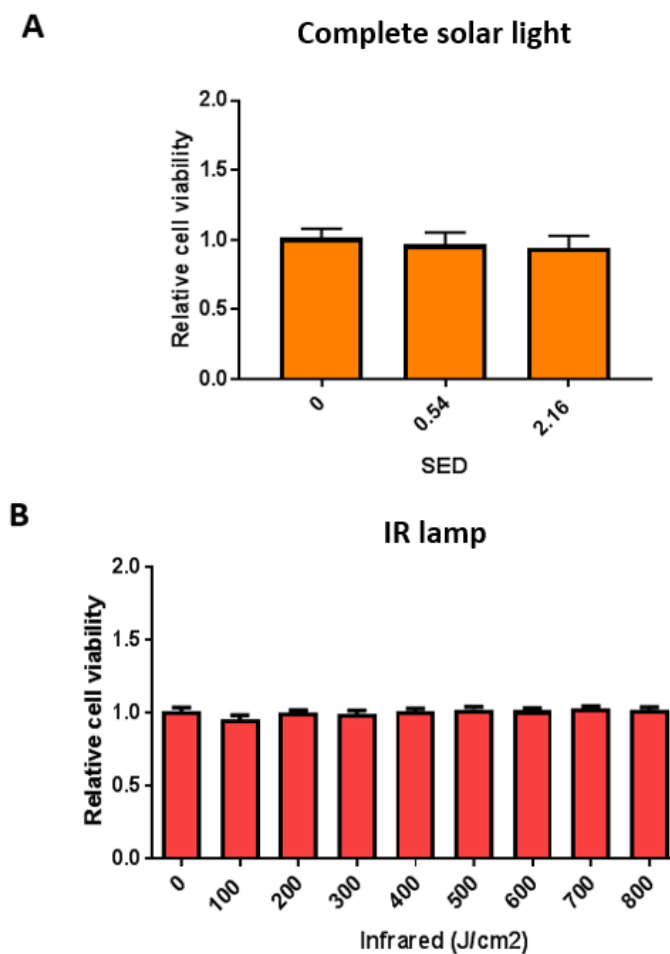


Figure 34: Effect of complete solar simulated light, and IR exposure on primary fibroblast viability

Primary fibroblast cells were treated with either full spectrum solar light or IR. Cell viability was assessed using the MTS assay. Cells treated with complete solar light (A) show no significant changes in relative cell viability at doses ≤ 2.16 SED. Similarly cells treated with IR show no significant effect on cell viability at doses ≤ 800 J/cm² (B). Statistical analysis was performed to compare all columns to the control (untreated) cells using a one-way ANOVA with Dunnett's post-hoc analysis * $P < 0.05$ (error bars represent the SEM) N=3, N=3 respectively.

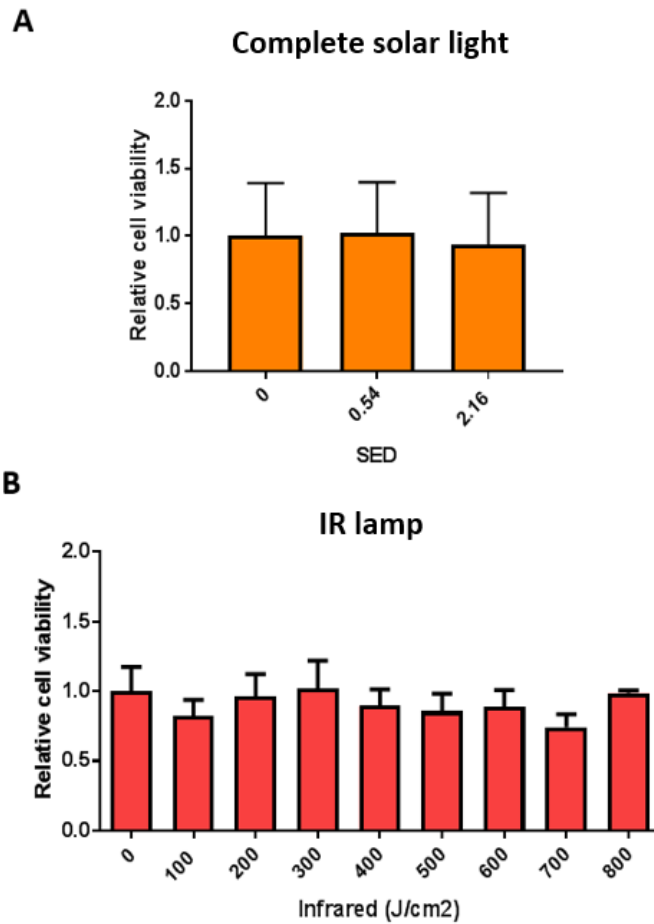


Figure 35: Effect of complete solar simulated light and IR exposure on primary keratinocyte cell viability

Primary keratinocyte cells were treated with either full spectrum solar light or IR with cell viability being assessed using the MTS assay. Cells treated with complete solar light (A) show no significant changes in relative cell viability at doses ≤ 2.16 SED. Similarly cells treated with IR show no significant effect on cell viability at doses ≤ 800 J/cm² (B). Statistical analysis was performed to compare all columns to the control (untreated) cells using a one-way ANOVA with Dunnett's post-hoc analysis (error bars represent the SEM) N=3, N=3 respectively.

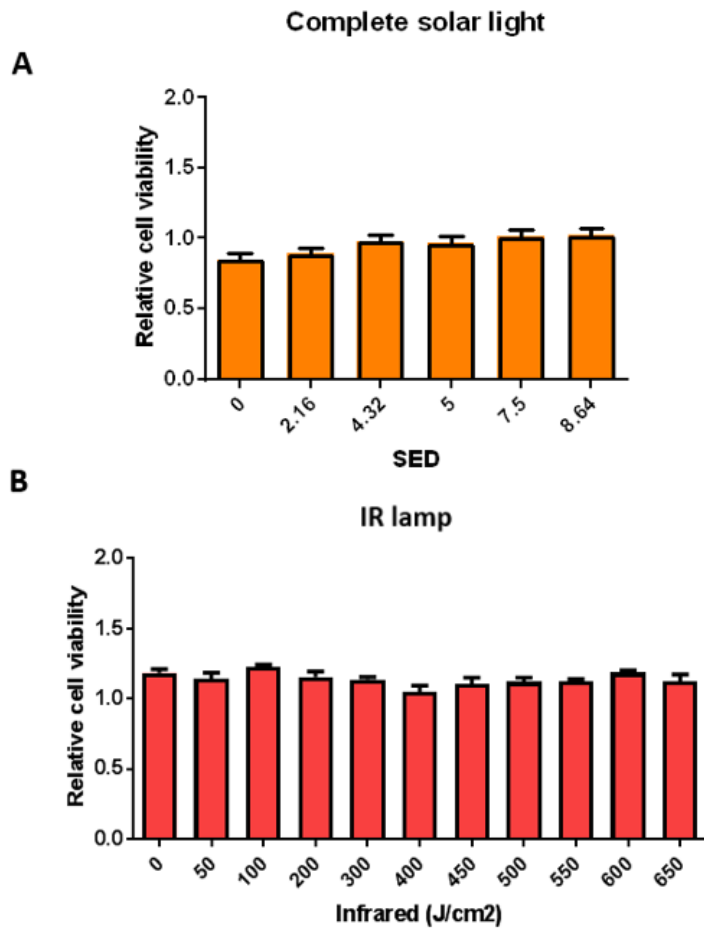


Figure 36: Effect of complete solar simulated light and IR exposure on HDFn cell viability

HDFn cells were treated with either full spectrum solar light (A) or IR (B) with cell viability being assessed using the MTS assay. Complete solar light had no significant effect on relative cell viability at doses ≤ 8.64 SED (A). IR had no effect on HDFn cell viability at doses ≤ 650 J/cm² (B). Statistical analysis was performed to compare all columns to the control (untreated) cells using a one-way ANOVA with Dunnett's correction (error bars represent the SEM) N=2, N=1 respectively.

3.3.4 ROS generation in response to solar light exposure

3.3.4.1 Measurements of ROS generation using the DCFDA assay

HDFn cells grown in monolayer were either exposed to full spectrum solar simulated light or solar UV and the DCFDA method was used to detect intracellular ROS generation (Figure 37). As can be seen in Figure 37A dosing HDFn cells with solar UV leads to a significant (0.33 fold) increase in the level of ROS at the higher dose of 7.5 SED ($P < 0.01$). Complete solar light produces significant ROS levels at a lower dose (4.32 SED) whereby a 0.5 fold increase is seen relative to control ($P < 0.001$) and a 1.16 fold increase is detected at a dose of 7.5 SED ($P < 0.001$) (Figure 37 B). When conditions are compared as shown in the re-plotted data (Figure 37 C) complete solar light leads to significantly greater levels of ROS at the 4.32 SED ($P < 0.05$) and 7.5 SED ($P < 0.001$) doses compared to solar UV.

HaCat cells assessed using the DCFDA method, did not produce any detectable ROS following exposure of cells to complete solar light. The ROS generation response may have been too low to be detected using the DCFDA assay. ROS could however be detected in HaCat cells using the DCFDA method following exposure to a H_2O_2 stimulus (100-500 μ M for 1h) (Appendix Figure 2).

3.3.4.2 Measurements of ROS generation using the ROS-Glo assay

Following on from the findings with the DCFDA assay (section 3.3.4.1), the ROS-Glo assay was used to further validate the data. ROS-Glo specifically detects the level of H_2O_2 generation within cells through a luminescence based approach. HDFn and HaCat cells were exposed to either full spectrum solar simulated light or solar UV. The level of ROS generation in HDFn cells obtained using the ROS-Glo assay (Figure 38) confirms the data seen previously with the DCFDA method (Figure 37). Furthermore, the ROS-Glo method appears to be more sensitive as higher levels of ROS can be detected at comparable doses. For example in HDFn cells a 4.77

fold increase in ROS is seen relative to control using the ROS-Glo method (Figure 38 B) compared to a 1.16 fold increase with the DCFDA assay (Figure 37 B). ROS generation in response to increasing doses of complete solar light shows a linearity relationship ($R^2= 0.83$) in HDFn cells (Figure 39). This linear relationship appears to be weaker when solar UV is assessed ($R^2= 0.47$) (Figure 39). The ROS-Glo assay was able to detect ROS levels in HaCat cells when solar light was used as a stimulus therefore further suggesting that it is a more sensitive assay when compared to DCFDA. ROS generation in HaCat cells follows a similar pattern to that found in HDFn cells whereby complete solar light results in greater levels of ROS compared to solar UV (Figure 40).

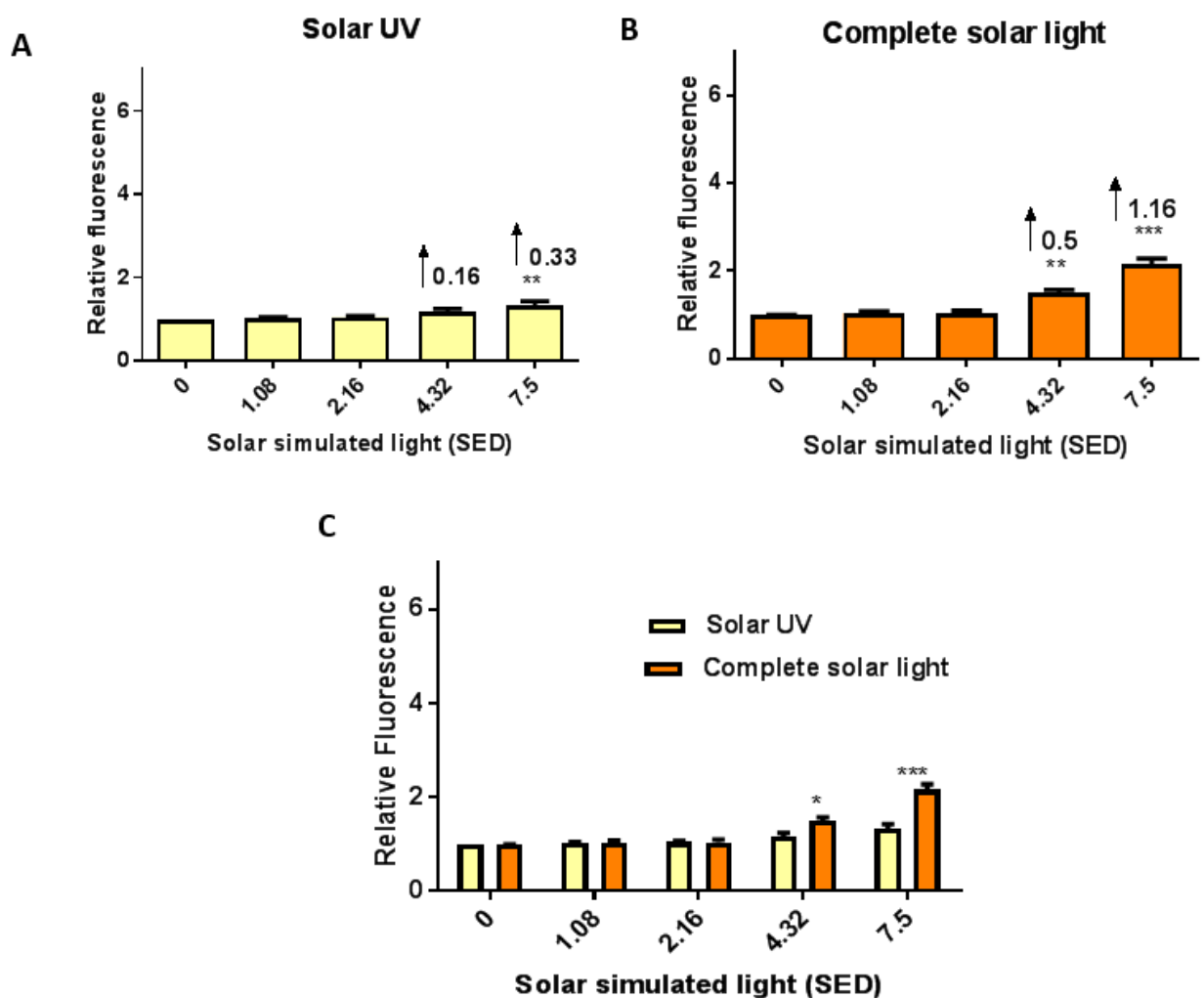


Figure 37: ROS generation in HDFn cells following exposure to solar simulated light

HDFn cells were dosed with either solar UV (A) or complete solar light (B) and the level of non-specific ROS generation was assessed using the DCFDA method. The relative level of fluorescence is equivalent to the level of ROS. Solar UV is seen to significantly contribute to ROS levels at 7.5 SED (A). Complete solar light is seen to produce significant ROS levels at a dose of 4.32 SED and 7.5 SED (B). Significant differences are detected when solar UV and complete solar light dosed cells are compared (C). Statistical analysis was performed to compare all columns to the 0 control (unirradiated) cells using a one-way ANOVA with Dunnett's correction ** P<0.01 ***P<0.0001. A one-way ANOVA with Bonferonni's post-hoc was used to compare the mean of each column with the mean of every other column * P<0.05, ***P <0.001 (error bars represent the SEM) N=3, N=3 respectively.

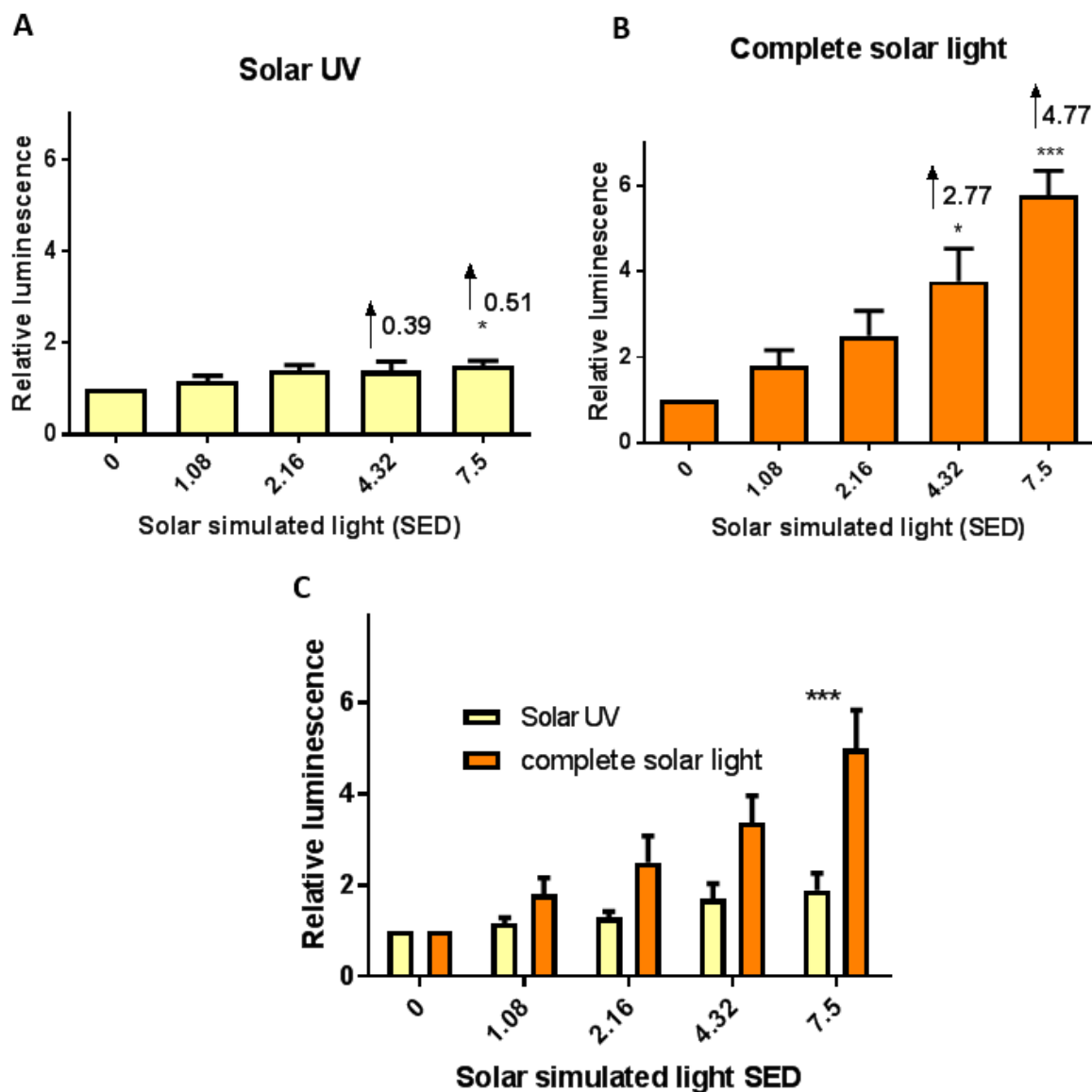


Figure 38: ROS generation in HDFn cells following exposure to solar simulated light

HDFn cells were dosed with either solar UV (A) or complete solar light (B) and the resulting level of ROS in the form of H₂O₂ was assessed using the ROS-Glo method. The level of H₂O₂ generation is equivalent to the relative luminescence measurements. Solar UV produces significant ROS levels at 7.5 SED (0.51 fold increase) (A). Complete solar light is seen to result in significant levels of ROS at 4.32 SED (2.77 fold increase) (B). At all doses assessed complete solar light produces greater levels of ROS relative to solar UV (C). Statistical analysis was performed to compare all columns to the control (unirradiated) cells using a one-way ANOVA with Dunnett's correction *P< 0.01, ***P<0.0001. A one-way ANOVA with Bonferonni's post-hoc was applied to compare the mean of each column with the mean of every other column (C) ***P<0.0001 (error bars represent the SEM) N=3, N=3 respectively.

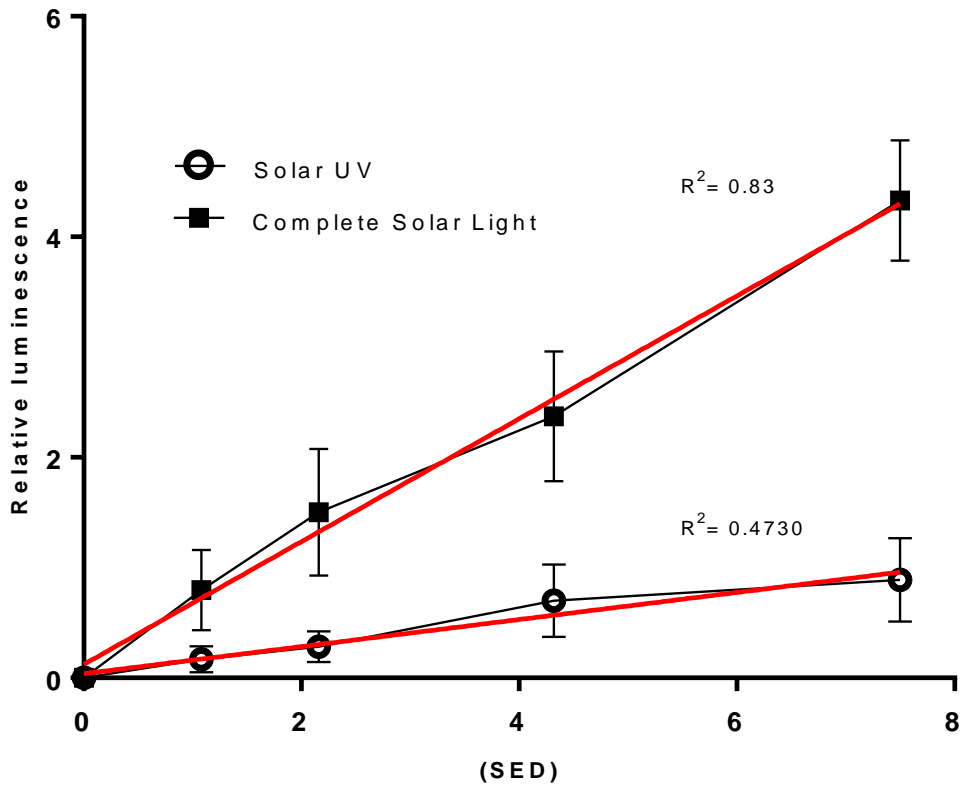


Figure 39: HDFn cell dose response following the application of complete solar light and solar UV

The response of HDFn cells to increasing doses of solar UV and complete solar light were measured using the ROS-Glo method. The level of luminescence is proportional to the H₂O₂ detected relative to the unirradiated control (0 SED). Statistical analysis was applied using linear regression analysis and the R² value calculated. A linear correlation can be seen when complete solar light is applied (R²= 0.83). A lower correlation level is seen with solar UV (R²= 0.473) (error bars are presented as the SEM), N=3, N=3 respectively.

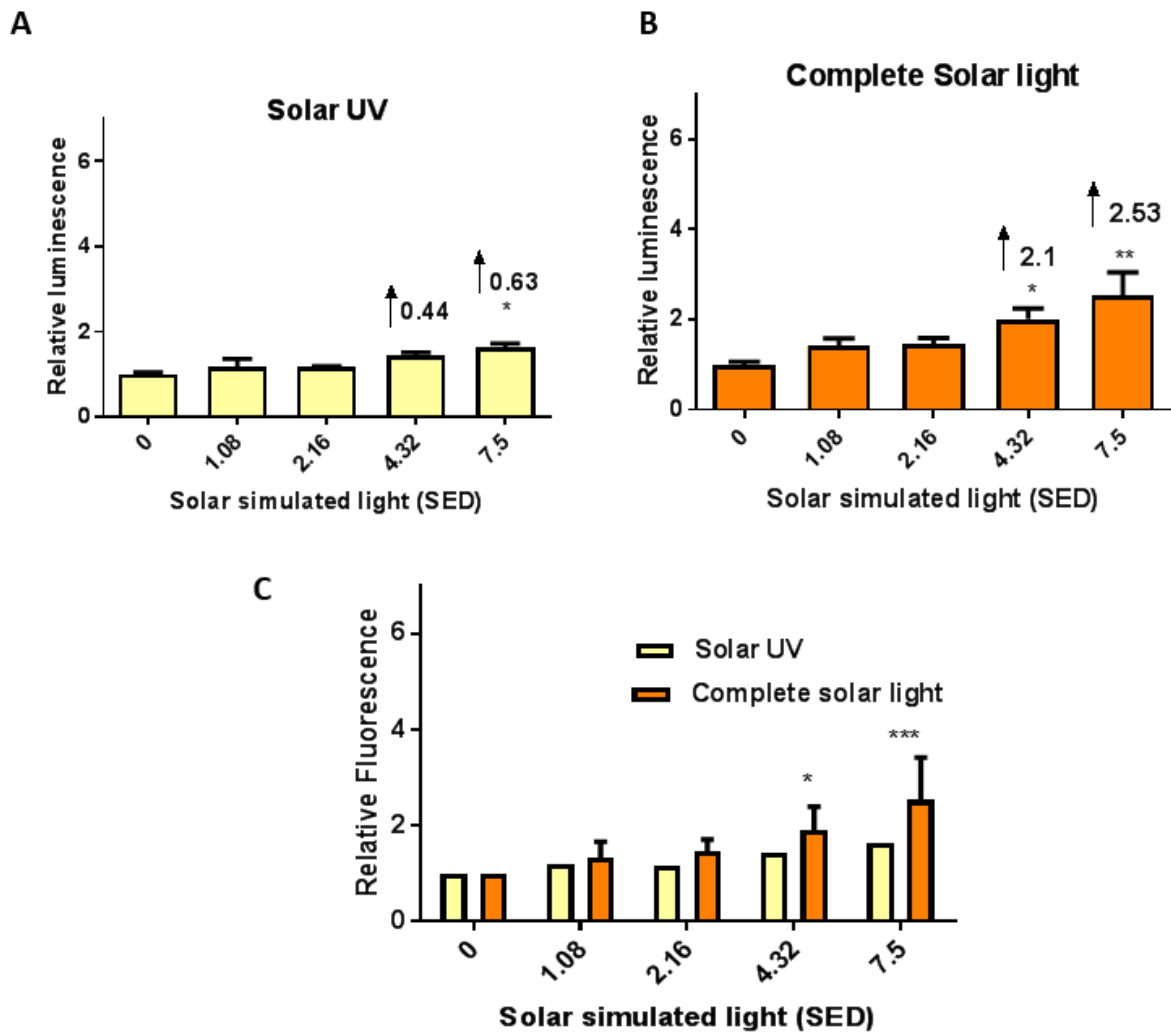


Figure 40: ROS generation in HaCat cells following exposure to solar simulated light

HaCat cells were dosed with either solar UV (A) or complete solar light (B) and the resulting level of ROS in the form of H₂O₂ was assessed using the ROS-Glo method. The level of H₂O₂ generation is equivalent to the relative luminescence measurements. Solar UV induces significant ROS levels at 7.5 SED (0.63 fold increase) (A). Complete solar light is seen to induce significant levels of ROS at 4.32 SED (2.1 fold increase) (B). Complete solar light produces significantly more ROS at 4.32 and 7.5 SED relative to solar UV (2.1 and 0.44 fold increase respectively at 4.32 SED) (C). Statistical analysis was performed to compare all columns to the control (unirradiated) cells using a one-way ANOVA with Dunnett's correction * P<0.01 ** P < 0.001. A one-way ANOVA with Bonferroni's post-hoc was carried out to compare the mean of each column with the mean of every other column * P < 0.05 ***P<0.001 (error bars represent the SEM) N=1, N=2 respectively.

3.3.4.3 Comparing HDFn and HaCat cell response to solar light

Figure 38 and Figure 40 have been re-plotted to compare the effect of HDFn and HaCat cells to complete solar light. Interestingly HDFn cells appear to be more sensitive to complete solar light when compared to the response of HaCat cells as significantly greater levels of ROS are

generated in HDFn cells at comparable doses (Figure 41 A). This suggests that like primary fibroblasts, HDFn cells are more sensitive to the longer wavelengths of solar light and similarly to primary keratinocytes, HaCat cells are seen to be less responsive. No such differences are detected when HDFn and HaCat cells are exposed to solar UV (Figure 41 B).

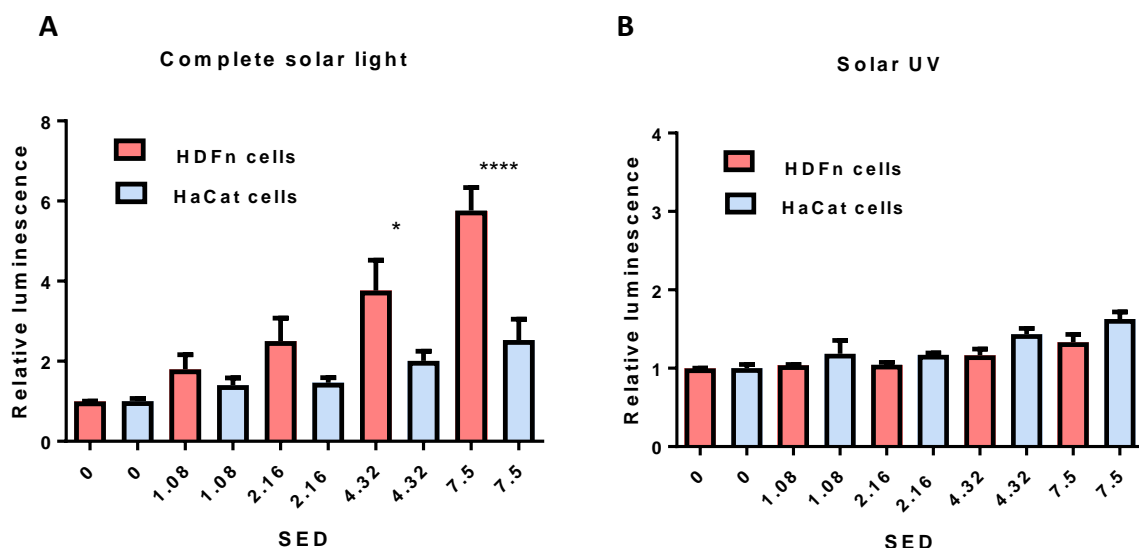


Figure 41: Comparison of HDFn and HaCat cell response to solar light

HDFn cells appear to be more responsive to complete solar light when compared to HaCat cells. The differences in response observed are significant at a dose of 4.32 SED (A). No statistical differences were found between the response of HDFn and HaCat cells to solar UV (B). Statistical analysis was performed to compare all columns to the control (unirradiated) cells using a one-way ANOVA with Bonferroni's correction * $P < 0.01$, **** $P < 0.0001$ (error bars represent the SEM) $N=3$, $N=2$ respectively.

3.3.4.4 Assessing the effect of individual components of solar light and combinations on ROS generation in HDFn and HaCat cells

Findings from the ROS detection assays have so far demonstrated that solar UV alone does not solely produce the increase in ROS generation detected within the skin cells assessed. The IR and or VIS components of solar light may therefore be contributing to the cellular response detected. This section of the chapter is concerned with assessing the effects of the individual components of solar light and components in combination in order to identify the wavelengths responsible for the level of ROS detection observed. Cells were immediately assessed following the application of the solar light doses.

As observed previously, solar UV (Figure 42) is seen to have marginal effects on the level of ROS generation when compared to complete solar light in both HDFn and HaCat cells. Similarly marginal ROS generation effects were detected in cells exposed to VIS (Figure 43), IR plus VIS (Figure 44) and UV plus VIS (Figure 45). Data which has been re-plotted shows no significant difference between HDFn and HaCat cells in terms of responses to IR plus VIS (Figure 44 C) and UV plus VIS (Figure 45 C). A range of IR doses have been previously investigated in the lab to assess the effects of IR exposure on ROS generation in HDFn cells. A single dose of IR ($400\text{J}/\text{cm}^2$) was found to produce marginal levels of ROS. The ROS generation response in HDFn cells did not show a linear response (Appendix Figure 3) HaCat cells were not assessed for ROS generation response following exposure to IR as they were previously found to be less responsive to longer wavelengths of light. Figure 46 illustrates the effect of the different dosing conditions on ROS generation. A combination of UV, IR and VIS clearly has a greater effect on ROS levels when compared to the individual effects and effects of any two components in combination. Complete solar light induced ROS generation in HaCat cells appears to show a less marked difference when compared to the effect of the other dosing conditions described (Figure 46 A).

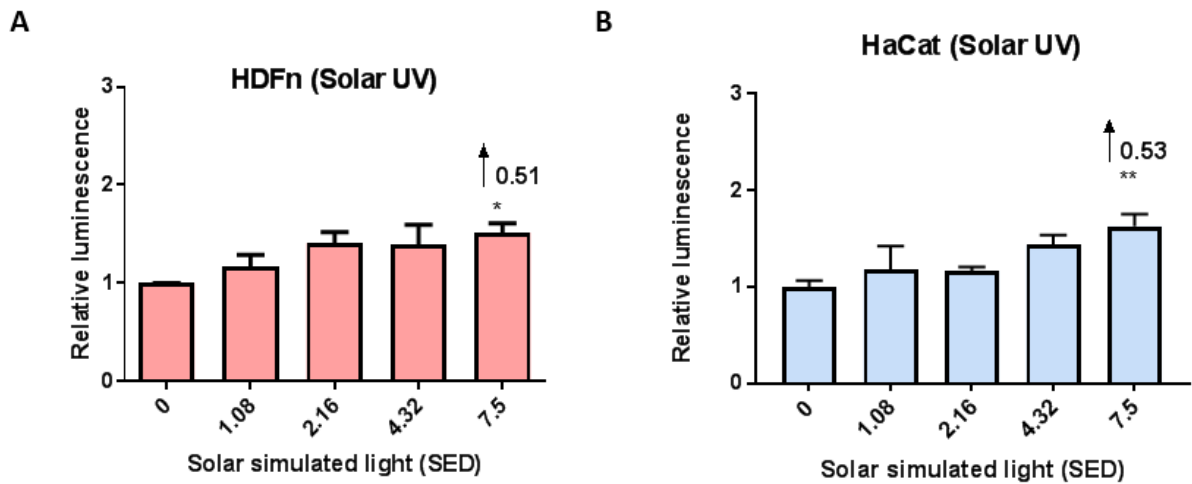


Figure 42: ROS generation in HDFn and HaCat cells following exposure to solar UV

Solar UV causes a significant increase in ROS levels as shown by the increase in relative luminescence at 7.5 SED in HDFn (A) and HaCat (B) cells. At 7.5 SED similar levels of ROS are seen between HDFn (0.51 fold increase) and HaCat cells (0.53 fold increase). Statistical analysis was carried out using the one-way ANOVA with Dunnett's correction to compare all columns to the control (untreated) cells *P<0.05, **P<0.001 (error bars represent the SEM) N=3, N=2 respectively.

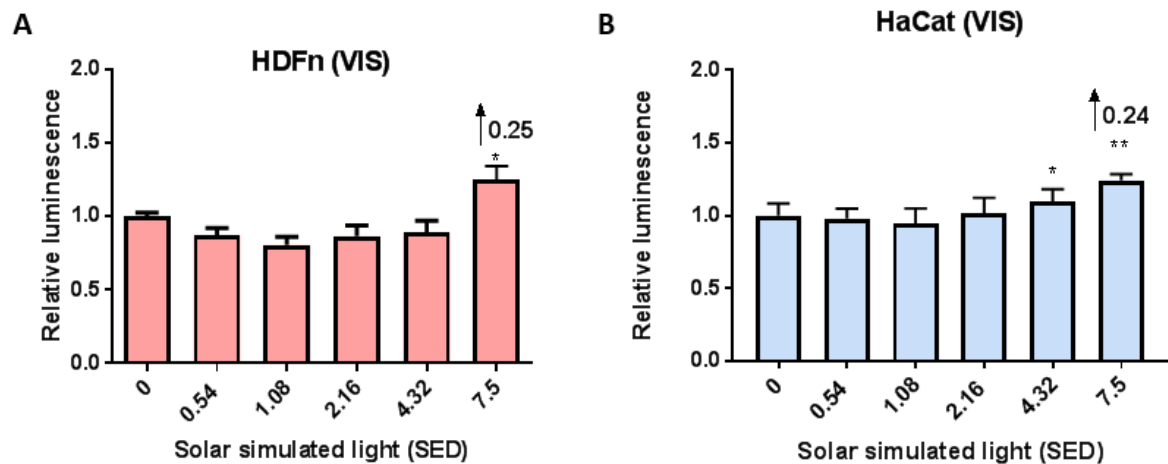


Figure 43: ROS generation in HDFn and HaCat cells following exposure to VIS

VIS causes a significant increase in ROS levels as shown by the increase in relative luminescence at 7.5 SED in HDFn (A) and HaCat (B) cells. At 7.5 SED similar levels of ROS are seen between HDFn (0.25 fold increase) and HaCat cells (0.24 fold increase). Statistical analysis was carried out using a one-way ANOVA with Dunnett's correction to compare all columns to the control (untreated) cells *P<0.05, **P<0.001 (error bars represent the SEM) N=3, N=2 respectively.

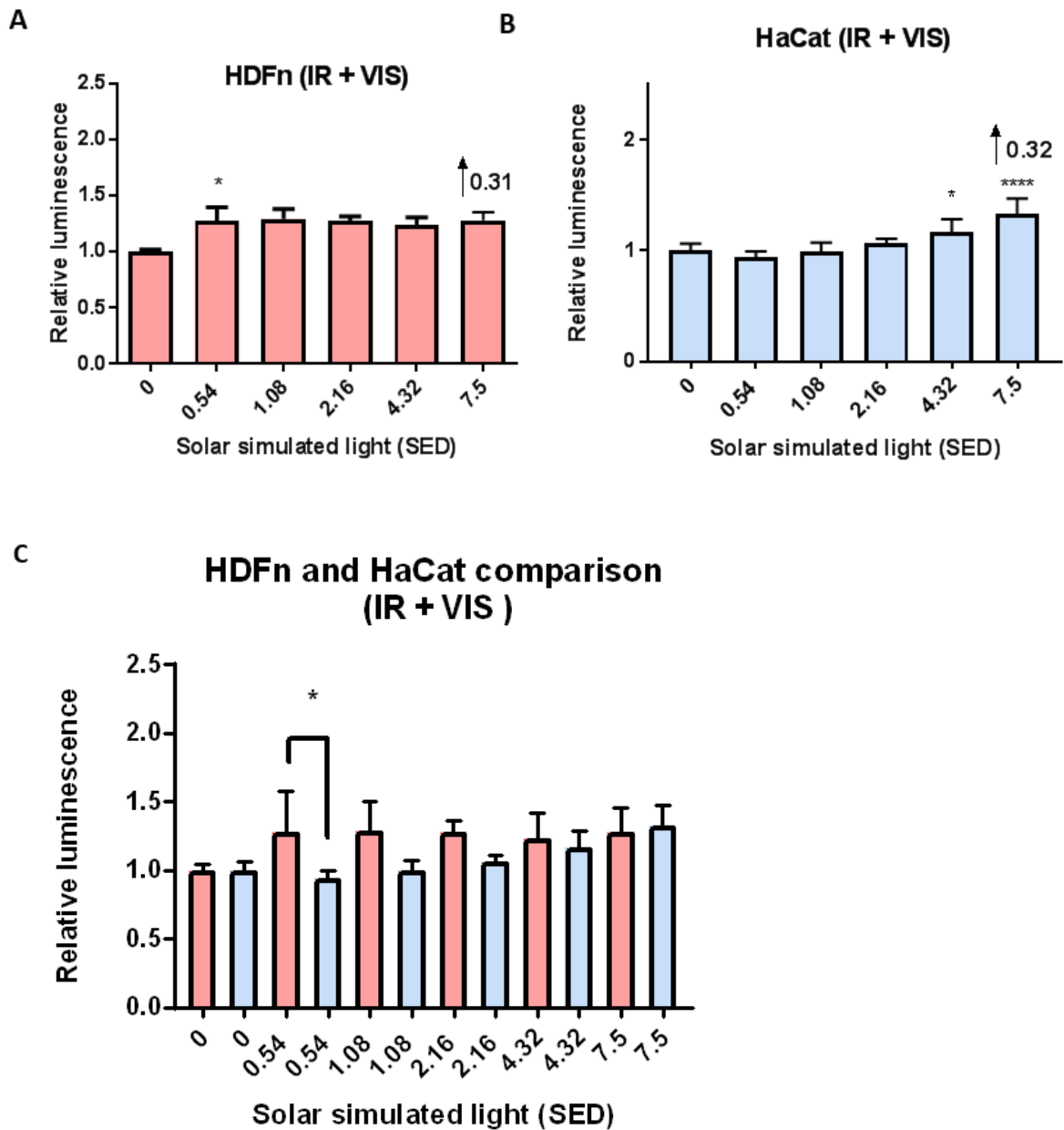


Figure 44: ROS generation in HDFn and HaCat cells following exposure to IR plus VIS

HDFn cells (A) appear to be more responsive to IR plus VIS when compared to HaCat cells (B) at the lower doses. The response to IR plus VIS however is similar at 7.5 SED (0.31 and 0.32 fold increase). ROS levels are represented by an increase in relative luminescence. No significant differences between HDFn and HaCat cells were detected at the higher SED doses (C). Statistical analysis was assessed using a one-way ANOVA with Dunnett's correction to compare all columns to control (untreated) cells. A one-way ANOVA with Bonferroni's correction was carried out to compare the mean of each column with the mean of every other column. *P< 0.05, ****P<0.0001 (error bars represent the SEM) N=3, N=2 respectively.

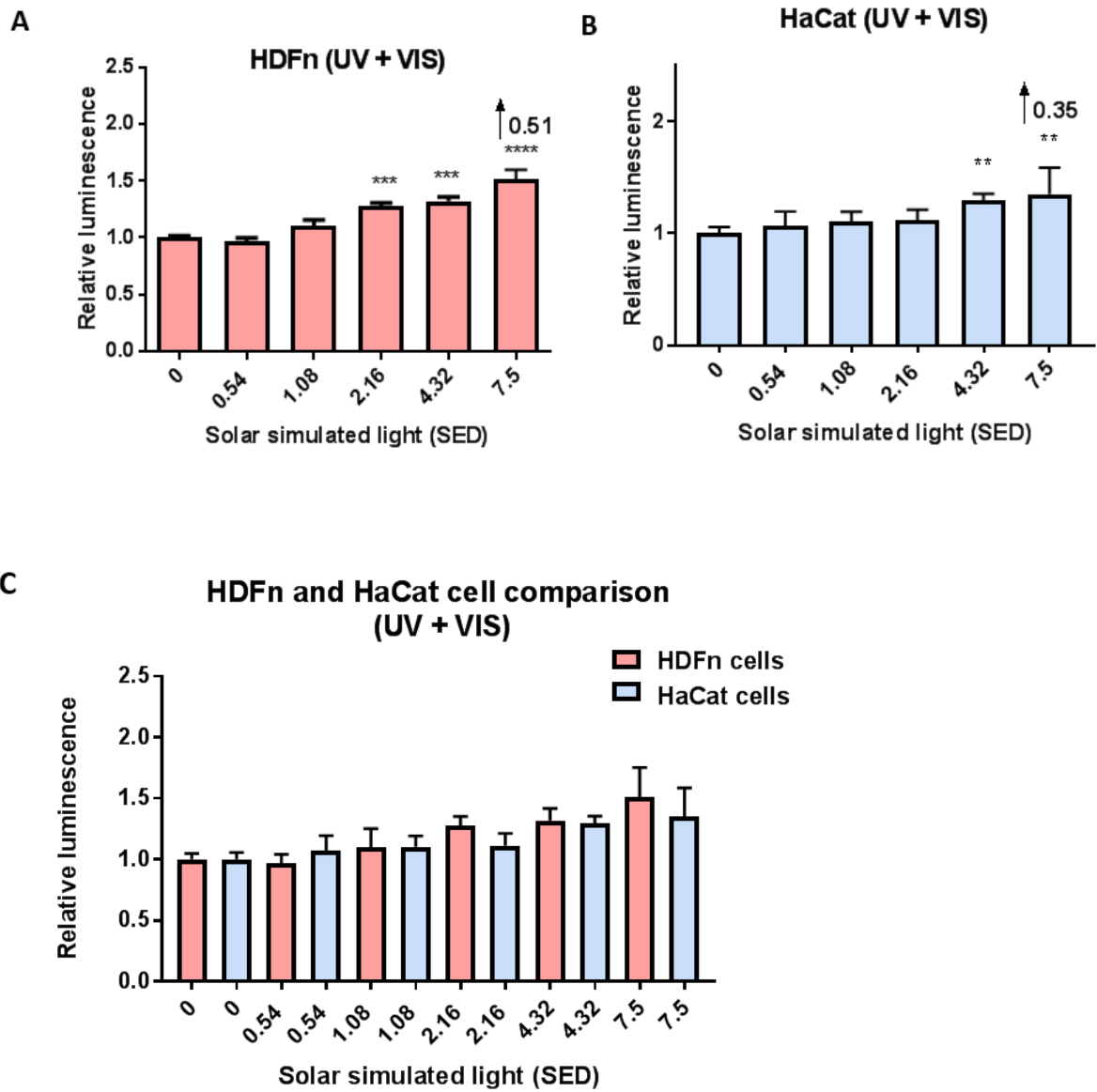
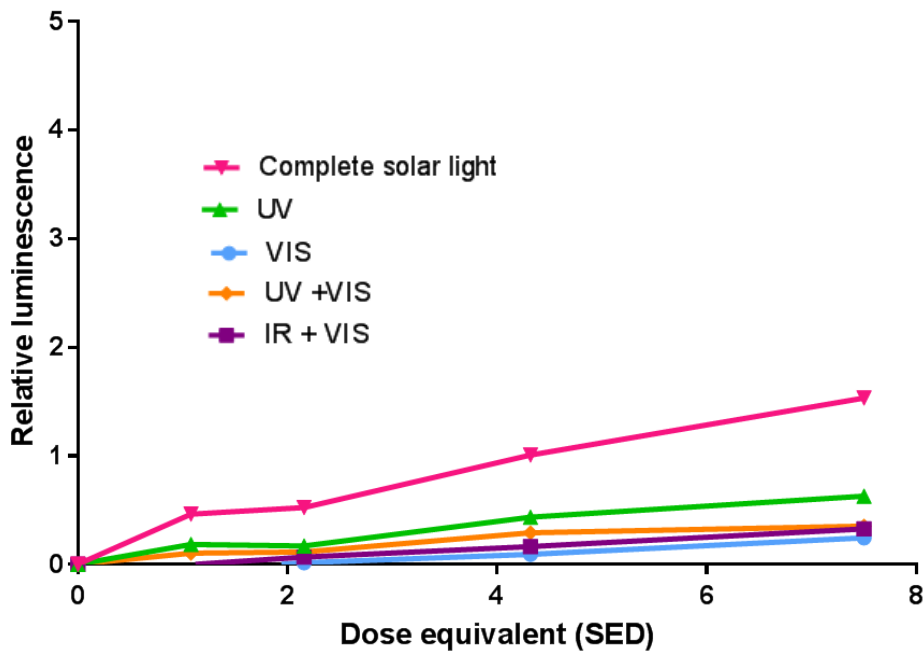


Figure 45: ROS generation in HDFn and HaCat cells following exposure to UV plus VIS

HDFn cells (A) appear to be more responsive to UV plus VIS when compared to HaCat cells (B) at the 7.5 SED dose (0.51 and 0.35 fold increase). ROS levels are represented by an increase in relative luminescence. No significant differences were however detected when HDFn and HaCat cell responses were compared (C). Statistical analysis was assessed using a one-way ANOVA with Dunnett's correction to compare all columns to control (untreated) cells. A one-way ANOVA with Bonferroni's correction was carried out to compare the mean of each column with the mean of every other column. *P< 0.05, ****P<0.0001 (error bars represent the SEM) N=3, N=2 respectively.

A HaCat cell response to components of solar light



B HDFn cell response to components of solar light

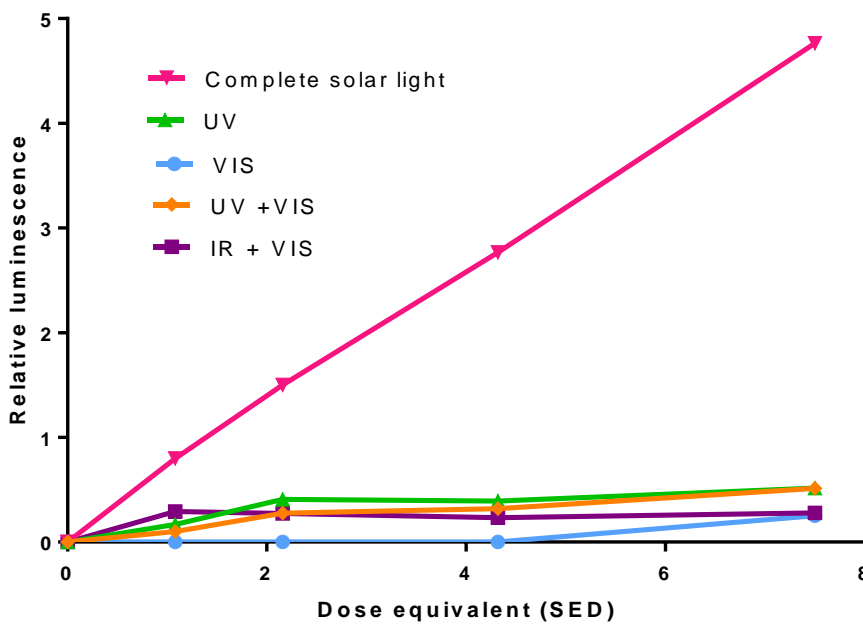


Figure 46: Summary of cellular ROS generation response in HDFn and HaCat cells following exposure to solar light dosing conditions

The ROS-Glo assay was used to assess the level of H₂O₂ generation. The response of HaCat (A) and HDFn (B) cells to the dosing conditions (complete solar light, UV, VIS, UV+ VIS and IR + VIS) are displayed.

3.3.4.5 Assessing the effect of individual components of solar light and combinations on ROS generation in primary skin cells

The individual components of solar light and components in combination were assessed in donor matched primary fibroblast, keratinocyte and differentiated keratinocyte cells. Data from the primary skin cells further confirms the findings from the HDFn and HaCat cell line experiments. The effect of the individual components of solar light and components in combination was marginal compared to complete solar light as can be seen in cells exposed to VIS (Figure 47), UV (Figure 48), IR (Figure 49), UV plus VIS (Figure 50) and IR plus VIS (Figure 51).

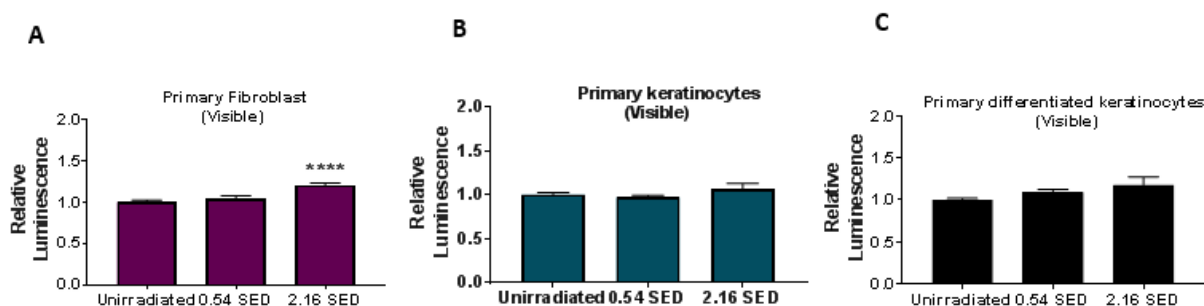


Figure 47: ROS generation in primary fibroblast, keratinocyte and differentiated keratinocyte cells following exposure to VIS

VIS induces a significant increase in relative luminescence (proportional to the level of H_2O_2 generation) in fibroblast cells at a dose of 2.16 SED (A). Data for the primary fibroblast cells was obtained by Dr Laura Hudson. No significant increase in ROS can be seen in donor-matched keratinocyte (B) and differentiated keratinocyte (C) cells. Statistical analysis was assessed using a one-way ANOVA with Dunnett's correction to compare all columns to the control (unirradiated) cells **** $P < 0.0001$ (error bars represent the SEM) $N=3$, $N=3$, $N=3$ respectively.

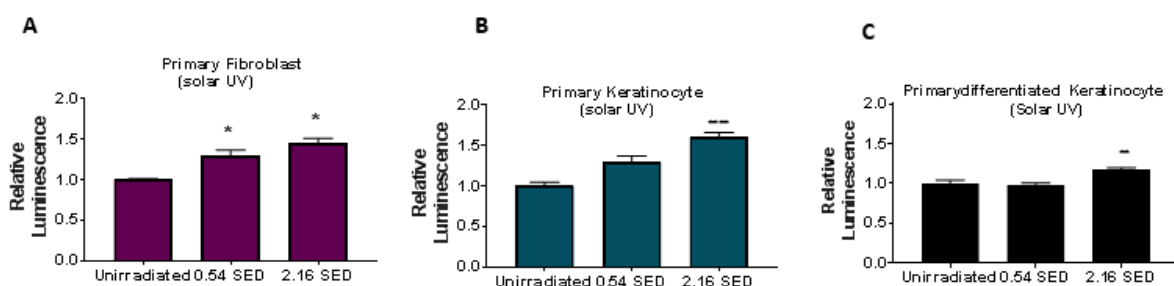


Figure 48: ROS generation in primary fibroblast, keratinocyte and differentiated keratinocyte cells following exposure to solar UV

Solar UV causes a significant increase in relative luminescence (proportional to the level of H_2O_2 generation) in fibroblast cells at a dose equivalent to 0.54 SED (A). Data for the primary fibroblast cells was obtained out by Dr Laura Hudson. A significant increase in ROS can be seen in donor matched keratinocyte (B) and differentiated keratinocyte (C) cells at a dose equivalent to 2.16 SED. Statistical analysis was assessed using a one-way ANOVA with Dunnett's correction to compare all columns to the control (unirradiated) cells * $P < 0.05$, **** $P < 0.0001$ (error bars represent the SEM) $N=3$, $N=3$, $N=3$ respectively.

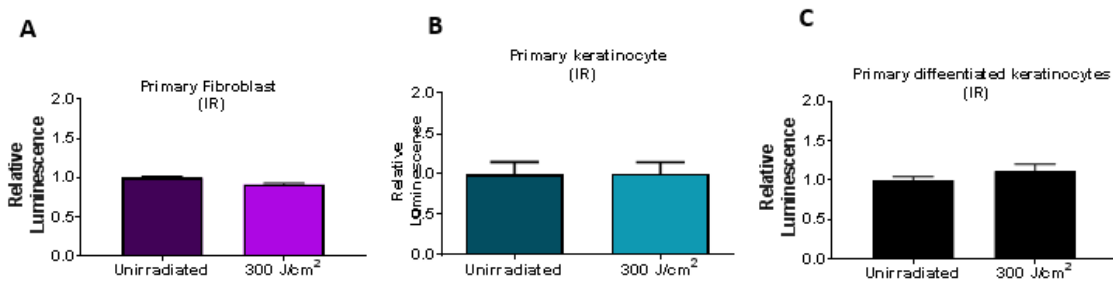


Figure 49: ROS generation in primary fibroblast, keratinocyte and differentiated keratinocyte cells following exposure to IR

IR (300J/cm²) did not cause a significant increase in relative luminescence (proportional to the level of H₂O₂ generation) in fibroblast cells (A). Data for the primary fibroblast cells was obtained by Dr Laura Hudson. Similarly no response can be seen in donor matched keratinocyte (B) and differentiated keratinocyte (C) cells. Statistical analysis was assessed using a one-way ANOVA with Dunnett's correction to compare all columns to control (unirradiated) cells (error bars represent the SEM) N=3, N=3, N=3 respectively.

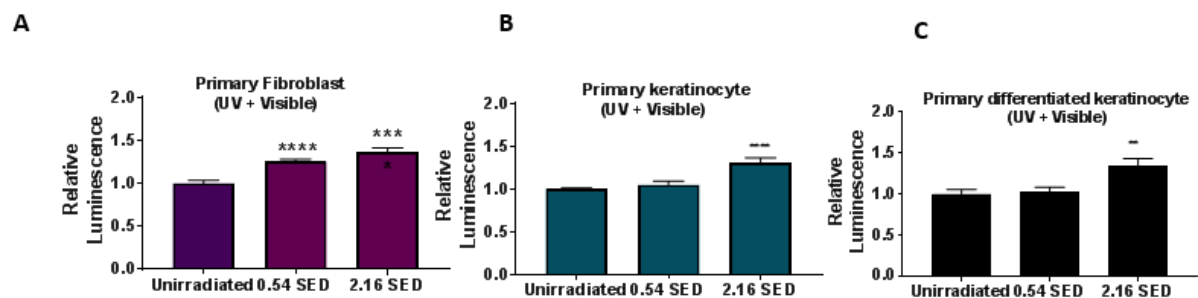


Figure 50: ROS generation in primary fibroblast, keratinocyte and differentiated keratinocyte cells following exposure to UV plus VIS

UV plus VIS at a dose equivalent to 0.54 SED causes a significant increase in relative luminescence (proportional to the level of H₂O₂ generation) (A). Data for the primary fibroblast cells was obtained by Dr Laura Hudson. A significant increase in ROS is seen in keratinocyte cells (B) and in differentiated keratinocyte cells (C) at a dose equivalent to 2.16 SED. Statistical analysis was assessed using a one-way ANOVA with Dunnett's correction to compare all columns to control (unirradiated) cells ****P<0.0001, **P<0.001 (error bars represent the SEM) N=3, N=3, N=3 respectively.

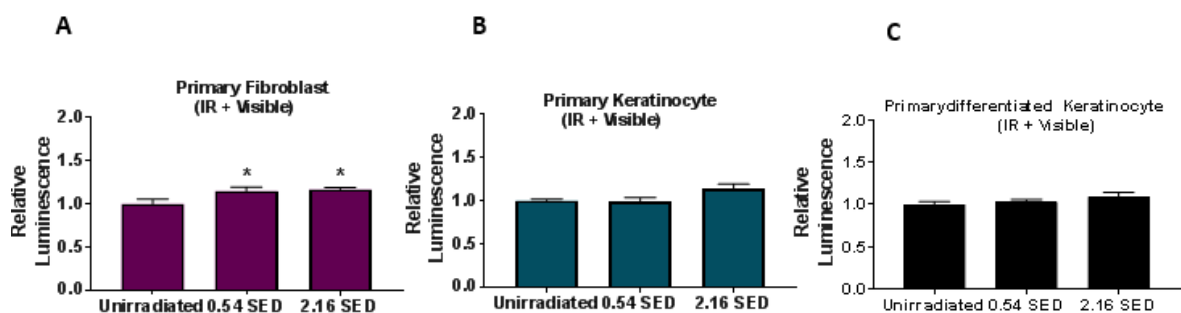


Figure 51: ROS generation in primary fibroblast, keratinocyte and differentiated keratinocyte cells following exposure to IR plus VIS

IR plus VIS at a dose equivalent to 0.54SED causes a significant increase in relative luminescence (proportional to the level of H₂O₂ generation) (A). Data for the primary fibroblast cells was obtained by Dr Laura Hudson. No significant increase in ROS is seen in keratinocyte (B) and differentiated keratinocyte (C) cells. Statistical analysis was assessed using a one-way ANOVA with Dunnett's correction to compare all columns to control (unirradiated) cells * P<0.05 (error bars represent the SEM) N=3, N=3, N=3 respectively.

3.3.4.6 Comparison of primary keratinocyte and HaCat cell response to solar light

HaCat cells have been reported to exhibit cellular differences when compared to normal human primary keratinocytes (Petit-Frère et al., 2000). A comparison was therefore made between the HaCat cell line and primary keratinocyte cells in terms of responsiveness to complete solar light and solar UV. No significant differences could be detected between the two cell types as shown in Figure 52.

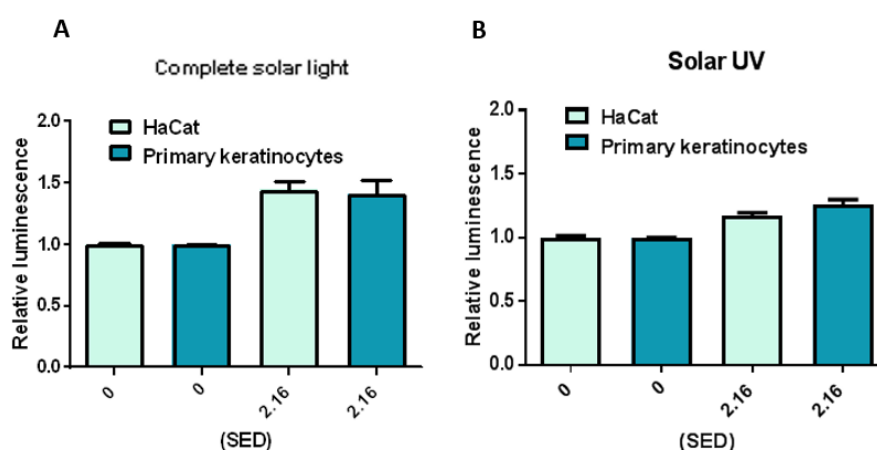


Figure 52: ROS generation response in HaCat and primary keratinocyte cells following exposure to complete solar light

No significant differences can be seen between HaCat and primary keratinocyte cell response to complete solar light (A) or solar UV (B) at a dose of 2.16 SED. Statistical analysis was assessed using a one-way ANOVA with Dunnett's correction to compare the mean of each column with the mean of every other column (error bars represent the SEM) N=2, N=3, respectively.

Data re-plotted from Figure 45 and Figure 50 shows that primary keratinocytes are more responsive to UV plus VIS as a response is seen with a lower dose of 2.16 SED compared to a significant response being seen in HaCat cells at 4.32 SED (Figure 53). At a comparable dose of 2.16 SED primary keratinocytes appear more responsive (0.31 fold increase) than the HaCat cells (0.11 fold increase in ROS) ($P < 0.005$). A similar response was detected in differentiated keratinocytes whereby they were more responsive to UV plus VIS when compared to HaCat cells ($P < 0.005$) (Figure 54).

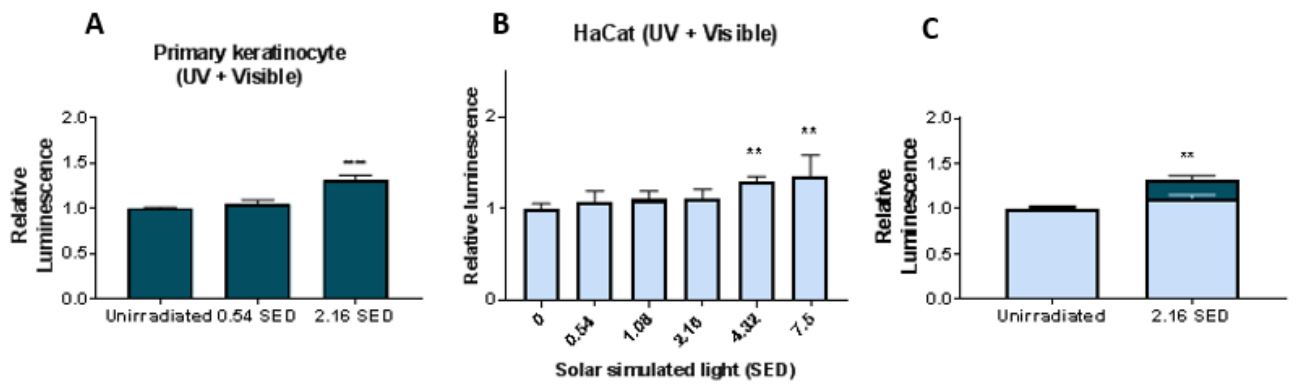


Figure 53: ROS generation comparison between primary keratinocyte and HaCat cells following exposure to UV plus VIS

The relative luminescence levels represent the amount of H₂O₂ generation following exposure of primary keratinocyte (A) and HaCat cells (B) to UV plus VIS. Primary keratinocytes show a ROS generation response at a dose equivalent to 2.16 SED (A). HaCat cells show a response at a dose equivalent to 4.32 SED (B). A significant difference can be seen between the response of primary keratinocyte and HaCat cells at a comparable dose of 2.16 SED (C). Statistical analysis was carried out to compare the mean of each column with the unirradiated control using a one-way ANOVA with Dunnett's correction. An unpaired T- test with Welch's correction was carried out to compare the mean of the two data sets (C) ***P<0.0001, **P<0.005 (error bars represent the SEM) N=3, N=3 respectively.

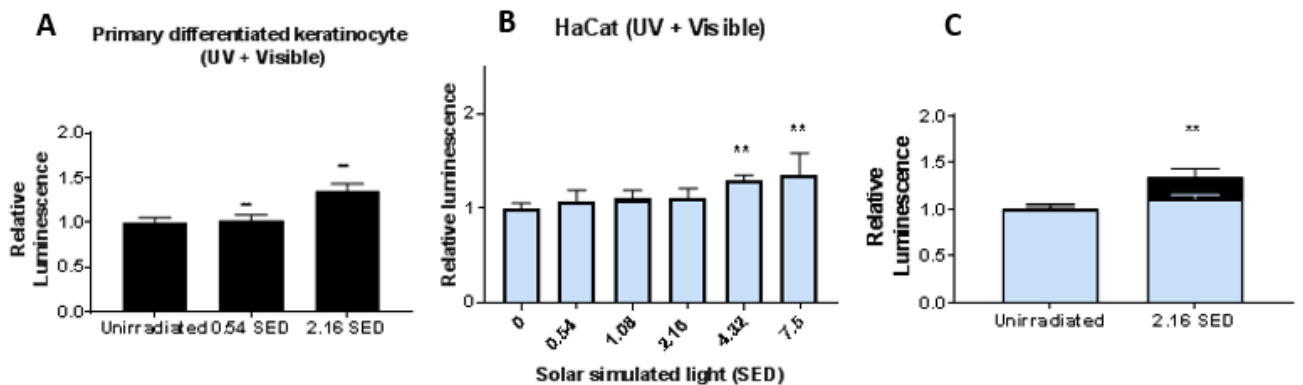


Figure 54: ROS generation comparison between primary differentiated keratinocyte and HaCat cells following exposure to UV plus VIS

The relative luminescence levels represent the amount of H₂O₂ generation following exposure of primary keratinocyte (A) and HaCat cells (B) to UV plus VIS. Primary keratinocytes show a ROS generation response at a dose equivalent to 0.54 SED (A). HaCat cells show a response at a dose equivalent to 4.32 SED (B). A significant difference can be seen between the response of primary keratinocyte and HaCat cells at a comparable dose of 2.16 SED (C). Statistical analysis was carried out to compare the mean of each column with the unirradiated control using a one-way ANOVA with Dunnett's correction. An unpaired T- test with Welch's correction was carried out to compare the mean of the two data sets (C) **P<0.005 (error bars represent the SEM) N=3, N=3 respectively.

3.3.5 mtDNA damage

The QPCR technique is also known as the long amplicon PCR or long extension PCR. The method can be used for measuring damage levels in nDNA and mtDNA without the need to separately extract cellular mitochondria. The QPCR method further allows for measurements of the relative mitochondrial genome copy numbers to be made. The principle of the assay relies on the fact that increased levels of DNA damage impede the progression of the DNA polymerase enzyme, thus resulting in a decreased amount of PCR product over a set amount of time (Bowman and Birch-Machin, 2015). The amount of PCR amplification product is inversely proportional to the level of intrinsic DNA damage present or induced following treatment with a genotoxic source. Treated samples are compared to untreated control samples and a relative level of damage can be quantified. Longer amplification products allow for an increased level of QPCR sensitivity as the polymerase enzyme is more likely to encounter a mutation. Damage can also be expressed as lesion frequency per 10kb through the Poisson distribution. The control DNA is defined as undamaged in this case. A small mitochondrial target is also amplified (usually 200bp or less) allowing for the normalisation of the mtDNA copy number as well as for measurements of changes to the mitochondrial copy number to be made (Baron and Suggs, 2014;Bustin, 2010;Bowman and Birch-Machin, 2015).

mtDNA is an excellent biomarker of solar damage as the DNA is able to withstand a high level of mutations. The DNA found within mitochondria has a limited number of repair mechanisms, for example it lacks the NER pathway which would otherwise remove UV damage and also lacks protective histones (Birch-Machin and Swalwell, 2010). Levels of mtDNA damage have been measured in previous studies using QPCR to amplify a long section of mtDNA, this is usually assessed within a large segment of mtDNA such as in the 11kb template (Swalwell et al., 2012a;Hunter et al., 2010;Ray et al., 2000a;Durham et al., 2003b;Eischeid et al., 2009;Kalinowski et al., 1992;Santos et al., 2002). Using QPCR analysis, the level of amplified double-stranded mtDNA product is detectable at each QPCR cycle via the binding of a dye which displays fluorescence once bound (Figure 55), the relative level of damage can therefore be determined by the number of cycles it takes before the level of amplified product reaches a certain threshold (CT) value. Therefore, those samples with a higher number of intact mitochondrial genomes (i.e. less damage) undergo more efficient amplification, and have a

lower CT value (Figure 56). The melting temperature of an amplification product is usually characteristic depending on the size of the amplicon product. This can be determined using melt curve analysis (Figure 57).

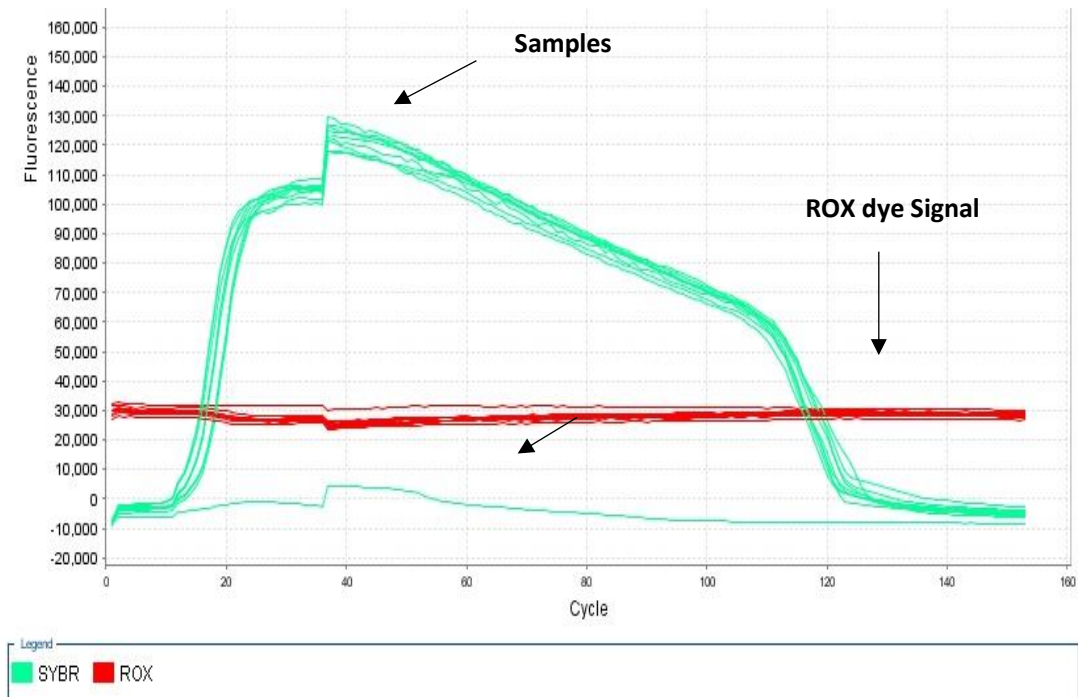


Figure 55: Showing a representative multicomponent plot

A representative image is shown with similar levels of SYBR Green being detected for each samples which suggests the presence of a similar amount of product amplification across the wells. Only SYBR green bound to the DNA was amplified. The signal measured is relative to that of the ROX baseline which had a fixed fluorescence (30,000 in all experiments assessed)

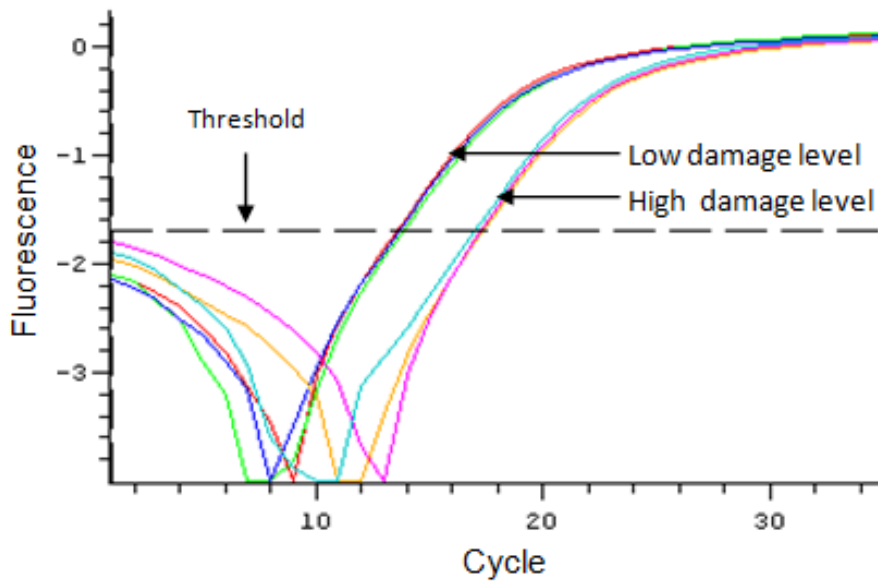


Figure 56: The principle of real-time QPCR.

The amplification plot shows two samples ran in triplicate, as shown by the coloured lines, one with low mtDNA damage and one with high mtDNA damage. A threshold is set, (black line) and the number of cycles it takes before the level of amplified DNA crosses this threshold is known as the CT, with a low value indicating low damage (or a high copy number) and a high value indicating high damage (or a low copy number).

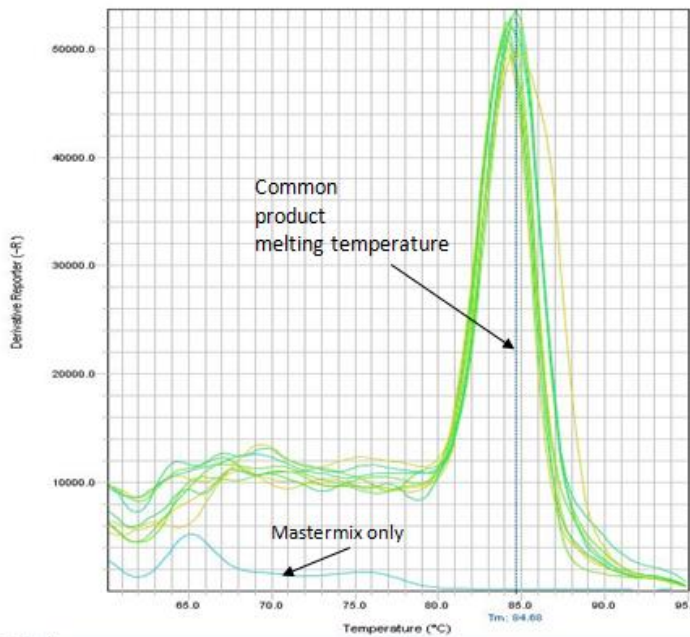


Figure 57: Showing a representative melt curve analysis

Products that have amplified specifically should show a characteristic melting temperature indicative of the product size (green line). No amplification should be detected in the negative control samples

3.3.5.1 mtDNA damage in HDFn cells following exposure to solar light

The level of mtDNA damage was assessed in HDFn cells using the 1kb fragment template QPCR assay. Further details on the assay can be found in the general methods (section 4.3.3). Cells in monolayer were dosed with either complete solar light or solar UV (2.16 SED) after which they were immediately processed for analysis. Complete solar light can be seen to cause greater levels of damage in HDFn cells compared to solar UV (Figure 58).

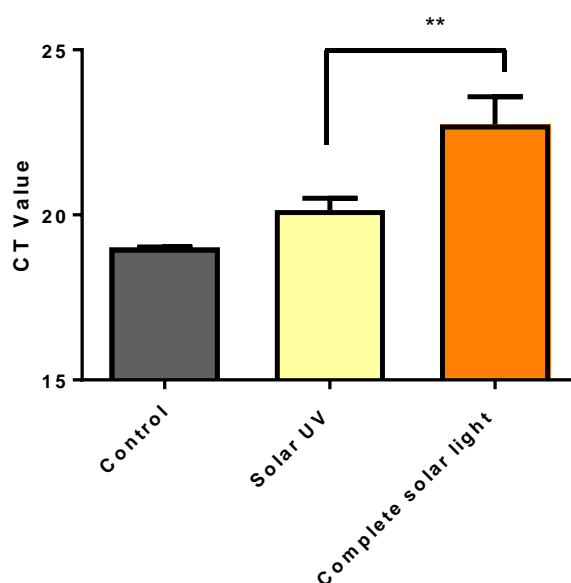


Figure 58: mtDNA damage in HDFn cells following exposure to solar UV and complete solar light

HDFn cells were exposed to either solar UV or complete solar light at a dose of 2.16 SED. The 1kb QPCR assay was used to assess the level of mtDNA damage relative to the unirradiated control. Statistical analysis was carried out to compare the mean of each column with the untreated control using a one-way ANOVA with Dunnett's correction $**P < 0.001$ (error bars represent the SEM) $N=4$.

3.3.5.2 Assessing mtDNA copy numbers following exposure to solar light

The mtDNA copy numbers were investigated using QPCR analysis through the amplification of an 83bp section from a control region within the D-Loop of mtDNA. A key requirement of the work was to determine the potential effect of different solar light sources on the cellular mtDNA copy numbers. This would establish how further assays involving mtDNA damage could be utilised. The QPCR assay used in this study has been described previously by Koch and co-workers (Koch et al., 2001). For their study, the authors used QPCR to determine

differences in mtDNA content between various patient samples. Furthermore, this assay has also been incorporated into a study where it was able to detect depleted mtDNA in immortalized (hTert) human fibroblasts by means of ethidium bromide exposure (Schroeder et al., 2008). The 83bp assay involves the amplification of a small 83bp segment of mtDNA. The principle of the assay is that this small segment of mtDNA is not located in any major/well documented deletion site and therefore amplification of this product is comparable to the amount of mtDNA present. Seeing as the QPCR method works on the basis of DNA quantification, it is crucial that the starting concentration of mtDNA is at a baseline level for each of the samples.

The mtDNA copy number was assessed in primary fibroblast (Figure 59) and keratinocyte cells (Figure 60) following exposure to 2.16 SED of complete solar simulated light. These experiments were carried to ensure that the higher dose of solar light did not cause a change in the mtDNA copy numbers. The CT values for each of the conditions tested were found to be within 1 CT meaning that the starting baseline levels of mtDNA were similar.

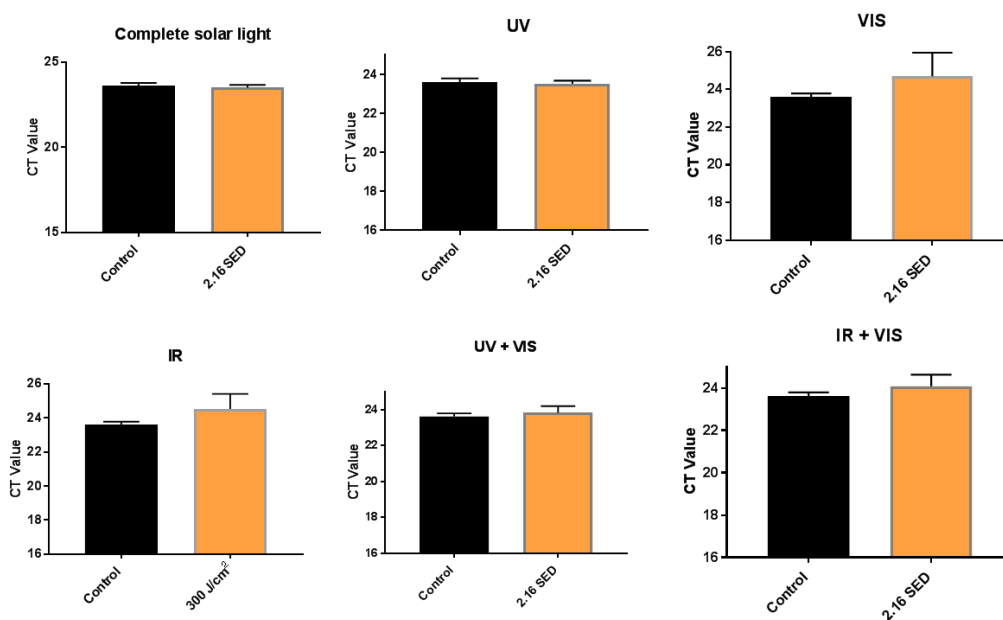


Figure 59: 83bp QPCR analysis showing mtDNA copy numbers in primary fibroblast cells following exposure to solar simulated light

Primary fibroblast cells were treated with each of the solar light dosing conditions (complete solar light, UV, VIS, IR, UV+VIS and IR+VIS) and the CT value compared to unirradiated control using the 83bp template QPCR assay. The level of mtDNA within the fibroblast cells was found to be unaffected by the solar light dosing conditions assessed. This suggests that the starting level of mtDNA was the same between irradiated and unirradiated control cells. Statistical analysis was assessed by applying an unpaired T test using Welch's correction, N=2.

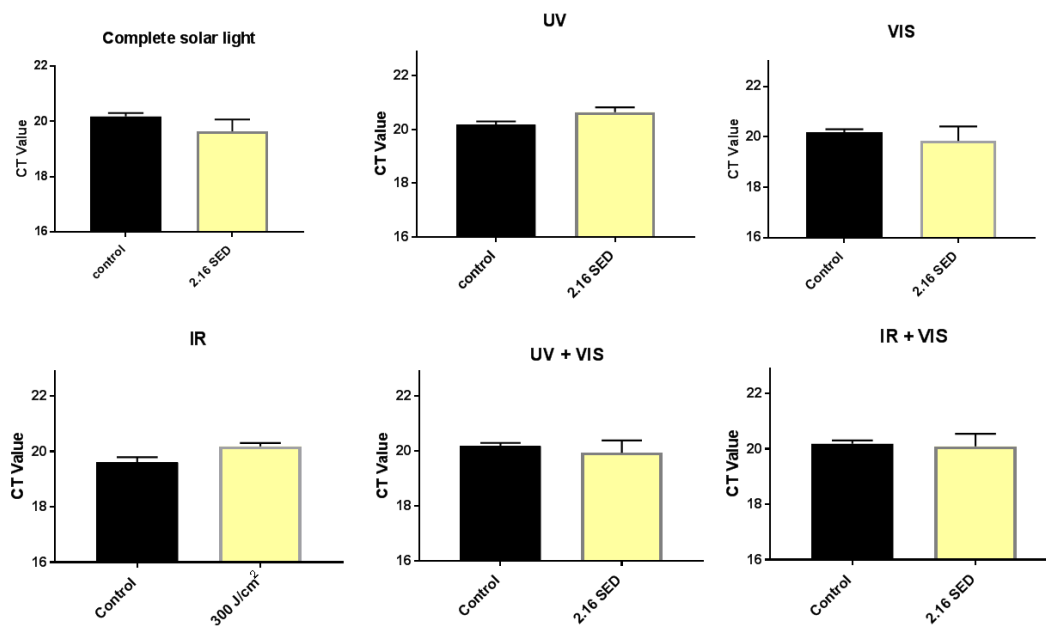


Figure 60: 83bp QPCR analysis showing mtDNA levels in primary keratinocytes following exposure to solar simulated light

Primary keratinocyte cells were treated with each of the solar light conditions (complete solar light, UV, VIS, IR, UV+VIS and IR+VIS) and the CT value compared to unirradiated control using the 83bp QPCR assay. The level of mtDNA within the keratinocyte cells was found to be unaffected by the solar light dosing conditions assessed. This suggests that the starting level of mtDNA was the same between irradiated and unirradiated control cells. Statistical analysis was assessed by applying an unpaired T test using Welch's correction, N=2.

3.3.5.3 Assessing mtDNA damage in primary skin cells following exposure to solar light

Following on from the ROS detection experiments, the level of mtDNA damage was assessed as a further biomarker in donor matched primary skin cells. Results for the QPCR data show similar findings to data obtained from the ROS detection assay. Low levels of mtDNA damage were detected when a dose of VIS (Figure 61), IR (Figure 62), IR plus VIS (Figure 63) and UV plus VIS (Figure 64) were applied. A 1CT significant difference relative to control can be seen in primary differentiated keratinocytes following exposure to 0.54 SED and 2.16 SED VIS ($P < 0.0001$) (Figure 61 C). Albeit the effects seen are marginal when compared to cells exposed to complete solar light (Appendix Figure 1.2).

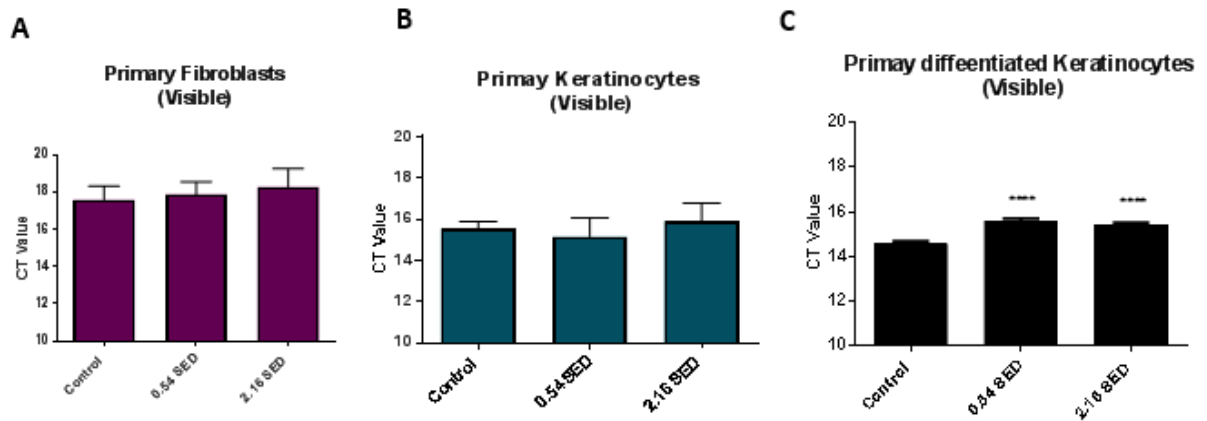


Figure 61: mtDNA damage in primary fibroblast, keratinocyte and differentiated keratinocyte cells following exposure to VIS

The level of mtDNA damage was assessed relative to the unirradiated control using the 11kb QPCR assay. VIS is not seen to have a significant effect on mtDNA damage in primary fibroblast (A) and primary keratinocyte (B) cells. A significant increase in CT is detected in primary differentiated keratinocytes exposed to VIS at doses equivalent to 0.54 and 2.16 SED (C). Statistical analysis was assessed using a one-way ANOVA with Dunnett's correction to compare all columns to control (untreated) cells ****P<0.0001 (error bars represent the SEM) N=3, N=3, N=3 respectively.

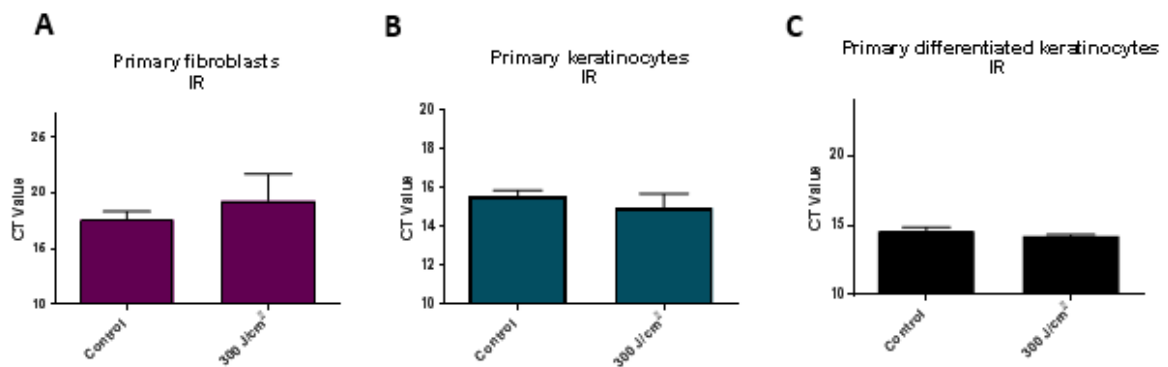


Figure 62: mtDNA damage in primary fibroblast, keratinocyte and differentiated keratinocyte cells following exposure to IR

IR (300J/cm²) does not cause a significant effect on mtDNA damage levels in primary fibroblast (A) keratinocyte (B) and differentiated keratinocyte (C) cells as assessed using 11kb QPCR assay. Statistical analysis was performed using a one-way ANOVA with Dunnett's correction to compare all columns to control (untreated) cells (the error bars represent the SEM) N=3, N=3, N=3 respectively.

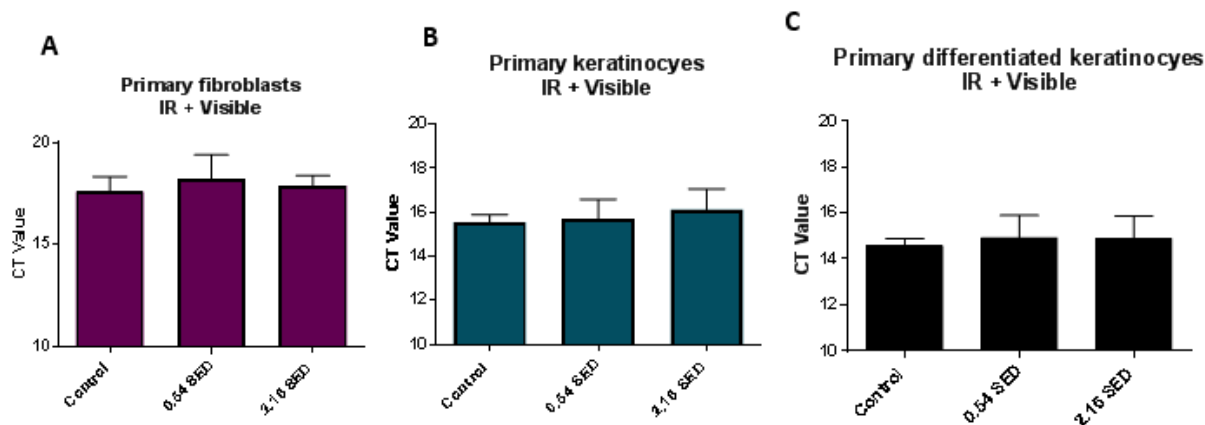


Figure 63: mtDNA damage in primary fibroblast, keratinocyte and differentiated keratinocyte cells following exposure to IR plus VIS

The mtDNA damage levels were assessed relative to unirradiated control cells following the application of IR plus VIS. This was carried out using the 11kb QPCR assay. IR plus VIS is not seen to have a significant effect on the level of damage in primary fibroblast (A) keratinocyte (B) and differentiated keratinocyte (C) cells. Statistical analysis was assessed using a one-way ANOVA with Dunnett's correction to compare all columns to control (untreated) cells (error bars represent the SEM) N=3, N=3, N=3 respectively.

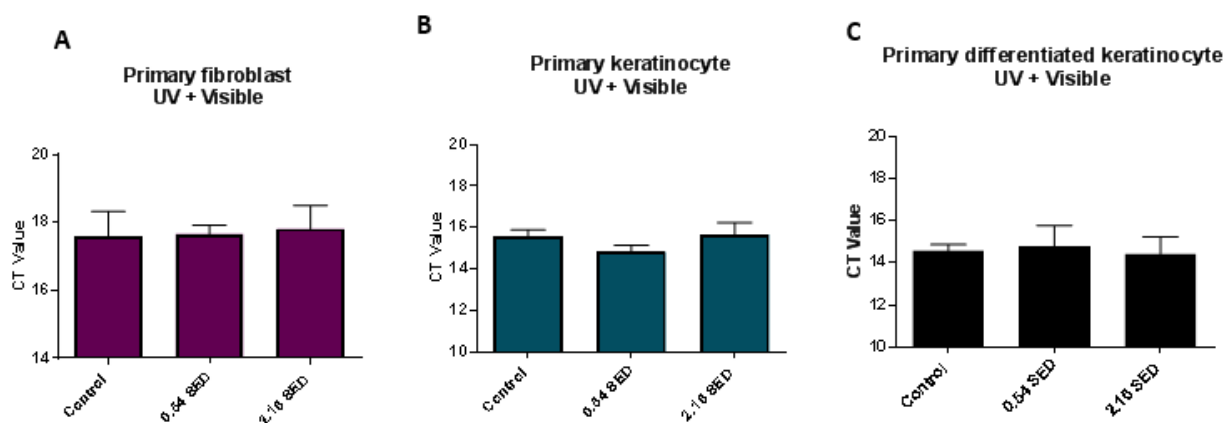


Figure 64: mtDNA damage in primary fibroblast, keratinocyte and differentiated keratinocyte cells following exposure to UV plus VIS

The mtDNA damage levels were assessed relative to unirradiated control cells following the application of UV plus VIS. This was carried out using the 11kb QPCR assay. UV plus VIS is not seen to have a significant effect on the level of damage in primary fibroblast (A) keratinocyte (B) and differentiated keratinocyte (C) cells. Statistical analysis was assessed using a one-way ANOVA with Dunnett's correction to compare all columns to control (untreated) cells (error bars represent the SEM) N=3, N=3, N=3 respectively.

3.3.6 Assessing UV and IR preconditioning in HDFn cells

A further question involved assessing whether pre-dosing fibroblast cells with IR followed by a dose of solar UV and vice versa influences the outcome of the biomarkers of damage detected. To investigate this question HDFn cells were dosed with IR (400J/cm²) and UV (4.32 SED) at doses which have previously been seen to induce detectable levels of ROS in the HDFn

cell type. The IR dose generated small amounts of ROS, whilst UV lead to a 2 fold increase in ROS generation compared to control (unirradiated) cells (Figure 65 A). When HDFn cells were dosed with UV followed immediately by IR, no significant difference was seen when compared to ROS generation in cells exposed to UV only. Similarly cells exposed to IR followed by UV showed no significant differences in terms of ROS generation (Figure 65 B).

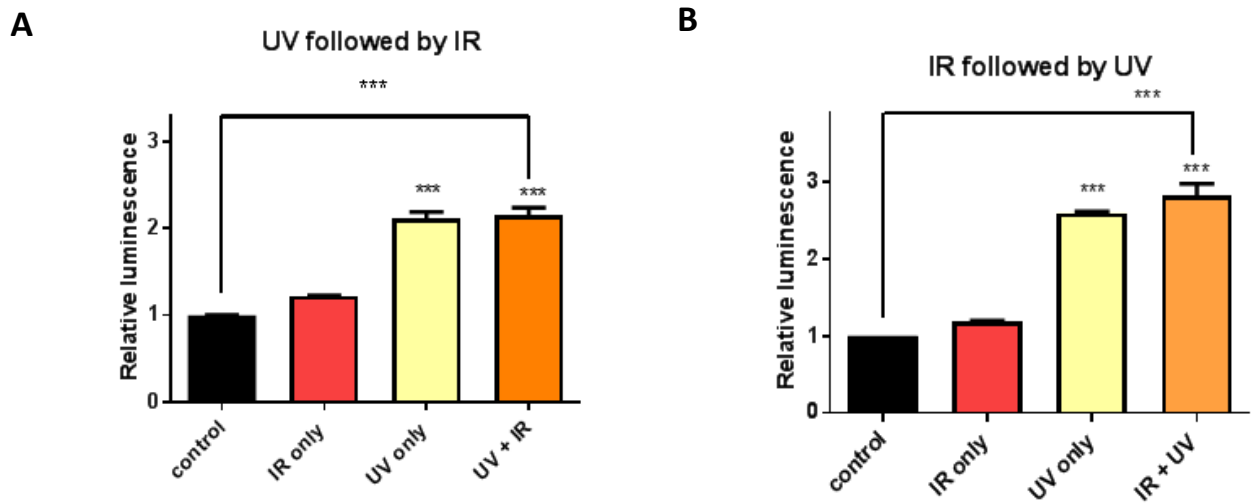


Figure 65: ROS generation response in HDFn cells following exposure to UV and IR

HDFn cells were irradiated with solar UV (4.32 SED) followed by a dose of IR (400J/cm²) and the level of ROS generation assessed using the ROS-Glo assay. Cells receiving a dose of UV followed by IR show no significant differences in ROS generation compared to UV only (A). Similar findings are seen when a dose of IR (400J/cm²) is applied prior to dosing the cells with UV (4.32 SED) (B). Statistical analysis was assessed using an unpaired T test using Welch’s correction (error bars represent the SEM) ***P<0.0001 N=2, N=3 respectively.

3.4 Discussion

3.4.1 Doses of complete solar light and IR assessed did not induce cytotoxicity

An essential aspect of the project involved determining sublethal doses of complete solar light and IR able to induce a detectable level of damage in cells. Single doses of complete solar light (0.54 and 2.16 SED) were not found to contribute to considerable cytotoxic effects in primary fibroblast and keratinocyte cells. In HDFn cells higher doses of solar light were applied with no cell death being detected at doses of up to 8.64 SED.

Similarly IR (800J/cm²) was not found to induce cytotoxic effects in the skin cells assessed. This is consistent with findings from Gonzalez et al., whereby a single dose of IRA ranging from 300-1220cm⁻² showed no effect on cell viability in fibroblasts (Gonzalez et al., 2015). Another paper did not find an effect on skin cell viability when using an irradiance of 1900w/m⁻² which according to the authors is 5 times greater than the level of IRA present within natural solar radiation (Piazena et al., 2014). Multiple irradiations (10 in total) of IRA at a dose of 20J/cm² were reported to induce cell death in human fibroblasts. The time span between irradiations was not however specified in the study (Tanaka and Gale, 2015).

The amount of IR dose received by the general public is not well defined in the literature due to the multiple factors involved (Akhlaya et al., 2014). There is a lack of data available on human exposure to solar radiation during recreational activities perhaps due to the absence of personal dosimeter devices (Diffey and Cadars, 2016). Exposure to IR is therefore estimated from predictions of the time spent outdoors in a horizontal or vertical stance from the sun as well as factors such as cloud cover and seeking shade. According to Diffey et al. 2016, the maximum human exposure to IR at the Earth's surface at noon during the summertime would be 250J cm² and for many people just a few tens of Jcm² (Diffey and Cadars, 2016).

3.4.2 Solar light sources used did not result in considerable heating effects

Changes in skin temperature have been reported to cause biological responses in skin cells such as the induction of heat shock protein. Heat generation in skin is thought to be involved in the ageing process, for example heat has been found to regulate the expression of tropoelastin and fibrillin-1, two major proteins of elastic fibres in human skin (Kim et al., 2005). Numerous studies have looked at IR effects in skin however it has been highlighted that some sources have also emitted UV and or VIS. It has also been argued that the doses received are in excess of real life exposure scenarios. Such factors have contributed to the contradictory findings within the literature (Diffey and Cadars, 2016). Numerous studies have used an IRA source without the application of a water filter or a contact cooling system. Such experiments risk a substantial amount of IRA energy being absorbed in the superficial skin layers, with only limited amounts of IRA energy being delivered to deeper tissues. The effects of the incident

IRA therefore would not be sufficiently evaluated as only the thermal effects, and not the non-thermal biological effects would be observed (Barolet et al., 2016; Tanaka and Gale, 2015).

The physiological temperature of skin is between 27.6-33.1°C, this can go up to 43-45°C when in the sun (Kleesz et al., 2012). Heating effects have been reported to induce the expression of (MMP) 1, 2 and 9 in human skin fibroblast (Park et al., 2004). When assessing the effects of IR on skin, such heating effects can act as a confounding factor (Akhalya et al., 2014). Whether the direct action of IR radiation and/or the secondary IR-induced heating effects are responsible for the pathological outcomes observed in human skin is yet to be clarified (Barolet et al., 2016).

An essential part of this chapter involved ensuring that the solar light sources were not creating considerable heat. Temperature measurements were taken over a time span that was representative of the dose that the cells would be exposed to during the experiments. No considerable heating effects could be detected above physiological level from the Hydrosun lamp or Newport Solar Simulator. This ensures that any potential damage response detected in the experiments carried out therefore cannot be equated to heat energy.

3.4.3 The level of cellular damage markers detected when UV, VIS, and IR are applied individually and in combination does not correspond to the level seen when all three components are present simultaneously

Work presented in this chapter involved assessing donor matched skin cells from patient samples. Use of donor matched cells reduces the risk of variability which may otherwise be seen due to possible biological differences between patient samples. For example experiments carried out by Schroeder et al., found that 20% of individuals were not seen to be responsive to the dose of IRA applied out of the 23 samples assessed (Schroeder et al., 2008). Such findings were also reported in in vitro whereby some of the cultured donor fibroblasts did not respond to IRA due to interindividual variability. No obvious correlation between skin type and response to IRA was reported however the authors mention that the cohort was small and all but one donors was either type I, II or III (Schroeder et al., 2008).

Donor matching was carried out for the samples assessed with skin pieces being initially selected for culturing and further analysis based on the samples morphological appearance and health. Prior to solar light dosing, cells were plated at similar times and at the same passage number. The different dosing conditions were carried out simultaneously on a single plate for each donor to minimise any experimental variability. ROS generation was assessed as this is thought to be one of the initial responses to complete solar light or solar UV exposure (Rinnerthaler et al., 2015;Hudson et al., 2016). An increase in the intracellular ROS levels may directly induce damaging effects or result in the activation of further downstream signalling pathways as reported by Pittayaprupek et al., 2016 (Figure 66). Exposure to IR has been shown to result in the generation of ROS however this topic remains controversial due to the different findings reported in the literature (Schieke et al., 2003;Barolet et al., 2016a;Tanaka and Gale, 2015;Jantschitsch et al., 2009). There is also evidence that ROS induction occurs following exposure to VIS later resulting in skin pigmentary effects (Randhawa et al., 2015). mtDNA damage was also assessed due to the close proximity of mtDNA to the main site of ROS generation (Hudson et al., 2016). The level of nDNA was investigated as a further biomarker of damage as solar radiation is known to induce nDNA damage responses within skin particularly during prolonged exposures (Kvam and Tyrrell, 1997;Rinnerthaler et al., 2015).

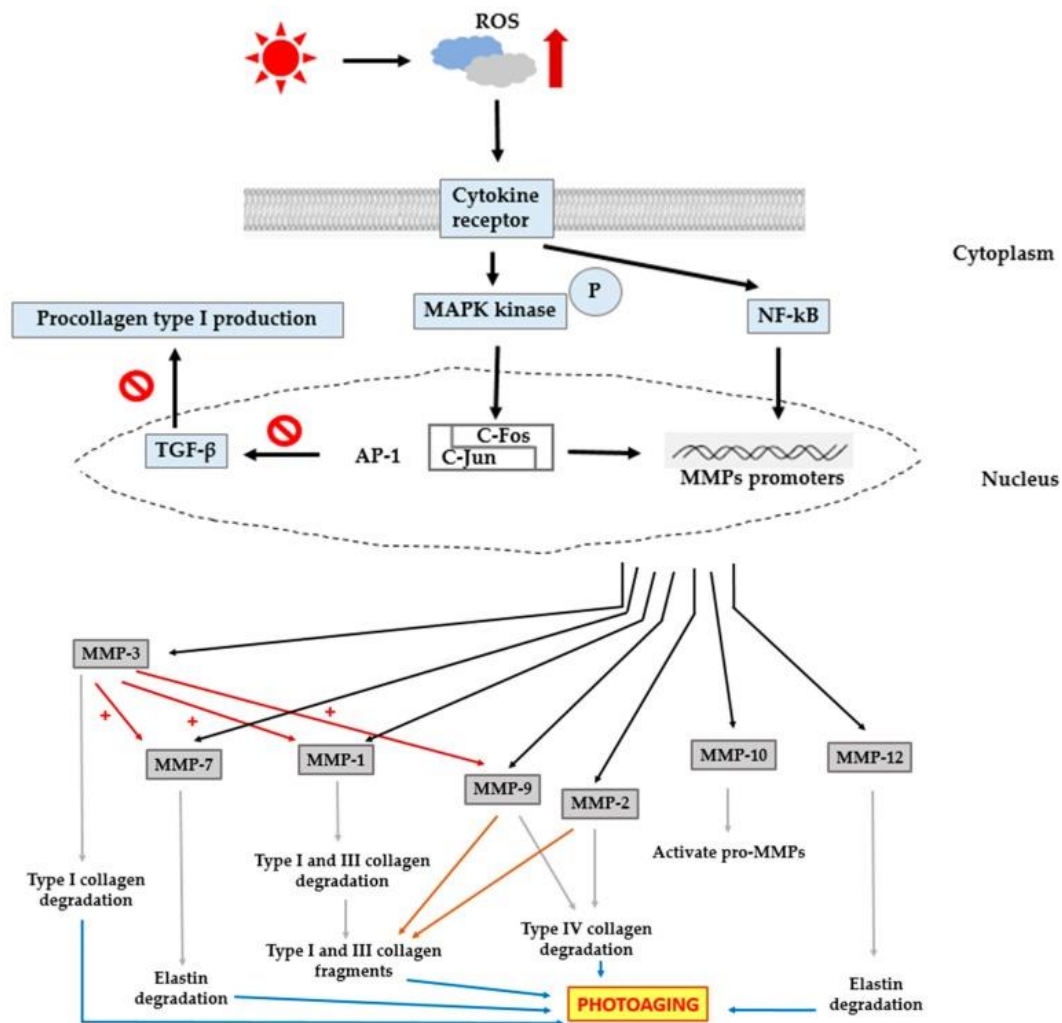


Figure 66: Schematic diagram showing an example of the effect of ROS on cellular response in skin (Pittayapruek et al., 2016).

UV-induced excess intracellular ROS activates mitogen-activated protein kinases (MAPKs) and nuclear factor-kappa B (NF-κB). This leads to the transcriptional regulation of MMPs, and results in the degradation of collagen and elastin thus subsequently leading to skin photoaging. As illustrated in Figure 66, AP-1 inhibits transforming growth factor beta (TGF-β) signalling, causing a reduction in procollagen synthesis therefore further contributing to the photoageing process (Pittayapruek et al., 2016).

DCFDA detects intracellular ROS in a non-specific ROS species manner. When used with the appropriate controls taking into account both background noise and factors which may affect probe stability, the DCFDA method can be used successfully to identify the levels of intracellular ROS present (Tetz et al., 2013; Boulton et al., 2011). Previous work in the lab has

demonstrated that irradiation of the DCFDA probe can cause instability leading to an overestimation of ROS levels (Boulton et al., 2011). For this reason the DCFDA probe was applied following the cellular irradiation steps with exposure to direct light being avoided during the course of the experiment. The ROS-Glo assay more specifically detects H₂O₂ levels present within a sample. Although both methods detected a similar trend in ROS generation, the ROS-Glo assay appears to be more sensitive. ROS-Glo was therefore used in subsequent experiments to allow for the detection of lower amounts of ROS which may otherwise be undetectable.

Experiments carried out in this chapter clearly demonstrate that removing the IR and VIS components from complete solar light markedly reduces the level of ROS generation in both primary fibroblast and HDFn cells. This suggests that IR and VIS may potentially be contributing either through an additive effect or alternatively the biomarkers of damage detected may be due to the synergistic effects of IR, VIS and UV.

Further confirmation of the role of IR and VIS in the ROS generation process was seen from experiments involving the assessment of the nDNA and mtDNA damage levels. More nDNA damage could be detected when IR, and VIS were present alongside UV. These findings prompted further investigations to assess the contribution of the individual components of solar light and components in combination. During the experiments the overall dose of solar light given was kept constant with only the wavelengths reaching the cells from the solar source being altered. The doses applied (IR, VIS, IR plus VIS and UV plus VIS) therefore represent the proportions of those wavelengths estimated to be present within a particular dose of complete solar light. Furthermore, effects of the individual components and components in combination gave a marginal increase in ROS and mtDNA damage. The effects of the individual components did not appear to be additive which therefore supports the occurrence of synergy.

Solar radiation is polychromatic and its effects on skin are not only the result of the separate action of each wavelength but rather the result of the interaction of the numerous wavelengths (Cho et al., 2009). Perhaps when acting as complete solar light the effects are exacerbated due to the synergistic disruptive effect of solar light on multiple cellular

processes. To my knowledge this is a novel finding as solar light effects have not been previously compared as carried out in this chapter. UVA, UVB, IR and VIS target different chromophores within the skin. UV is absorbed mainly by DNA and some aromatic amino acids whilst IR is absorbed predominantly by the mitochondrial cytochrome C complex. Less is known about the chromophores for VIS however potential chromophores reported include, riboflavin, bilirubin and hemoglobin as well as melanin and β -Carotene all of which have been shown to have the ability to absorb in the VIS region and are present in skin (Liebel et al., 2012). Although IR, VIS and UV have been reported to generate ROS within cells, they do so through different mechanisms. Calles et al., carried out a microarray analysis on primary human skin fibroblasts and found 599 IRA-regulated transcripts (Calles et al., 2010). The transcriptome observed following exposure to IR (860J/cm²) differed from that found when fibroblasts were exposed to UV radiation. The authors selected 13 of these IRA induced genes for further analysis using real-time PCR. The genes were involved in processes such as calcium homeostasis, apoptosis, stress signalling and the extracellular matrix regulation. A major part of the response was triggered by mitochondrial ROS and to a lesser extent non-mitochondrial induced ROS (Calles et al., 2010).

Solar UV, particularly the UVA component is known to lead to ROS generation resulting in the indirect DNA damaging effects observed (de Gruijl, 2000). UV also induces damage through the peroxidation of membrane lipids via the generation of lipid peroxides. A depletion in the level of endogenous antioxidants and various skin enzymes may also be seen. This includes a reduction in the levels of ubiquinone, glutathione reductase and catalase (Liebel et al., 2012). An increase in proinflammatory cytokine levels including interleukin-1 α (IL-1 α) and tumour necrosis factor- α (TNF- α) has been found in fibroblast and keratinocyte cells following exposure to UV (Bashir et al., 2009). UVA and UVB have been demonstrated to induce ROS production in human skin equivalents leading to the downstream expression in MMP-1 and IL1- α (Liebel et al., 2012). Further to this, UV is well known to lead to an increase in both nDNA and mtDNA (Birch-Machin and Wilkinson 2008). It was therefore expected that solar UV would lead to the generation of damage albeit at low levels at the doses assessed.

Only a small number of studies have assessed the effect of VIS on skin. Liebel et al., 2012 suggested that VIS with a solar irradiance of 50mW cm² applied at a dose of 40-240J cm² would be equivalent to 15-90 min outdoors in the mid-summer sun in Houston TX. The authors

demonstrated that at these doses VIS was able to induce ROS in human epidermal skin equivalents as the level of intracellular H₂O₂ was seen to increase. Doses of 65, 130 and 180J/cm² were reported to induce a 5, 9 and 18 fold increase in ROS respectively. An increase in MMP-1 expression and a dose dependent increase in IL1- α were also observed. The finding that VIS leads to ROS generation was confirmed in human skin in vivo using a chemiluminescence detection method whereby free radical generation was detected. This generation was later partially decreased following the application of sunscreen formulations containing antioxidants (Leibel et al., 2012). When assessing the effects of VIS on nDNA damage, no damage was seen in terms of thymine dimer formation even when doses that were high enough to produce the ROS effects were used. The authors do however mention that other forms of DNA damage may exist such as 8-Oxoguanine which were not accounted for in the study. Exposure of AS52 Chinese hamster cells to VIS (400-450nm) has previously been shown to result in the formation of 8-Oxoguanine DNA lesions (Kielbassa et al., 1997).

IRA is thought to exhibit effects on skin through two main mechanisms with one being a direct interaction with the mitochondrial cytochrome C component leading to the disruption of the ETC, inadequate energy production and a substantial level of ROS production. Alternatively an indirect action may occur due to heat generation resulting in the mobilisation of heat stressor proteins and heat sensors promoting the inward flux of calcium in to cells. Both these mechanisms are thought to lead to the generation of MMP and the associated skin ageing phenotype.

IR doses as small as 30J/cm² and 54J/cm² have been reported to have an effect on fibroblast cells (Danno et al., 2001; Schroeder et al., 2007). Studies have shown IRA to induce the expression of MMP-1 both at the mRNA and protein level in dermal fibroblasts. Kim et al., report that this was independent of heating effects as heat shock protein 70 was not expressed (Kim et al., 2006). Grether-Beck showed an increase in the mRNA level of MMP-1 following the exposure of human dermal fibroblasts to 360J/cm² IRA (Grether-Beck et al., 2015). IR has also been found to increase MMP-3, MMP-13 mRNA as well as increasing the expression of UV induced MMP-2 and MMP-9 in hairless mice (Kim et al., 2005). Furthermore, MMP secretion has been reported in keratinocytes and inflammatory cells following exposure

to IR (Cho et al., 2009). Schroeder et al., carried out an in vivo study on human buttock skin in order to assess the relevance of the in vitro findings. Human skin was subjected to physiologically relevant doses of IR (360 and 720J/cm²) thought to be achievable within a few hours on a summers day in central Europe (Schroeder et al., 2008). It has however been suggested that these doses may be too high in relation to physiological levels (Diffey and Cadars, 2016). Schieke et al., predicted the exposure to IR on a summers day as being 75J/cm²/h (Schieke et al., 2003).

Some studies have found no response following exposure of skin cells to IR. Kim et al., 2016 did not find an increase in the level of MMP-1 expression following a single exposure despite the findings of Schroeder et al., 2007. The authors reported that a single IR dose did not cause any increase in MMP-1 expression however multiple doses were able to induce a response (Kim et al., 2006). Another study assessed dermal fibroblasts taken from donors between the ages of 40-54. A dose of IR from the hydrosun lamp was applied (20-162J/cm²) and fluorescence immediately recorded via the DCFDA method whereby it was found that 40J/cm² was able to produce significant levels of ROS (Robert et al., 2015). In an experiment carried out by Cho et al., buttock skin of healthy volunteers aged 24-43 was dosed with natural sunlight (1-1.3 MED). Regions were either covered with a UV filter or black cloth to eliminate UV or IR respectively. Skin samples were analysed for MMP, type I procollagen and inflammatory cell expression 24h later. The authors mention that heating effects were controlled for prior to the irradiation process. Complete natural sunlight, UV only and IR plus VIS plus heat were all found to increase the production of MMP-1 and MMP-9 in human skin both at the mRNA and protein level. Similarly type I procollagen was decreased following exposure to the different conditions described, both these occurrences are thought to contribute to skin ageing effects (Cho et al., 2008).

3.4.4 Fibroblasts are more sensitive to longer wavelengths of solar light when compared to keratinocytes

Primary fibroblasts appear to be relatively more sensitive to the longer components of solar light (IR and VIS) when compared to keratinocyte cells. This finding was also seen in cell line whereby HDFn cells appear to be more responsive relative to HaCat cells. Higher doses of solar light were applied to the HDFn and HaCat cells with the same trend in responsiveness to longer wavelengths being seen at doses beyond those used in primary cells. Keratinocytes have previously been shown to be less sensitive to IRA (Latimer et al., 2015). Experiments carried out in this chapter demonstrate that keratinocyte cells are less responsive to both the IR and VIS components of solar radiation. The lower sensitivity of keratinocytes to longer wavelengths may be due to their antioxidative capacity which is several fold higher than that of fibroblasts (Applegate et al., 1995). This therefore enables keratinocytes to withstand exposure to higher doses of IR and VIS. The main way in which the IR component acts is through eliciting a retrograde signalling response which is initiated in the mitochondrial ETC (Schroeder et al., 2007). Keratinocytes have also been reported to have a relatively smaller mitochondrial electron transport chain relative to fibroblasts (Hornig-Do et al., 2007). IR is mainly absorbed by the Cytochrome C oxidase (COX) components in mammalian cells. COX serves as a generator of ROS in keratinocyte cells therefore the smaller ETC would mean less generation of ROS following exposure to IR as there is a lower level of ETC activity (Applegate et al., 1995; Akhalaya et al., 2014; Latimer et al., 2015). Less is currently known about the mechanism of action of VIS and the interaction between VIS and IR (Sklar et al., 2013; Barolet et al., 2016a).

3.4.5 Primary keratinocytes show signs of greater sensitivity when compared to HaCat cells

Due to HaCat cells being an immortalised cell line (Boukamp.P and Fusenig, 1988) concerns over potential abnormalities has been reported previously in the literature (Seo et al., 2012). Primary human keratinocytes have been demonstrated to show different sensitivity levels when compared to cell line. For instance Hoh and Maier reported that primary keratinocytes showed lower sensitivity levels relative to the HaCaT or 3T3 cells (Hoh and Maier, 1993). Further investigations were carried out in this chapter to assess whether the response seen in

HaCat cells is similar to that found in primary keratinocytes. The experiments indicated no significant differences in terms of response to complete solar light. HaCat cells were however significantly less responsive to the UV plus VIS component of solar light when compared to primary keratinocytes. Similar effects are also observed when HaCat cells are compared to differentiated keratinocytes following exposure to UV plus VIS.

3.4.6 Skin cells assessed had similar baseline mtDNA copy numbers

The mtDNA numbers can vary between individual patient samples as well as regionally within the body and can also differ with the age of the donor skin (Venegas et al., 2011). For quality assurance samples that are to be investigated for mtDNA damage levels first undergo determination of mtDNA copy number through the use of the 83bp fragment template QPCR assay. This is to ensure that the same amount of mtDNA is used at the start of the experiment as the amount of DNA can be a confounding factor in the QPCR assay. What was also of interest was any difference in mtDNA content created by irradiation as this may over/under estimate any damage induction recorded. The baseline levels of mtDNA between the different donor cells assessed were similar. No significant differences in CT value between the conditions assessed were detected therefore it was concluded that the various conditions assayed did not alter the mtDNA content.

3.4.7 Treating cells with IR followed by UV has no effect on ROS generation

The VIS and IR components of solar light are interestingly the predominant wavebands of solar radiation during the morning hours. At around noon UVA and UVB become the predominant wavebands. This has led to the theory that IR preconditioning primes skin cells before being exposed to the higher levels of damaging solar radiation at noon (Frank et al., 2006). There is evidence that priming cells with doses of IR prior to UV exposure results in protective effects in skin fibroblasts. Experiments have been carried out previously in vitro using human fibroblasts and in vivo using murine models. Priming human dermal fibroblast cells with IR was essentially found to provide a photoimmunoadaptive response whereby the cells were better able to resist subsequent UVB induced damage (Frank et al., 2006). Exposure to IR followed by UV has been reported to provide protection in rat skin however UVB exposure followed by

IR was found to cause damage (Gonzalez et al., 2015). Experiments carried out in this chapter did not show any effect on ROS generation in HDFn cells when priming with IR prior to UV dosing and vice versa. According to other studies, only at high doses is IR able to generate highly reactive singlet oxygen and hydroxyl radicals in human skin. For example at low doses (1–10 J/cm²), IR is not thought to generate highly reactive singlet oxygen and hydroxyl radicals, whilst at high doses (>120 J/cm²) these effects have been reported (Akhalya et al., 2014). Experiments by Tanaka illustrate that skin tumours appear faster after irradiation with complete solar light compared to irradiation with UV alone (Tanaka, 2012). The UV component of solar light is well known to contribute to skin cancer, there have been no reports however of skin cancers arising as a result of the IR component solely. It has however been speculated that when IR and UV interact together they lead to an enhancement in tumour development (Kimeswenger et al., 2016). Other studies have shown harmful effects following IR pre-exposure such as a decrease in the rate of UVB induced apoptosis therefore leading to an increase in the survival rate of cells with greater DNA mutation levels. IR has been found to confer resistance to UV-induced apoptosis by reducing the amount of DNA damage and up regulating the level of antiapoptotic proteins (Jantschitsch et al., 2009). Murine keratinocyte cells were used to assess the interplay between IR and UV with regards to UV induced apoptosis. IR preconditioning was found to decrease UVB induced apoptosis following exposure which was assessed 16h later. At the same time an increase in nucleotide excision repair (NER) was seen in keratinocyte cells and in vivo in wildtype mice. IR on its own did not induce sunburn cells as assessed histological in the epidermis via hematoxylin and eosin (H&E) staining. IR (250J/cm²) plus UVA (55mJ/cm²) was found to reduce apoptosis in murine model keratinocytes. The authors demonstrated that DNA damage levels were lower in mouse keratinocyte cells pre-exposed to IR (135J/cm²) followed by UVB 3h later (Jantschitsch et al., 2009).

In vivo photocarcinogenesis studies were performed in a mouse model where Jantschitch et al., treated mice with UV only, IR only and a combination. Mice given doses of UV were expected to develop tumours within 200 days. The median time for tumour development in the combined dose of IR followed by UV was 74 weeks whereas in UV only the median time was 9 weeks. A decrease in the level of p53 mutated clone in skin was also seen, however once developed the tumours in mice pre-treated with IR grew faster as shown by the

enhanced expression of Ki-67. More sarcomas and epithelial tumours were seen amongst the group of mice pre-treated with IR indicative of more aggressive cancers. The authors state that IR may delay the onset of UV-induced tumours however it might also contribute to a worse outcome by shifting the tumour into a more aggressive type. Essentially such work would serve as evidence to incorporate IR protection into sunscreens (Jantschitsch et al., 2011). Dover et al., 2015 argued that IR alone may be carcinogenic however this was not seen to be the case in mice as no tumours were seen with IR only.

Kimeswenger et al., investigated the link between melanoma and IR plus UV as either a simultaneous exposure or through preconditioning human primary melanocyte cells. The authors investigated the effect of IR followed by UV exposure on DNA damage repair and UVB induced apoptosis. The balance between the two mechanisms is thought to affect malignant transformation. IR was found to reduce the level of UVB induced apoptosis by altering the expression and activity of apoptotic proteins mainly in the extrinsic pathway, no effect on the DNA repair mechanisms was seen in melanocytes. The authors conclude that IR may contribute to melanomagenesis by increasing the survival rate of melanocyte cells carrying defective DNA mutations (Kimeswenger et al., 2016).

3.5 Summary of main findings:

- Solar UV alone has moderate effects on ROS generation therefore suggesting a role for the IR and VIS components.
- The level of ROS generation detected following the application of UV, VIS, IR and combinations does not correspond to the level seen with complete solar light. Data for the mtDNA and nDNA damage is in agreement with ROS generation experiments.
- Fibroblast cells appear to be more sensitive to longer wavelengths of solar light when compared to keratinocytes.
- Priming HDFn cells with IR followed by UV exposure has no effect on ROS generation, this was also seen when cells were dosed with UV followed by IR.

**Chapter 4 – Protection Against
Solar Radiation Induced Damage
in Human Skin**

4 Chapter Overview

High doses of solar light and/or excessive unprotected exposures may have detrimental effects on human skin those of which including premature ageing as well as the development and progression of skin cancer (Birch-Machin and Wilkinson, 2008). This is in contrast to the positive and health promoting effects of moderate solar light exposure such as the role of the UVB component in vitamin D production, increase in nitric oxide (NO) levels and the general feeling of wellbeing during exposure (Holick, 2016). Attitudes towards solar light exposure and protective strategies have changed over time. Initially people were seeking protection from the sun to avoid painful burns and darkening of the skin. Darker skin was seen to be a mark of lower socio-economic status for a long time until the popularisation of the tan in the early 1920's. Darker tanned skin later became associated with recreational outdoor activities and being able to access sun filled holiday destinations (Picton, 2013). Interestingly sunscreens have been available since the time of the Egyptians where they are thought to have existed in forms such as clay and mineral powders. During the time of the ancient Greeks sunscreens in the form of a mixture of oil and sand were used to protect skin against sunburn (Schalka and Reis, 2011).

The link between sun exposure and skin cancer was suggested in the early 20th century and was later established by an Australian scientist, Norman Paul. A few years later German scientists, Wilhelm Vahle and Karl E discovered the association between UVB exposure and sunburn (Kligman, 1969). Consequently exposure to other wavelengths in the solar spectrum was considered safe and the emergence of the “safe tan” began with some products being marketed as “tanning lotion” (Bargoil and Erdman, 1993).

Modern day products that incorporate UVB blocking organic compounds were formulated with initial formulations being marketed by the company L'Oréal under the name of “AmbreSolaire”. During this period the “dark ages” of tanning were practiced with many believing that “tanning lotions” were allowing for safe sun exposure. Such marketing is now prohibited certainly within the EU under the regulations concerned with products providing solar radiation protection (Dupont et al., 2013;Aldahan et al., 2015). In the 1960's Franz Greiter, Switzerland, suggested the concept of the sun protection factor “SPF”. According to this concept a sunscreen with an SPF 15 allows the user to stay out in the sun 15 times longer before burning than would be

possible for bare skin. During the late 1960's further research showed UVB to have a role in skin cancer development as well as contributing to the structural damage leading to skin ageing (Baron and Suggs, 2014).

By the 1970's UVA was beginning to be recognised as a contributing factor to skin ageing and cancer. Such discoveries influenced the industrial and marketing companies as well as the attitude of consumers towards solar light exposure (Diffey and Farr, 1991;Forman et al., 1989). During the 80's the labelling of "suntan lotion" was replaced with what is now known as "sunscreen". Commercially available products were beginning to offer protection against the UVA component as well as UVB (Baron and Suggs, 2014;Nash et al., 2006;Wahie et al., 2007).

Currently the fact that skin ageing may be accelerated by both internal and external factors is well recognised. The list of external factors contributing to skin ageing and cancer is continuing to expand (Naidoo and Birch-Machin, 2017;Abel and Haarmann-Stemmann, 2010). There are currently debates as to whether protection against solar radiation should be expanded further beyond the UV region and whether protection against IR and/ or VIS should also be included (Diffey and Cadars, 2016).

The damaging effects of UV on skin are well characterised by the reddening, blistering and burning that occurs as a result of over exposure. The focus of the research and the protective strategies so far have been centred on the UV portion of the spectrum. UV however accounts for approximately 7% of the solar light energy (Birch-Machin et al., 2013b), which many have argued underlines the necessity to consider the potential deleterious effects from other parts of the spectrum. Current literature findings have proposed a need for dermal protection against IR in particular as it has been demonstrated to cause alterations in the gene expression of skin cells resulting in accelerated skin aging as described in more detail in chapter 1. A number of studies, as described in chapter 3, have investigated the contribution of IR to skin cancer development, particularly when involving the interaction of IR with solar UV.

So far, experimental evidence from chapter 3 suggests that all three components of solar light act synergistically to produce the increase in ROS, nDNA and mtDNA damage levels detected. Conventional sunscreens within the EU block the majority of UVB along with a proportion of the UVA rays (Aldahan et al., 2015). With this knowledge in mind further investigations were

carried out in this chapter to assess the level or percentage at which UV is required to be present alongside the IR and VIS components of solar light before the apparent synergy is no longer observed. Filters with UVB and UVA blocking abilities were used to alter the proportion of solar UV present within the complete solar light doses applied. Experiments were carried out on skin cells in monolayer as described previously using both cell line (HDFn and HaCat) and donor matched primary skin cells (fibroblast, keratinocyte and differentiated keratinocyte). ROS generation and mtDNA damage levels were assessed following the application of various light sources. Parallel to these experiments sunscreen formulations were assessed for their ability to provide acellularly as well as cellular protection against solar light exposures as measured by the level of mtDNA damage. The level of damage following exposure to intermittent doses of solar light and to an equivalent single dose of solar light was also assessed.

The real time-QPCR assay is a powerful method which allows for the detection of DNA damage. The Birch-Machin lab have previously utilised this technique to pioneer the detection of lesions present within mtDNA (Birch-Machin and Swalwell, 2010; Swalwell et al., 2012b; Krishnan et al., 2004; Parr et al., 2006) A range of templates may be utilised to amplify sections of the mtDNA genome depending on the level of damage present or induced following exposure to stimuli. Longer templates are generally used to identify lower levels of damage and allow for greater sensitivity levels to be achieved as the CT values obtained are usually higher. The greater the level of damage present the more likely it is to be detected with shorter fragment template amplifications. Shorter fragment templates also have the advantage of enabling a quicker amplification time. This is more desirable particularly when screening a large number of samples as the run time is shorter and usually more cost effective (Bowman and Birch-Machin, 2015).

QPCR involving amplicon sizes of up to 1000bp has been described in the literature. This allows for the determination of DNA lesions in small, well-defined regions along the mitochondrial genome. In the past, there has been speculation about a variable vulnerability to oxidative stress along the mitochondrial genome therefore four areas approximately 1kb each were selected from different regions within the genome. Comparing several independent regions evenly distributed along the mitochondrial genome, the level of lesions induced by H₂O₂ was

found to be greater in the fragment harbouring the regulatory D-Loop. Results from the paper indicated the existence of at least one mitochondrial DNA hot spot, namely the D-Loop, as this was shown to be more prone to ROS-derived damage (Rothfuss et al., 2010). In this chapter various 1kb regions described previously by Rothfuss et al., 2010 were used to assess damage induction along the mtDNA in HDFn cells following exposure to complete solar light. This was carried out to identify potential differences in solar light induced damage across the different regions of the mtDNA genome.

4.2 Chapter aims

- Assess the effect of reducing the UV component of complete solar light on biomarkers of damage in skin cells and compare responses between cell types.
- Investigate the level of mtDNA damage caused over time due to intermittent and equivalent single doses of solar light exposure and assess the ability of sunscreens in providing protection.
- Compare the sensitivity of the 1kb and 11kb assay.
- Assess the level of cellular damage induction along regions of the mitochondrial genome following exposure to solar light.

4.3 Chapter specific methods

Methods for cell culture, the ROS-Glo assay, solar light dosing (Newport Solar Simulator, Hydrosun lamp and UV sources) and the assessment of sunscreen cellular protection levels can be found in the general methods section (Chapter 2).

4.4 Results

4.4.1 ROS generation in skin cells following a reduction in the level of UV from complete solar light

4.4.1.1 ROS generation in HDFn and HaCat cells following exposure to solar light plus filters

HDFn cells were assessed for the generation of ROS using various doses of complete solar light (0-7.5 SED) with and without the application of the plastic and glass filters (Figure 67). Experiments were initially carried out in cell line prior to assessment in primary cells. Higher doses of solar light were used in cell line to determine whether the effects being seen are consistent over a higher range of doses.

At a dose of 4.32 SED (Figure 67) a 2.95 fold increase in the level of ROS was seen compared to the unirradiated control ($P < 0.005$). Following the application of the glass filter the level of ROS generation compared to control was reduced from a 2.95 fold increase to a 0.93 fold increase ($P < 0.005$) and a further decrease (0.34 fold increase in ROS generation compared to control) was seen when the plastic filter was applied ($P < 0.0001$). No significant differences in ROS generation could be detected between the untreated control sample and the glass or plastic filter at the 4.32 SED dose (Figure 67).

A dose of 7.5 SED complete solar light (Figure 67) resulted in a 5.34 fold increase in the level of ROS in comparison to unirradiated control ($P < 0.0001$). Following the application of the glass filter, the level of ROS generation decreased to a 1.6 fold increase relative to control ($P < 0.005$). A 0.46 fold increase in ROS was seen when the plastic filter was applied ($P < 0.0001$) (Figure 67). A significant difference was seen in ROS generation between the unirradiated control sample and the glass filter ($P < 0.005$) however no such significance was detected between the control and plastic filter. HDFn data from the 7.5 SED dose has been re-plotted (Figure 68) as this gave the greatest response. The level of ROS generation indicates that the increase detected with the glass filter (1.59 fold increase) is greater than the values from the IR plus VIS (0.28 fold increase) and solar UV values combined (0.52 fold increase).

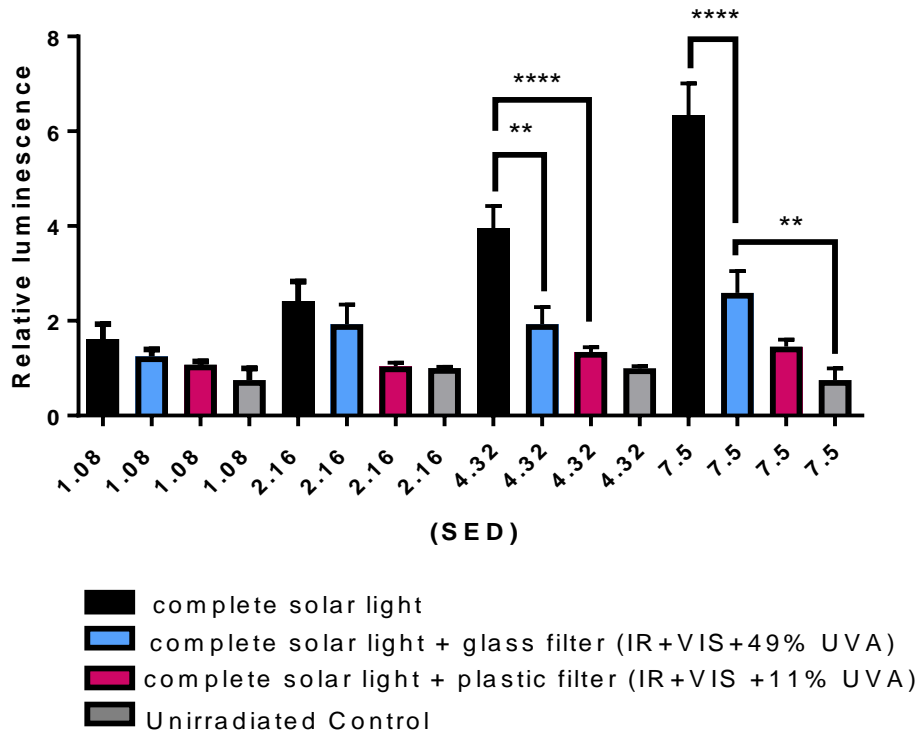


Figure 67: ROS generation in HDFn cells following exposure to complete solar light with varying levels of UVA and UVB

HDFn cells were exposed to doses of solar light (0-7.5 SED) with conditions being either complete solar light (black bar), complete solar light plus glass filter (blue bar), complete solar light plus plastic filter (pink bar) or unirradiated control (grey bar). A ROS-Glo assay was carried out to assess the relative luminescence level (proportional to the level of H₂O₂). The different conditions assessed within each dose (SED) were compared relative to cells treated with the same dose of complete solar light. Statistical analysis was applied using a Kruskal-Wallis one-way ANOVA with Dunn's multiple comparison test ****P<0.0001, **P<0.005 (error bars represent the SEM) N=2.

At a dose of 7.5 SED complete solar light HaCat cells showed a significant 1.53 fold increase in the level of ROS compared to the unirradiated control (P<0.05) (Figure 69). When a glass filter was applied the level of ROS generation dropped to a 0.18 fold increase and a similar 0.18 fold increase in ROS was seen compared to control following the application of the plastic filter. The levels of ROS following the application of the plastic or glass filter is significant when compared to the unirradiated control cells.

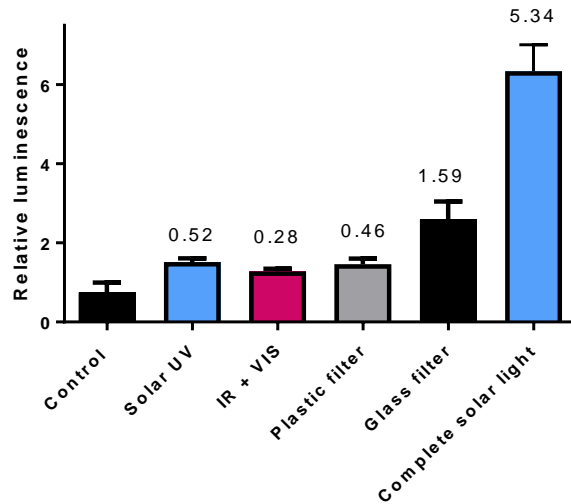


Figure 68: ROS generation in HDFn cells following exposure to complete solar light with varying levels of UVA and UVB

Data shows the relative luminescence levels following irradiation of HDFn cells with a dose of 2.16 SED complete solar light. The fold change in luminescence is displayed relative to the unirradiated (control) cells.

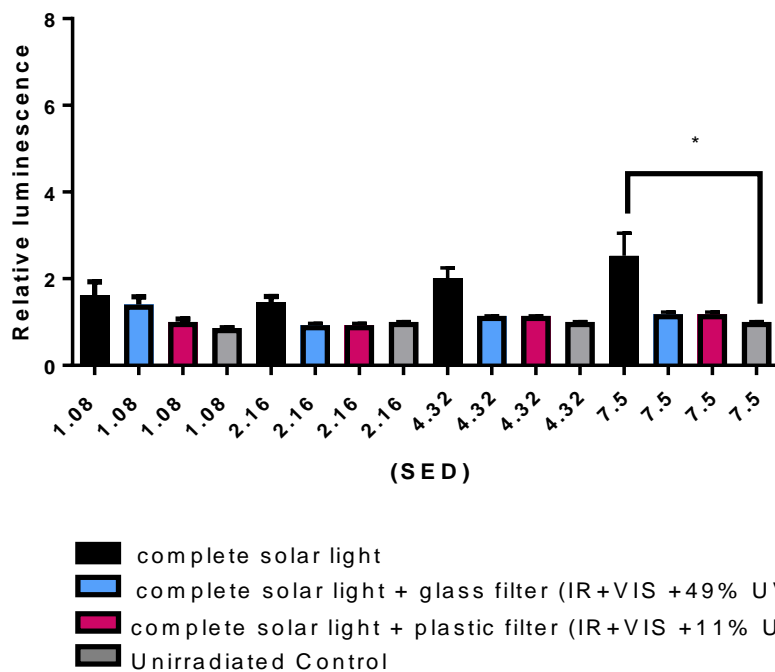


Figure 69: ROS generation in HaCat cells following exposure to complete solar light with varying levels of UVA and UVB

HaCat cells were exposed to doses of solar light (0-7.5 SED) with conditions being either complete solar light (black bar), complete solar light plus glass filter (blue bar), complete solar light plus plastic filter (pink bar) or unirradiated control (grey bar). A ROS-Glo assay was carried out to assess the relative luminescence level (proportional to the level of H₂O₂). The different conditions assessed within each dose (SED) were compared relative to cells treated with the same dose of complete solar light. Statistical analysis was assessed using a Kruskal-Wallis one-way ANOVA with Dunn's multiple comparison test*P<0.05 (error bars represent the SEM) N=2.

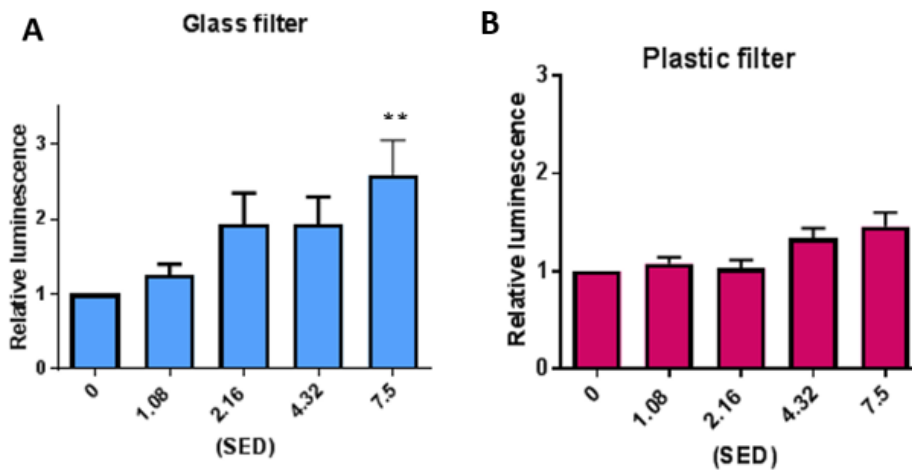


Figure 70: ROS generation in HDFn cells following exposure to complete solar light plus glass or plastic filters
 Data shows the relative luminescence level (proportional to H₂O₂ generation) in HDFn cells with increasing doses of complete solar light (0-7.5 SED) plus glass filter (A) or plastic filter (B). Statistical analysis was performed to compare all columns to the control (unirradiated) cells using a one-way ANOVA with Dunnett's correction **P<0.01 *P<0.05 (error bars represent the SEM) N=2, N=2 respectively.

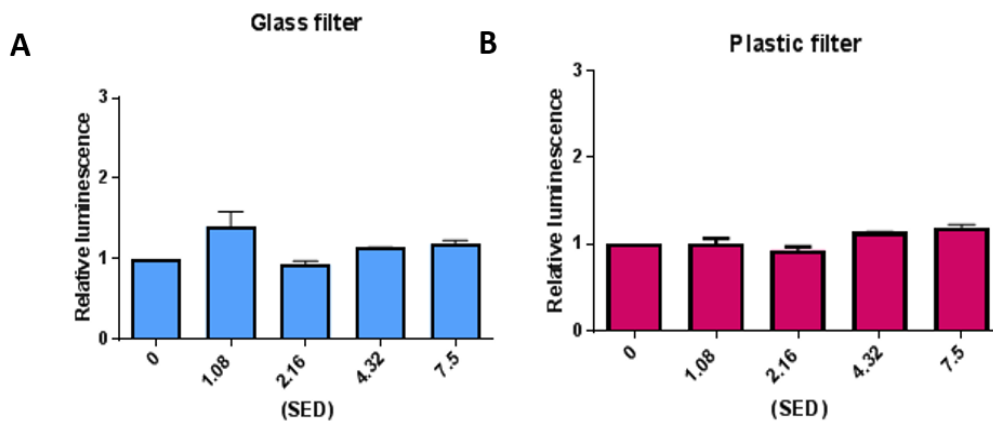


Figure 71: ROS generation in HaCat cells following exposure to complete solar light plus glass or plastic filters
 Data shows the relative luminescence level (proportional to H₂O₂ generation) in HaCat cells with increasing doses of complete solar light plus glass filter (0-7.5 SED) (A) or plastic filter (B). Statistical analysis was performed to compare all columns to the control (unirradiated) cells using a one-way ANOVA with Dunnett's correction **P<0.01 *P<0.05 (error bars represent the SEM) N=2, N=2 respectively.

Data from Figure 67 and Figure 69 were re-plotted in order to establish whether a dose dependent response in ROS generation could be observed when the glass and plastic filters were applied alongside complete solar light. No dose dependent increase in ROS was seen with increasing SED of complete solar light following the application of the glass (Figure 70 A) or plastic (Figure 71 B) filters in HDFn cells. HaCat cells appeared to be less sensitive than HDFn cells and showed no dose dependent response effect following the application of the glass (Figure 71 A) or plastic filters (Figure 70 B).

4.4.1.2 ROS generation in primary skin cells following exposure to solar light plus filters

Primary skin cells were dosed with the relevant wavelengths of solar light and the level of ROS generation was measured immediately following exposure. Data from the three donors assessed (primary keratinocyte (Figure 72), differentiated keratinocyte (Figure 73) and fibroblast cells (Figure 74)) indicate that full spectrum light leads to an increase in ROS generation at both the 0.54 and 2.16 SED dose. An increase in ROS is also seen when the glass filter is applied at both doses of 0.54 and 2.16 SED. The ROS generation values for each of the donor matched skin cell types is summarised in Table 10. The data is in support of the wavelengths of solar light acting synergistically. As would be expected the ROS generation seen with the glass filter is not as high as levels detected with complete solar light. No significant difference between the plastic filter and unirradiated control was seen which suggests that the 11% UVA present alongside the IR and VIS is perhaps not sufficient to lead to the synergistic effects in primary keratinocyte (Figure 72), differentiated keratinocyte (Figure 73) and fibroblast cells (Figure 74).

Skin cell type	Complete solar light	IR plus VIS	Solar UV	Glass filter	Plastic filter	Difference between glass filter and additive effects of UV plus IR and VIS
Primary fibroblast	98%	16%	19%	66%	25%	Synergistic effects detected with glass filter = 66% Synergistic effects detected with plastic filter = 25% Additive effects of solar UV plus IR and VIS = 35%
Primary keratinocytes	93%	13%	10%	99%	17%	Synergistic effects detected with the glass filter = 59% Synergistic effects detected with the plastic filter = 17% Additive effects of solar UV plus IR and VIS = 23%
Primary differentiated keratinocytes	85%	9%	19%	58%	19%	Synergistic effects detected with the glass filter= 58% Synergistic effects detected with the plastic filter = 19% Additive effects of solar UV plus IR and VIS= 28%

Table 10: Summarising the percentage increase in ROS relative to unirradiated control following exposure of primary skin cells to solar light (2.16 SED)

A 0.1 fold increase in ROS compared to control was seen when solar UV was applied to keratinocytes (Figure 72). A 0.13 fold increase was detected when IR plus VIS was applied however when the glass filter was applied giving an output dose consisting of IR plus VIS plus 49% UVA, a 0.59 fold increase in ROS could be detected ($P < 0.0001$). This value was higher than the ROS level increase with solar UV (0.1 fold increase) and IR plus VIS (0.13 fold increase) combined suggesting the effects were not additive. This further suggests that the solar light wavelengths are acting synergistically on keratinocyte cells. As would be expected the ROS seen with the glass filter (0.59 fold increase) is not as high as that detected with the full spectrum light (0.93 fold increase). No significant difference between the plastic filter and untreated control was seen which suggest that the 0.11% UVA present alongside the IR and VIS is perhaps not enough to lead to the synergistic effects.

Differentiated primary keratinocyte cells show a 0.85 fold increase in ROS compared to the unirradiated control at a complete solar light dose of 2.16 SED ($P < 0.005$). When the glass filter is applied the level of ROS generation decreases to a 0.58 fold increase relative to unirradiated control and 0.19 fold increase when the plastic filter is applied (Figure 73). Findings from the differentiated keratinocytes are similar to the data obtained from non-differentiated keratinocytes (Figure 73) in that the ROS level for solar UV (0.19 fold increase) and for IR plus VIS (0.09 fold increase) are additively less than the value obtained with the glass filter (0.58 fold increase). This suggests that synergy is occurring in the differentiated keratinocytes. Similarly again, the plastic UVB filter which allows only 11% UVA through is not sufficient to cause synergistic effects.

Primary fibroblast cells show a 0.98 fold increase in ROS compared to the untreated control at a dose of 2.16 SED complete solar light ($P < 0.0001$). When the glass filter was applied the level of ROS generation was reduced to a 0.66 fold increase ($P < 0.0001$) and a 0.25 fold increase in ROS was seen when the plastic filter was applied (Figure 74). The value for the plastic filter appears to be significant compared to the untreated control ($P < 0.001$) however the ROS values for the plastic filter (0.25 fold increase) are less than the additive effects of the solar UV (0.19 fold increase) and IR plus VIS (0.16 fold increase) data obtained. Data from the fibroblast cells also suggests that the effects of IR, VIS and UV are synergistic. Although data from the plastic filter shows an increase in ROS that is statistically significant compared to control it does not indicate that there is synergy occurring when an 11% UVA level is applied alongside the IR and VIS solar wavelengths.

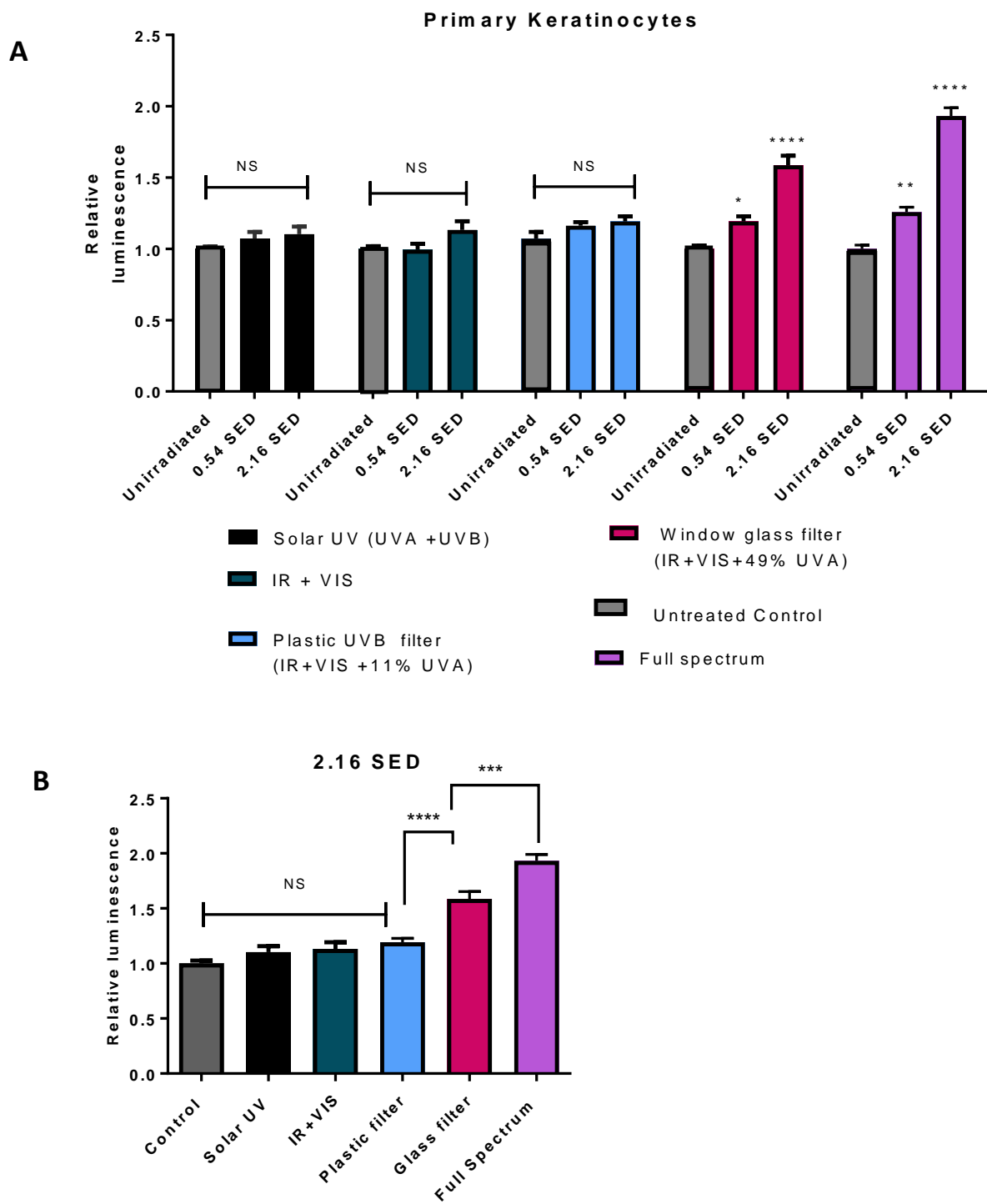


Figure 72: ROS generation in primary keratinocytes following exposure to full spectrum solar simulated light with varying UVA and UVB levels

Primary keratinocyte cells were exposed to a dose of solar light (0-2.16 SED) (A). Cells were exposed to either complete solar light (black bar), complete solar light plus glass filter (blue bar), complete solar light plus plastic filter (pink bar) or unirradiated control (grey bar). A ROS-Glo assay was carried out to assess the luminescence level (proportional to the level of H₂O₂ generation). The different conditions assessed within each SED dose were compared relative to cells treated with the same SED of complete solar light. Results of the higher dose (2.16 SED) are displayed separately for comparison (B). A Kruskal-Wallis one-way ANOVA with Dunn's multiple comparison test was used to assess significance * p<0.05 ****, p<0.0001 (error bars represent the SEM) N=3.

A

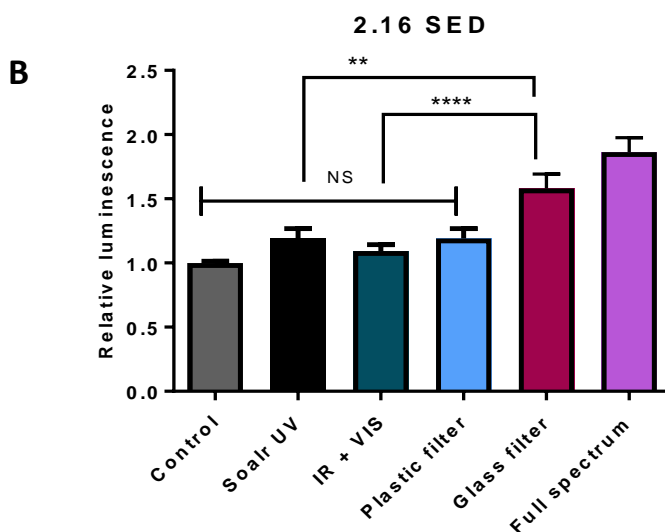
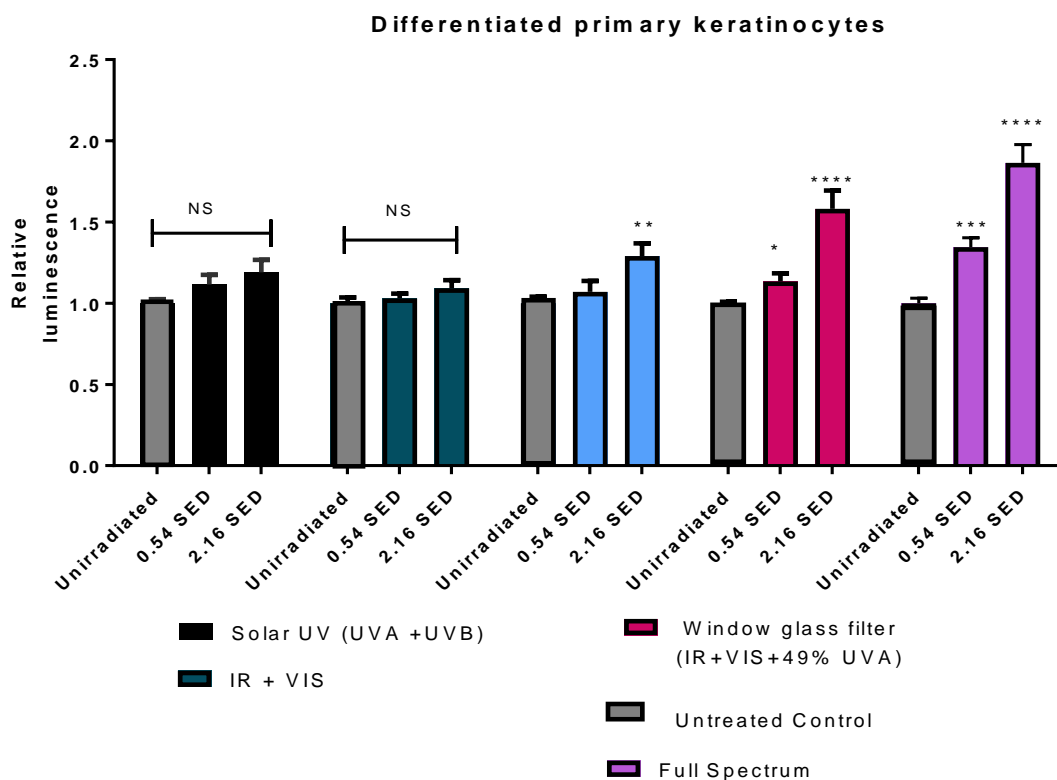


Figure 73: ROS generation in differentiated primary keratinocytes following exposure to full spectrum solar simulated light with varying UVA and UVB levels

Primary differentiated keratinocyte cells were exposed to a dose of solar light (0-2.16 SED) (A). Cells were exposed to either complete solar light (black bar), complete solar light plus glass filter (blue bar), complete solar light plus plastic filter (pink bar) or unirradiated control (grey bar). A ROS-Glo assay carried out to assess the luminescence level (proportional to the level of H₂O₂ generation). The different conditions assessed within each SED dose were compared relative to cells treated with the same SED of complete solar light. Results of the higher dose (2.16 SED) are displayed separately for comparison (B). A Kruskal-Wallis one-way ANOVA with Dunn's multiple comparison test was used to assess significance *p<0.05, **p<0.001, ****p<0.0001 (error bars represent the SEM) N=3.

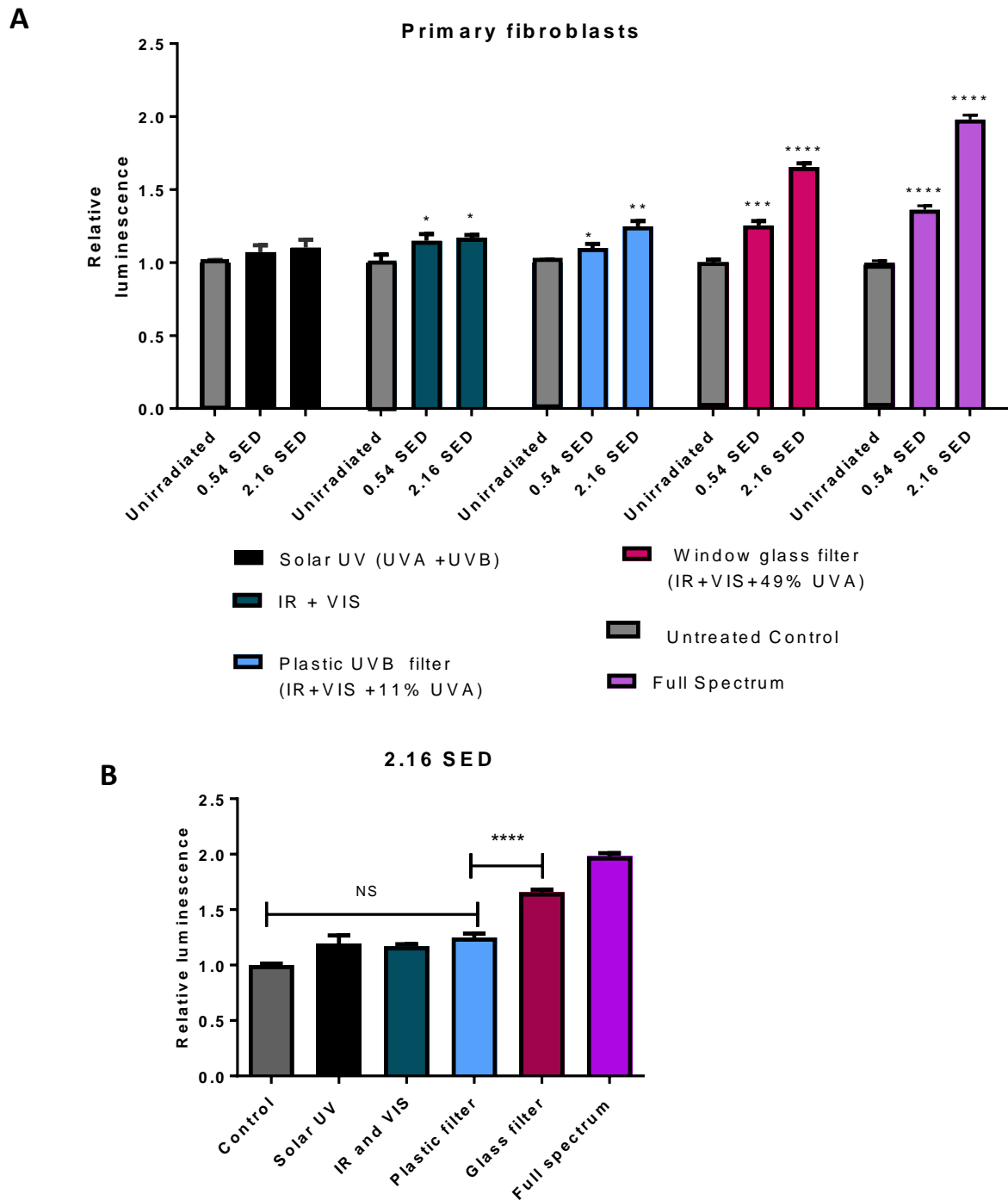


Figure 74: ROS generation in differentiated primary fibroblasts following exposure to full spectrum solar simulated light with varying UVA and UVB levels

Primary fibroblast cells were exposed to a dose of solar light (0-2.16 SED) (A). Cells were exposed to either complete solar light (black bar), complete solar light plus glass filter (blue bar), complete solar light plus plastic filter (pink bar) or unirradiated control (grey bar). A ROS-Glo assay carried out to assess the luminescence level (proportional to the level of H_2O_2 generation). The different conditions assessed within each SED dose were compared relative to cells treated with the same SED of complete solar light. Results of the higher dose (2.16 SED) are displayed separately for comparison (B). A Kruskal-Wallis one-way ANOVA with Dunn's multiple comparison test was used to assess significance * $P < 0.05$, *** $P < 0.001$, **** $P < 0.0001$ (error bars represent the SEM) $N = 3$.

4.4.2 mtDNA damage in primary skin cells following exposure to solar UV plus filters

The level of mtDNA damage was assessed as a further biomarker of damage following the reduction in the UV portion of the solar spectrum. Cells were assessed immediately following exposure to complete solar light (0.54 and 2.16 SED) plus or minus the glass or plastic filters. The 0.54 SED dose did not show detectable changes in CT value under the conditions tested, data was therefore not included. Primary keratinocytes show an average of a 2 CT difference between the mtDNA in the irradiated and unirradiated control. A 1 CT difference was seen between the glass filter and unirradiated control and a 0.5 CT between the IR plus VIS filter and unirradiated control. No difference was detected between the plastic filter and unirradiated control. The differences between the IR plus VIS and glass filter were not statistically significant (Figure 75). Similarly primary fibroblasts show a 2 CT increase in mtDNA damage levels following exposure to complete solar light when compared to unirradiated control. No difference in CT compared to control was seen with the IR plus VIS component. The glass filter does show a 1 CT difference compared to control however when compared to the IR plus VIS filter no significant changes in CT value can be seen (Figure 76). Data for the differentiated keratinocyte cells shows similar findings to the keratinocyte and fibroblast cells although a higher damage level between irradiated and unirradiated control was detected (3.5 CT) (Figure 77). This lack of cellular response in terms of the level of mtDNA damage detection may be due to no UVB being present when the glass or plastic filters are applied as the UVB component causes direct damage to DNA (Bowman and Birch-Machin, 2015; Birch-Machin and Wilkinson, 2008).

Primary keratinocytes (2.16SED)

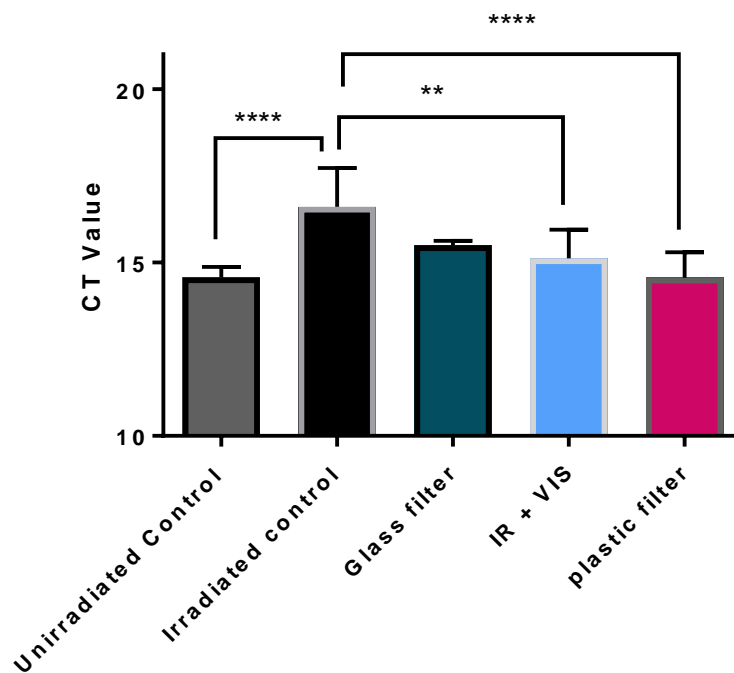


Figure 75: mtDNA damage in primary keratinocytes following exposure to full spectrum solar simulated light plus or minus plastic and glass filters

Primary keratinocyte cells were exposed to a dose of complete solar light (2.16 SED) and the level of mtDNA damage relative to the unirradiated control assessed using the 11kb QPCR assay. Cells were either unirradiated (grey bar) or exposed to complete solar light (black bar), complete solar light plus glass filter (green bar), IR + VIS (blue bar), complete solar light plus plastic filter (pink bar). A Kruskal-Wallis one-way ANOVA with Dunn's multiple comparison test was used to assess significance ** $P < 0.005$, **** $P < 0.0001$ (error bars represent the SEM) $N = 3$.

Primary fibroblasts (2.16 SED)

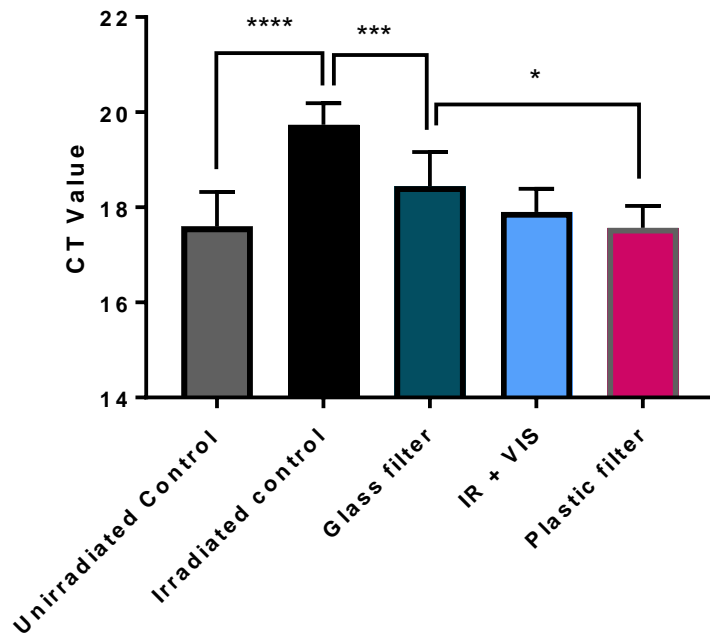


Figure 76: mtDNA damage levels in primary fibroblasts following exposure to full spectrum solar simulated light plus or minus the plastic and glass filters

Primary fibroblast cells were exposed to a dose of complete solar light (2.16 SED) and the level of mtDNA damage relative to the unirradiated control assessed using the 11kb QPCR assay. Cells were either unirradiated (grey bar) or exposed to complete solar light (black bar), complete solar light plus glass filter (green bar), IR + VIS (blue bar), complete solar light plus plastic filter (pink bar). A Kruskal-Wallis one-way ANOVA with Dunn's multiple comparison test was used to assess significance * $P < 0.05$, *** $P < 0.0001$ (error bars represent the SEM) $N=3$.

Differentiated primary keratinocytes (2.16SED)

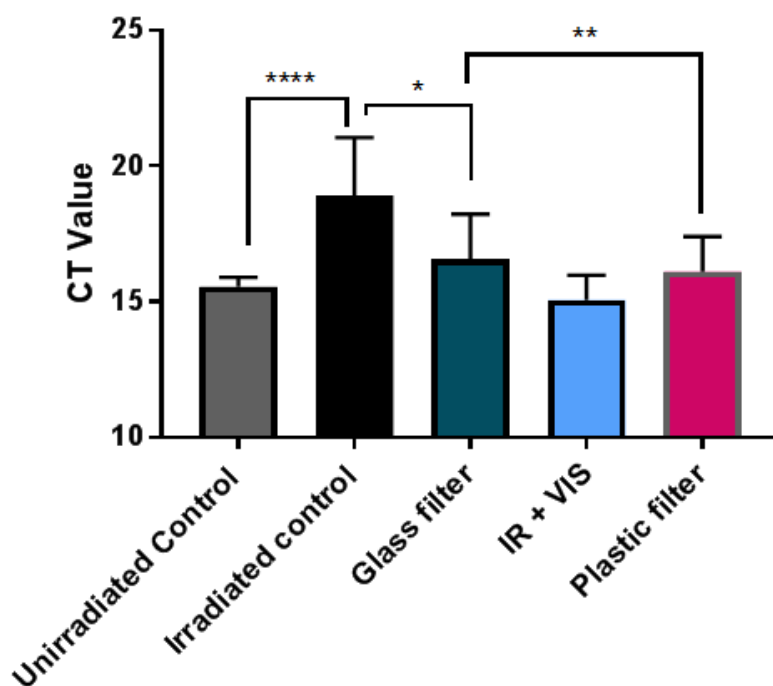


Figure 77: mtDNA damage in differentiated primary keratinocytes following exposure to full spectrum solar simulated light plus or minus the plastic and glass filters

Differentiated primary keratinocyte cells were exposed to a dose of complete solar light (2.16 SED) and the level of mtDNA damage relative to the unirradiated control assessed using the 11kb QPCR assay. Cells were either unirradiated (grey bar) or exposed to complete solar light (black bar), complete solar light plus glass filter (green bar), IR + VIS (blue bar), complete solar light plus plastic filter (pink bar). A Kruskal-Wallis one-way ANOVA with Dunn's multiple comparison test was used to assess significance * $P < 0.05$, ** $P < 0.005$, **** $P < 0.0001$ (error bars represent the SEM) $N = 3$.

4.4.3 Comparison of primary cell response to the reduction in solar UV levels

The response of primary fibroblast, keratinocyte and differentiated keratinocyte cells to doses of complete solar light following the application of the glass and plastic filters was compared. Data from Figure 72, Figure 73 and Figure 74 is represented in Figure 78. No difference can be seen between the response of the skin cells to the glass and plastic filters. HDFn cells were however seen to be more responsive to solar UV when compared to keratinocyte and differentiated keratinocyte cells ($P < 0.0001$) (Figure 79).

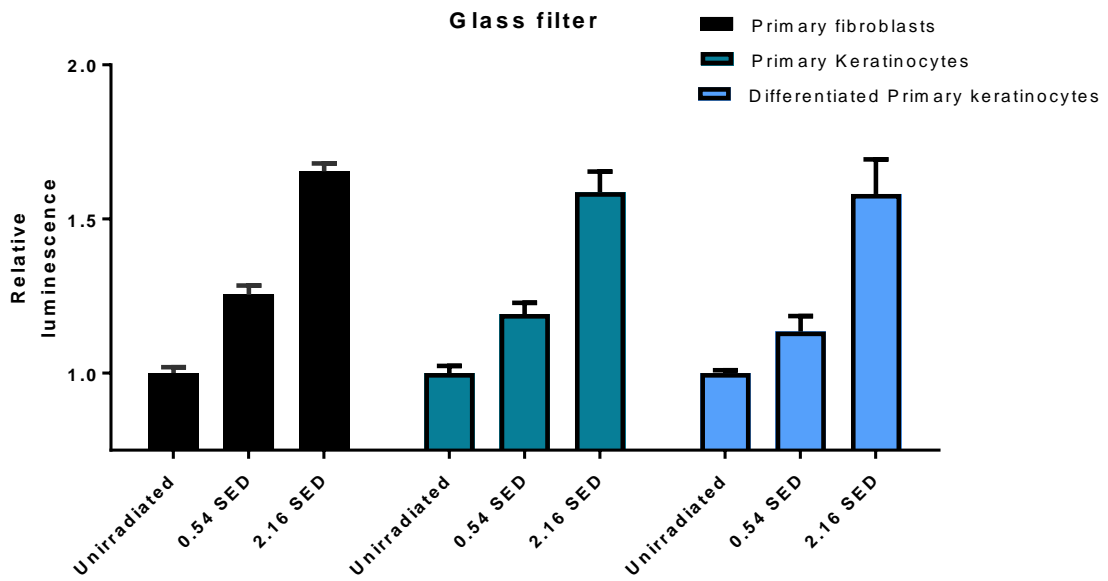
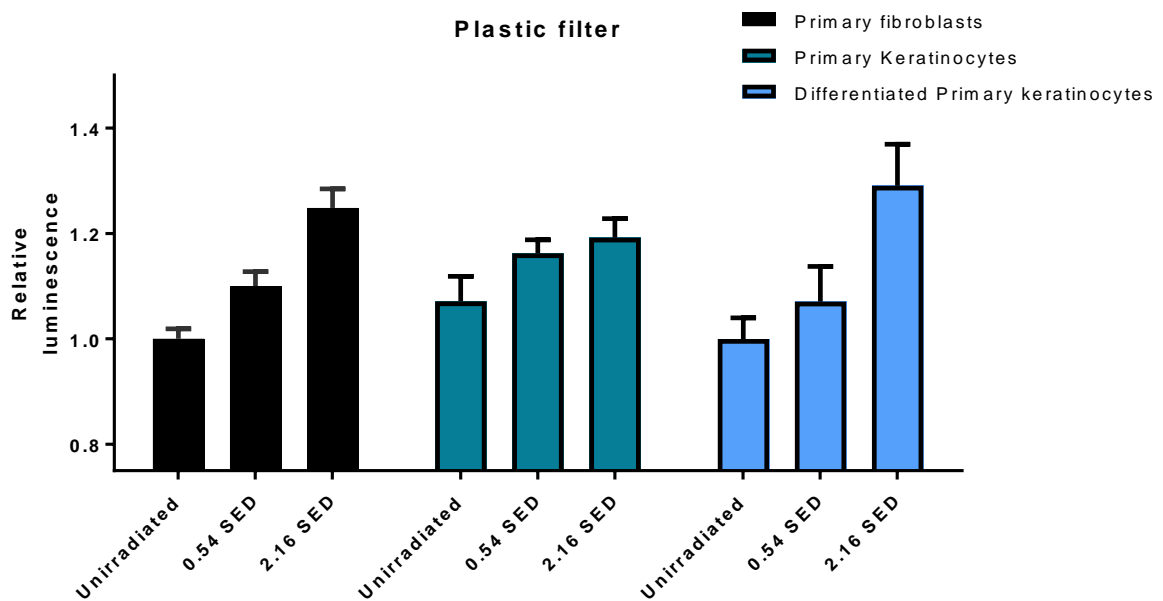
A**B**

Figure 78: Comparison of ROS generation in primary fibroblast, keratinocyte and differentiated keratinocyte cells following exposure to full spectrum solar simulated light plus or minus the plastic and glass filters
 Primary fibroblast, keratinocyte and differentiated keratinocyte cells are seen to respond in a similar way when complete solar light is applied along with the glass or plastic UVB filters. Statistical analysis was assessed using a one-way ANOVA with Bonferonni's post-hoc to compare the mean of each column with the mean of every other column (error bars represent the SEM) N=3.

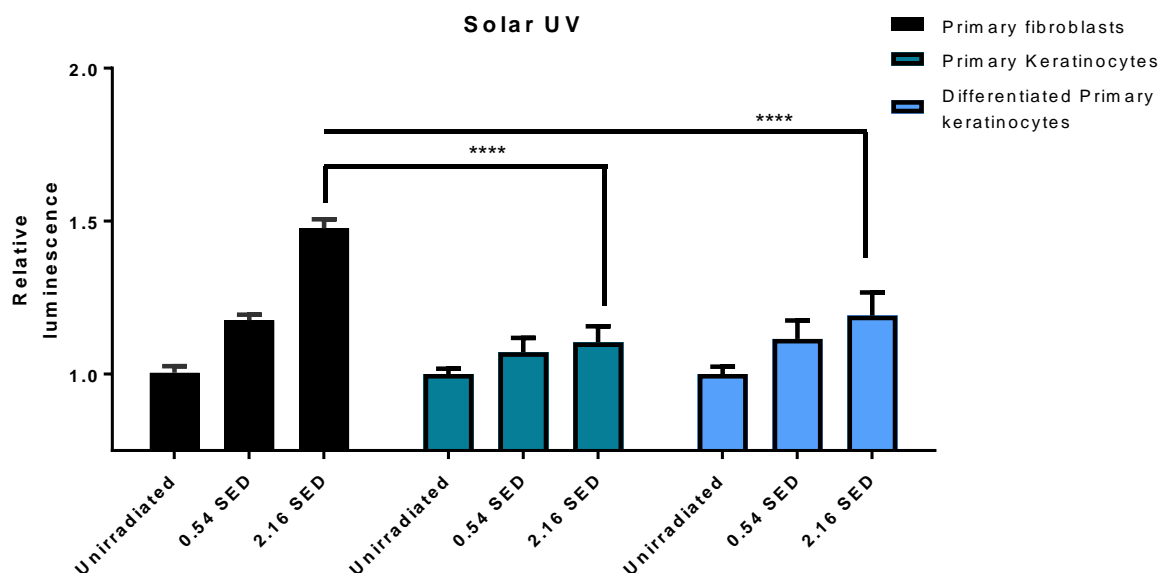


Figure 79: Comparison of ROS generation in primary fibroblast, keratinocyte and differentiated keratinocyte cells following exposure to solar UV

HDFn cells are seen to generate more ROS in response to solar UV when compared to keratinocyte and differentiated keratinocyte cells. Statistical analysis was assessed using a one-way ANOVA with Bonferonni's post-hoc to compare the mean of each column with the mean of every other column ****P<0.0001 (error bars represent the SEM) N=3.

4.4.4 Protective effects of sunscreens against solar radiation exposure

Sunscreens are conventionally assessed for the level of protection they offer to skin when applied at the recommended amount of 2mg/cm² (Burnett and Wang, 2011). The ability of sunscreens to provide protection against mtDNA damage levels was assessed following exposure to solar light. A baseline formulation containing no SPF was used as a control alongside the same baseline formulation containing SPF 15 and SPF 30 protection. In vitro experiments were carried out to demonstrate the protective ability of the sunscreen formulations when used at a dose of 2mg/cm² (Figure 80). Formulations were assessed for protection against complete solar simulated light, UVA, UVB and IR. In all cases the baseline formulation provided some level of protection perhaps due to the white tint effect reflecting light. The SPF 15 formulation was seen to protect against complete solar light, UVA and UVB dosing conditions whilst as expected, SPF 30 gave even further protection (Figure 80). This is consistent with findings in the literature whereby SPF 15 was able to provide protection against solar radiation induced DNA damage (Phillips et al., 2000). The tape control only blocks a proportion of the UVB and IR rays. Similarly, baseline formulation blocks a proportion of the

IR as seen in Figure 80 . Sunscreen formulations both SPF 15 and 30 were not able to provide protection against IR when compared to the no SPF baseline formulation.

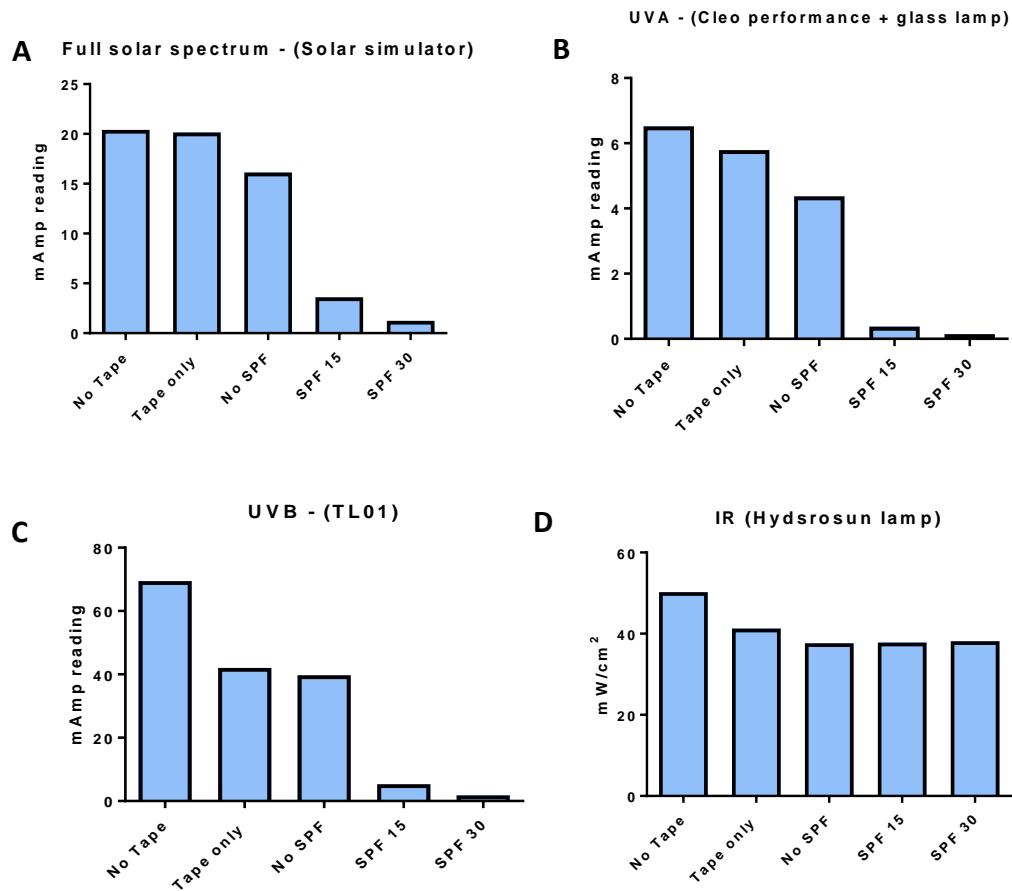


Figure 80: Protective effects of sunscreen formulations - acellular

Sunscreen formulations (baseline no SPF, SPF15 and SPF30) were placed on transpore tape at the recommended amount ($2\text{mg}/\text{cm}^2$) and assessed for ability to block against the solar light doses applied, full solar spectrum (A), UVA - Cleo performance + glass (B), UVB - TL01 (C) and IR (D). The lower readings compared to tape only control are indicative of the protective action of the sunscreen formulations.

The ability of sunscreens to provide protection against mtDNA was assessed in HDFn cells. Sunscreens were applied on to micropore tape to mimic the epidermal layer of skin and placed on top of the wells where the cells resided. HDFn cells were dosed with complete solar light and the level of mtDNA damage was assessed using the 1kb QPCR assay.

One of the questions investigated during the project is whether the pattern of solar light exposure received effects the level of DNA damage accumulation over time. Experiments were carried out whereby HDFn cells were dosed with solar light over 4 days with each dose being equivalent to 30 min in the Mediterranean sun at noon during the summer months. Parallel to this HDFn cells were given a single large dose equivalent to 2h under the same conditions and the levels of damage compared between the two groups using QPCR. Two different dosing conditions were carried out with one group of cells receiving a dose of 0.54 SED over 4 days (Figure 81 A) and the other cells receiving a single 2.16 SED dose (Figure 81 B). Both dosing conditions showed that complete solar light was able to induce significant mtDNA damage with the no SPF baseline cream formulation ($P < 0.001$). The application of SPF 15 sunscreen protected the cells exposed to multiple doses of solar light (0.54 SED) over 4 days as well as protecting against the single 2.16 SED dose of complete solar light (Figure 80). No significance was detected between the SPF 15 and SPF 30 sunscreen formulations in terms of the protection offered to mtDNA. No mtDNA damage was seen to be induced following HDFn cell exposure to solar UV (Figure 82). A level of damage was however detected following the application of arimed B (Figure 83), sunscreens were able to protect against damage induction during the intermittent (0.54 SED over 4 days) and single (2.16 SED) dose exposures.

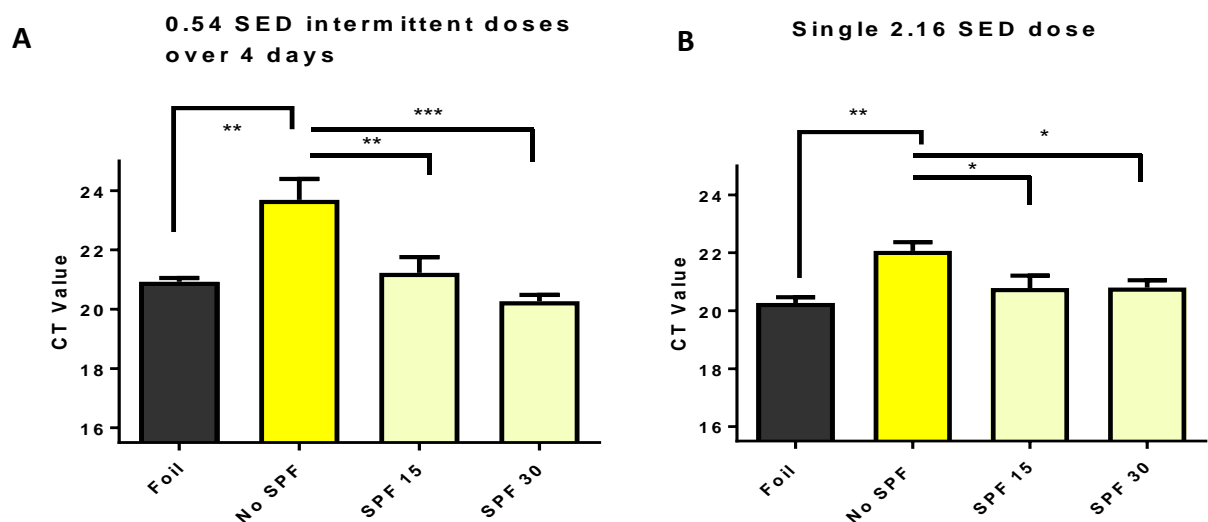


Figure 81: Protective effects of sunscreens against complete solar light induced mtDNA damage in HDFn cells Sunscreen formulations (baseline no SPF, SPF15 and SPF30) were placed on transpore tape at the recommended 2mg/cm² amount and assessed for ability to provide protection to HDFn cells against the complete solar light dose applied. Complete solar light was either applied intermittently (A) or as a single 2.16 SED dose (B). A 1kb QPCR assay was carried out to measure the level of mtDNA damage relative to the unirradiated (foil) control. Statistical analysis was assessed using a one-way ANOVA with Dunnett's correction to compare the mean of each column with the mean of every other column * $P < 0.05$ ** $P < 0.001$, *** $P < 0.0001$ (error bars represent the SEM) N=2, N=2 respectively.

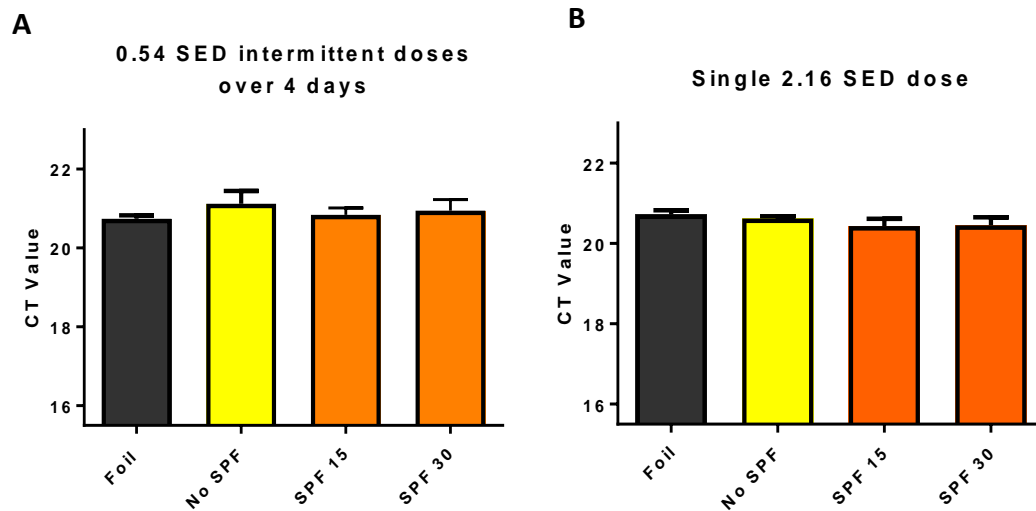


Figure 82: Protective effects of sunscreens against solar UV induced mtDNA damage in HDFn cells
 Sunscreen formulations (baseline no SPF, SPF15 and SPF30) were placed on transpore tape at the recommended 2mg/cm² amount and assessed for ability to provide protection to HDFn cells against the solar UV dose applied. Solar UV was either applied intermittently (A) or as a single 2.16 SED dose (B). A 1kb QPCR assay was carried out to measure the level of mtDNA damage relative to the unirradiated (foil) control. Statistical analysis was assessed using a one-way ANOVA with Dunnett's correction to compare the mean of each column with the mean of every other column (error bars represent the SEM) N=2, N=2 respectively.

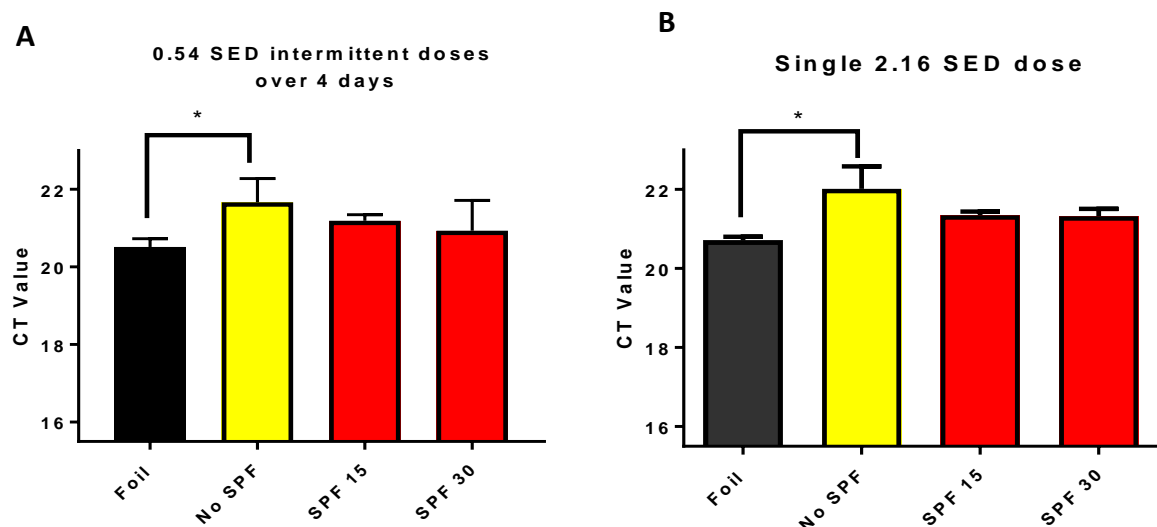


Figure 83: Protective effects of sunscreens against arimed B induced mtDNA damage in HDFn cells
 Sunscreen formulations (baseline no SPF, SPF15 and SPF30) were placed on transpore tape at the recommended 2mg/cm² amount and assessed for ability to provide protection to HDFn cells against the arimed B dose applied. Arimed B was either applied intermittently (A) or as a single 2.16 SED dose (B). A 1kb QPCR assay was carried out to measure the level of mtDNA damage relative to the unirradiated (foil) control. Statistical analysis was assessed using a one-way ANOVA with Dunnett's correction to compare the mean of each column with the mean of every other column *P< 0.05 (error bars represent the SEM) N=2, N=2 respectively.

Further experiments involved assessing cells which were displaced during the experimental wash steps. Following cellular irradiations, a wash step was carried out and the cells which

were displaced from the wells were collected and processed separately in order to measure the level of damage. Cells which detach may theoretically have a higher amount of DNA damage, cells within the washes would otherwise not be included in the analysis. No significant amounts of DNA could be extracted from the detached cells which suggested a low cell count in the wash steps. Total levels of DNA from the cells was assessed using the nanaodrop machine with no detectable levels of DNA obtained.

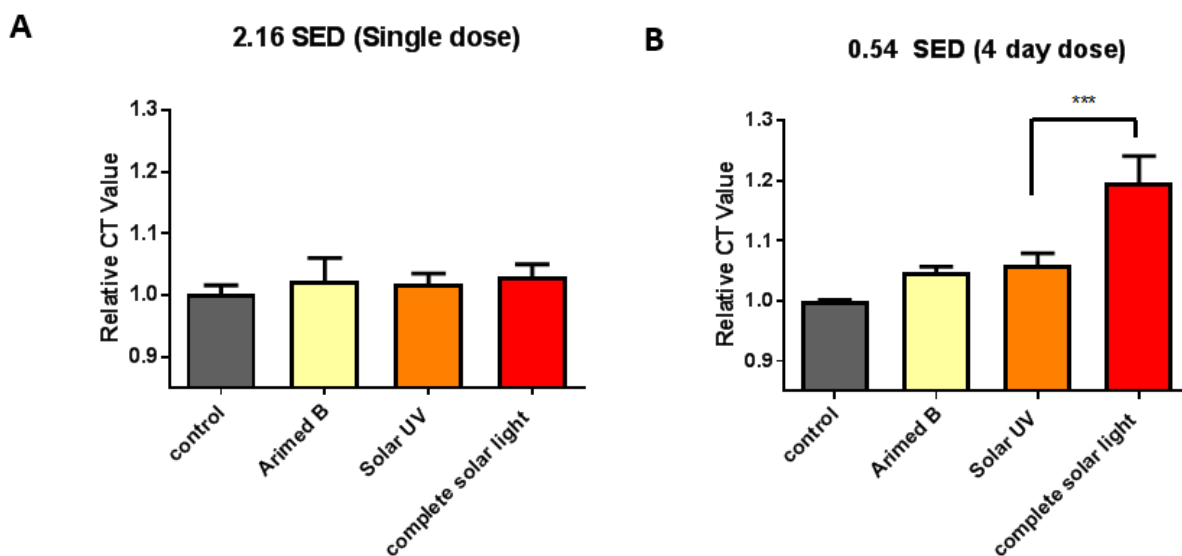


Figure 84: Comparison of mtDNA damage levels in HDFn cells following exposure to different solar light sources and dosing conditions

HDFn cells were dosed with either Arimed B, solar UV or complete solar light and the level of mtDNA damage assessed. Doses were either given as a single 2.16 SED dose (A) or as equivalent intermittent doses of 0.54 SED over 4 days (B) Statistical analysis was assessed using a one-way ANOVA with Dunnett's correction to compare all columns to control (unirradiated) cells ***P<0.001 (error bars represent the SEM) N=4.

4.4.5 mtDNA damage accumulation over time following exposure to intermittent doses of solar light

Damage in mtDNA as a result of intermittent UV exposure was seen to be progressive following exposure to either arimed B (Figure 85 A), solar UV (Figure 85 B) or complete solar light (Figure 85 C). In all cases damage was seen to commence on day 2 and 3 following irradiation. The Δ CT following arimed B dosing is seen to increase significantly on day 4. Solar UV causes a significant Δ CT on day 4 compared to day 1. Complete solar light causes damage on day 2 and 3 with significantly higher levels of damage being seen on day 4 compared to day 3 (Figure 85)

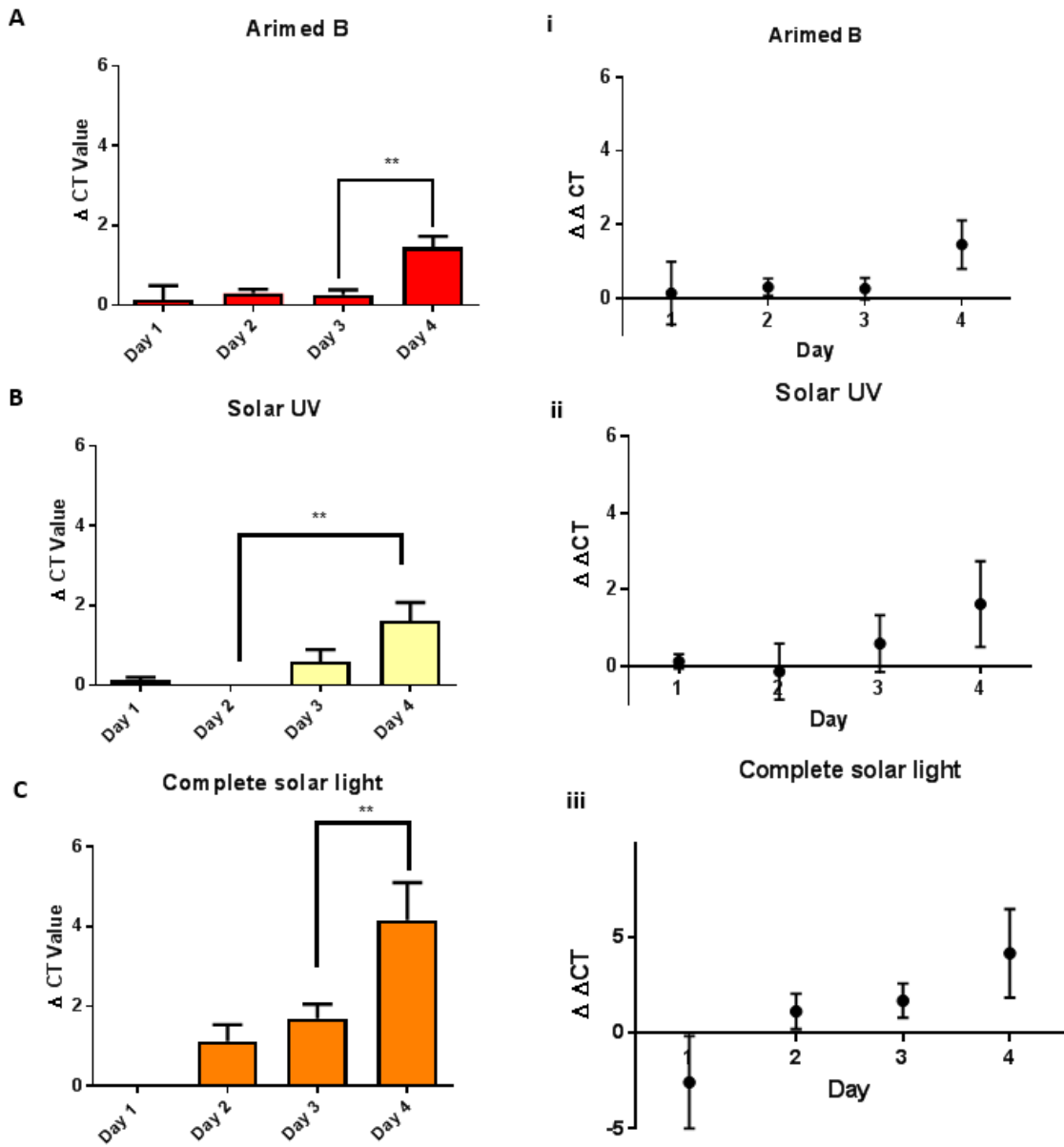


Figure 85: Level of mtDNA damage accumulation over 4 days following exposure to single or intermittent doses of solar light

HDFn cells were exposed to intermittent doses of arimed B (A and i), solar UV (B and ii) or complete solar light (C and iii). The level of mtDNA damage accumulation relative to unirradiated control was measured following each day (1-4) and the change in CT calculated using 11kb QPCR analysis. Statistical analysis was assessed through a one-way ANOVA with Dunnett's correction to compare the mean of each column with the mean of every other column **P<0.005 (error bars represent the SEM) N=2.

4.4.6 Comparison of mtDNA damage following exposure to intermittent and an equivalent single dose of solar light

The level of mtDNA damage detected using the 1kb QPCR assay showed differences depending on the dosing pattern applied. More damage was observed when a dose of complete solar light was applied at a dose of 0.54 SED over 4 days compared to a single 2.16 SED dose (Figure 86). Similar findings were seen with solar UV (Figure 86). Data for the Arimed B lamp was not seen to be significant (Figure 88). The same experiments were analysed for mtDNA damage using an 11kb template QPCR assay. The level of damage with complete solar light was similar with both dosing patterns as no significance between the single and intermittent dose was observed (Figure 89). HDFn cells exposed to a single 2.16 SED dose show little change (0.014 fold increase) in CT value with the 1kb assay. Cells exposed to Multiple 0.54 SED doses show a greater increase in CT (0.19 fold increase) compared to unirradiated control. The difference detected between the single and intermittent dose is statistically significant ($P= 0.0107$).

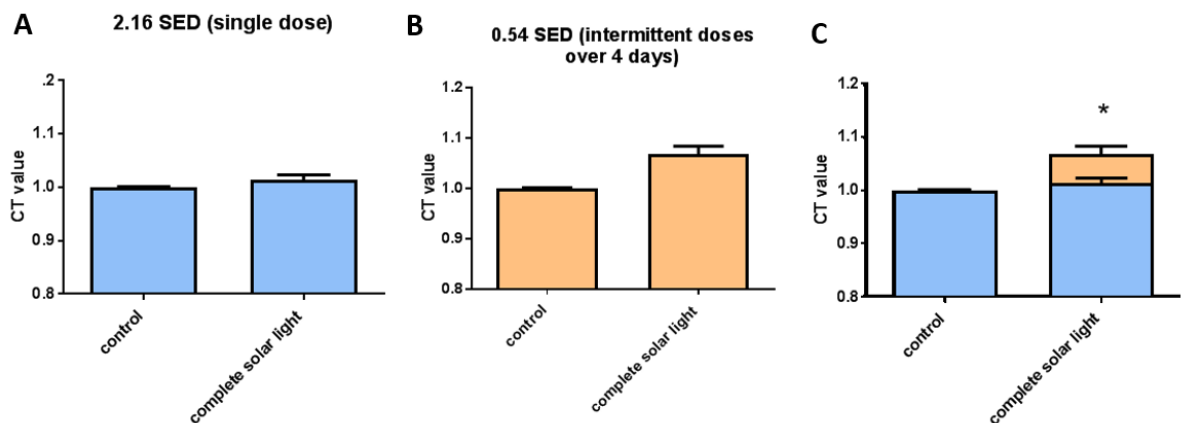


Figure 86: mtDNA damage in HDFn cells following exposure to intermittent and single doses of complete solar light

HDFn cells were treated with a single dose (2.16 SED) of complete solar light (A) or an equivalent dose applied intermittently over 4 days (B). The level of mtDNA damage was assessed relative to the unirradiated control using the 1kb assay. The difference in response between single and intermittent exposures is shown (C). Statistical analysis was assessed through an unpaired T test using Welch's correction* $P<0.05$ (error bars represent the SEM) $N=4$, $N=3$ respectively.

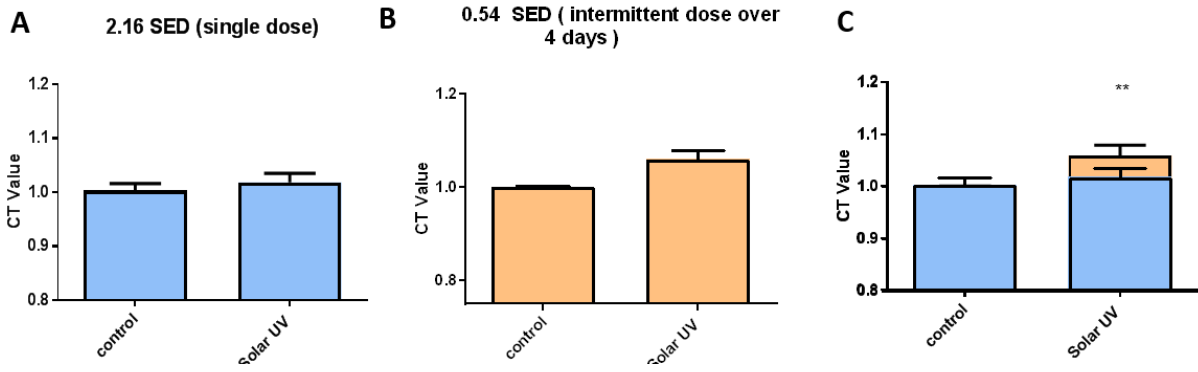


Figure 87: mtDNA damage in HDFn cells following exposure to either an intermittent dose single dose of complete solar

HDFn cells were treated with a single dose (2.16 SED) of solar UV (A) or an equivalent dose applied intermittently (B). The level of mtDNA damage was assessed relative to the unirradiated control using the 1kb assay. The difference in response between single and intermittent exposures is displayed (C). Statistical analysis was assessed though an unpaired T test using Welch's correction $**P < 0.01$ (error bars represent the SEM) N=4, N=3 respectively.

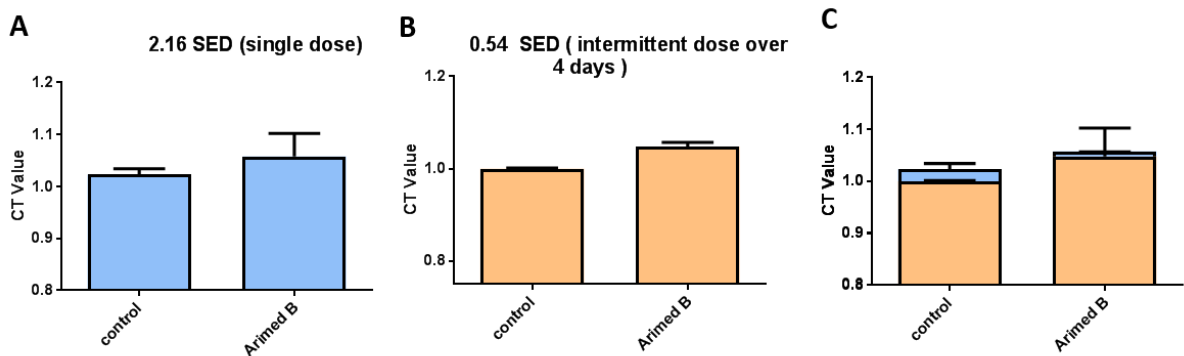


Figure 88: mtDNA damage in HDFn cells following exposure to either an intermittent or a single dose of arimed B

HDFn cells were treated with a single dose (2.16 SED) of arimed B (A) or an equivalent dose applied intermittently (B). The level of mtDNA damage was assessed relative to the unirradiated control using the 1kb assay. The difference in response between single and intermittent exposures is displayed (C). Statistical analysis was assessed though an unpaired T test using Welch's correction (error bars represent the SEM) N=4, N=3 respectively.

4.4.7 Comparison of mtDNA damage following exposure to intermittent and an equivalent single dose of solar light -11Kb QPCR assay

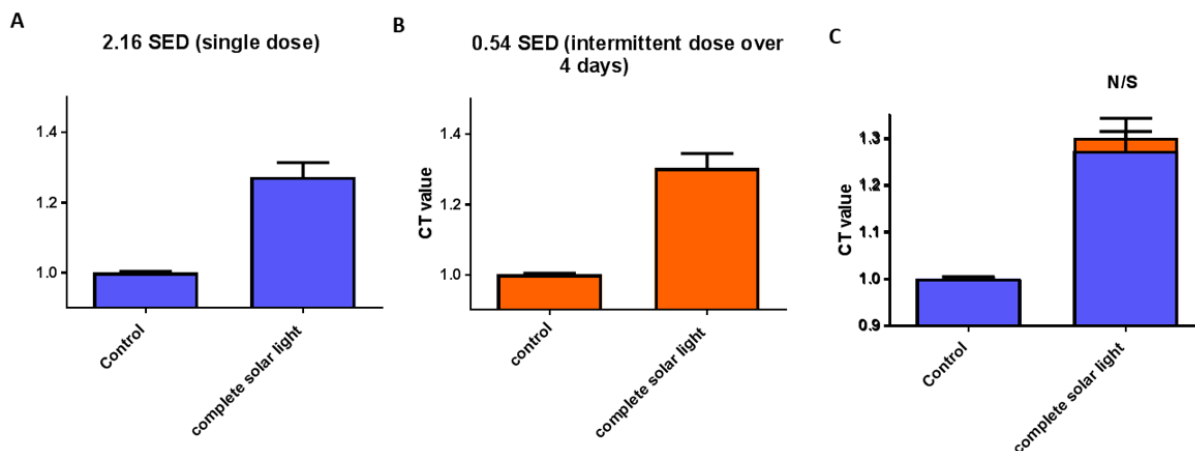


Figure 89: mtDNA damage in HDFn cells following exposure to either an intermittent or a single dose of complete solar light

HDFn cells were treated with a single dose (2.16 SED) of complete solar light (A) or an equivalent dose applied intermittently (B). The level of mtDNA damage was assessed relative to the unirradiated control using the 11kb assay. The difference in response between single and intermittent exposures is shown (C). Statistical analysis was assessed through an unpaired T test using Welch's correction. N=3, N=3 respectively.

The 1kb template was initially used to quantify the mtDNA damage levels. Greater levels of damage were detected in cells dosed intermittently this implied that receiving intermittent doses of solar light was more damaging than a single large dose. Following on from this finding the levels of damage were reassessed using the 11Kb QPCR assay. The 11kb fragment template spans a wider area of the mitochondrial genome (Figure 90) and has been reported to have greater levels of sensitivity from previous work carried out in the lab. This was confirmed in the samples assessed as higher CT values could be detected using the 11kb assay (Figure 91). HDFn cells dosed with a single 2.16 SED dose of complete solar light or intermittent doses at 0.54 SED were seen to have similar levels of damage when assessed using the 11kb assay with no significant differences in Δ CT value compared to unirradiated control.

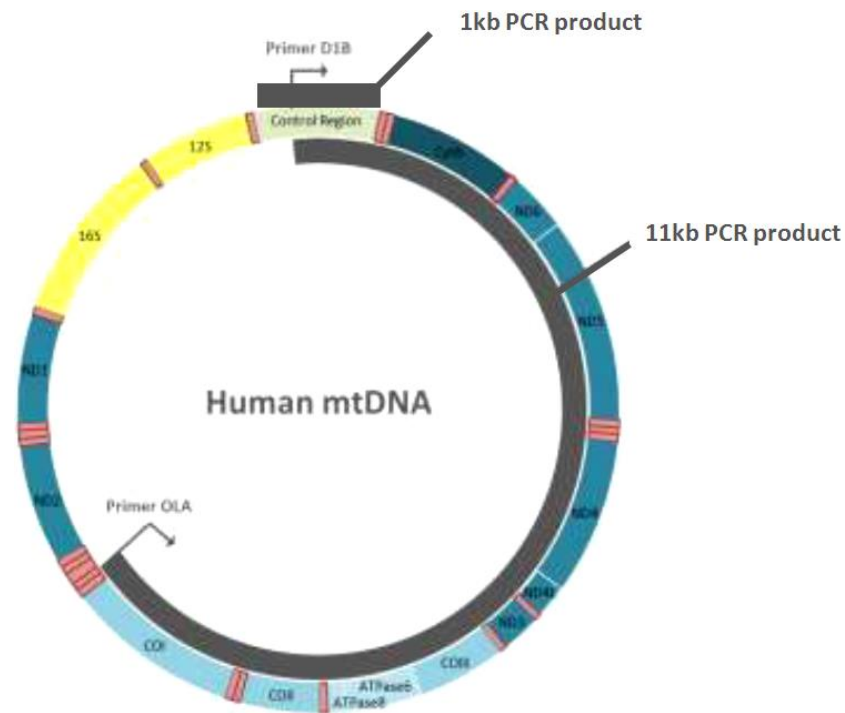


Figure 90: Amplification regions of the 1kb and 11kb QPCR fragments

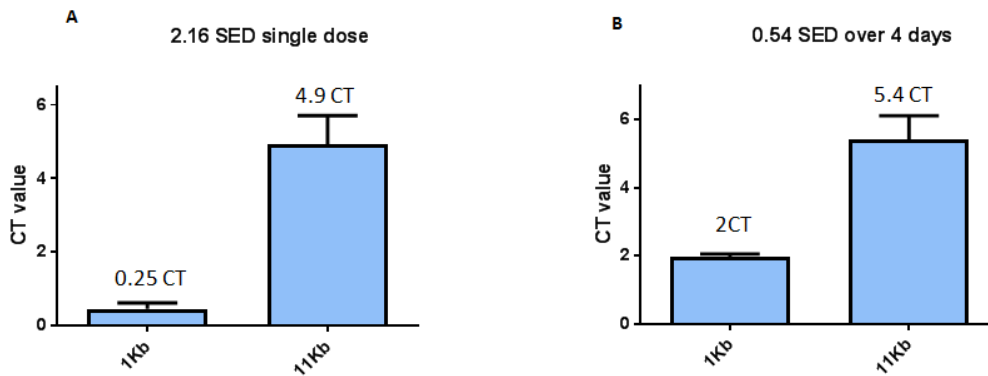


Figure 91: mtDNA damage detection using the 1Kb and 11kb fragments following single and intermittent dose exposure to solar light

The 1kb assay is seen to detect a 0.25 Δ CT following exposure of HDFn cells to a single dose of 2.16 SED complete solar light (A). Intermittent 0.54 SED doses of complete solar light over 4 days show a greater difference in CT value (2 CT) (B) compared to the single dose exposure (A). The Δ CT detected with the 11Kb assay is similar across both dosing patterns (A and B).

4.4.8 mtDNA damage susceptibility

Further investigations were carried out using 1Kb fragment QPCR analysis to identify whether regions across the mtDNA genome may display different susceptibility levels to solar light induced damage. Primer pairs were initially assessed for their ability to amplify DNA across a range of mtDNA concentrations and establish the linear range for the QPCR amplification experiments. Unirradiated control mtDNA samples from HDFn cells were used to establish the dose response curves using the primer pairs described (Figure 92). A linear relationship (R^2 equal to or close to 1) between mtDNA concentration and CT value could be seen with a 1CT increase being detected with each mtDNA doubling. This linearity was observed with all four primer pairs tested (Figure 92). The efficiency of the QPCR was also been calculated (E) from the slope of the graph using the following equation:

$E = 2^{(-1/-\text{slope})}$ (Log² is applied as a 1:1 dilution of the DNA samples was carried out)

$\%E = (\text{slope value} - 1) \times 100$

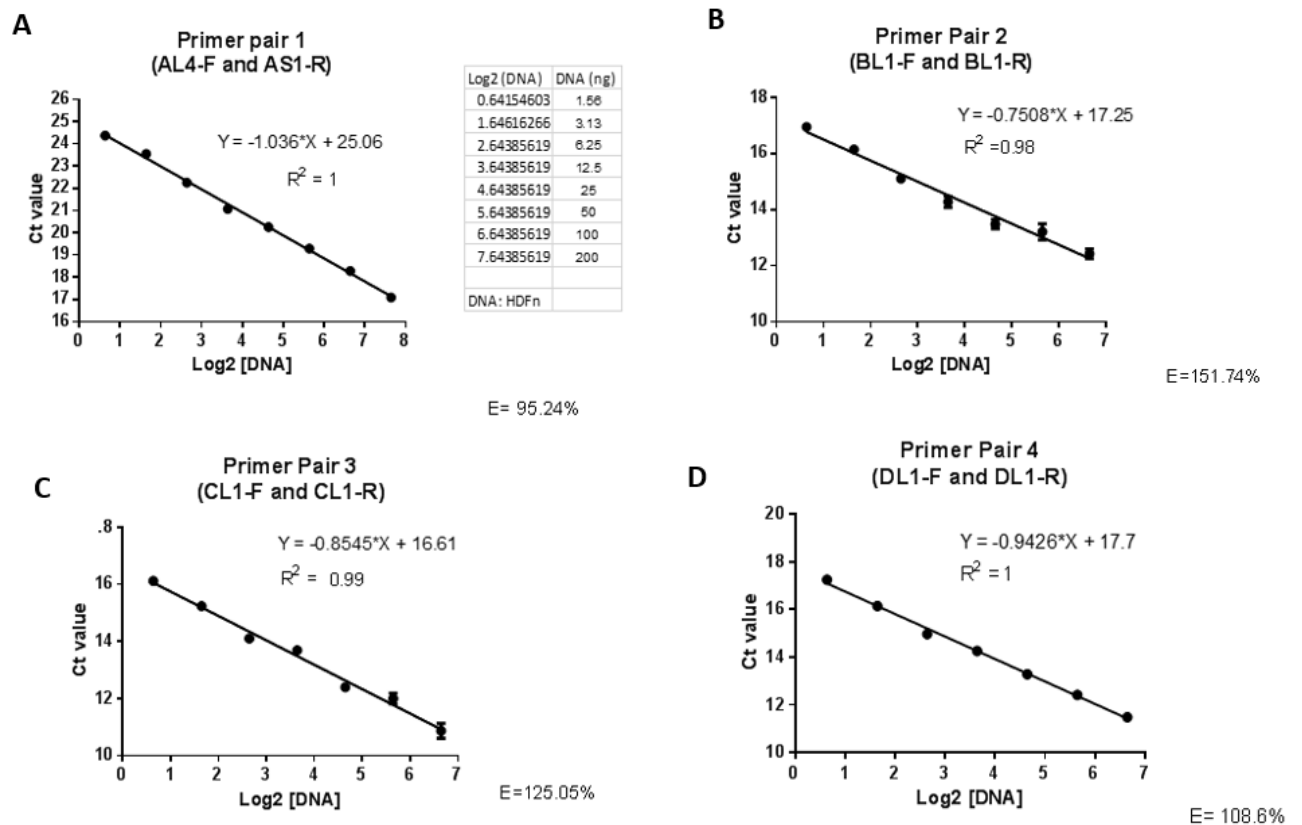


Figure 92: Standard curve assessing the linear range amplified by the 1kb primer pairs

DNA samples extracted from untreated HDFn cells were diluted at the concentrations shown in the table. The DNA samples were used to assess the level of damage detected by each of the primer pairs AL4-F and AS1-R (A), BL1-F and BL1-R (B), CL1-F and CL1-R (C), DL1-F and DL1-R (D). A linear relationship between DNA concentration and CT value was detected as shown by the R² value. E represents the efficiency of the primer pairs, Statistical analysis was carried out using linear regression analysis N=3.

Primer Pair	PCR efficiency (%) found from experimental samples assessed	PCR efficiency (%) (Rusforth et al., 2010)
AL4.F and AS1.R	95.24	69.4
BL1.F and BL1.R	151.74	89.0
CL1.F and CL1.R	125.05	85.1
DL1.F and DL1.R	108.06	85.4

Table 11: QPCR efficiency for each primer pair and comparison with previous findings in the literature (Rothfuss et al., 2010)

4.4.9 Assessing the level of mtDNA damage across the mtDNA genome following exposure to solar light

The level of damage detected by each of the primer pairs targeting different regions of the mitochondrial genome was investigated. Samples of mtDNA from three independent experimental repeats were extracted from HDFn cells receiving an intermittent dose of 0.54 SED over 4 days. A change in CT of approximately 2 compared to the unirradiated control was detected for each of the experiments 1-3 (Figure 93) as shown by the Δ CT value.

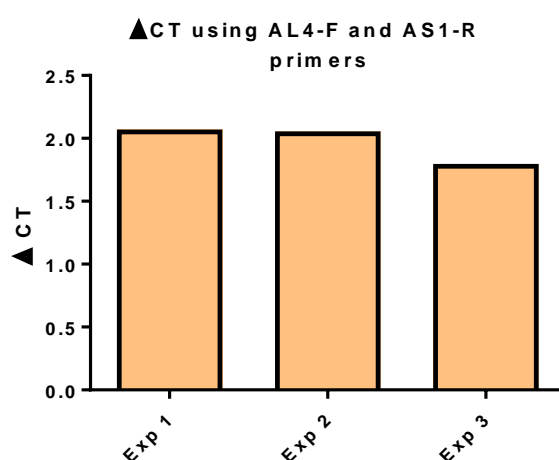


Figure 93: mtDNA damage level in HDFn cells following exposure to complete of solar light

HDFn cells were treated with complete solar light (0.54 SED over 4 days) and the level of mtDNA damage assessed relative to the unirradiated control cells. The Δ CT values from three independent experiments are displayed. All three experimental repeats show a similar level of mtDNA damage induction.

DNA from the three independent repeats were subsequently assessed for mtDNA damage levels using each of the 4 primer pairs described in Table 11 and the Δ CT compared between the primer pairs. No significant differences in Δ CT were found across mtDNA in the different regions assessed (Figure 94). This suggests that the damage susceptibility level along the mitochondrial genome is similar in the regions tested following exposure to complete solar light.

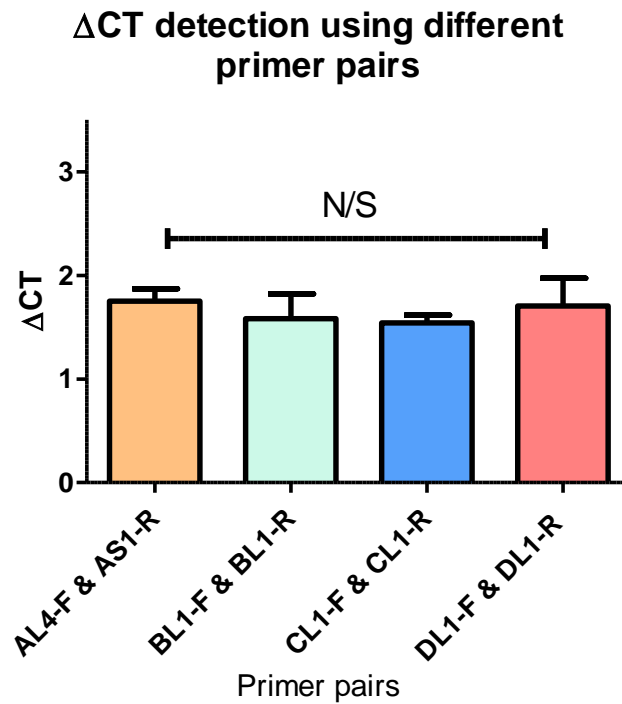


Figure 94: Level of mtDNA damage detection across different regions of the mitochondrial genome.

Primer pairs spanning different regions of the mitochondrial genome (each approximately 1kb in size) were used to amplify DNA from HDFn cells following the treatment of cells with complete solar light (2.16 SED). The results represent the change in mtDNA damage relative to the unirradiated control cells. A one-way ANOVA with Bonferroni's post-hoc was carried out to compare the mean of each column with the mean of every other column (error bars represent the SEM) N=3.

4.5 Discussion

4.5.1 Presence of a reduced amount of UV alongside IR and VIS leads to synergistic ROS generation in skin cells

Sunscreen formulations usually contain a mixture of active ingredients immersed in the oil and/or water phase. Conventional sunscreens are designed to block against UVB along with a proportion of the UVA rays (Diffey, 2016; Gilbert et al., 2013). The European standard for the level of UVA protection offered by sunscreens is set in place by Cosmetics Europe. The Personal Care Association requires that the ratio of UVA protection offered to be at least one third of the SPF intended (Fourtanier et al., 2012).

Not all sunscreens claim to provide protection against IR and VIS (Diffey and Cadars, 2016), although some active ingredients such as the mineral compounds TiO₂ and ZnO do provide partial protection in the IR and VIS regions (DiSomma and Brion, 1999). In order to simulate the UV blocking ability of sunscreens in vitro glass and plastic filters were used to remove UVB and partially block UVA rays from complete solar light. Filters were selected on the basis of their availability and compatibility for use with the Newport solar simulator device.

The results demonstrate that when a percentage of solar UVA in the range of 49% acts alongside the IR and VIS bands, a synergistic effect in terms of ROS generation can be seen as demonstrated in both cell line and in primary cells. The level of ROS generation is greater with the glass filter compared to the additive effects of the IR plus VIS and solar UV dosing conditions combined. Use of the plastic filter did not lead to synergy perhaps due to the low level of UVA passing through. Such findings have not been demonstrated previously and provide further evidence to the synergistic effects described in chapter 3. When UVA is present alongside IR and VIS the cell may be more susceptible to ROS generation due to the IR, VIS and UVA targeting different chromophores within the skin (Sinha and Häder, 2002). Further investigations may be required to establish these initial findings.

4.5.2 No synergy in mtDNA damage levels was detected when a percentage of UVA was present alongside IR and VIS

Solar light with reduced levels of UV does not produce synergistic effects in terms of mtDNA damage. This may be due to the different mechanistic action of solar light in producing damaging effects in mtDNA. As mentioned previously DNA damage can be induced both directly through UVB absorption and indirectly via UVA mediated ROS generation (Sinha and Häder, 2002). As well as reducing the UVA rays to 49%, the glass filter removes the UVB component which therefore eliminates the direct UVB DNA damaging effects which may otherwise occur.

4.5.3 Sunscreen formulations are able to provide cellular protection against mtDNA damage

Experiments were carried out to determine whether the sunscreen formulations assessed are able to protect against solar radiation. Protection was seen against complete solar light, UVA and UVB bands following the application of SPF 15 and SPF 30 formulations. The sunscreens did not however provide protection against IR which was not surprising as neither formulation claimed to do so. Many formulations that provide IR protection rely on antioxidants being present (Meinke et al., 2011). It may be that formulations are required to be in direct contact with the cells to enable protection. Such experiments involving the use of commercial sunscreens would not be feasible in cell culture monolayers. Commercial sunscreen formulations may however be assessed on whole skin models.

Sunscreens are typically assessed for their ability to provide protection against erythema following application ($2\text{mg}/\text{cm}^2$). It is assumed that sunscreens with a high SPF provide protection against mtDNA, this has not however been shown directly (El-Boury et al., 2007). The level of mtDNA damage provides an excellent biomarker for measuring damage arising from solar radiation exposure. This is due to the fact that mitochondria can accumulate multiple mutations as a result of their limited repair mechanism and compensatory ability due to the large numbers present within a cell. Erythema is used as a marker for assessing the SPF property of sunscreen formulations. mtDNA damage however can occur sooner as the reddening effect of skin is the resulting response to damage (Diffey et al., 1997). Sunscreens ($2\text{mg}/\text{cm}^2$) were shown to have a protective effect on HDFn cells against solar light both when a single large dose was applied and during intermittent dosing exposures. No significant difference in terms of protection against mtDNA damage was seen between the SPF 15 and SPF 30 formulations. This is not surprising as SPF 15 blocks approximately 93% of the UVB whilst SPF 30 blocks 97% (Gilbert et al., 2013; Fourtanier et al., 2012).

4.5.4 Exposure to intermittent and single doses of solar light both lead to similar levels of mtDNA damage as demonstrated using the 11kb QPCR assay

The level of mtDNA damage accumulation was assessed following exposure to a single large dose and smaller intermittent doses of solar light over time. Consistent with the previous findings, complete solar light leads to the greatest level of mtDNA damage. Doses of arimed B and solar UV show lower levels of mtDNA damage relative to complete solar light. The damage seen in the intermittent dosing experiments was progressive starting at days 2-3. The 1kb assay showed higher levels of damage when intermittent doses were applied compared to the single equivalent dose. This finding may however be due to the dynamics of the 1kb fragment template region. The experiments carried out demonstrate the greater sensitivity of the 11kb assay. Data for the 11kb assay shows similar levels of damage following intermittent and single dose exposures to complete solar light. The results of the 11kb QPCR data suggest a reciprocal effect of solar radiation whereby mtDNA damage accumulates progressively over time following each exposure. The Bunsen-Roscoe law (BRL) of reciprocity states that a certain biological effect is directly proportional to the total energy dose irrespective of the administered regime (Barolet et al., 2016a). These findings perhaps highlight the need for protection against solar radiation over time as mtDNA damage is seen to accumulate. Mitochondria have been associated with the carcinogenic process due to their role in apoptosis as well as somatic mutations as observed in a wide range of tumours in humans. It is not however clear whether mtDNA damage is directly linked to skin cancer development. Nevertheless mtDNA damage is thought to act as a good indicator for the level of nDNA instability in cells (Penta et al., 2001; Durham et al., 2003a).

4.5.5 mtDNA damage levels were seen to be similar across the regions of the genome assessed following exposure to solar light.

Levels of mDNA as well as nDNA damage can be detected using a broad spectrum of methodically different approaches. Many of these techniques however are tedious, involve radioactive labelling, or require considerable optimisation efforts and a high amount of genomic DNA. One of the most prominent and widely used methods is Southern blot analysis,

which is able to detect DNA strand breaks semi quantitatively via a multi-step procedure and requires high amounts of sample material. Single Cell Gel Electrophoresis, commonly known as the comet assay, enables the detection of single-and double-strand breaks as well as alkali-labile DNA sites under alkaline conditions. Such techniques however deliver only partially quantifiable values (Evans et al., 2016). High-performance liquid chromatography (HPLC) in combination with different detection methods, e.g. electrochemical (ECD) or the more recently described isotope dilution and tandem mass spectrometry (MS) display a quantitative approach to detect specifically damaged DNA products (Frelon et al., 2000).

The QPCR assay has the advantage of being able to detect a wide range of DNA lesions which are capable of disrupting the progression of DNA polymerase. This includes the detection of strand breaks as well as DNA adducts. No prior knowledge of the specific DNA lesions is required. The ability to detect changes in mtDNA copy numbers is advantageous as some treatments may lead to changes in the mtDNA copy numbers. The QPCR assay permits the analysis of both mtDNA and nDNA simultaneously as target primers are specific and can be used to compare how genotoxins effect different parts of the genome. The assay requires small amounts of DNA (as little as 1ng per sample), which allows for small samples to be used (Bowman and Birch-Machin, 2015).

One limitation of the QPCR method is that the damage detected is relative to the untreated control. It cannot be used to obtain absolute values from the treated samples and compared to a standard curve of treated samples. The non discriminatory nature of PCR in terms of DNA damage may also be seen as a weakness as well as being a strength. Notably the 8-hydroxydeoxy-guanosine does not cause disruption of the DNA polymerase enzyme and is therefore not detected (Maslov et al., 2013).

The application of sequence-specific primers allows for the investigation of putative hot spots for mtDNA vulnerability along the mitochondrial genome and enables the study of any

genomic in the mitochondria as well as in the nucleus in a real-time approach (Bowman and Birch-Machin, 2015).

Interestingly, DNA mutations are thought to be localised along the entire mitochondrial genome but predominantly in the non-coding regulatory D-Loop suggesting an increased susceptibility for mutations in human samples. Employing the QPCR method the authors were able to show that the D-Loop is more prone to ROS derived DNA damage relative to other mtDNA loci. A 95% efficiency was found with primer pair 1 in HDFn cells exposed to solar light compared to a 69.4% efficiency found in experiments carried out by Rothfuss et al., 2010. This difference may be due to the higher range of dilutions used by the authors as efficiency is taken as an average value. The reasons for the reported differential mtDNA damage remains unknown, the partially triple-stranded displaced structure in the D-Loop has been suggested as a plausible explanation for the predisposition of this region to excessive DNA damage (Rothfuss et al., 2010). Increased susceptibility in the D-Loop however was not seen in the experiments carried out to investigate the effects of solar light induced damage on HDFn cells.

4.6 Summary of main findings:

- The synergistic effects of complete solar light could be observed through ROS generation when UVB was removed and the level of UVA reduced to approximately 50%. Synergy was not however observed in terms of mtDNA damage perhaps due to the role of UVB component in the direct damage of DNA bases.
- Sunscreens assessed acellularly at a dose of 2mg/cm² provided protection against complete solar light, UVA and UVB with SPF 15 and SPF 30. No protection was seen against IR. Sunscreens were able to provide protection against solar light induced mtDNA damage when applied during intermittent and a single large dose exposure.
- Discrepancies were highlighted between the 1 and 11kb fragment QPCR assays. The 11kb fragment was found to be more reliable in identifying mtDNA damage levels

following exposure to a single dose of solar light. mtDNA damage in intermittently dosed experiments was progressive starting at days 2-3.

- The 1kb fragment assay was found to detect similar levels of damage across the different mitochondrial genome regions assessed.
- The 1kb fragment however showed higher levels of damage when multiple doses of solar light were applied which suggests that it may not be suitable for damage detection during multiple dosing experiments.
- As expected the 11kb was found to be more sensitive when compared to the 1kb assay.

**Chapter 5 – Assessing the
Apparent Health Hazards of
Nanoparticulate TiO₂**

5 Chapter overview

TiO₂ is a mineral compound widely used as an active ingredient in sunscreens due to its ability to provide broad-spectrum protection whilst remaining chemically stable on the skin surface. TiO₂ is compatible with sensitive skin types which makes the compound an excellent alternative for use in place of the chemical filters (SCCP, 2013). Older generation sunscreens containing TiO₂ are regarded as less aesthetically appealing to consumers due to the white tint appearance and viscous feel they leave following application. Formulations containing mineral sunscreens have been improved by further micronizing the TiO₂ compound within the nanoscale range. Examples of the range and size in which TiO₂ particles are available are shown in Table 12. The word nano is loosely defined as an entity with one or more of its dimensions being within the size of 1-100nm (Stankovich, 2007;Teo et al., 2010). Having particles within this size range allows for more transparent formulations to be achieved with a broader UV blocking efficiency (Fakin et al., 2015).

TiO₂ is known to be a relatively inert compound however when photoactivated it is able to exhibit photocatalytic properties (SCCP, 2013). Such reactivity becomes concerning with smaller particles as the surface area becomes larger with decreasing particle size leading to higher levels of reactivity. Such interactions primarily result in the formation of ROS along with further downstream effects such as DNA damage and cell signalling responses (Hongbo Shi, 2013b).

TiO₂ is used within industry for a wide variety of applications such as for example in water cleaning systems due to its photocatalytic properties (Falck et al., 2009b). Such properties however are undesirable in sunscreen formulations therefore the TiO₂ used in newer sunscreen formulations is either doped and/ or coated with materials to reduce the ROS activity by 90% of that of the original parent compound (Yuan et al., 2010)

Particle name	Manufacturer	Crystal type	Average crystal size	Coating materials and concentrations
T805 Degussa20/80 RU/AN	Degussa	rutile/ anatase	21 nm	silicone dioxide <2.5%
T817 Degussa79/12/2 RU/AN/Fe	Degussa	rutile/ anatase	21 nm	silicone dioxide <2.5% (also doped with di-iron trioxide 2%)
UV-Titan M160	Kemira	rutile	17-20 nm	alumina 5.5-7.5%, stearic acid 10%
UV-Titan M212	Kemira	rutile	20 nm	alumina 5-6.5%, glycerol 1%
UV-Titan X161	Kemira	rutile	15 nm	alumina 8.5-11.5%, stearic acid 10%
UV-Titan X200	Kemira	rutile	20 nm	none
Eusolex T-2000	Merck	unknown	14 nm	alumina 8-11%, simethicone 1-3%
TTO 51A	Merck	rutile	35 nm	alumina 11%, silica 1-7%
TTO 51C	Merck	rutile	35 nm	alumina 11%, silica 1-7%, stearic acid 3-7%
MT-100 AQ	Mitsubishi/Tayca	rutile	15 nm	alumina 4-8%, silica 7-11%
MT-100 AR	Mitsubishi/Tayca	unknown	15 nm	alumina 4-8%, silica 7-10%
MT-100 T-L-1	Mitsubishi/Tayca	rutile	15 nm	alumina 3.3-7.3%, stearic acid 5-11%
MT-100SA	Mitsubishi/Tayca	rutile	15 nm	alumina 4-7.5%, silica 2-4%
MT100TV (or MT-100TV)	Mitsubishi/Tayca	rutile	15 nm	alumina 1-15% or 3-8%; aluminum stearate 1-13% or 1-15% or stearic acid 5-11%
MT100Z (or MT-100Z)	Mitsubishi/Tayca	rutile	15 nm	alumina 6-10%, stearic acid 10-16%
MT-500SA	Mitsubishi/Tayca	rutile	35 nm	alumina 1-2.5%, silica 4-7%
Mirasun TiW60	Rhodia	anatase	60 nm	alumina 3-7%, silica 12-18%
UV-Titan M262	Rhodia and Kemira	rutile	20 nm	alumina 5-6.5%, dimethicone 1-4%
Tioveil dispersions	Uniqema	rutile	10-28 nm	alumina 10.5-12.5% or 5-15% and silica 3.5-5.5%; alumina 5-15% and aluminum stearate 5-15%

Table 12: Showing examples of the range of TiO₂ particles available (SCCNFP, 2000)

A large body of evidence published both from academic institutes and regulatory body studies suggests that TiO₂ does not penetrate or otherwise bypass the skin surface and therefore does not come in to contact with viable skin cells (Miquel-Jeanjean et al., 2012). The majority of the studies carried out however have focused on investigating healthy skin. This has led to debates over the potential effects of nano TiO₂ use particularly in compromised skin states such as sunburnt, wounded and diseased skin (SCCP, 2013). Disruption of the skin barrier function however may allow for contact of TiO₂ with viable keratinocyte and potentially fibroblast cells. The amount of compound reaching the cells may accumulate over time with increasing use of the sunscreens. Further work is therefore required which will contribute to the discussion regarding the use of nano sized TiO₂ particles in sunscreen formulations (Teeguarden et al., 2007; Peira et al., 2014; Elena Peira a and Luigi Battaglia a, 2014).

The work in this chapter aims to optimise the use of existing methodologies to assess the effect of nanoparticulate TiO₂ on skin barrier function. Initial stages of the project involved creating dispersions of TiO₂ in physiologically relevant media suitable for use in cell monolayers. The suspensions were characterised for their stability and particle size as these

parameters may influence the experimental outcome seeing that the effects of TiO₂ are size dependent (Francesco Turci, 2013). Viability assays were also carried out to determine cytotoxicity and identify the sublethal dose of TiO₂ that may be used in later experiments.

TiO₂ has been shown to be internalised by fibroblast cells however, there is disagreement in the literature as to whether internalisation occurs in keratinocytes (Kiss et al., 2008). In the present study genotoxic effects were assessed in HDFn cells following the application of TiO₂ both with and without exposure to UV. Being a compound used in sunscreens the level of protection offered by the specific TiO₂ aerioxide (P25) was also investigated. Levels of ROS generation were assessed cellularly and acellularly using both the DCFDA and ROS-Glo method. A chemical sunscreen compound, Parsol HS, was tested for its ability to induce ROS and provide protection alongside TiO₂ due to its different mechanism of action.

Sunscreens are classified differently around the world and are regarded as cosmetics within the EU whilst for example in the US are over the counter drugs (Aldahan et al., 2015). In vivo animal testing of finished cosmetics is now prohibited with the application of the testing ban on finished cosmetic products being applied since September 2004, and the testing ban on ingredients or combination of ingredients applied since March 2009 (EuropeanCommission, 2013). Use of in vitro methods for studying compounds is therefore necessary. Existing in vitro methods have not been validated for the assessment of nano materials, however human skin or porcine ear skin are recommended sources of ex vivo skin within the Organization for Economic Cooperation and Development (OECD) guidelines (Shi et al., 2013) for absorption studies of chemicals in vitro. Reconstructed skin models are also available, although the integrity of their permeability barrier is somewhat lower than that of native skin (Abd et al., 2016).

Evidence exists to suggest that uncoated TiO₂ can enhance penetration of chemicals through the skin which in sunscreens may in turn result in local or systemic sensitization (Crosera et al., 2015). The effect of nanoparticulate TiO₂ on the percutaneous absorption of radiolabelled chemical compounds through human skin was investigated in vitro. Solar simulated light was

applied to skin in the presence of TiO₂ to assess the potential effects on the disruption of skin barrier function. Such disruption may also suggest the possible permeation of smaller size TiO₂ particles through the skin which would require further confirmation. A further percutaneous absorption model CutaFlex™ was assessed to investigate the potential effect of flexion on skin. The CutaFlex™ model is theorised as being a more representative model of compound absorption through the skin as skin flexion may contribute towards the permeation of compounds across the skin layers (Viegas, 2014).

This chapter of the thesis is presented as two sections with section I focusing on the characterisation of TiO₂ suspensions and assessment of both the protective effects and the toxicity profile of TiO₂. Section II addresses the potential influence of TiO₂ on of skin barrier disruption.

Chapter 5 - Section I

5.1 Chapter aims

- Optimise and characterise TiO₂ dispersion and stability in suspension.
- Assess a selection of the available cell viability assays for investigating the effect of nano TiO₂ cytotoxicity.
- Assess the ability of the TiO₂ compound under study in providing protection against solar light.
- Determine the level of ROS generation, genotoxicity and internalisation following exposure of skin cells to TiO₂.

5.2 Chapter specific methods

Details of the Solar simulated light (plus or minus IR and VIS) dosing and UV lamp dosing experiments (Cleo performance plus glass, TL01 and UV6) can be found in the general methods section (Chapter 2). A description of the cell viability assays (MTS and RT-Glo assay), cell culture methods and ROS detection methods (ROS-Glo and DCFDA assay) can also be found in chapter 2.

5.2.1 Dispersions and suspension characterisation

5.2.1.1 Reagents

Uncoated TiO₂ (aeroxide P25) was purchased from Evonik and has a primary particle size ranging between 20-30nm with 98.03% purity comprising of 81% anatase and 19% rutile (W/W) crystalline form (French et al., 2009). 2-Phenyl-5-benzimidazolesulfonic acid (Parsol HS) was obtained from DSM. The Tiron antioxidant compound was purchased from Sigma.

5.2.1.2 TiO₂ oil in water suspension

Concentrations of TiO₂ (0-5mg) were initially dispersed in PBS along with a range of glycerol at between 0-10% (V/V). TiO₂ was initially dispersed in suspension by vortexing for 30 seconds before being assessed visually for signs of settling.

5.2.1.3 TiO₂ working suspensions

Dry powder TiO₂ was suspended in deionised water (1mg/ml), vortexed for 15 sec and sonicated for 15 min using a bath sonicator (Grant ultrasonic bath XB2) as described by (Ji et al., 2010). Working suspensions were later made by aliquoting TiO₂ suspension from 1mg/ml stock solution into either PBS or 10% FCS in DMEM (Figure 95). A further 15 min sonication step was carried out.

5.2.1.4 Peak absorbance of TiO₂

TiO₂ (1mg/ml) in PBS plus 10% glycerol was diluted multiple times (1:1) to create a range TiO₂ suspensions. Photospectrometry was used to measure the absorbance of each dilution across a range of wavelengths (250-450nm). The maximum absorbance peak was recorded for each dilution. The average maximum absorbance value was taken as the characteristic peak for TiO₂ and used as the wavelength for assessing suspension absorbencies in further experiments.

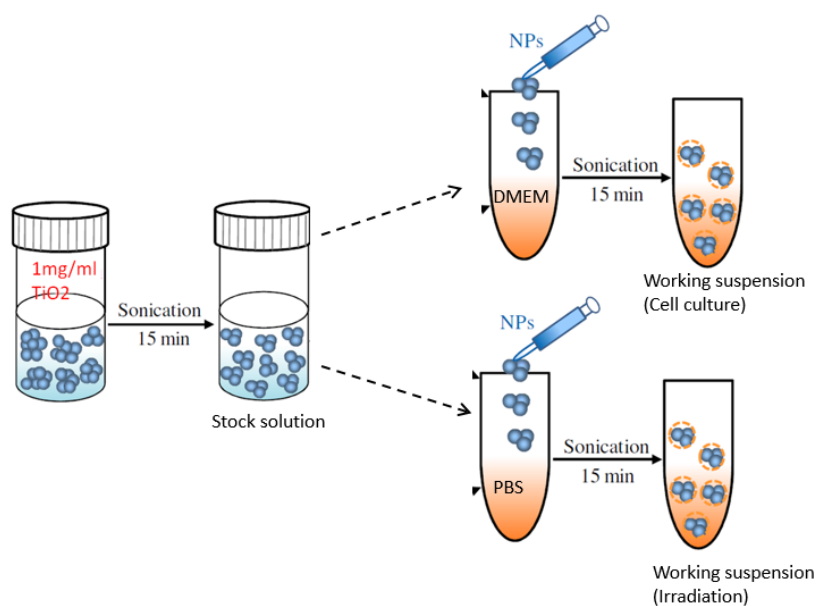


Figure 95: Outline of method used to creat TiO₂ working suspensions (Ji et al., 2010)

5.2.1.5 TiO₂ stability in suspension

Working suspensions of TiO₂ were prepared as described in section 5.2.1.3. Samples (2ml) were placed in plastic cuvettes and occluded for the duration of the experiment. Absorbance readings were assessed over time at a wavelength of 350nm. Readings were recorded every 10 min for a duration of 72h.

5.2.1.6 TiO₂ particle sizing

Nanosight NAS (Malvern) equipment was used to assess the size of TiO₂ particles in dispersion. The mode and mean sizes of the particles were recorded. Three samples were prepared for each condition and an average of the readings was taken as the final value. The method relies on the Brownian motion of particles in dispersion which can be visualised and measured. Larger particles scatter light at a greater level and move more slowly, these can be seen more clearly relative to the smaller particles which move more rapidly, scatter less light and appear to be dimmer during visualisation.

5.2.2 TiO₂ internalisation

HDFn cells were plated in 12 well plates at a density of 5000 cell/well and dosed with TiO₂ suspensions (0-50µg/ml) in DMEM the following day. Suspensions were prepared as described in section 5.2.1.3. Prior to visualisation using phase contrast microscopy cells were washed with PBS three times and incubated in PBS either for 0, 4 or 24h.

5.2.4 Assessing the protective abilities of compounds (TiO₂ and Parsol HS)

5.2.4.1 Acellular experiments

Dispersions of TiO₂ and Parsol HS compound were prepared in PBS at various concentrations as described in section 5.2.1.3. Dispersions were weighed to calculate a dose of 2mg/cm² before applying to transpore tape fixed to a custom made scaffold. The Hydrosun meter (Hydrosun lamp) or spectrophotometer (Solar Simulator) was placed under the transpore tape and readings taken to determine the ability of the dispersions to block the solar radiation energy.

5.2.4.2 Cellular experiments

Dispersions were applied to transpore tape as described above (section 5.2.4.1). The tape was then placed on top of a 96 well plate before cells were dosed with the appropriate solar light source. The level of ROS generation was determined using the DCFDA method (Chapter 2 section 2.3.3).

5.3 Results

5.3.1. Characterisation of TiO₂ suspensions

The TiO₂ assessed in this chapter is available in powder form and requires dispersion prior to use. Suspensions were prepared in various dispersion media including water, PBS (plus or minus glycerol) and DMEM (plus or minus FBS). Previous work carried out on nano TiO₂ has highlighted the importance of suspension characterisation as the toxicological effects of suspensions may be attributed to their nano size range. It should be noted that TiO₂ in the micronised form is considered inert (SCCP, 2013). Toxicological concerns have been suggested to arise when particles are further micronised into the nano range as described in more detail in chapter 1. Experimental outcomes may therefore vary depending on the size and distribution of the particles in suspension.

Following the dispersion of TiO₂, rapid settling was observed in physiologically relevant media (PBS and DMEM), this was not however the case for water where TiO₂ remained stable. These settling observations were quantified using spectrophotometry to establish a time period whereby the suspensions remain stable. This would then allow for suspensions to be used in experiments during the estimated stable phase. The level at which light is absorbed through the test suspensions is an indication of the amount of TiO₂ in suspension.

TiO₂ (1mg/ml) was initially dispersed in PBS plus 10% (V/V) glycerol to make a stock suspension. This was diluted multiple times (1:1) before measuring the absorbance of the dilutions using spectrophotometry across a range of wavelengths (250-450nm). Absorbance was normalised to a blank PBS plus glycerol control in each case. The maximum absorbance peak was recorded for each dilution (Figure 96) with the average maximum absorbance value being taken as the characteristic peak for the TiO₂ compound. This was used as the wavelength for assessing suspension absorbance in further experiments.

Following the analysis of the dilutions assessed, the maximum absorbance peak for TiO₂ was determined to be 350nm. This wavelength was later used in successive experiments to determine the level of absorption in further test suspensions as it gave the highest peak for the specific compound used. TiO₂ dispersions in PBS alone were the least stable as suspensions were seen to settle completely within 1h. Glycerol was added to PBS to create a potentially nontoxic oil-in-water emulsion to replicate the composition found within sunscreen formulations. TiO₂ in water showed the greatest level of stability with very little settling occurring over a 3 day period. Due to the hypotonic nature of water it could not be used in cell culture and irradiation experiments.

Sonication is reported in the literature to aid the dispersion of TiO₂ in suspension (Ji et al., 2010;Faure et al., 2013). Test suspensions were sonicated as described in the chapter specific methods (section 5.2.1.3). Settling experiments however showed sonication to have no effect on the rate of TiO₂ settling over time (Figure 100). Use of 10% (W/V) FCS was seen to aid TiO₂ stability in the DMEM cell culture medium (Figure 97).

The level of TiO₂ settling in working suspensions, 10% FCS in DMEM (Figure 98) and PBS (Figure 99) at different concentrations was determined over 72 h by measuring the absorbance of suspensions at various time intervals. The level of settling over 72 h was calculated as a percentage of the original concentration. Settling levels could then be taken into consideration as a factor when performing experiments.

Nanomaterials in the soluble and /or biodegradable group may be adequately assessed using mass metrics. For the insoluble group (including TiO₂) a consideration of other metrics such as the number, distribution and surface area of the particles is required as size and aggregation state effects the analysis and interpretation of experimental results. For toxicological analysis an ideal nano TiO₂ suspension should be stable, homogenous and have particles within a similar size range. Although numerous papers have used TiO₂ on skin and non-skin cell lines, it is not clear how stable the suspensions are and whether TiO₂ remains “nano” during the course of the experiment (SCCS, 2013). This has made it difficult to compare data between

different studies as conditions for assessing nanoparticles are not standardised (Jaeger et al., 2012;Saquib et al., 2012;Gurr et al., 2005b;Peira et al., 2014).

Cell culture work in this project requires stable suspensions in media (DMEM) as well as stable suspensions in PBS for cell irradiation. PBS suspensions are required as studies carried out previously have shown that irradiating cells in culture media results in spurious results due to the proteins absorbing UV and becoming unstable (Boulton et al., 2011).

To assess the particle sizes of TiO₂ in suspension a zeta-sizer was used over at PHE labs with the help of Dr Graham Holliman. The mode value for TiO₂ particle sizes in PBS at 1mg/ml was 51.75nm. Sonication for 20min in a water bath had no effect on size (51.33nm) (Figure 101). The mode value for TiO₂ in water at 1mg/ml was 41.66, which appeared to be smaller than the size of particles in PBS. Sonication was seen to reduce the particle size. Similar effects were observed with the higher concentration (5mg/ml) TiO₂ in water whereby sonication reduced the mode size of particles in suspension. As can be seen from the mean particle sizes, there was a wide range of particle sizes as indicated by the large SEM of the bars.

TiO₂ dispersions in DMEM take a similar length of time to reach 50% of the starting concentration when a range of doses are assessed within PBS dispersions, the lower concentration suspensions of TiO₂ were found to be more stable than the higher concentrations (Figure 101).

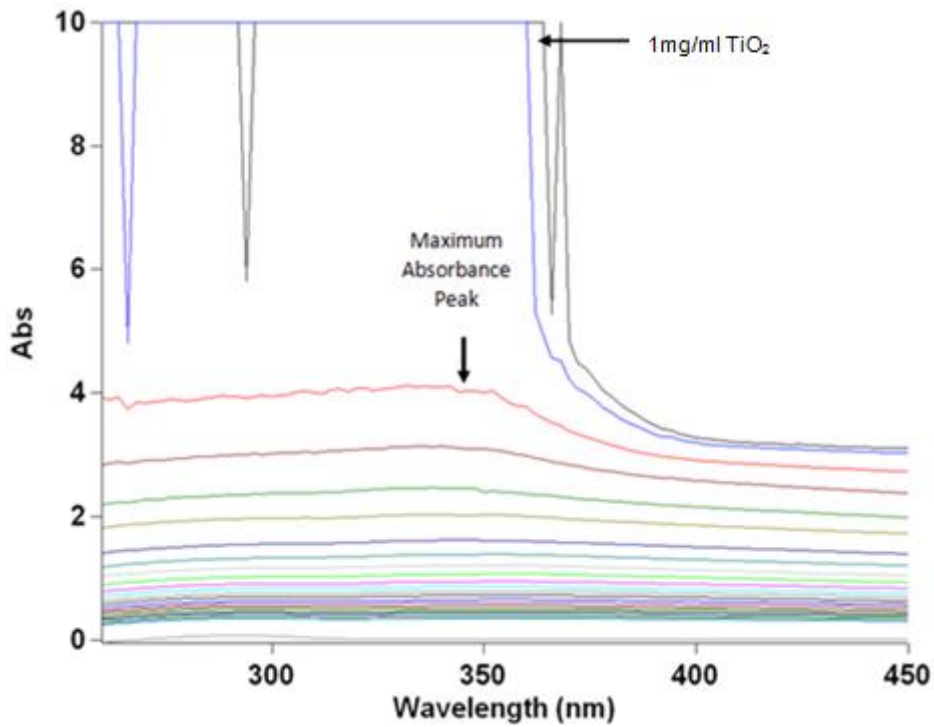


Figure 96: Absorbance profile of TiO₂ suspensions at different concentrations

TiO₂ was dispersed in PBS plus 10% glycerol as a stock suspension of 1mg/ml. The 1mg/ml dose was too high and showed maximal absorbance readings. A 1:1 dilution of the suspension was carried out to achieve a range of lower concentrations. The successive lines represent a 1:1 dilution of the TiO₂ suspensions in PBS plus 10% glycerol. Absorbance readings were taken at wavelengths between 250-450nm. The highest peak from each absorbance reading was used to determine the average maximum absorbance peak for TiO₂. This was found to be within 350nm as shown on the graph N=2.

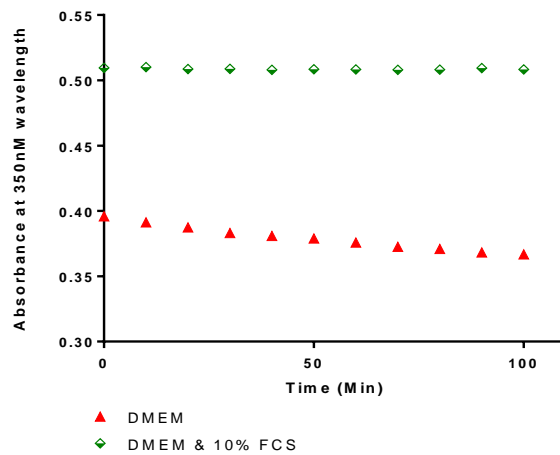
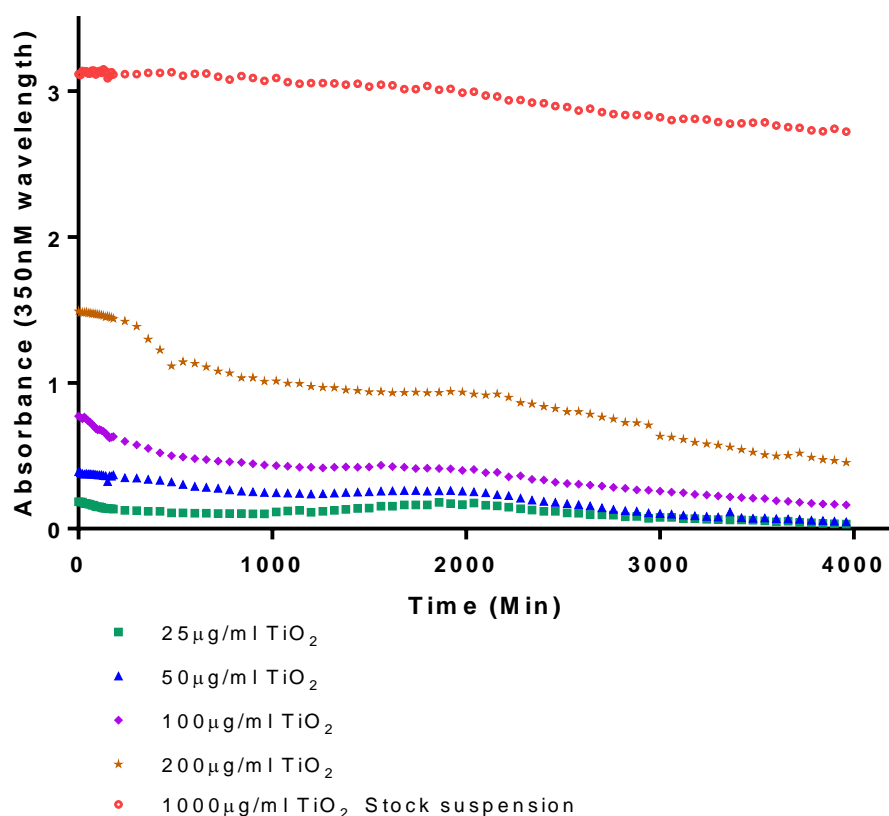


Figure 97: Comparison of TiO₂ settling with and without the addition of 10% FCS to DMEM cell culture medium
DMEM remains more stable relative to the time 0 control when 10% FCS is added

Stability of TiO₂ in DMEM

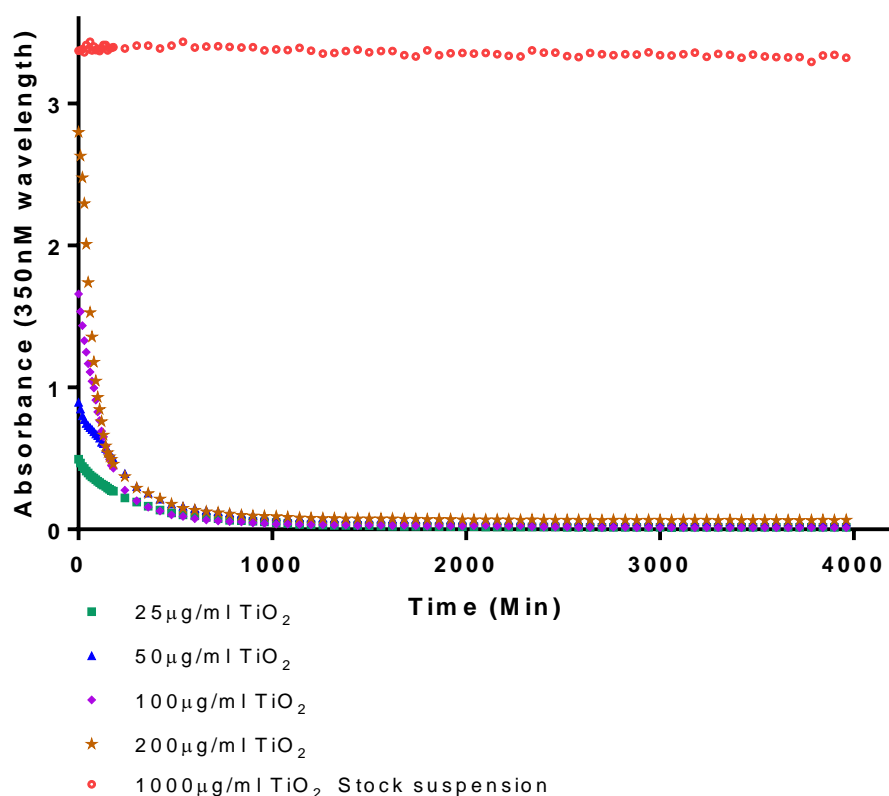


Working solution concentration (µg/ml)	Settling following 24h (%)	Settling following 48h (%)	Settling following 72h (%)	Time taken (h) to reach 50% concentration
25	25	55	83	46
50	35	70	88	39
100	45	65	79	35
200	37	51	70	46
1000 (stock suspension)	2	9	13	N/A

Figure 98: Absorbance analysis of TiO₂ in DMEM plus 10% FCS illustrating TiO₂ settling levels over 72h

Spectrophotometry was used to measure the absorbance of TiO₂ working suspensions in DMEM plus 10% FCS at 10 min time intervals over a time span of 72h. Complete settling can be seen at 150min. The TiO₂ stock solution (red line) remained stable for the duration tested. The table shows the percentage of TiO₂ settling at 24h time intervals along with the time taken to reach 50% of the original concentration. Data was obtained with guidance from Dr Sarah Jayne Boulton.

Stability of TiO₂ in PBS



Working solution concentration (µg/ml)	Settling following 24h (%)	Settling following 48h (%)	Settling following 72h (%)	Time taken (h) to reach 50% concentration
25	94	95	95	3
50	92	91	91	3
100	98	98	98	1.7
200	97	97	97	1.2
1000 (Stock solution)	0	0	0.5	N/A

Figure 99: Absorbance analysis of TiO₂ in PBS illustrating TiO₂ settling levels over 72h

Spectrophotometry was used to measure the absorbance of TiO₂ working suspensions in PBS at 10 min time intervals over a time span of 72h. Complete settling can be seen at 150min. The TiO₂ stock solution (red line) remained stable for the duration tested. The table shows the percentage of TiO₂ settling at 24h time intervals along with the time taken to reach 50% of the original concentration. Data was obtained with guidance from Dr Sarah Jayne Boulton.

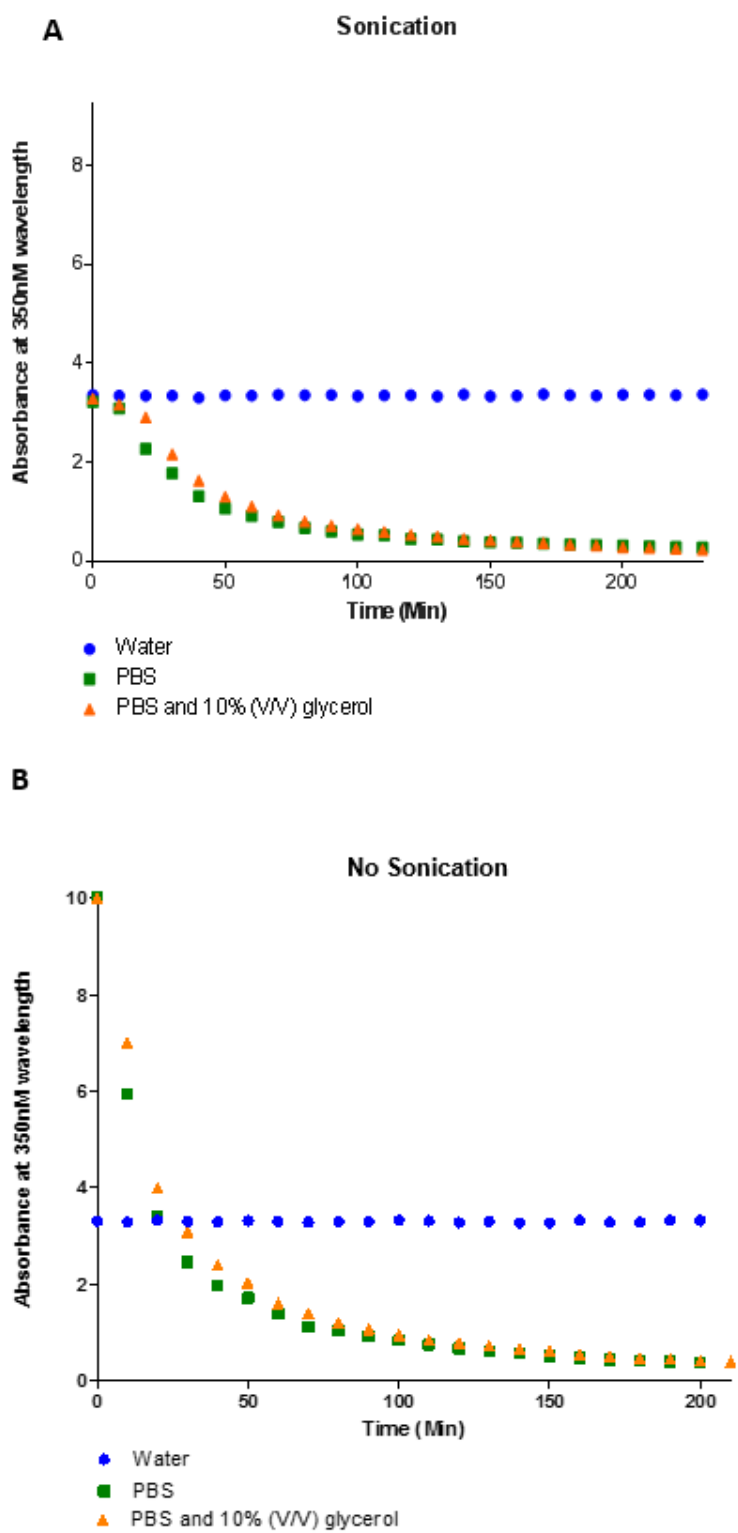


Figure 100: Effect of sonication on TiO₂ settling in PBS suspension
 Sonication for 20 min using a water bath sonicator (A) showed little effect on TiO₂ settling in PBS and PBS plus 10% glycerol when compared to no sonication (B). TiO₂ in water remained stable under both conditions.

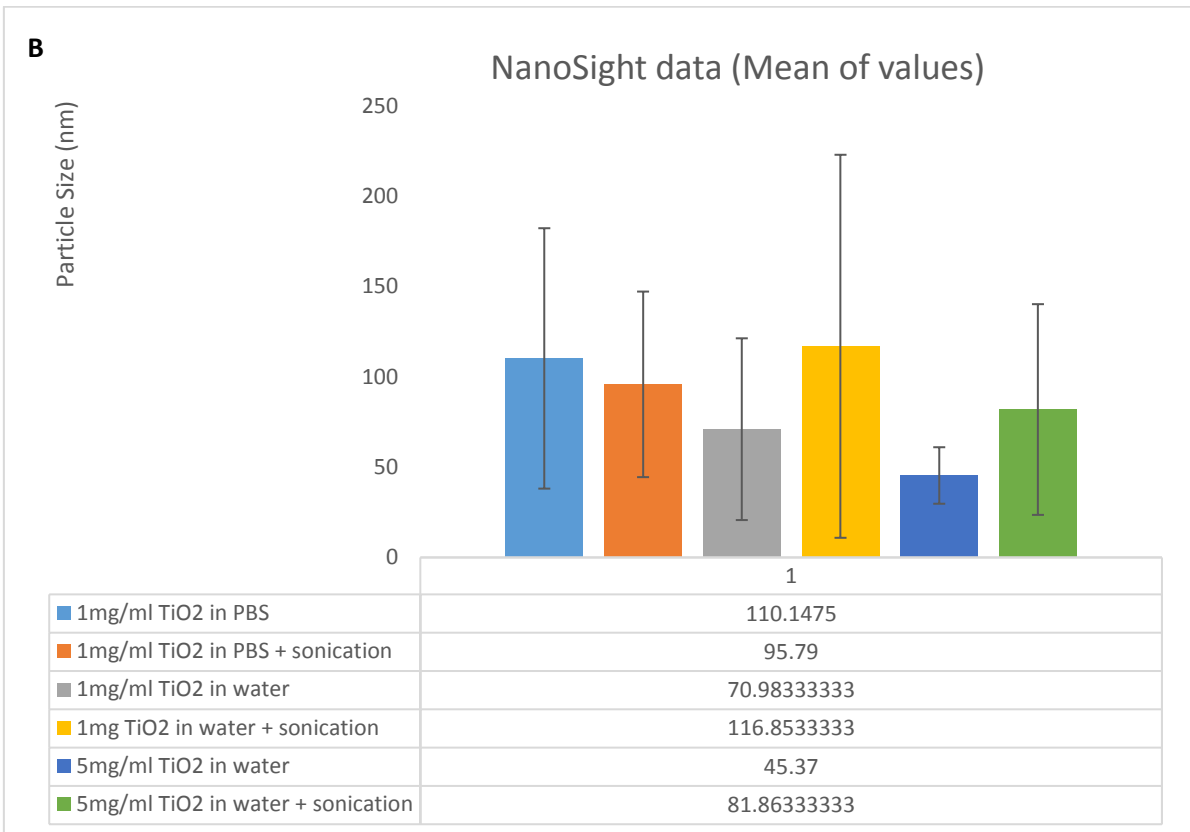
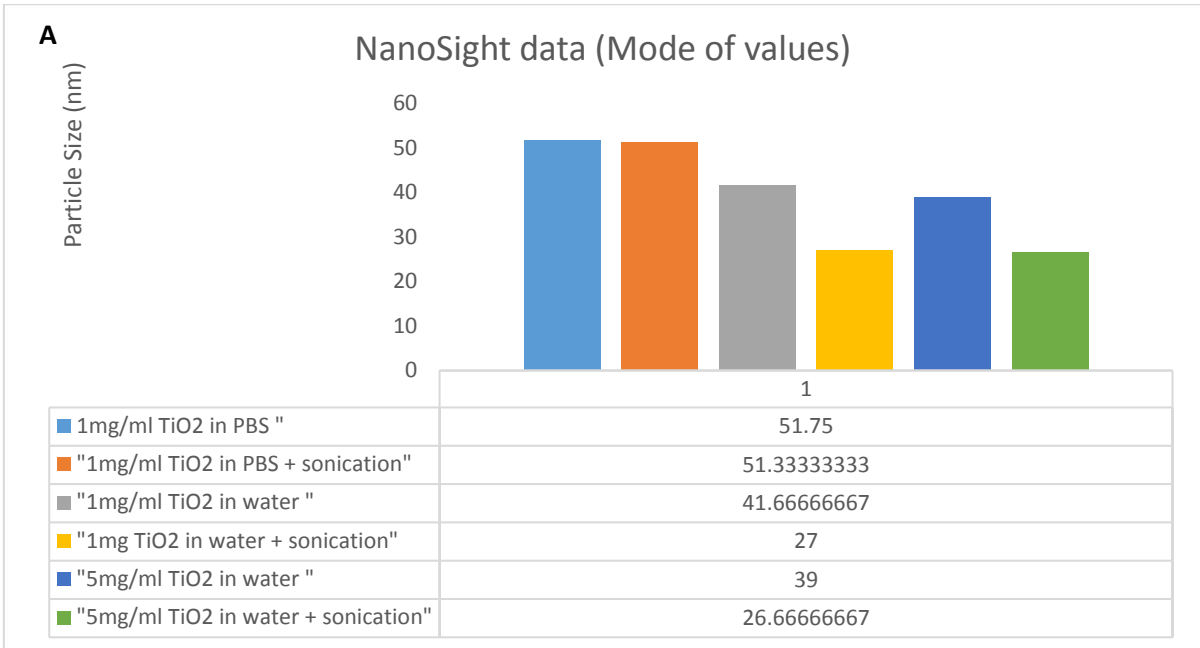


Figure 101: Assessing the average size of nano TiO₂ particles in suspension

TiO₂ particles were dispersed at a concentration of 1- 5mg/ml in either water or PBS. Suspensions were then assessed using the NanoSight instrument to determine the average size of the particles. The mode (A) and mean (B) particle sizes are shown (error bars represent the SEM) N=3

5.3.2 Cell viability assays for the assessment of TiO₂ and positive control compounds (Tiron and Parsol HS)

TiO₂ dispersions were assessed for cytotoxic effects on cells. This was carried out to identify the sub-lethal dose for use in further experiments. Various cytotoxicity assays were initially assessed with the aim of finding a more effective alternative to the MTS assay which is routinely used in the lab. The MTS assay assesses cell viability through the reduction of MTS, a tetrazolium compound, in to cell culture medium soluble formazan by the mitochondrial NAD(P)H-dependent dehydrogenase enzymes. This results in a colour change from golden yellow to orange/red which can be assessed through absorption analysis (Wang et al., 2010; Selim Uzunoglu and Uslu, 2010). The antioxidant compound Tiron was also used as a positive control where appropriate as this compound has been previously assessed in the lab and has shown cell death at higher concentrations.

RT-Glo is a more recently developed method that assesses cell viability in real-time through measurements of bioluminescence which relies on the reducing potential of cells. The assay involves adding NanoLuc[®] luciferase and a cell-permeant pro-NanoLuc[®] substrate to cells in culture. Viable cells reduce the proprietary pro-substrate to generate a substrate for NanoLuc[®] luciferase. This substrate diffuses from the cells into the surrounding culture medium, where it is rapidly utilised by the NanoLuc[®] enzyme to produce a luminescent signal correlating to the number of viable cells. The RT-Glo method has a numerous advantages as the reagents are stable, non-toxic for a time span of up to 72 h and may be added at any stage of the experiment. The assay also allows for multiple fluorescence readings to be made. No cell washing, removal of medium or further reagent addition is required to determine the number of viable cells. The same cells assessed with RT-Glo may also be used at the end of the experiment for further analysis such as multiplexing and nucleic acid analysis (Promega, 2016).

Parsol HS, a chemical sunscreen compound with broadband UVB protection was used as a further sunscreen active compound for assessment alongside TiO₂ in subsequent experiments. Being a chemical compound it protects against solar radiation through a different mechanism compared to TiO₂ (Aldahan et al., 2015). As mentioned previously TiO₂ mainly reflects and scatters light with some level of absorption whilst Parsol HS absorbs the solar radiation. Due to these differences in properties both sunscreen compounds were used for assessment where relevant.

Cell viability experiments were carried out on HDFn cells. The Tiron compound used as a positive control for the MTS assay showed a decrease in cell viability with increasing concentration as would be expected (Figure 102). Parsol HS concentrations above 5mg/ml lead to an 80% decrease in cell viability as seen in Figure 103. The MTS and RT-Glo assays were used in further experiments whereby HDFn cells were incubated with a range of TiO₂ doses (0-2mg/ml) for 24h after which the level of viable cells was measured. Lower concentrations of TiO₂ did not have an effect on cell viability, at higher concentrations however (>100µg/ml), the relative cell viability appeared to show an increase with both the MTS (Figure 104) and RT-Glo assay (Figure 105). This apparent increase may potentially be due to interference from the TiO₂ particles as observations under the microscope showed that TiO₂ particles remain adsorbed on to the cell surface following the wash steps. Modifications to the MTS assay such as allowing TiO₂ to settle and transferring the solutions from the well into a fresh 96-well plate prior to reading gave similar outcomes. Following on from these findings, a wide range of TiO₂ doses were used in subsequent experiments in accordance with previous literature studies (Tucci et al., 2013).

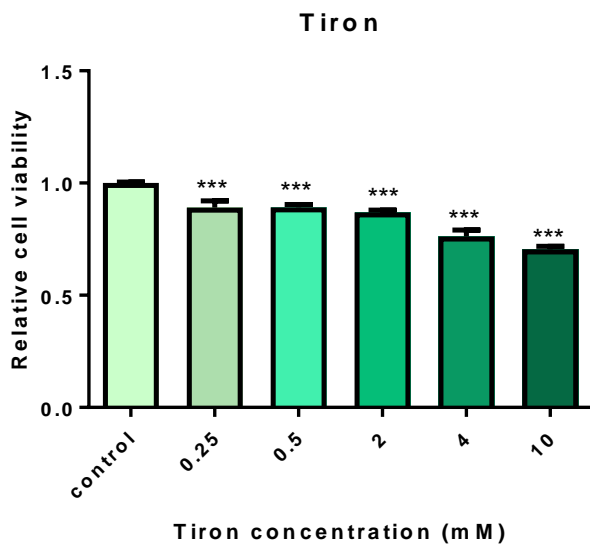


Figure 102: HDFn cell viability following exposure to Tiron

HDFn cells were incubated with Tiron concentrations (0-10mM) for 24h. An MTS assay was carried out to assess the cell viability and to determine the sublethal dose. A one-way ANOVA with Dunnett's correction was carried out to compare treated cells to the non-treated control) *** $P < 0.0001$ (error bars represent the SEM) N=3.

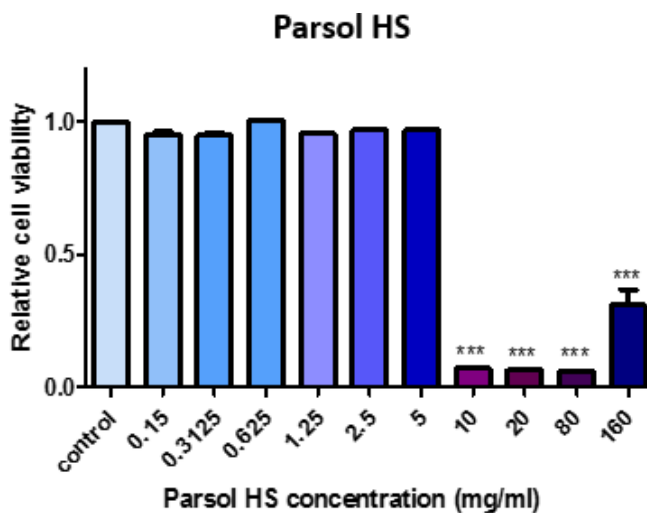


Figure 103: HDFn cell viability following exposure to Parsol HS

HDFn cells were incubated with Parsol HS concentrations (0-160mg/ml) for 24h. An MTS assay was carried out to assess the cell viability and to determine the sublethal dose. A one-way ANOVA with Dunnett's correction was carried out to compare treated cells to the non-treated control) *** $P < 0.0001$ (error bars represent the SEM) N=3.

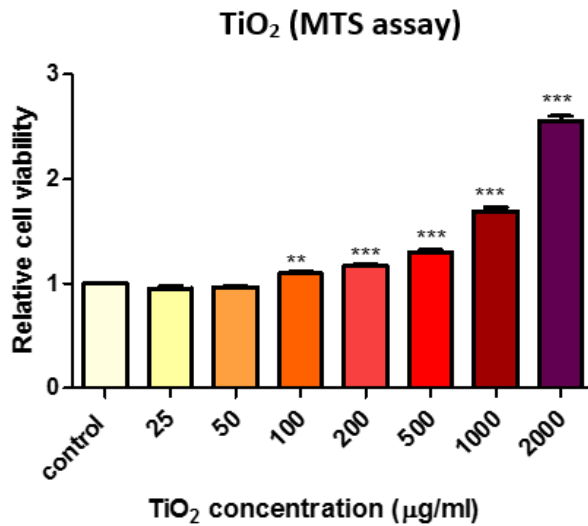


Figure 104: HDFn cell viability following exposure to TiO₂

HDFn cells were incubated with TiO₂ concentrations (0-2000µg/ml) for 24h. An MTS assay was carried out to assess the cell viability and to determine the sublethal dose. A one-way ANOVA with Dunnett's correction was carried out to compare treated cells to the non-treated control ***P < 0.0001 (error bars represent the SEM) N=4.

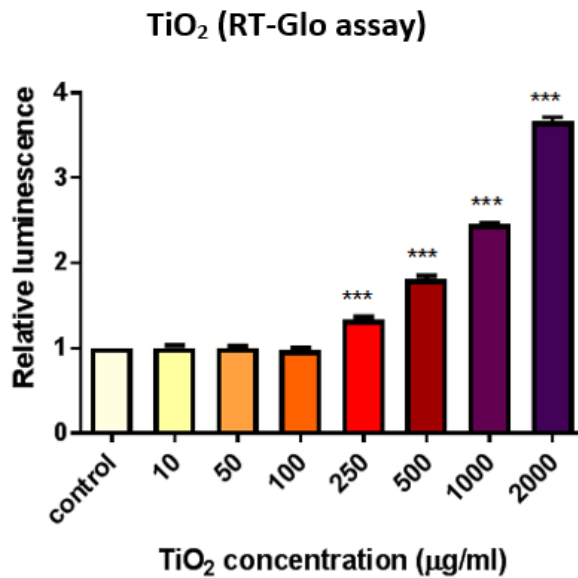


Figure 105: HDFn cell viability following exposure to TiO₂

HDFn cells were incubated with TiO₂ concentrations (0-2000µg/ml) for 24h. An RT-Glo assay was carried out to assess the cell viability and to determine the sublethal dose. A one-way ANOVA with Dunnett's correction was carried out to compare treated cells to the non-treated control ***P < 0.0001 (error bars represent the SEM) N=2.

5.3.3 Cellular TiO₂ internalisation in HDFn cells

The cellular internalisation of nanoparticles has been suggested to influence the resulting level of toxicity (Halamoda-Kenzaoui et al., 2017;Wills et al., 2016). A number of studies have assessed TiO₂ internalisation in a range of cell types including dermal fibroblasts, keratinocytes and melanocytes (Nanoderm, 2007;Pan et al., 2009b). Visualisation methods such as TEM and phase contrast microscopy have been utilised. Through the use of phase contrast microscopy, data from the nanoderm study found that fibroblasts were able to internalise TiO₂ following a 24h incubation period (Figure 106). Within the same study and others similar, internalisation was not seen to occur in keratinocytes perhaps due to their effective role at providing a barrier function to skin (Kiss et al., 2008;Shukla et al., 2011a;Jaeger et al., 2012). Figure 107 shows an example of TiO₂ internalisation detected through TEM analysis detection.

As a pilot study phase-contrast microscopy was used to visualise TiO₂ internalisation in HDFn cells (Figure 108). HaCat cells were also assessed although they were not seen to grow well in the presence of TiO₂. A range of TiO₂ concentrations (0-50µg/ml) were applied under different incubation times (0, 4 and 24h). What appears to be internalisation could be observed in HDFn cells after 24 h, it was however difficult to distinguish true internalisation from cell surface adsorption events. Small amounts of TiO₂ were used to assess internalisation in order to minimise the level of TiO₂ adsorption on to cells following the wash steps.

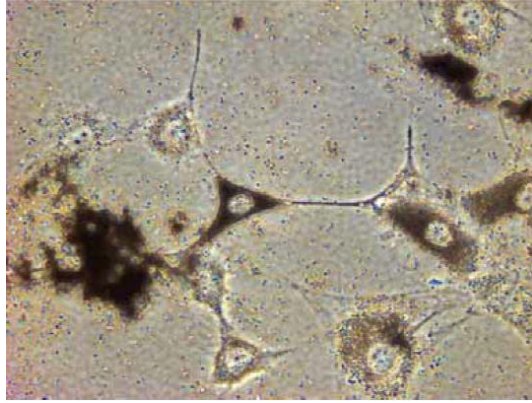


Figure 106: Showing internalization in NIH 3T3 fibroblasts following exposure to uncoated TiO₂ nanoparticles (15µg/cm²) (Nanoderm, 2007).

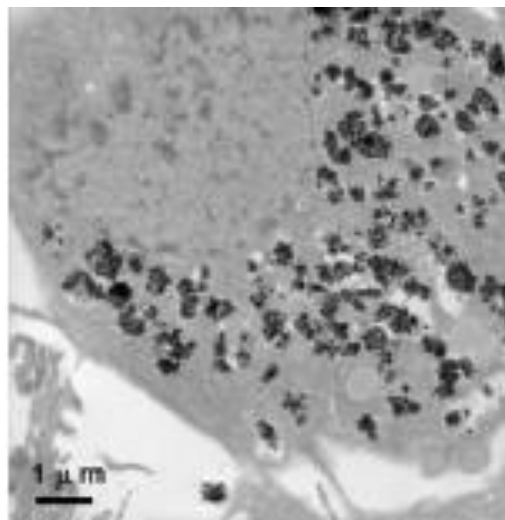


Figure 107: TEM image of human fibroblast cell incubated with TiO₂ nanoparticles (0.4 mg/ml) for two days. A typical cell with nanoparticle clusters is shown (Pan et al., 2009a)

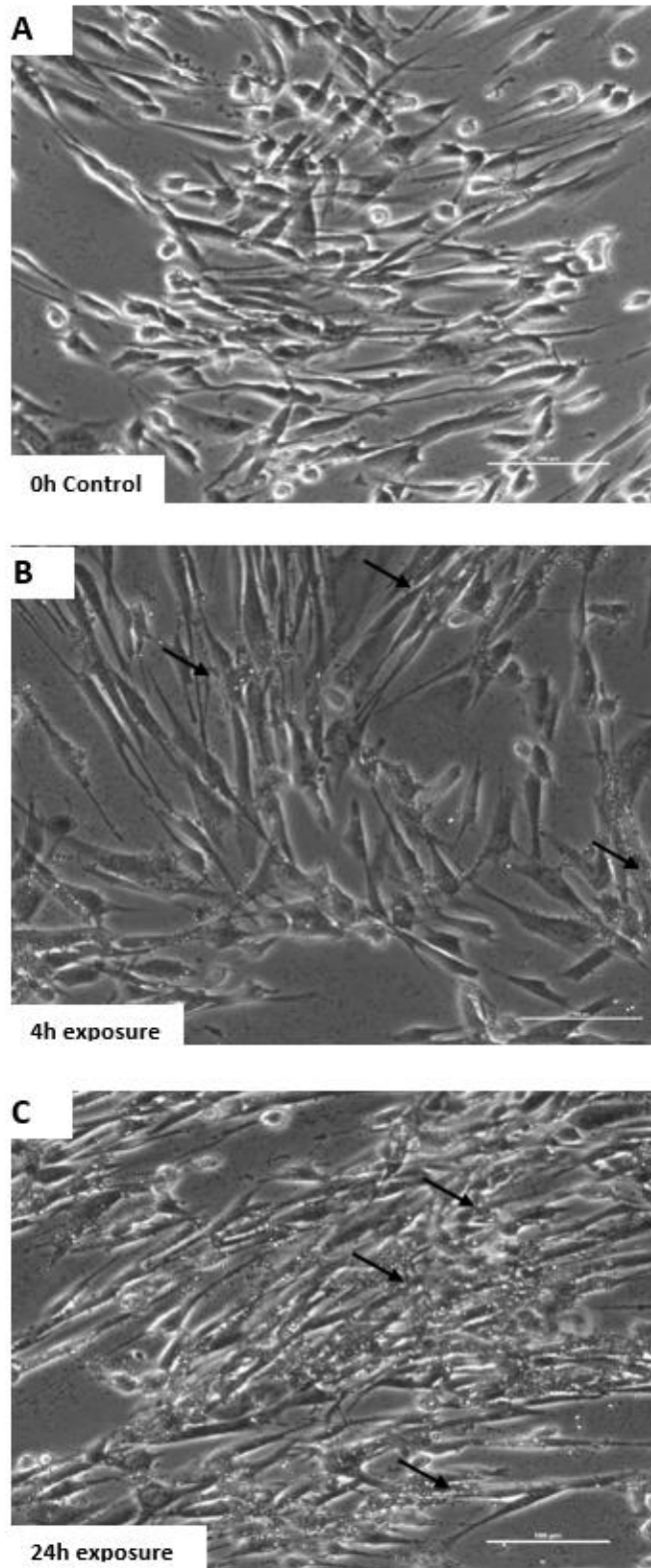


Figure 108: Showing representative images of potential TiO₂ internalisation by HDFn cells following exposure to TiO₂

The images represent HDFn cells in an area of the plate containing no TiO₂ (A), TiO₂ (25 µg) incubated for 4h (B) and TiO₂ (25 µg) incubated for 24h (C). Images were taken with the help of Dr Alex Laude (scale bars represent a length of 100 µm).

5.3.4 Genotoxicity

The comet assay was used to investigate the genotoxic effect of TiO₂ on HDFn cells by measuring the level of DSB. Cells were incubated with TiO₂ (0-50µg/ml) for 24h after which the compound was removed and various doses of solar simulated light (0-2.16 SED) were applied. Lower concentrations of TiO₂ were used in the comet assays as the higher concentrations were observed in earlier experiments to adhere to the cells and remain in the gel during the analysis process. Further wash steps were included in subsequent experiments to remove any remaining TiO₂. Analysis was carried out to determine the level of nDNA damage by scoring the tail length of the comets with each comet representing a nucleus from a single cell (n=100). A dose of 0.54 and 1.08 SED were not found to induce significantly detectable levels of nDNA damage in the control HDFn cells, 2.16 SED was therefore applied in subsequent experiments. Controls for the comet assay are shown in Figure 109. H₂O₂ was used as a positive control as this has been used previously in the lab and has been shown to induce significant levels of nDNA damage. Significantly longer tail lengths (indicative of DSB) can be seen in the unirradiated HDFn cells exposed to 25 and 50µg/ml TiO₂ when compared to the no TiO₂ control (Figure 110). Irradiated samples that have been exposed to 25 and 50µg/ml TiO₂ also show a significant fold increase in tail length when compared to the no TiO₂ irradiated control (N=2). Irradiated cells treated with TiO₂ show higher levels of nDNA damage relative to the unirradiated TiO₂ treated samples. These findings demonstrate that at relatively low concentrations TiO₂ has the capacity to induce genotoxicity in HDFn cells. When photoactivated TiO₂ has the capacity to induce even greater levels of nDNA damage.

An enzyme modified comet assay was later carried out to uncover any further potential nDNA damage which may be present. The human 8-hydroxyguanine DNA-glycosylase (hOGG1) enzyme was used as this recognizes and removes oxidatively damaged DNA lesions such as 8-Oxoguanine creating further DNA DSB (Bjørås et al., 1997;Boiteux and Radicella, 1999). Addition of hOGG1 during the comet assay was able to uncover further levels of oxidative DNA damage in both irradiated and unirradiated TiO₂ treated samples as shown in Figure 111 and Figure 112.

The European Standards Committee on Oxidative DNA Damage (ESCODD) recommends the use of the lesion specific repair enzyme, formamidopyrimidine DNA glycosylase (FPG) in the comet assay to detect oxidative DNA damage (Smith et al., 2006). A study has been carried out by Smith et al., whereby FPG was compared with endonuclease III (ENDOIII) and hOGG1 for its ability to modify the sensitivity of the comet assay (Smith et al., 2006). The data obtained indicated that all three endonucleases recognize oxidative DNA damage and, in addition, FPG and ENDOIII also recognized alkylation damage. The use of hOGG1 in the modified comet assay was reported to offer a useful alternative to FPG and is apparently more specific for 8-oxoguanine and methyl-fapy-guanine (Smith et al., 2006).

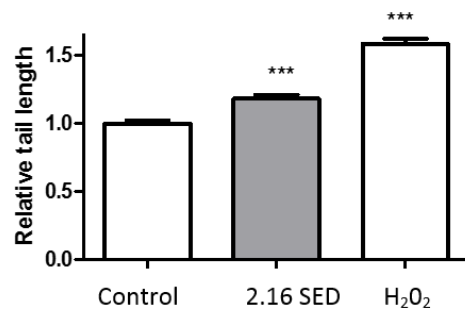


Figure 109: Comet assay control conditions

HDFn cells were dosed with either solar simulated light (2.16 SED) or H₂O₂ (10 μ M) for 1h. The average tail lengths are shown. Statistical analysis was carried out using a one-way ANOVA with Dunnett's correction to compare treated cells to the 0 SED control *** P<0.0001 (error bars represent the SEM) N=2.

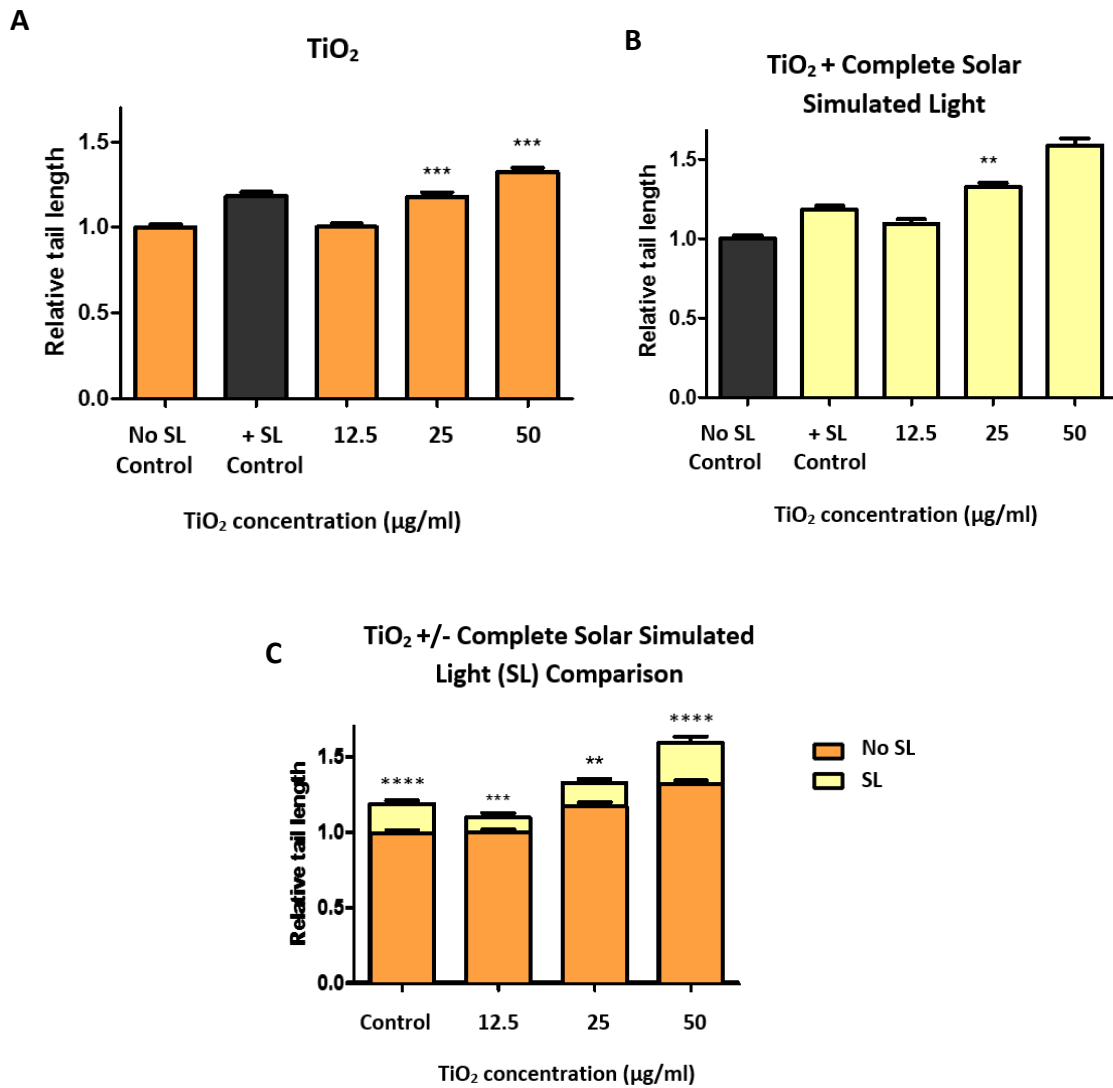


Figure 110: nDNA damage following exposure of HDFn cells to TiO₂ +/- complete solar simulated light.

HDFn cells were incubated with TiO₂ for 24h after which the compound was removed and cells assessed for the level of nDNA damage induction (A). Alternatively, cells were irradiated with complete solar simulated light (SL) (2.16 SED) prior to assessing nDNA damage levels (B). Nuclei from 100 cells were selected at random for each of the test conditions assessed and were analysed for tail length. The tail length is proportional to the level of DNA DSB and are displayed as relative values to the appropriate non TiO₂ treated (control) cells. Data has been replotted (C) to illustrate comparisons between the inert and photoactivated TiO₂ effects on genotoxicity in HDFn cells. Statistical analysis was performed to compare all columns to the control (untreated) cells using a one-way ANOVA with Dunnett's correction ** P < 0.001 *** P < 0.0001. A one-way ANOVA with Bonferroni's post-hoc was carried out to compare the mean of each column with the mean of every other column (C) ***P < 0.001 (error bars represent the SEM) N=2, N=2 respectively.

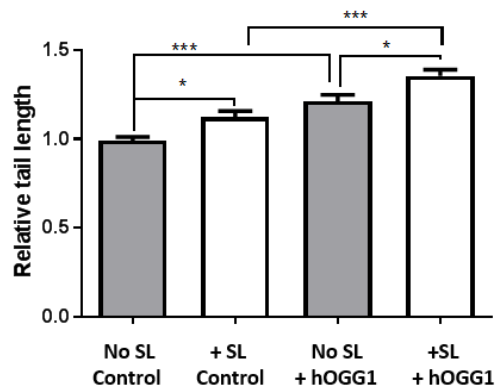


Figure 111: Enzyme modified (hOGG1) comet assay control conditions

HDFn cells were dosed with complete solar simulated light (SL) (2.16 SED) and the level of nDNA damage assessed using the comet assay +/- the hOGG1 enzyme. The average tail lengths are shown. Statistical analysis was carried out using a one-way ANOVA with Dunnett's correction to compare treated cells to the unirradiated (no SL) control * $P < 0.05$ *** $P < 0.0001$ (error bars represent the SEM) $N = 1$.

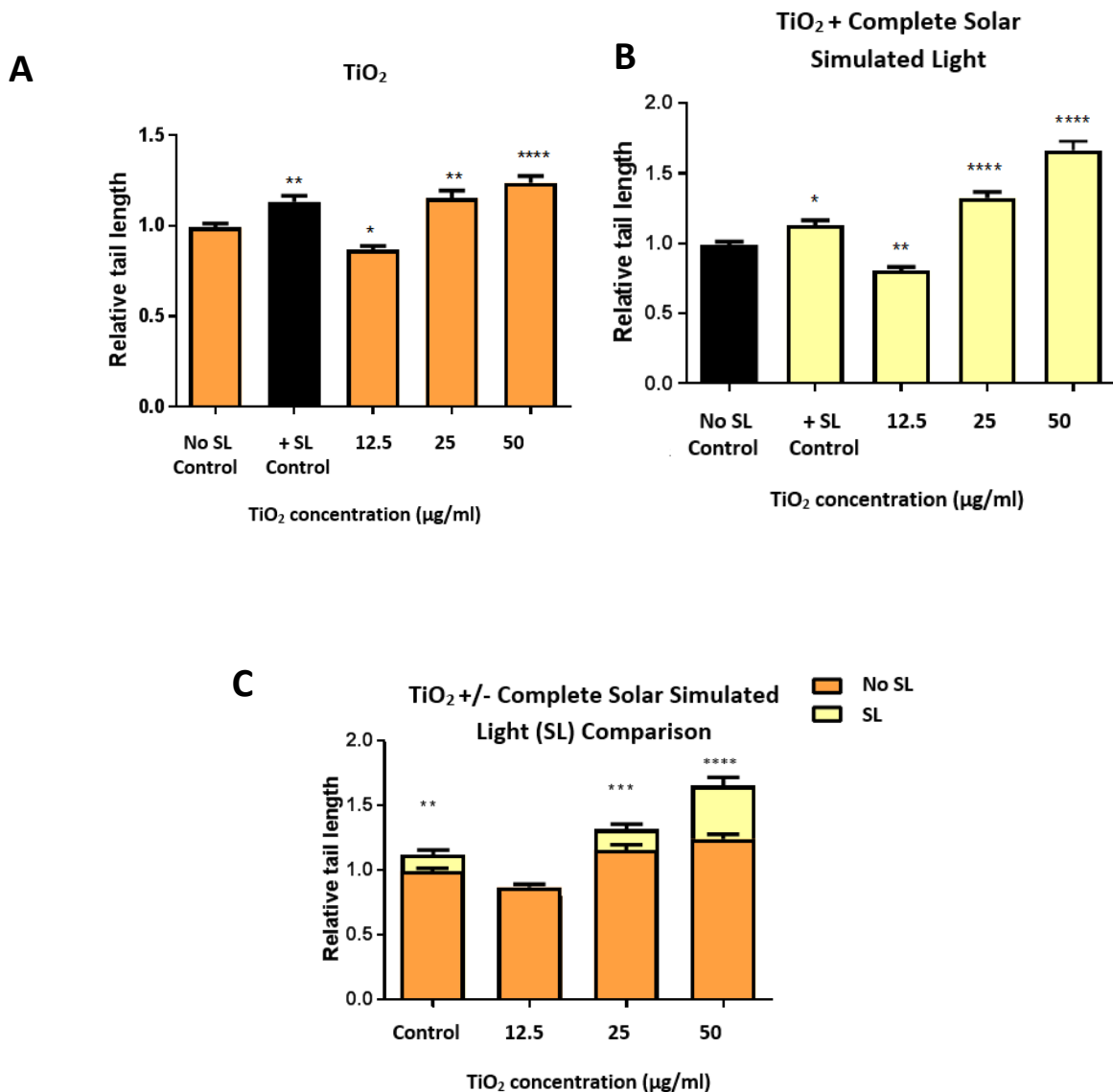


Figure 112: nDNA damage detection following exposure of HDFn cells to TiO₂ +/- complete solar simulated light- enzyme modified assay.

HDFn cells were incubated with TiO₂ for 24h after which the compound was removed and cells assessed for the level of nDNA damage induction (A). Alternatively, cells were irradiated with complete solar simulated light (SL) (2.16 SED) prior to assessing nDNA damage (B). Both experiments (A and B) involved the use of the hOGG1 enzyme to identify further DNA lesions. Nuclei from 100 cells were selected at random for each of the test conditions assessed and were analysed for tail length. The tail length is proportional to the level of DNA DSB and are displayed as relative values to the appropriate non TiO₂ treated (control) cells. Data has been replotted (C) to illustrate comparisons between the inert and photoactivated TiO₂ effects on genotoxicity in HDFn cells. Statistical analysis was performed to compare all columns to the control (untreated) cells using a one-way ANOVA with Dunnett's correction ** P < 0.001 *** P<0.0001. A one-way ANOVA with Bonferroni's post-hoc was carried out to compare the mean of each column with the mean of every other column (C) ** P <0.05 ***P<0.001 (error bars represent the SEM) N=1, N=1 respectively.

5.3.5 Protective effects of TiO₂

TiO₂ is widely used as an active mineral compound in sunscreen formulations due to its ability to reflect, scatter and partially absorb the encountered solar radiation (Jacobs et al., 2010a). The ratio of UVA to UVB protection offered by TiO₂ is size dependent (Wang and Tooley, 2011). The level of protection offered by the aeroxide formulations created in the lab were therefore assessed both cellularly and acellularly. TiO₂ suspensions in PBS were initially tested for their ability to block against UV from solar simulated light and IR. A TiO₂ dose dependent UV and IR blocking ability was observed (Figure 113). A greater capacity to block against solar UV was however seen at 1mg/ml whereby approximately 80% of the solar simulated light was blocked compared to only 50% protection being offered against IR at an equivalent TiO₂ dose (Figure 113).

Parsol HS also provided protection against solar simulated light although much higher concentrations were required to achieve a similar level of protection to that obtained with the TiO₂ suspension. TiO₂ offers moderate protection against IR at higher concentrations (Figure 114) whereas Parsol HS shows marginal protection even when higher concentrations are applied (Figure 114).

The level of cellular protection offered by TiO₂ was tested in HDFn cells (Figure 115). Formulations were applied on to transpore tape at a concentration of 2mg/cm² to simulate

the application of sunscreen on to skin. The transpore tape was positioned on top of the wells to cover the cells prior to the irradiation step in PBS media. Protection against solar simulated light (4.32 SED) can be seen at TiO₂ concentrations of 200-1000µg/ml as significantly lower levels of ROS were detected compared to the irradiated control cells (Figure 115). This demonstrates that the dispersions made were able to act as sunscreens and provide protective effects.

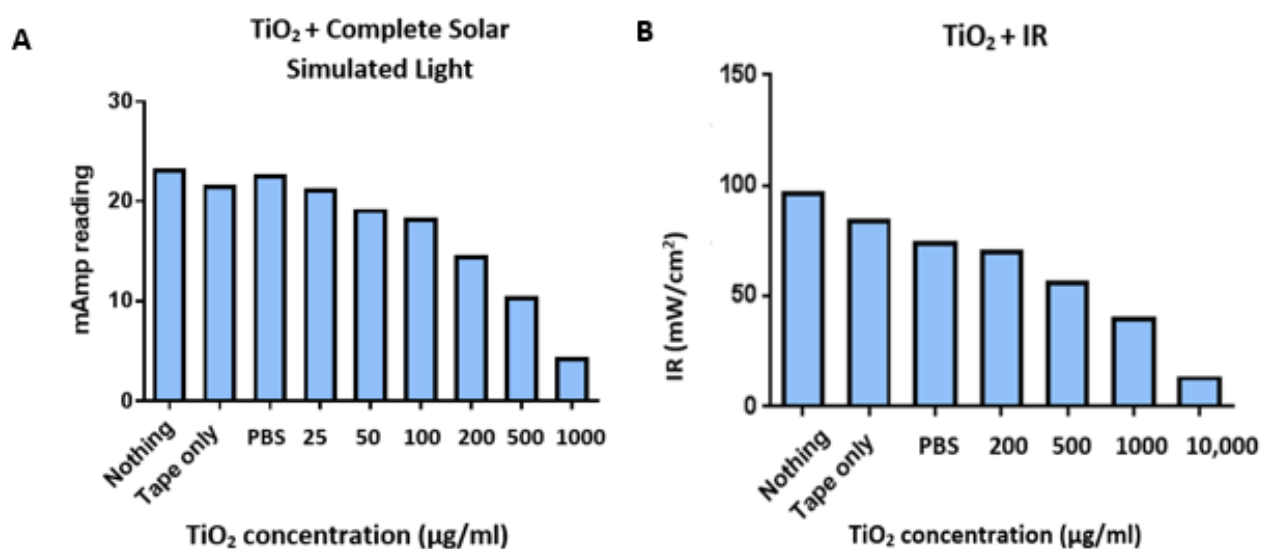


Figure 113: Protective effects of TiO₂ suspensions- acellular

TiO₂ suspensions (0-10,000µg/ml) were placed on transpore tape and assessed for ability to block against the complete solar simulated light (A) and IR (B) applied. The lower readings compared to the tape only (control) are indicative of the protective action of the TiO₂ formulations N=1.

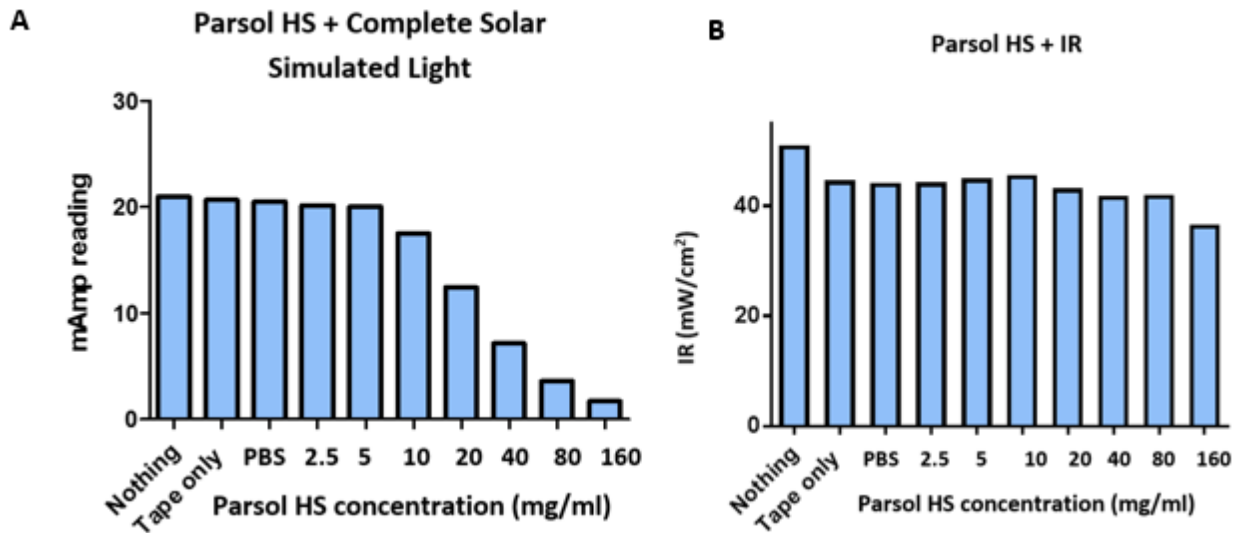


Figure 114: Protective effects of Parsol HS in solution- acellular

Parsol HS solutions (0-160mg/ml) were placed on transpore tape and assessed for ability to block against the complete solar simulated light (A) and IR (B) applied. The lower readings compared to the tape only (control) are indicative of the protective action of the Parsol HS formulations N=1.

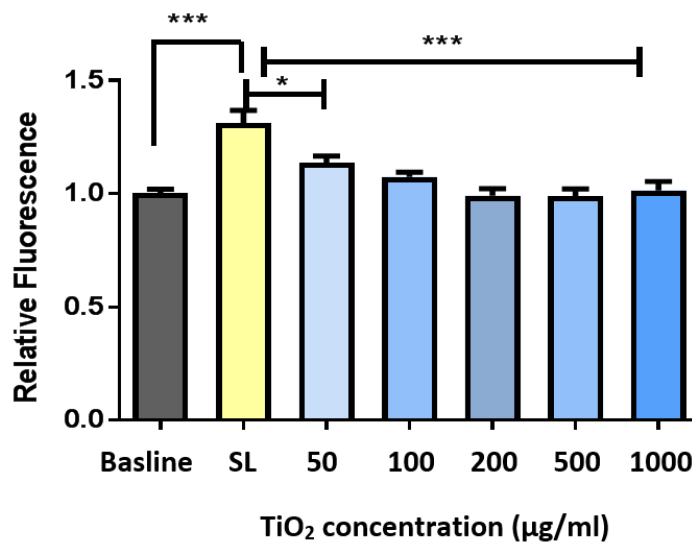


Figure 115: TiO₂ protective effects against complete solar light induced ROS generation in HDFn cells

TiO₂ formulations (0-1000 µg/ml) were placed on transpore tape and assessed for ability to provide protection to HDFn cells against the complete solar light (2.16 SED) dose applied. A DCFDA assay was carried out to measure the level of ROS generation relative to the baseline (unirradiated) control. A one-way ANOVA with Bonferonni's post-hoc was used to compare the mean of each column with the mean of every other column *P< 0.05 ***P<0.0001 (error bars represent the SEM) N=3.

5.3.6 ROS generation following exposure to TiO₂ and Parsol HS sunscreen compounds

As mentioned previously, one of the main toxicological concerns associated with exposure to nano size TiO₂ is ROS generation (Shi et al., 2013). Secondary effects of ROS generation include downstream cellular signalling events as well as the indirect nDNA and or mtDNA damage (Woodruff et al., 2012).

This area of the project aimed to quantify levels of ROS generation from the sunscreen active compounds and compare the use of the DCFDA ROS detection probe method to a more recently developed ROS-Glo method. Acellular work was carried out to identify possible artefacts generated from the use of the test compounds of interest, namely TiO₂ and Parsol HS. A range of TiO₂ and Parsol HS concentrations were applied and the effects of photoactivation using various solar light components were assessed.

The DCFDA probe is commonly used for ROS detection in order to measure hydroxyl, peroxy and various other ROS activity within the cell. After diffusion into the cell, DCFDA is deacetylated by cellular esterases to a non-fluorescent compound, which is later oxidized by ROS into 2',7'-dichlorofluorescein (DCF). DCF is a highly fluorescent compound which can be detected by fluorescence spectroscopy (Boulton et al., 2011). From previous work in the lab, DCFDA has been found to be a reliable method for detecting general ROS species. Due to the unstable nature of the compound however, controls are required along with measures to minimise the instability of the probe (Boulton et al., 2011). For instance exposure to direct light must be avoided where possible and irradiations should not be carried out in the presence of the probe as this may result in false positive readings.

Acellular DCFDA experiments were carried out to measure the level of non-cell specific ROS generation. TiO₂ and Parsol HS suspensions were exposed to UV sources prior to being incubated with DCFDA (Figure 116 and Figure 117 respectively). The ROS generation observed in the acellular experiments may be due to DCFDA becoming unstable or alternatively due to autofluorescence from the test compounds following exposure to the test conditions

particularly at higher concentrations. HDFn cells were incubated with TiO₂ suspensions for 24h after which irradiation was carried out. TiO₂ was later removed and ROS levels measured using DCFDA (Figure 118, Figure 119 and Figure 120). Similarly the effect of Parsol HS on HDFn ROS generation was also assessed (Figure 121, Figure 122 and Figure 123). The net level of ROS production was calculated by subtracting the values corresponding to the UV exposed cells from the non-UV exposed cells. Significant ROS production could be detected with the Cleo performance + glass lamp however higher TiO₂ concentrations resulted in a decrease in ROS perhaps due to cell death influencing the amount of intracellular DCFDA remaining for analysis. Alternatively the TiO₂ may be having a protective effect on the cells by blocking the solar light. Further experiments would be required to determine this. The ROS-Glo method was therefore applied following these findings to assess ROS levels further.

The DCFDA probe method was not able to detect ROS in HaCat cells. Optimisation experiments were carried out such as increasing the UV doses applied. The ROS levels generated by HaCat cells may have been too low for detection with the DCFDA method. ROS was however detected using DCFDA in HaCat cells which have been exposed to H₂O₂, albeit not in a dose dependent manner (data shown in appendix Figure 2).

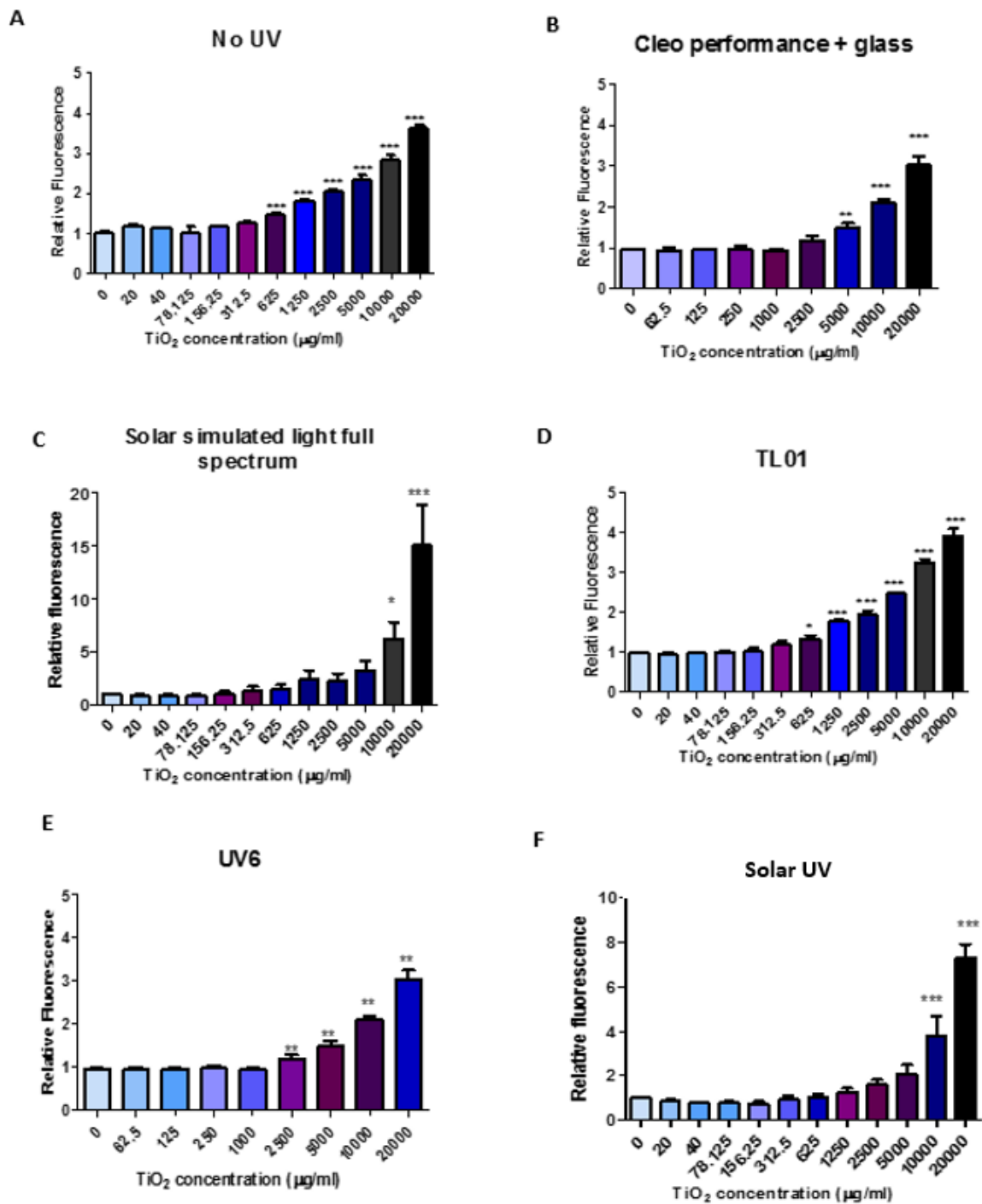


Figure 116: TiO₂ acellular ROS generation following exposure to solar light sources

The DCFDA ROS detection method was used to assess the level of acellular ROS generation following exposure to TiO₂ plus either no UV (A), cleo performance + glass (B), solar simulated light full spectrum (C) TL01 (D) UV6 (E) or solar UV (F). A one-way ANOVA with Dunnett's correction was used to compare all columns to the 0 control *** P < 0.0001 (error bars represent the SEM) N=1, N=4, N=2, N=3, N=1, N=2 respectively.

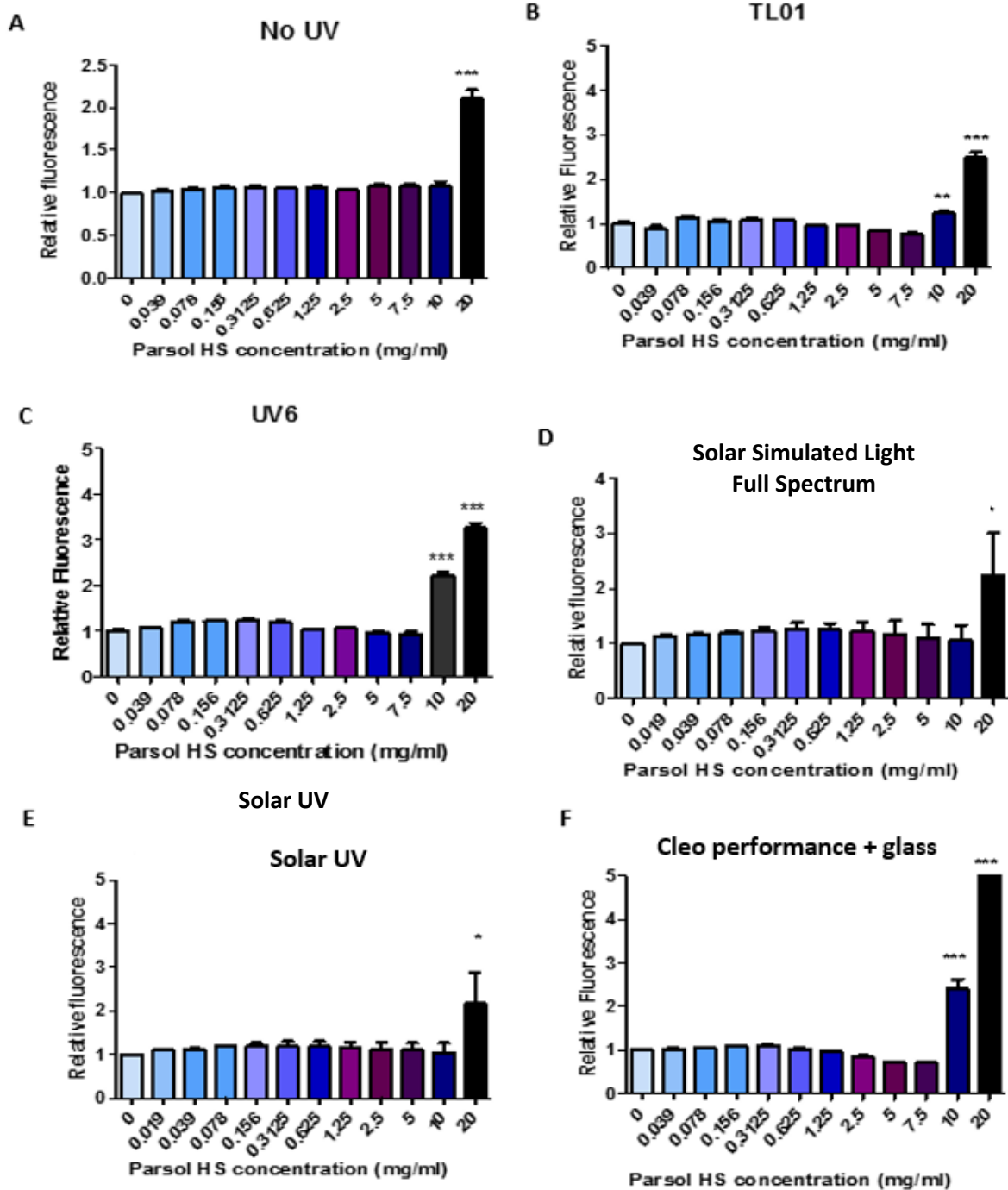


Figure 117: Parsol HS acellular ROS generation following exposure to solar light sources

The DCFDA ROS detection method was used to assess the level of acellular ROS generation following exposure to Parsol HS plus either no UV (A), TL01 (B), UV6 (C), solar simulated light full spectrum (D) solar UV (E) or cleo performance + glass (F). A one-way ANOVA with Dunnett's correction was used to compare all columns to the 0 control *** P < 0.0001 (error bars represent the SEM) N=1, N=1, N=1 N=2, N=2, N=2 respectively.

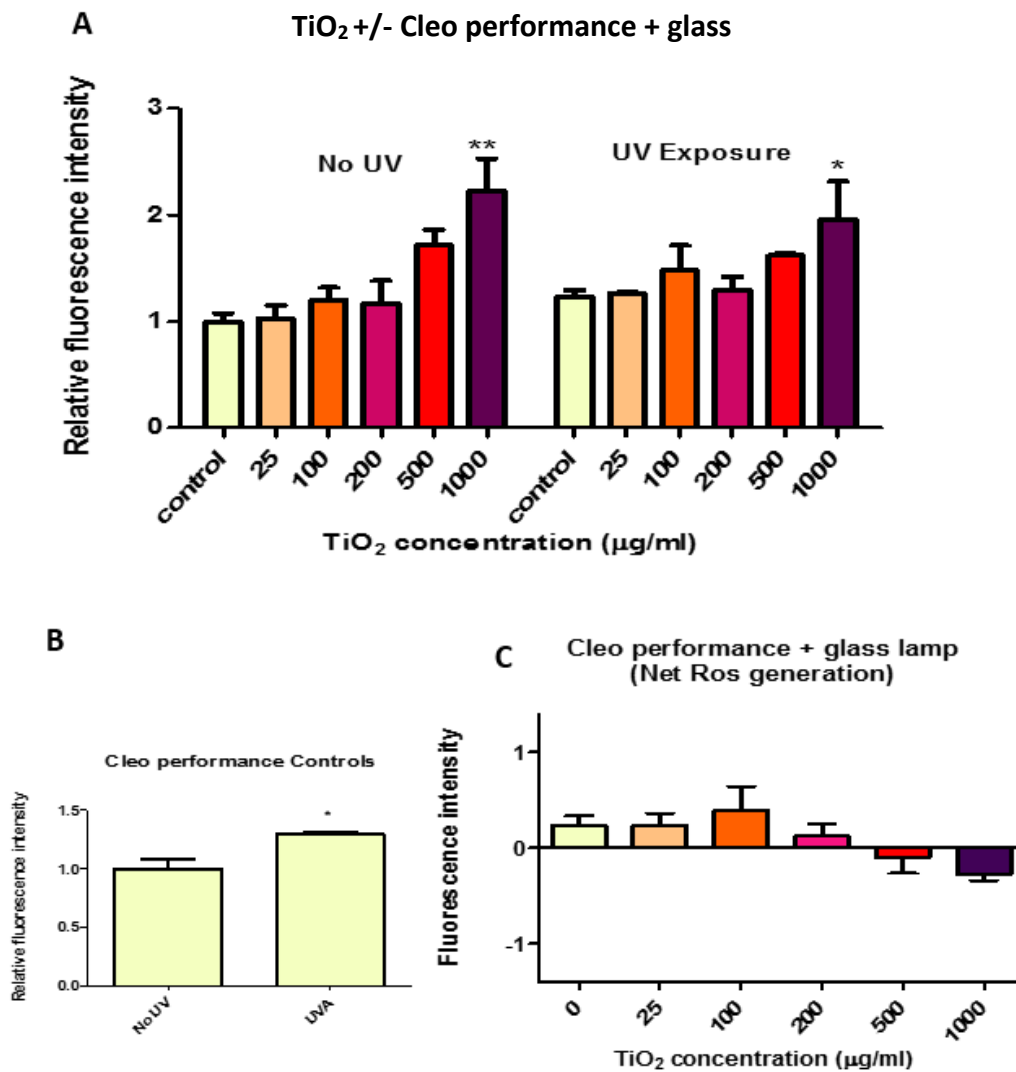


Figure 118: Assessing the protective effect of TiO_2 on HDFn cells following exposure to Cleo performance + glass

Cells were incubated with TiO_2 suspensions for 24h after which a dose of Cleo performance + glass was applied ($10\text{J}/\text{cm}^2$). TiO_2 was later removed and the level of ROS generation measured using the DCFDA method. The effect of increasing TiO_2 concentrations on ROS generation and the influence of TiO_2 photoactivation following UV exposure (Cleo performance + glass) was assessed (A). Control treated and untreated cells are displayed (B). The net level of ROS generation has been replotted by subtracting the values of the UV dosed TiO_2 from the non UV dosed samples (C). A One tailed T-test was used to analyse significance of the control samples (B) * $P < 0.05$. A one-way ANOVA with Dunnett's correction was used to analyse significance * $P < 0.05$, ** $P < 0.001$ (error bars represent the SEM) $N=3$, $N=3$ respectively.

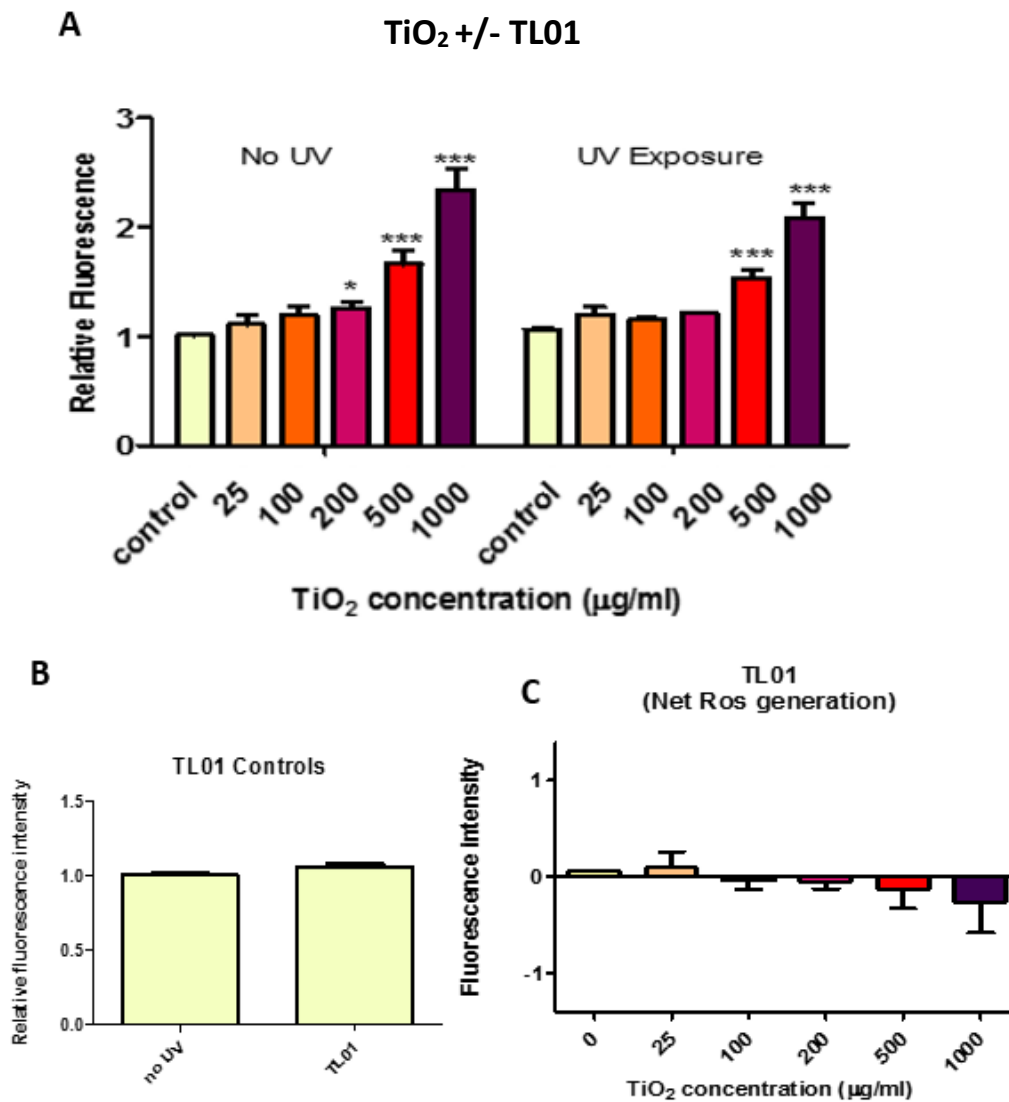


Figure 119: Assessing the protective effect of TiO_2 on HDFn cells following exposure to TL01

Cells were incubated with TiO_2 suspensions for 24h after which a dose of TL01 was applied ($10\text{J}/\text{cm}^2$). TiO_2 was later removed and the level of ROS generation measured using the DCFDA method. The effect of increasing TiO_2 concentrations on ROS generation and the influence of TiO_2 photoactivation following UV (TL01) exposure was assessed (A). Control treated and untreated cells are displayed (B). The net level of ROS generation has been replotted by subtracting the values of the UV dosed TiO_2 from the non UV dosed samples (C). A One tailed T-test was used to analyse significance of the control samples. A one-way ANOVA with Dunnett's correction was used to analyse significance) * $P < 0.05$, ** $P < 0.001$ (error bars represent the SEMN) $N=3$, $N=3$ respectively.

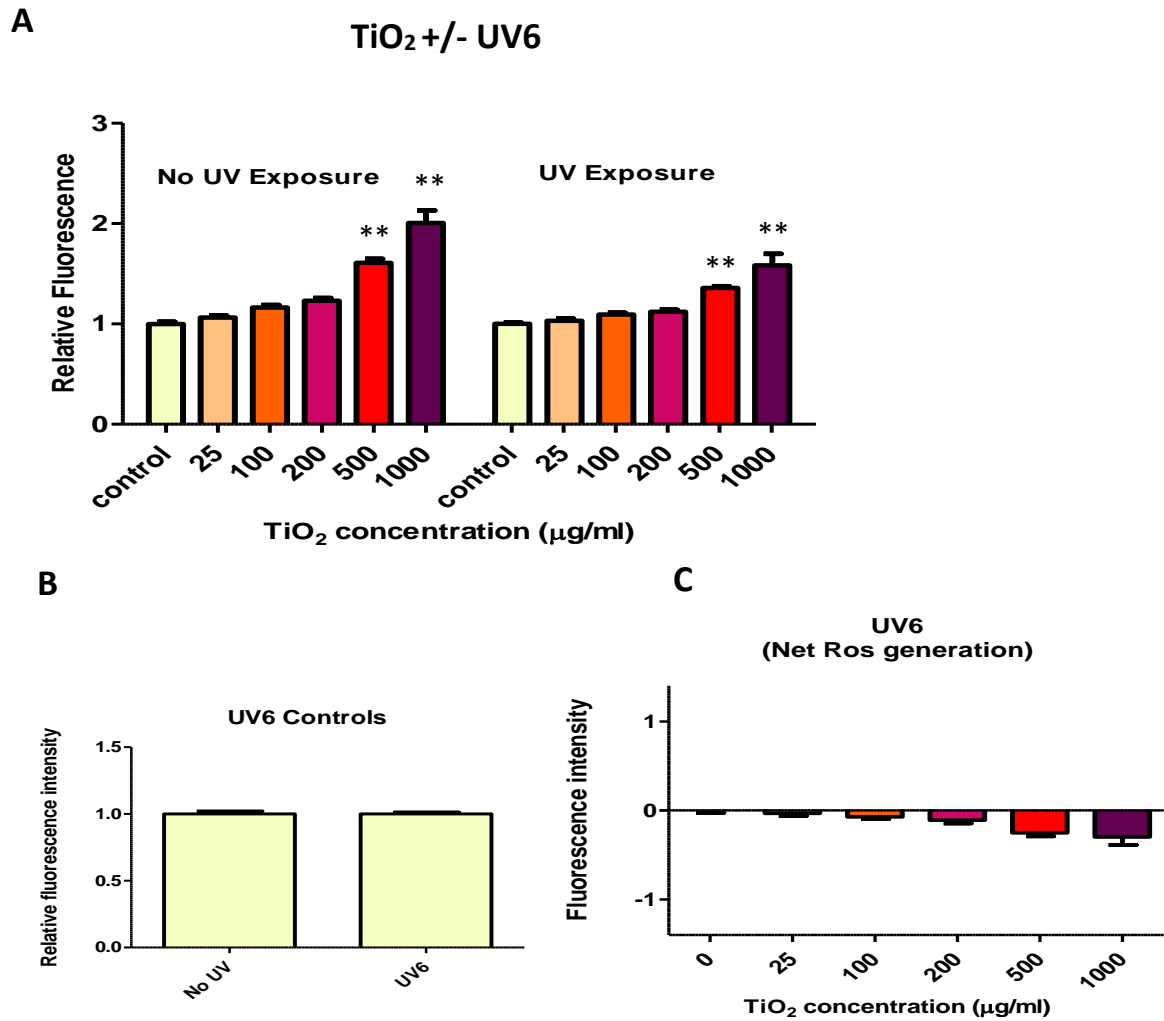


Figure 120: Assessing the protective effect of TiO₂ on HDFn cells following exposure to UV6

Cells were incubated with TiO₂ suspensions for 24h after which a dose of UV6 was applied (10J/cm²). TiO₂ was later removed and the level of ROS generation measured using the DCFDA method. The effect of increasing TiO₂ concentrations on ROS generation and the influence of TiO₂ photoactivation following UV (UV6) exposure was assessed (A). Control treated and untreated cells are displayed (B). The net level of ROS generation has been replotted by subtracting the values of the UV dosed TiO₂ from the non UV dosed samples (C). A One tailed T-test was used to analyse significance of the control samples. A one-way ANOVA with Dunnett's correction was used to analyse significance* P <0.05 ** P <0.001 (error bars represent the SEM) N=3, N=3 respectively.

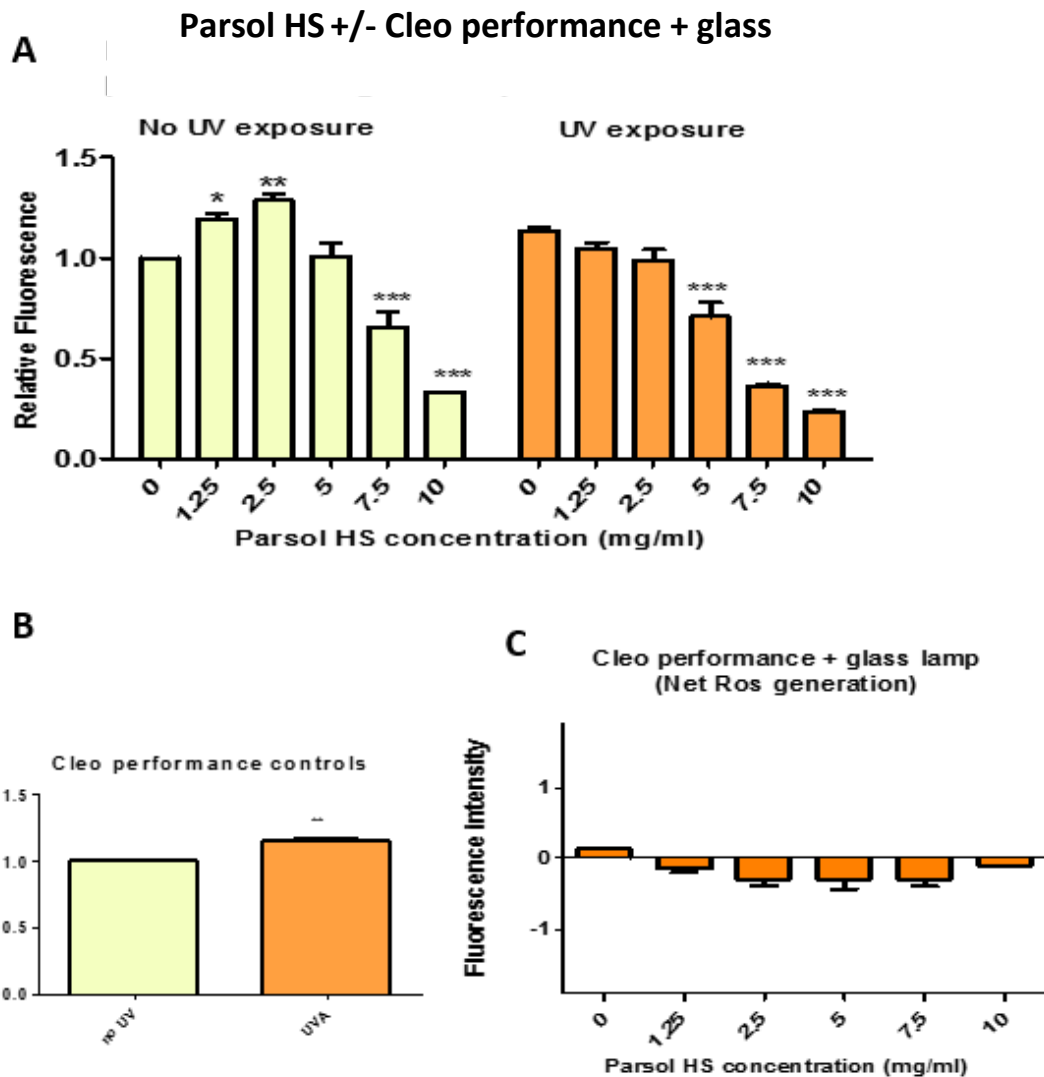


Figure 121: Assessing the protective effect of Parsol HS on HDFn cells following exposure to Cleo performance + glass

Cells were incubated with Parsol HS suspensions for 24h after which a dose of Cleo performance + glass was applied ($10\text{J}/\text{cm}^2$). The Parsol HS compound was later removed and the level of ROS generation measured using the DCFDA method. The effect of increasing Parsol HS concentrations on ROS generation and the influence of photoactivation of the compound following UV (Cleo performance + glass) exposure was assessed (A). Control treated and untreated cells are displayed (B). The net level of ROS generation has been replotted by subtracting the values of the UV dosed Parsol HS from the non UV dosed samples (C). A One tailed T-test was used to analyse significance of the control samples. A one-way ANOVA with Dunnett's correction was used to analyse significance * $P < 0.05$, ** $P < 0.001$ (error bars represent the SEM) $N=3$, $N=3$ respectively.

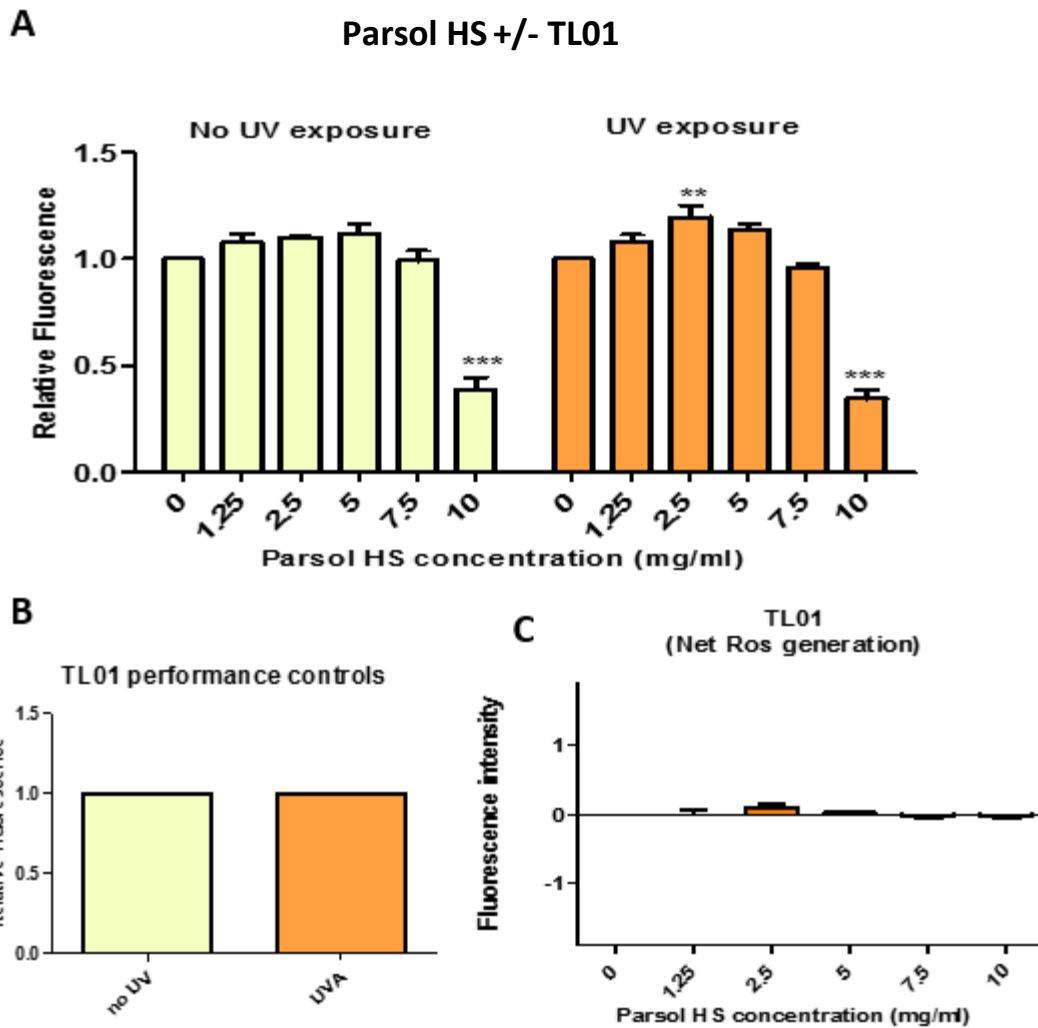


Figure 122: Assessing the protective effect of Parsol HS on HDFn cells following exposure to TL01

Cells were incubated with Parsol HS suspensions for 24h after which a dose of TL01 was applied (10J/cm²). The Parsol HS compound was later removed and the level of ROS generation measured using the DCFDA method. The effect of increasing Parsol HS concentrations on ROS generation and the influence of photoactivation of the compound following UV (TL01) exposure was assessed (A). Control treated and untreated cells are displayed (B). The net level of ROS generation has been replotted by subtracting the values of the UV dosed Parsol HS from the non UV dosed samples (C). A One tailed T-test was used to analyse significance of the control samples. A one-way ANOVA with Dunnett's correction was used to analyse significance * P < 0.05, ** P < 0.001 (error bars represent the SEM) N=3, N=3 respectively.

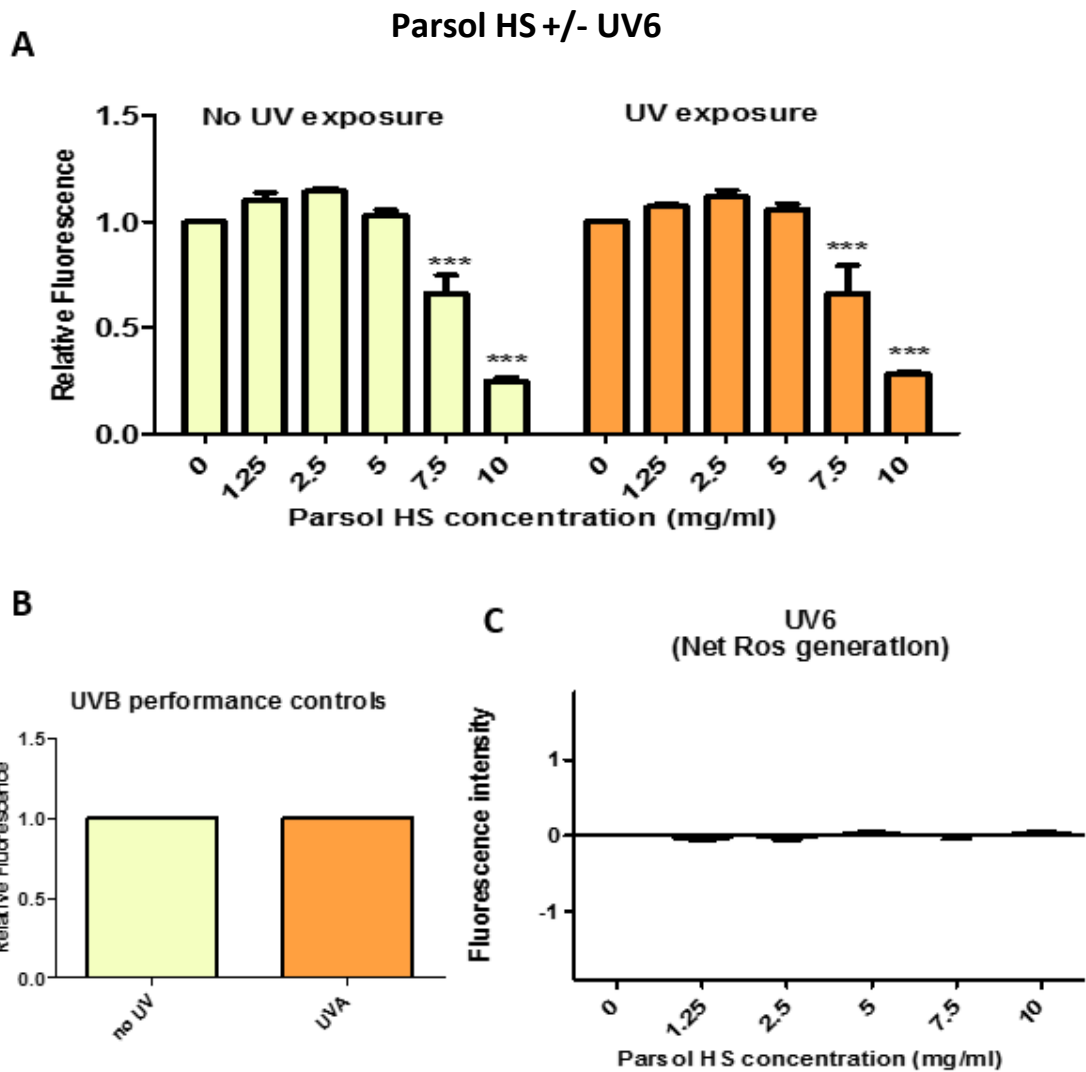


Figure 123: Assessing the protective effect of Parsol HS on HDFn cells following exposure to UV6

Cells were incubated with Parsol HS suspensions for 24h after which a dose of UV6 was applied (10J/cm²). The Parsol HS compound was later removed and the level of ROS generation measured using the DCFDA method. The effect of increasing Parsol HS concentrations on ROS generation and the influence of photoactivation of the compound following UV (UV6) exposure was assessed (A). Control treated and untreated cells are displayed (B). The net level of ROS generation has been replotted by subtracting the values of the UV dosed Parsol HS from the non UV dosed samples (C). A One tailed T-test was used to analyse significance of the control samples. A one-way ANOVA with Dunnett's correction was used to analyse significance * P <0.05, ** P <0.001 (error bars represent the SEM) N=3, N=3 respectively.

Acellular experiments were carried out to determine the effect of both inert and photoactivated TiO_2 on the ROS-Glo assay (Figure 124). Addition of TiO_2 leads to a modest increase in ROS generation with no further increase being seen at the higher doses (Figure 124 A). When TiO_2 becomes photoactivated (Figure 124 B) an increase in ROS could be seen at higher concentrations perhaps due to TiO_2 interference. A decline in ROS was seen after $625\mu\text{g/ml}$ which may be due to quenching of the luminescence signal with increasing TiO_2 concentration (Figure 124 B).

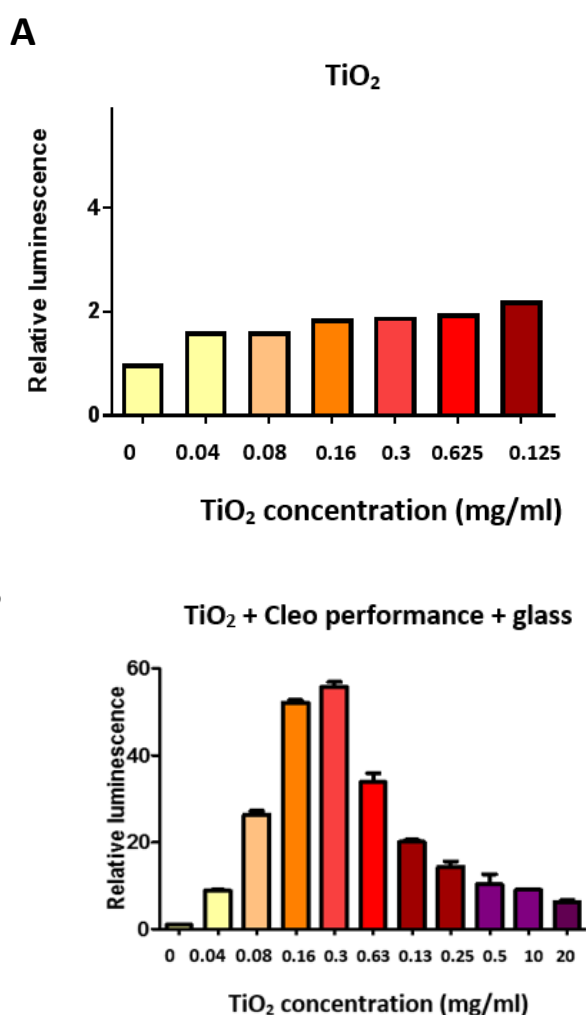
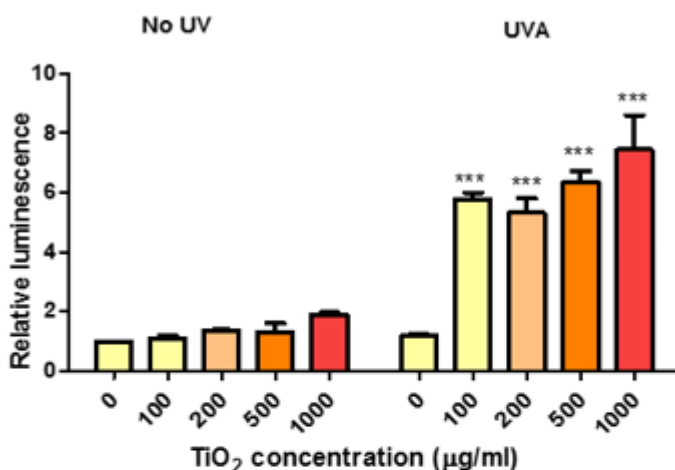


Figure 124: TiO_2 acellular ROS generation following exposure to Cleo performance + glass

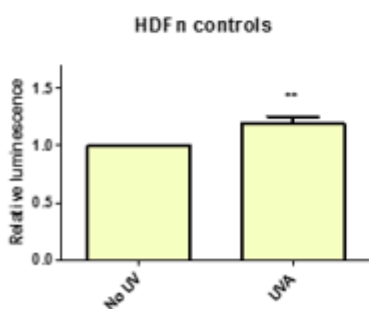
The ROS-Glo detection method was used to assess the level of acellular ROS generation following exposure to TiO_2 (A) and TiO_2 plus Cleo performance + glass (10J/cm^2) (B). A one-way ANOVA with Dunnett's correction was used to compare all columns to the non dosed (0 TiO_2) control *** $P < 0.0001$ (error bars represent the SEM) $N=1$, $N=2$ respectively.

Cellular ROS generation as a result of TiO₂ exposure was measured in HDFn cells. The net level of ROS production was calculated by subtracting the values of the UV dosed cells from the non-UV dosed (Figure 125). Application of inert TiO₂ has little effect on the level of ROS generation in HDFn cells relative to untreated control. Photoactivated TiO₂ however shows a significant 6-fold increase in the level of ROS observed. Similar outcomes were seen with increasing concentrations of TiO₂. From the net ROS generation (Figure 125 C) it can be seen that the ROS generated is not dose dependent. The level of ROS generation was assessed in HaCat cells with similar findings being observed to that found in HDFn cells (Figure 126). Parsol HS was not assessed using the ROS-Glo assay due to limited resources and a similar trend being seen between the DCFDA and ROS-Glo assay in terms of ROS-generation pattern.

A TiO₂ +/- Cleo performance + glass



B



C

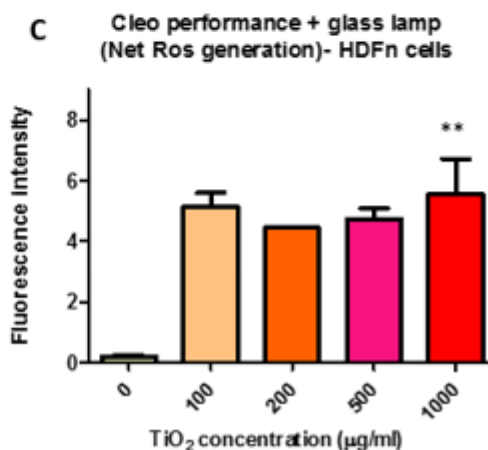


Figure 125: ROS generation in HDFn cells following exposure to TiO₂ +/- Cleo performance

HDFn cells were dosed with TiO₂ +/- Cleo performance + glass and the level of ROS generation was assessed using the ROS-Glo method (A). The level of ROS generation is displayed relative to the non-treated TiO₂ control. Control treated and untreated cells are displayed (B). The net level of ROS generation has been replotted by subtracting the values of the UV dosed TiO₂ from the non UV dosed samples (C). A One tailed T-test was used to analyse significance of the control samples. A one-way ANOVA with Dunnett's correction was applied to analyse significance ** P < 0.001, *** P < 0.0001 (error bars represent the SEM) N=4, N=4 respectively.

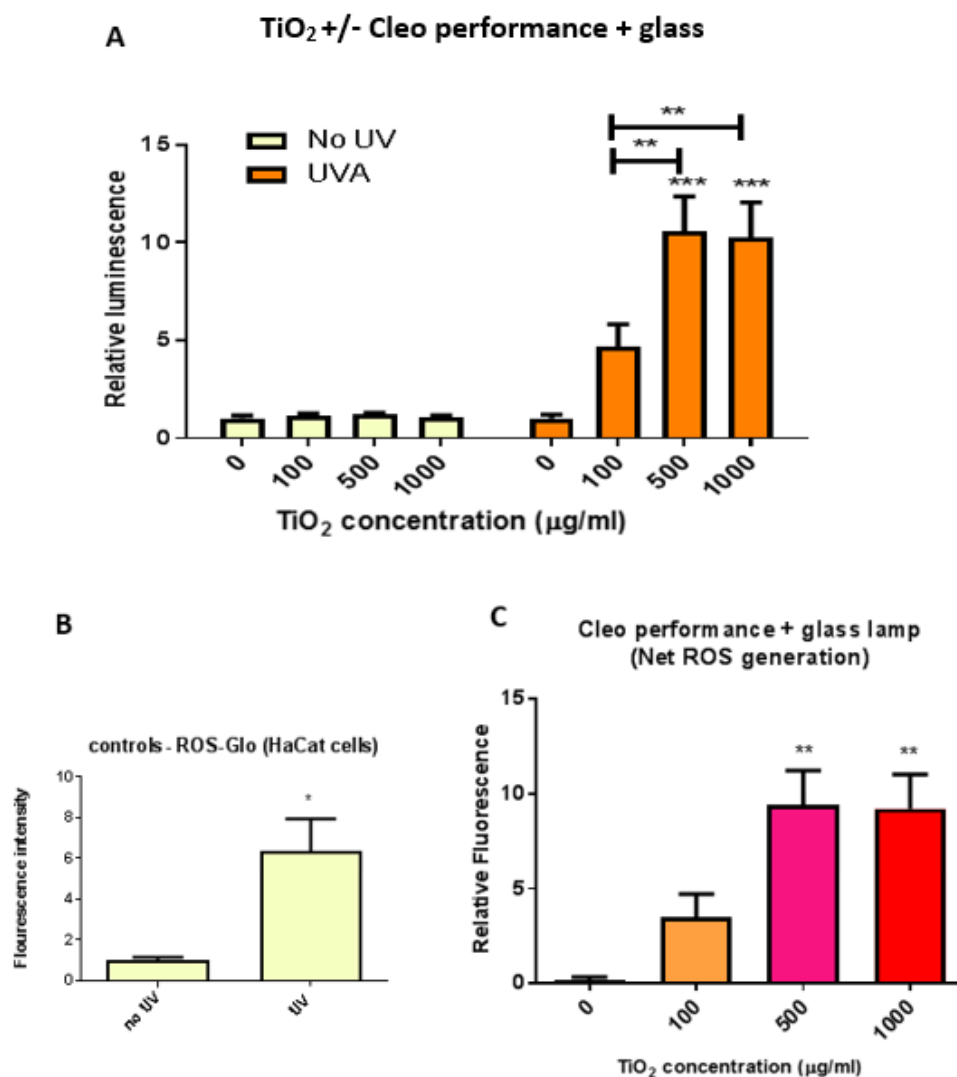


Figure 126: ROS generation in HaCat cells following exposure to TiO₂ +/- Cleo performance

HaCat cells were dosed with TiO₂ +/- Cleo performance + glass and the level of ROS generation was assessed using the ROS-Glo method (A). The level of ROS generation is displayed relative to the non-treated TiO₂ control. Control treated and untreated cells are displayed (B). The net level of ROS generation has been replotted by subtracting the values of the UV dosed TiO₂ from the non UV dosed samples (B). A One tailed T-test was applied to analyse significance of the control samples. A one-way ANOVA with Dunnett's correction was used to analyse significance * P < 0.05, ** P < 0.001, *** P < 0.0001 (error bars represent the SEM) N=2, N=2 respectively.

5.4 Discussion

TiO₂ colloidal suspensions suitable for experimental use under physiological conditions have proven difficult to achieve due to the higher tendency for agglomeration at neutral pH. At lower pH (below 4), TiO₂ remains stable as the point of zero charge (PZC) is in the range of 4.2–6.8 (Pacia et al., 2014). The DLVO theory explains that the stability of a colloidal suspension is based on the balance of two forces, attractive van der Waals and electrostatic repulsive forces. To make a stable suspension with dispersed particles, the repulsive force should overcome the attractive leading to the prevention of particle aggregation. The charge associated with the particles (zeta potential) should be high in order to maintain the repulsive forces between the individual entities (Derjaguin and Landau, 1941).

The starting concentration of TiO₂ in suspension is thought to have an effect in some cases on the level of aggregation observed. TiO₂ dispersed in cell culture media has been shown to have greater aggregation levels when higher starting concentrations are used. It has been suggested that this may be due to the high ionic strength of culture media leading to increased particle agglomeration (Meißner T. et al., 2014). Similar effects have also been reported in PBS. TiO₂ in water has been reported to have similar aggregate sizes at a wide range of concentrations (2-100µg/ml) (Meißner T. et al., 2014). In the experiments carried out TiO₂ in PBS showed an increased rate of sedimentation with the higher starting concentration however TiO₂ in DMEM showed similar levels of sedimentation regardless of the starting concentration.

Ji et al., carried out a study whereby TiO₂ (aeroxide P25) was dispersed in six different cell culture media with either FCS or BSA (Bovine serum albumin) to aid dispersion (Ji et al., 2010). As little as 1% FCS was found to be efficient at dispersing TiO₂ across all the medias tested. FCS was able to aid dispersion due to the effect of protein corona formation. The three day settling experiments carried out in this chapter involved the dispersion of TiO₂ plus 10% FCS in either DMEM or PBS. FCS (10%) in DMEM was chosen as this is routinely used in culture media and would be suitable to use for further experiments. Suspensions were occluded

during the three day investigations to minimise evaporation with cuvettes being marked with a line to monitor the fluid levels over time.

TiO₂ dispersions may be made thicker to help minimise particle aggregation and instability as in the case of sunscreen formulations. Surfactants, proteins and serum can be used to enhance nanoparticle stability. Care is however required when choosing dispersing agents as compounds such as tween 20 and sodium dodecyl sulphate may be toxic to cells in monolayer (Faure et al., 2013). Use of glycerol with PBS at various concentrations as a potentially nontoxic dispersing agent did not seem improve dispersion at the various doses assessed. Use of such suspensions was therefore excluded from further analysis and data was therefore not included in this chapter.

Sonication has been used to obtain suspensions containing smaller aggregate sizes. This process involves breaking up larger TiO₂ aggregates into smaller ones allowing for higher dispersion levels (Faure et al., 2013). Assessment of suspension stability following water bath sonication did not show any further increase in stability levels. For example sonication of TiO₂ particles dispersed in water, PBS, or PBS plus glycerol seemed to have minimal effects on TiO₂ settling. More powerful methods of sonication are available such as the use of a sonication probe, this method however requires contact with the suspensions thus resulting in non-sterile suspensions unsuitable for use in cell culture systems (Meißner T. et al., 2014; Faure et al., 2013; Yoshiura et al., 2015).

The TiO₂ compound was found to be present in variable size aggregates in suspension as shown by the data obtained from the Nanosight. This finding corroborates with earlier reports (Limbach et al., 2005; Xia et al., 2006). Size of the TiO₂ particles in suspensions is important as the potential reactivity of the TiO₂ is dependent on the size being close to the nano range. TiO₂ exists in a wide range of aggregate sizes within sunscreen formulations. This provides the broad spectrum protection offered due to the range of sizes blocking different wavelengths of solar radiation (Smijjs and Pavel, 2011). In an analysis of four sunscreen formulations, researchers found that the particle size of the raw materials was not changed, i.e., the initial

nanoparticle materials remained within the nano range in the sunscreen formulations (Wokovich et al., 2009). Bennett et al., reported that both natural ambient light and artificial light have the ability to disaggregate TiO₂ particles held together by weak DLVO forces. This was observed 30min following irradiation with UV. Ambient light was also found to have the ability to induce disaggregation (Bennett et al., 2012). Aggregation was later seen to occur within 5min of removing the irradiation source (Bennett et al., 2012).

5.4.2 No cell death was detected following exposure of HDFn cells to TiO₂

HDFn cell viability was assessed using the MTS assay following exposure to TiO₂ dispersions. Consistent data were obtained whereby no cell death was detected at the TiO₂ concentrations assessed. At the higher concentrations TiO₂ may have interfered with the assay perhaps due to its physical properties as indicated by the apparent increase in viability seen. Due to the physical and chemical properties of TiO₂ many have reported interference with various dyes and their products used in colorimetric and fluorometric assays thus leading to the possibility of misinterpretation of data (Doak et al., 2009;Monteiro-Riviere et al., 2009;Stone et al., 2009;Baer et al., 2010;Dhawan and Sharma, 2010). Other studies however report no such interference with the MTT and Neutral red assay (Shukla et al., 2011a).

Earlier studies assessing TiO₂ cytotoxicity in different mammalian cell types have been inconclusive with some experimental data showing a cytotoxic response (Jin et al., 2008;Simon-Deckers et al., 2008;Di Virgilio et al., 2010) whilst others showing a negative outcome (Park et al., 2007;Wang et al., 2007b) using the MTS assay. According to a study no cytotoxicity was found in primary human skin fibroblast (BJ cells) or human skin fibroblast immortalised with hTERT (BJhTERT) when exposed to doses of 10-100µg/cm² TiO₂ (Saqib et al., 2012). Prasad et al., assessed fibroblast cells isolated from neonatal foreskin following exposure to anatase form TiO₂ (15 nm primary article size) for 24h at a concentration of up to 1mg/ml. Using the Trypan dye exclusion assay the authors showed a concentration-dependent decrease in cell viability (Prasad et al., 2013). Other studies found significant levels of cytotoxicity following exposure to 30 and 100µg/ml TiO₂ (Lewinski et al., 2008;Arora et al., 2012). Cytotoxic effects were seen in human neonatal foreskin fibroblast cells (BJ) following

exposure to a TiO_2 concentration of $250\mu\text{g/ml}$ (Setyawati et al., 2013). Shukla et al., demonstrated that TiO_2 Nanoparticles have a mild cytotoxic effect on human epidermal cells (A431). Results from the MTT assay, used for studying the expression of the mitochondrial succinate dehydrogenase enzyme, showed that there was a significant reduction in the viability of human skin epidermal cells when exposed to 8 and $80\mu\text{g/ml}$ TiO_2 for 48h (Shukla et al., 2011a).

TiO_2 has been reported to induce toxicity in HaCat cells following a 24h exposure period at concentrations as low as $0.5\mu\text{g/ml}$ using the MTT assay (Gao et al., 2015). Contrary to this Tucci et al., found no cytotoxicity in HaCat cells incubated with $5\text{-}100\mu\text{g/ml}$ TiO_2 for 24h (P Tucci, 2013). Johnston et al., assessed cytotoxicity in Hacat cells using various assays (MTT, Alamar Blue and propidium iodide, PI, uptake assays) after 24h, 48h, and seven days of exposure. The authors demonstrated that TiO_2 induced cytotoxic effects only at very high concentrations, reducing cell viability after seven days of exposure (Johnston et al., 2009).

Due to the multiple routes of TiO_2 exposure and speculated targeting effects in the body studies have investigated the cytotoxic effects of TiO_2 on numerous cell types. For example no significant decrease in cell survival was seen after a 24h exposure to TiO_2 on human lung epithelial cells (A549 and BEAS- 2B) and lung fibroblasts as measured using the SRB, Trypan blue and MTT assay (Gurr et al., 2005a;Bhattacharya et al., 2009;Wan et al., 2012). Other work demonstrated the ability of TiO_2 to induce cytotoxic effects using the MTT assay in human skin fibroblasts, epidermal (A431) and bronchial epithelial cells (BEAS-2B) (Falck et al., 2009a;Shukla et al., 2011b;Prasad et al., 2012). In human amnion epithelial (WISH) cells, TiO_2 was able to induce cytotoxicity at concentrations between $0.625\text{-}10\mu\text{g/ml}$ as assessed by the MTT assay (Saquib Q, 2012). Such TiO_2 induced apoptosis is thought to be attributed to the destabilization of the lysosomal membrane and lipid peroxidation in human monoblastoid and bronchial epithelial cells (Vamanu et al., 2008;Zhao et al., 2009;Hussain et al., 2010). According to Shukla et al., TiO_2 nanoparticles do not cause any significant loss of mitochondrial potential, however lysosomal membrane destabilization occurs. This further leads to the release of lysosomal proteases like cathepsin B, and may directly cause proteolysis or activate caspases, as a pathway for TiO_2 induced death as assessed in bronchial epithelial (16HBE14o-) cells

(Shukla et al., 2011a). Tucci et al., found no alteration of the cell cycle and no increase in apoptosis after a 24 h exposure to TiO₂ nanoparticles, suggesting that the cell is not halting the cell cycle to repair DNA damage nor is it inducing death due to such damage (Tucci et al., 2013).

Magdolenova et al., suggested that the method of dispersing the nanoparticles prior to treatment may affect the resulting toxicity. In their study, two different methods of dispersal were utilized that resulted in either a stable dispersion of TiO₂ nanoparticles or an unstable dispersion with a larger agglomerate size in the other suspension (Setyawati et al., 2013). The unstable dispersion induced cytotoxicity in monkey kidney fibroblasts (Cos-1), while the stable dispersion did not. Interestingly, one previous study has utilized two different cytotoxicity assays in the same cell line after exposure to the same TiO₂ nanoparticles and obtained different results. The authors measured cytotoxicity in lung epithelial cells (A549) after exposure to TiO₂ nanoparticles of various concentrations (12 - 140 nm). After a 48h exposure, a significant decrease in cell viability measured by the MTT assay was seen, but no significant decrease was measured using the clonogenic proliferation assay. Although the results of the MTT assay were significant, the authors note that less than 25% cell death was seen even with the most cytotoxic TiO₂ nanoparticles (Magdolenova et al., 2012). The specific TiO₂ characteristics such as anatase and rutile crystalline form as well as doped and coated versions may have contributed to the differential response in cellular systems. The same applies in the case of TiO₂ sample preparation (Shukla et al., 2011b).

Data from the RT-Glo assay in this chapter showed consistency within the experimental repeats carried out. The RT-Glo assay was not able to detect cell death in HDFn cells following exposure to TiO₂ and an apparent increase in viability is seen again perhaps due to TiO₂ interference occurring.

Further optimisations of the MTS and RT-Glo assay were carried out such as increasing the cellular incubation times with TiO₂ to 48 and 72h. UV was also applied to HDFn and HaCat cells following TiO₂ to induce photo activation effects however no decrease in cell viability was detected and data was therefore not included. The MTS reagents were also transferred into a fresh plate prior to absorbance readings being carried out in order to eliminate any remaining

TiO₂ in suspension. An apparent increase in absorbance with increasing TiO₂ concentration was however still seen. Due to time constraints further optimisation was not carried out.

Although the MTS assay is a simple and reproducible method, other methods such as those involving the use of a resazurin compound have been reported to provide greater sensitivity during colorimetric detection (Eirheim et al., 2004). A limitation of the MTS assay is that mitochondrial stress may lead to an increase in the reductive capacity of a cell, this may be misinterpreted as an increase in cell viability (Eirheim et al., 2004). Further cytotoxicity assays such as the ROS-Glo, resazurin and neutral red assays were also investigated during this study. The neutral red method relies on the active uptake of a vital dye into the cell particularly in low pH regions such as lysosomes. Limitations of the neutral red method include cells being washed away and the vital dye seeping out of cells during the wash steps (Eirheim et al., 2004). Resazurin is a cell permeable redox indicator used to assess cell viability through the reduction of resazurin to resarufin. This results in the production of a pink fluorescent colour which may be measured using a fluorometer. Resazurin reduction is thought to be carried out by a number of reductive enzymes (O'Brien et al., 2005). Incubation time requires optimisation as a compromise between the toxic effect of resazurin on cells and an adequate fluorescent signal is required. A concentration of 0.03% resazurin in PBS was initially used to incubate HDFn cells over the recommended period of 90min. Incubation time was extended (120min and 150min) for optimisation of the fluorescence signal. Low value readings were however obtained despite the increase in incubation time. Lower concentrations of resazurin (0.015% and 0.0075% in PBS) were later assessed with cells being incubated for 90min. Variability in the results was seen along with low readings.

It has been suggested that the clonogenic survival assay may be considered a gold standard among cytotoxicity assays as it depends on the survival and proliferation of cells which therefore makes it more sensitive than other cytotoxicity assays (Franken et al., 2006). The clonogenic survival assay may therefore be assessed in future studies to investigate the cytotoxic potential of nano size TiO₂ particles.

5.4.3 TiO₂ internalisation is suspected to have an effect on the level of cellular toxicity induced

The cellular internalisation of nanoparticles forms an important part of the toxicological analysis although many studies concerned with nanotoxicity have not investigated this in the past (Woodruff et al., 2012). It has been suggested that negative toxicity data particularly regarding genotoxicity may be attributed to a lack of cellular uptake rather than an absence of toxicity (Woodruff et al., 2012).

Browning et al., showed that TiO₂ nanoparticles can penetrate into the cytoplasm and nucleus of human skin fibroblast cells following an exposure time of 24h (Browning et al., 2014). Interestingly the authors found that TiO₂ nanoparticles did not induce cytotoxicity or chromosomal aberrations after 24h, even though they bypassed both the cellular and nuclear membranes. No internalisation was reported by the authors in keratinocyte cells (Browning et al., 2014). Shukla et al., showed TiO₂ nanoparticles to either be internalized in to the human skin epidermal cells or adhere to the cell membrane depending on their size (Shukla et al., 2011b). Other authors found nanoparticles of 30–100 nm in size to be internalized into the cytoplasm, vesicles and also the nucleus, whilst larger particles(>500 nm) remained outside the cells (Suzuki et al., 2007;Xu et al., 2009). Nanoparticles in culture medium are reported to enter cells through endocytosis, and have been suggested in further studies to be localised in vacuoles within the cytoplasm (Hussain et al., 2010;Jaeger et al., 2012). TiO₂ nanoparticles (anatase form with primary particle size of 9nm) were found to be internalized by in vitro cultured fibroblasts and melanocytes but not by keratinocytes and sebocytes (Kiss et al., 2008). Contrary to this Tucci et al., showed that HaCat cells incubated with 5-100µg/ml TiO₂ for 24h were able to internalise TiO₂ (Tucci et al., 2013). The TiO₂ however remained in the phagosomes and did not enter the nucleus or other cytoplasmic organelles. TiO₂ was also reported to lead to altered mitochondrial function and an increase in cellular stress response (Tucci et al., 2013). Goa et al., also reported TiO₂ (aeroxide P25) internalisation by Hacat cells following a 24h incubation at a concentration of 0.5-25µg/ml (Gao et al., 2015).

Micronucleus (MN) formation was found to be significantly increased 24h after treatment with 10µg/ml and 48h after treatment with 5µg/ml TiO₂. Mitochondrial DNA damage measured as “common deletion” was observed to be significantly (14-fold) increased 72h after treatment with 10µg/ml TiO₂ nanoparticles when compared to control. TEM analysis showed that in mouse fibroblast cells (L929) cultured in a medium containing 300µg/ml TiO₂, the number of lysosomes increased, and some cytoplasmic organelles were damaged (Jaeger et al., 2012). In addition, a significant increase in oxidative stress at higher TiO₂ nanoparticle concentrations (>60µg/ml) was found (Traynor et al., 2008¹).

Preliminary investigations carried out in this chapter showed that it was not possible to distinguish with certainty between absorption and adsorption of TiO₂ in cell monolayers. Further work is required to investigate this matter, for example internal cell structures may be stained to visualise the plane at which TiO₂ particles reside within the cells. This would help to distinguish true internalisation from adsorption effects through the use of microscopy techniques the field of focus should help identify where the TiO₂ particles reside within the cells.

5.4.4 TiO₂ induces nDNA damage in HDFn cells with further significant levels of nDNA damage being detected following the photoactivation of TiO₂

Genotoxicity has been defined by the International Conference of Harmonization in the ICH-Guideline as the deleterious change in the genetic material induced by any mechanism (Rajapakse et al., 2012). Damage to DNA results in cellular dysfunction which may in turn initiate and promote mutagenesis, carcinogenesis, or impact fertility (Sathya et al., 2010). Data on the genotoxicity of a given compound is therefore of great importance in regulatory health risk assessment studies (Rajapakse et al., 2013). DS breaks are a serious form of DNA damage that can lead to chromosomal aberrations if they are not repaired prior to the cell entering mitosis (Shukla et al., 2011b). It has been reported that TiO₂ nanoparticles can bind directly to DNA or repair enzymes leading to the generation of strand breaks (Reeves et al., 2008). There

is disagreement in the literature on the genotoxic effects of TiO₂ within cells with some studies being in support of genotoxicity (Falck et al., 2009a;Jugan et al., 2012;Trouiller et al., 2009) whilst others reporting no effect (Warheit et al., 2007;Theogaraj et al., 2007;Bhattacharya et al., 2009). Such studies have been carried out in a variety of cell types however not much work has been done on skin cells (Browning et al., 2014) . A number of authors have shown that TiO₂ nanoparticles are able to induce damage in a wide range of cell types as detected by the comet assay method (Dunford et al., 1997;Karlsson et al., 2008;Reeves et al., 2008;Wang et al., 2007b). Shukla et al., have also shown oxidative DNA damage which was evident by the results of the Fpg-modified comet assay (Shukla et al., 2011b). These results are in accordance with Kang et al., who reported that TiO₂ nanoparticles induced ROS generation in human lymphocytes (Kang et al., 2008). This is also in accordance with data reported by Gurr et al., 2005a which showed that TiO₂ (10µg/ml) induced genotoxicity in BEAS 2B cells. However the concentrations at which DNA damage was observed is lower than that reported by previous authors (Wang et al., 2007a;Falck et al., 2009a).

TiO₂ nanoparticles have also been found to activate key DNA double strand break repair proteins such as the ATM-Chk2 DNA damage response in human dermal fibroblasts after 24 h exposure (Browning et al., 2014). TiO₂ has been reported to induce genotoxic effects at concentrations as low as 10µg/ml after 24h incubation where gamma-H2AX induction was seen to occur (Setyawati et al., 2013). An alternative perspective for phosphorylated H2A.X is that it also serves as a marker of senescence (Widodo et al., 2009). Thus, rather than measuring breaks, the H2A.X foci or some fraction of them, may actually reflect senescent cells.

Saquib et al., were able to detect nDNA damage in human amnion epithelial cells using the neutral comet assay. The authors suggest that at the lower TiO₂ concentrations (10µg/ml), a modulation in the antioxidant enzymes level can be observed, whilst at the critical concentration of (20µg/ml) nDNA damage could be seen (Saquib et al., 2012). Gurr et al., demonstrated that in the human bronchial epithelial (BEAS-2B) cell line, anatase TiO₂ (10 and 20 nm in size) in the absence of photoactivation was able to induce oxidative DNA damage and cause increased H₂O₂ and NO production (Gurr et al., 2005a).

The experiments carried out on HDFn cells in this chapter showed that TiO₂ was able to induce nDNA damage in the absence of photactivation however lower amounts could still be detected in the absence of photoactivation. Vevers and Jha reported similar findings whereby TiO₂ nanoparticles caused DNA damage in the absence of UV light in goldfish skin cells (GFSk-S1) (Vevers and Jha, 2008). Other studies however have shown no toxic effects in the absence of UV. (Reeves et al., 2008). Zijno et al., investigated the genotoxicity of TiO₂ nanoparticles induced by oxidative stress on human colon carcinoma cells (Caco-2 cells). They measured free radical production under acellular conditions using the Electron Paramagnetic Resonance technique and genotoxicity through the micronucleus and comet assays. The comet did not reveal any significant levels of DNA damage (Zijno et al., 2015). According to Browning no one has looked at the clastogenic potential of TiO₂ particles in human skin cells despite this being a well-recognised hallmark of cancer. Following further investigations the authors did not detect clastogenic effects from TiO₂ as chromosomal aberrations (Browning et al., 2014). Woodruff et al., report that the uptake of TiO₂ nanoparticles by TK6 cells was seen to occur however, there was no significant induction of DNA breaks in the standard comet assay nor was there oxidative DNA adducts in the enzyme-modified comet (Woodruff et al., 2012). Similar negative results from the comet assay were observed in human diploid fibroblasts, human bronchial epithelial cells, human carcinoma intestinal cells and human keratinocytes following exposure to TiO₂ (Bhattacharya et al., 2009; Gerloff et al., 2009; Serpone, 2006). Gerloff et al., found no detection of damage using the comet assay under dark conditions, and only found a concentration-dependent induction of DNA damage in the light condition (Gerloff et al., 2009).

It has been suggested that the different experimental outcomes published may be due to the inconsistent comet assay conditions during experiments. It is necessary to take into consideration light exposure while utilizing the comet assay to assess the genotoxicity of TiO₂ (Browning et al., 2014). Petersen et al., showed that DNA samples incubated in the dark for 24 with TiO₂ (0.5–50 µg/ml) did not lead to the formation of base lesions. When the same DNA is exposed to either VIS (400 to 800 nm) for 24h or UVA (370 nm) for 30 min however there was significant formation of lesions at the 50µg/ml dose for the VIS exposure and a significant formation of lesions at the 5 and 50µg/mL doses for the UVA exposure. The authors suggest that the commercial P25 TiO₂ nanoparticles do not have an inherent capacity to oxidatively

damage DNA bases in the absence of sufficient photoactivation. However, TiO₂ exposed to electromagnetic radiation within the VIS portion of the radiation spectrum can induce the formation of DNA lesions (Petersen et al., 2014). Experimental data presented in this chapter shows that aerioxide P25 is able to induce nDNA damage in HDFn cells despite cells being kept under dark conditions throughout the experimental process.

Magdolenova et al., have suggested that differences in the genotoxicity results may result from the proteins and sonication process used in the dose preparation steps (Magdolenova et al., 2012). The duration of sonication and content of proteins need to be considered in these studies. The amount of proteins in dispersion might also be important as they may cover nanoparticles to form protein corona. Results show that the presence of serum in stock dispersion medium and the length of sonication may modify the surface of nanoparticles and affect their behaviour. As mentioned previously serum proteins adhere to their surface forming a protein corona and in doing so help disperse the nanoparticles in suspension (Magdolenova et al., 2012).

As suggested by Warheit et al., 2007, the manner in which genetic damage is measured varies among different test systems; and some assays could be ill-suited for evaluating particular types of nanomaterials. For example, bacterial mutagenicity-based assays may not be suitable for detecting the genotoxicity of nanoparticles as prokaryotic cells may lack the ability that eukaryotic cells have to intake particles through endocytosis. Prokaryotic cell walls have been reported to block the entry of nanoparticles contrary to the eukaryotic cell membrane (Woodruff et al., 2012).

5.5 Summary of main findings:

- TiO₂ was stable in water and was unstable when dispersed in physiologically relevant media. Addition of FCS to DMEM increased TiO₂ stability, the application of sonication however was not seen to aid stability in suspension.
- Interference in cell viability assays (MTS and RT-Glo) was seen possibly due to TiO₂ interactions with light.
- TiO₂ induced cytotoxicity in HDFn cells when present without the influence of solar light. Application of UVA alongside TiO₂ induced further levels of damage. The enzyme modified method (hOGG1) was able to further uncover oxidative damage levels.
- TiO₂ displayed protection against solar radiation in both acellular and cellular systems and also demonstrated protective abilities against IR.
- TiO₂ interfered with fluorescence and luminescence measurements in both the DCFDA and ROS-Glo assays as demonstrated in the acellular experiments. The ROS-Glo assay was found to be a more sensitive method for ROS detection relative to the DCFDA assay. Photoactivated TiO₂ induced ROS generation effects in both HDFn and HaCat cells.

Chapter 5 - Section II

5.6 Chapter aims:

- Optimise experimental conditions for investigating the effect of nanoparticulate TiO₂ on whole skin models of dermal absorption.
- Investigate the effect of TiO₂ plus or minus UV in the perturbation of skin barrier function.
- Assess the effect of skin flexion on dermal absorption levels using the Cutaflex model.

5.7 Absorption studies- Franz cell model

The Franz-type cell (Figure 127) has a fixed volume receptor chamber which is kept under controlled temperatures and is stirred continually during the course of the experiment to minimise interference with the level of compound diffusion through the membrane under study. The sampling port allows for sample collection during the duration of the study (Gummer et al., 1987).

Human tissue *ex vivo* is the gold standard for use either as fresh or that which has been previously frozen. Porcine skin has been used extensively as a surrogate for human skin as it is very similar to human in terms of morphology and function. Synthetic polymeric membranes which are inert may also be used, this includes membranes such as polysulfone and cellulose acetate, and hydrophilic polymeric membranes with a pore size of 0.45 µm are usually used. Human skin equivalents (HSEs) may also be utilised in absorption studies. These are engineered 3D skin constructs that use a combination of cultured human skin cells and extracellular matrix components under controlled culture conditions. HSEs allow for skin cell viability to be maintained, the permeability of the simulated tissue however is generally higher than that of the *in vivo* situation. These models allow for the investigation of metabolism, penetration, and distribution of the compound of interest. Caution is often required when relating the findings back to human skin *in vivo* (Schmook et al., 2001; Godin and Touitou, 2007).

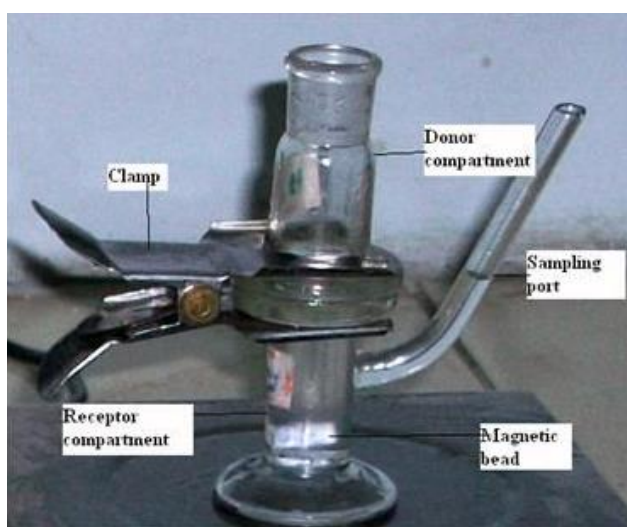


Figure 127: Photograph of a Franz type diffusion cell (Bharadwaj et al., 2011)

The Franz-cell method allows for the evaluation of compound uptake through a membrane. The finite dose permeation, steady state flux of compounds (either alone or in formulations), permeability of the compound and permeability of the membrane under study may be assessed. Considerations are required for the compound under study as the use of a highly permeable molecule with a small receptor chamber eventually leads to the build-up of compound in the receiver chamber which reduces the concentration gradient and therefore slows the flux of the compound (non-sink conditions). Sink conditions must be maintained in this instance by using a large volume of receptor fluid for example or reducing the dose of the highly permeant compound (Bartosova and Bajgar, 2012). If a low permeability compound is used then detection in a large volume receptor chamber may become a problem.

5.7.1 Experimental design (donor chamber, receiver chamber and permeant compound)

The compound of interest can be prepared in a variety of formulations, this includes liquid solutions, suspensions, creams, gels, ointments, lotions, pastes, powders, or adhesive patches. The formulation chosen for study should mimic the human exposure scenarios where possible. The application of either an infinite or finite dose (concentration of the permeant) depends on the study aims. An infinite dose is one in which the concentration of the permeant will not be depleted from the donor formulation over the course of the experiment (Bartosova and Bajgar, 2012). This dosing will produce fundamental permeation

behaviour and is usually used when testing that behaviour in the presence of permeability enhancers. A finite dose mimics the amount of permeant that would be present in a real life situation for example, a specific amount of drug to be administered to a patient. Finite dosing can also be used to mimic compounds that would only be present on the skin for a short amount of time before being removed (Chen et al., 2011).

PBS and water are good vehicles for the donor compartment as they allow for basic permeation data to be achieved. Lipophilic compounds have a low aqueous solubility and may require alternative vehicles such as water/ alcohol mixtures or propylene glycol. It must be noted that these additives may interact with the structure and permeability barrier of the tissue and thus change the flux of the permeant (Vaddi et al., 2002). For each compound of interest assessed it is recommended that at least a minimum of three parallel cells should be used for every run. Due to the biological variability in skin, in many cases 5-6 replicates should be run per group. Evaporation of compounds, solvents, or formulations from donor chambers may occur, especially if the cells are maintained at high temperatures. Samples may therefore be occluded bearing in mind that the occlusion process increases the level of permeation through the skin. Although occlusion prevents the evaporation of the test compound, it also increases the hydration of the rate limiting membrane by preventing the evaporation of water from the rate limiting membrane (Bronaugh and Stewart, 1985; Moss et al., 2015).

The choice of receptor fluid depends on the nature of the permeant and the type of diffusion cell used. An ideal receptor medium for an in vitro permeability study should mimic the in vivo situation. In the static Franz Type cells the permeant is not continually cleared therefore caution is required so not to reach saturation which would affect the diffusion gradient and could slow down the passive diffusion process. The solubility of the compound should be taken into consideration so that the compound is at its desired form in the donor formulation. Aqueous receptors are common for hydrophilic and moderately lipophilic permeants. PBS (pH 7.4) is also commonly used. More lipophilic permeants or permeants with low aqueous solubility may require additional solubilising agents such as surfactants, protein (BSA) or organic solvents (ethanol/water systems), in order to maintain "sink" conditions. The effect that such solubilisers have on the penetration of the compound of interest however needs to be considered. Such compounds are recommended for use at the minimum concentration necessary to solubilise the permeant (Moss et al., 2015).

5.7.2 Detection of the permeant compound

Detection of the permeant compound may be carried out using chromatographic or spectroscopic methodologies. Alternatively the use of radiolabelled permeates may be employed. The flux of a compound can be converted to an amount of compound in ng or μg per time interval per unit surface area of exposed skin (Council, 2000; Moss et al., 2015). Information about the time points of the specific samples collected is required to calculate the quantity of the compound in the collected sample per time interval, regardless of volume.

Radiolabelled compounds can be detected in very small amounts and in a large volume of receptor medium. Analysis is usually quite rapid and accurate. The collected volume can be counted using a scintillation counter, and then the flux or permeability coefficient (K_p) calculated from the measured radio activity obtained. This can be converted to the amount of compound in any given sample at any given time interval by knowing the specific activity of the labelled compound, however radiolabelled purity must be taken into account when using such compounds. Non-radiolabelled compounds can also be used in permeability experiments and detected with methods including high-performance liquid chromatography (HPLC), enzyme-linked immunosorbent assay (ELISA), and fluorescence. Such methods allow the investigator to determine whether the same species of compound that permeated the membrane was that which was applied. The disadvantage of such methods is that very small quantities of compound can go undetected or under-detected because of the large volume in the receptor chambers. This issue can be overcome by decreasing the volume of the sample by drying it down to a total quantity of sample that can then be analysed however such analysis would give the amount of compound penetrating a membrane over time and not the amount at different time intervals. Samples should be taken quickly and consecutively from all receptor chambers so that the time interval is consistent for all samples. If there is a delay of minutes between taking samples instead of seconds, this should be taken into account when performing calculations (Moss et al., 2015; Gulson et al., 2015).

5.8 Chapter specific methods – section II

Details of UV dosing (Cleo performance + glass lamps) carried out in this chapter are outlined in the general methods section (chapter 2)

5.8.1 Franz-type diffusion cell skin processing

Percutaneous absorption studies were carried out using full thickness surplus human breast and abdominal skin from surgical procedures obtained from normally discarded tissue following consent. Ethical approval for use of adult normally discarded surplus human tissue was obtained by the Newcastle Dermatology Biobank. Skin was mounted on static Franz cell diffusion chambers with an area of 0.79cm^2 and total receptor volume of 1.5ml as a modification of the method described previously (Moore et al., 2014). Skin was processed by removing subcutaneous fat and connective tissue and freezing at -20°C until use. Before use, skin was thawed on ice at RT for approximately 1h prior to placing on diffusion cells. Whole skin pieces were cut to approximately 3cm sizes and sandwiched between the donor and receiver chamber, diffusion cells were placed in a heated manifold connected to a circulating water bath at 38°C to maintain a skin temperature of 32°C . The receiver chamber was filled with 0.9% (W/V) saline solution and skin samples left to equilibrate for 1 h. A magnetic stirrer was used to keep the receiver media in constant motion. Receiver chamber fluid ($50\mu\text{l}$) was taken from each diffusion cell as the time 0 sample to measure background radiation.

5.8.1.1 Dose preparation

Control dose samples were prepared by mixing an infinite dose (10mg/ml) radiolabelled (C^{14}) caffeine (Figure 128) in water. TiO_2 test sample doses were prepared by adding TiO_2 (5mg/ml) to the radiolabelled compounds in water and stirring till compounds appeared homogenous in suspension. Later experiments involved suspension preparation by aliquoting TiO_2 from the 1mg/ml stock suspension as described in section 5.2.1.3. Radioactivity of the dose samples was determined by taking an average reading of three $50\mu\text{l}$ samples prior to applying $500\mu\text{l}$ of the dose to each skin surface.

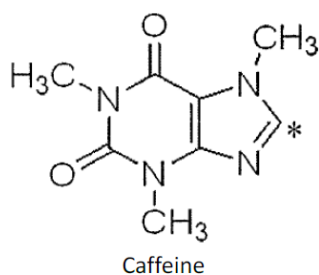


Figure 128: Showing the structure of radiolabelled carbon-14 caffeine.
The position of the carbon-14 isotope is indicated by the asterisk (*)

5.8.1.2 Sampling

At appropriate time intervals (0-24h) 50µl samples were collected from the receiving medium and analysed for the presence of radiolabelled compound, cells were immediately refilled with fresh receiver medium (50µl). At the end of the permeation experiment (24h), the total receptor fluid was collected in pre-weighed tubes and analysed for presence of radiolabelled compound.

5.8.1.3 Mass balance

The inside of the receiver chambers was washed with PBS and the wash collected for analysis. The donor chamber was also swabbed twice with cotton wool balls soaked in soap and water followed by a single dry cotton wool swab. All swabs were placed in 10ml scintillation fluid and left overnight.

5.8.1.4 Tape stripping

Skin was allowed to dry following skin surface swabbing (1-2h) before the amount of test compound in the stratum corneum was measured using tape stripping. Adhesive tape (scotch 3M) was applied to the skin surface (stratum corneum side up) pressed down with forceps

and pulled gently from the skin. This was repeated 10 times for each skin sample. Tape strips were placed in 10ml scintillation fluid and left to enable the stratum corneum to dissociate from the tape strips for 72h before analysis.

5.8.1.5 Skin digest

Following tape stripping the remaining skin was placed in 1.5 M potassium hydroxide (2ml) in 80% (V/V) ethanol in water and left for 48 h to digest before adding 10ml scintillation fluid.

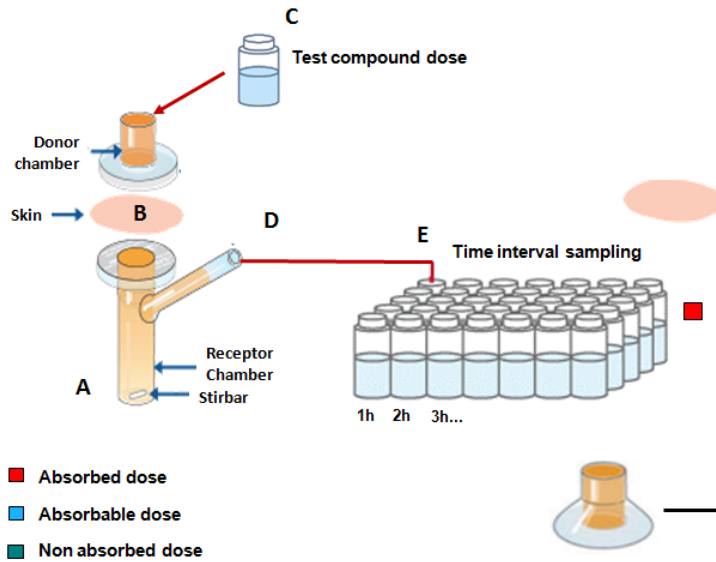
5.8.1.6 Analysis

All samples were analysed through scintillation counting using Beckman LS6500 with automatic quench correction. The mass balance and radiolabelled compound distribution was calculated from the amount of chemical in all the compartments of the diffusion cell and expressed as a percentage of the applied dose. The radioactivity in the dose solutions was determined from triplicate aliquots. For the distribution profile, “unabsorbed” was the sum of the skin surface, donor chamber, tape strips 1-2 and non-dosed skin. “Absorbed” was the cumulative dose measured in receptor fluid during the experimental period plus washes of the receiver chamber. “Dosed skin” was the combined epidermis and dermis after removal of the stratum corneum. “Absorbable” was dosed skin plus the value for absorbed. A summary of the mass balance terminology can be found in section 5.8.1.8.

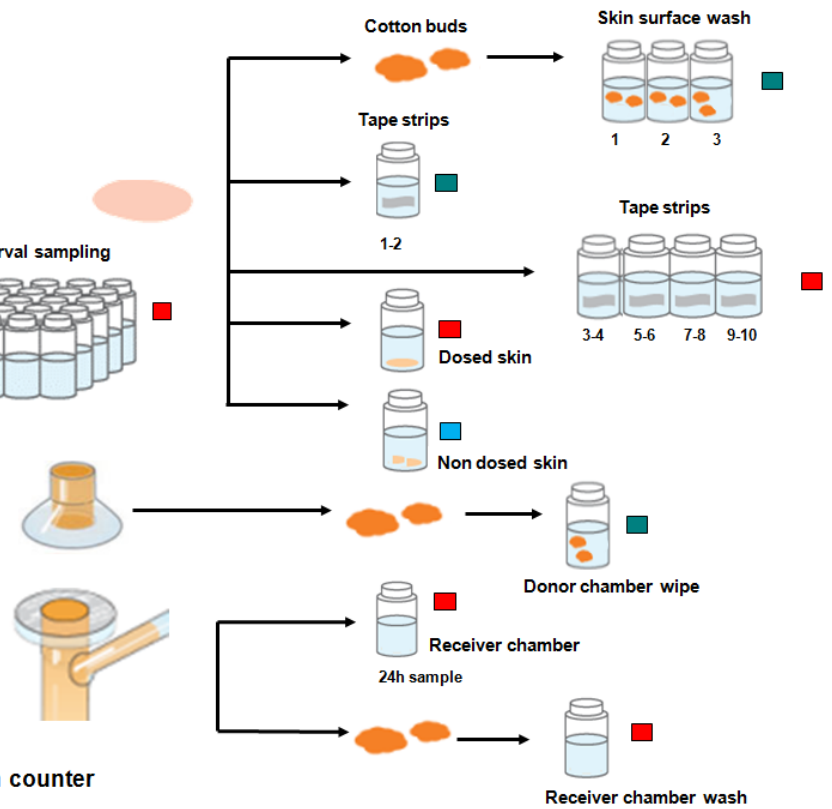
5.8.1.7 Statistical analysis

The Shapiro-Wilk test was used to assess data for normal distribution due to the small sample sizes studied. Data determined to be normally distributed was then analysed using a T-test to identify potential significance in differences between the two groups (test and control).

1) Franz -type diffusion cell



2) Mass balance compartments



❖ All samples were analysed using a scintillation counter

Figure 129: Outline of percutaneous absorption study methodology using the Franz-type diffusion cell.

(1) Franz type diffusion cells (A) were used for static cell percutaneous absorption studies. Whole thickness human breast skin (B) was mounted on to the diffusion cells and allowed to perfuse for 1h before dosing (C). Receptor media samples (D) were taken at various time intervals (E) for a period of 24h after which a mass balance analysis was carried out as shown in (2). All samples were analysed for presence of the radiolabelled chemical marker compound using scintillation counting.

5.8.1.8 Mass balance terminology:

Skin surface = dose retrieved from the skin surface through the wash steps

Donor chamber = dose retrieved from the donor chamber compartment of the Franz cell

Non-dosed skin = area of skin in-between the donor and receiver chambers that is non exposed

Tape strips = amount of compound in the stratum corneum with each tape strips (1-2 are dead cells of the stratum corneum and are not regarded as absorbed. Tape strips 3-10 in human skin are regarded as absorbed)

Dosed skin = amount of compound present in skin following tape stripping

Absorbed= amount of compound detected in receptor fluid

Non-absorbed= the sum of compound in skin surface, donor chamber, tape strips 1-2 and non-dosed skin

Absorbed= compound in fluid collected from acceptor compartment and acceptor compartment wash

Absorbable= amount of compound available on dosed skin plus the value of absorbed

Total= the sum of all the compartments

5.8.2 Cutaflex

The flexing skin cell (CutaFlex™) is based on a modification of the standard Franz cell and was manufactured by BM Injections (Winchester, UK). The modified cells are constructed from inert (PTFE) plastic and incorporate a bifurcated receptor sampling arm. The upper arm has been modified to accommodate a removable air-tight cap. The lower arm accommodates a latex bladder which is connected to an external Watson-Marlow 520Di peristaltic pump (Falmouth, U.K.), controlled by bespoke software provided by Watson-Marlow (v1.0) which allows for timed control of the pump. This allows a controlled inflation/deflation of the latex bladder to be achieved.

Skin sections were mounted and clamped to the donor chamber. The receptor chamber in each diffusion cell (static and CutaFlex™) was filled with PBS. The assembled diffusion cells were then placed in a metal chamber on a magnetic stirrer, which mixed the receptor chamber

fluid via two (12 x 6 mm) Teflon™ coated iron stir bars placed in each receptor chamber. The jacket of each diffusion cell was connected to a Grant Instruments GD120 (Cambridge, U.K.) re-circulating water heater via the diffusion cell manifold in order to ensure a regulated temperature.

Skin deflection in the CutaFlex™ diffusion cell was driven by air displacement generated by the peristaltic pump under controlled parameters (Figure 139). Skin deflection height was measured using a custom-made laboratory apparatus that sat on top of the skin surface and contained a piston with a ruler displaying markings (mm). For the displacement of air as facilitated by the peristaltic pump, twelve revolutions per minute was the chosen speed for both forward (upwards) movement of 14 sec and reverse (downwards) movement of 13 sec as optimised previously (Viegas, 2014). This led to approximately 2 flexes/min. The maximum average of height for displacement was approximately 3 mm.

5.8.3 Porcine skin preparation

Full thickness porcine skin was obtained from a reputable supplier within a few hours postmortem. Sections were wrapped in aluminium foil and stored flat at -20°C for up to 3 months before use. Skin was defrosted for approximately 24 h at 5°C and dermatomed to a thickness of 1000µm using a Humecca D42 dermatome (Eurosurgical Ltd.) prior to the experiment. Skin thickness was confirmed using a digital micrometer (Tooled-Up). Dermatomed skin was cut into squares measuring approximately 3 x 3 cm in preparation for mounting into diffusion cells.

5.9 Results

5.9.1 The effects of TiO₂ compound on skin barrier function

Radiolabelled [1-methyl ¹⁴C] caffeine was utilised as a marker compound to assess the potential effects of TiO₂ as a dermal penetration enhancer in human skin samples. Any disruption in the skin barrier function as a result of TiO₂ interaction with the skin surface can then be detected as an increase in the rate of [1-methyl ¹⁴C] caffeine influx through the skin. TiO₂ appeared to show no effect on the rate of caffeine absorption through healthy intact human skin. The percutaneous absorption of [1-methyl ¹⁴C] caffeine (2.9 mg/cm²) was measured through human skin in the presence or absence of dispersed TiO₂ nanoparticles at 5 mg/ml (Figure 130, Figure 131 and Table 13) or 50µg/ml in water (Figure 132, Figure 133 and Table 14). Franz-type diffusion cells (surface area 0.79 cm², receiver chamber volume 1.5 ml) were used to assess the level of radiolabelled caffeine absorption. Skin was exposed to ambient light conditions throughout the course of the experiment.

Absorption of caffeine after 24h amounted to $22.8 \pm 10 \mu\text{g}/\text{cm}^2$ with water alone and $27.5 \pm 6 \mu\text{g}/\text{cm}^2$ with 5mg/ml TiO₂ in water ($P>0.05$) (Figure 130). There was a similar lack of effect of TiO₂ on the disposition of caffeine in the SC or dosed skin (Figure 131). The results demonstrate that 5mg/ml TiO₂ had no significant effect on percutaneous absorption of caffeine. This may indicate that human breast skin maintained its natural barrier function when TiO₂ was applied under the influence of ambient light. An experimental repeat was carried out using a lower concentration of TiO₂, this was carried out to minimise the level of TiO₂ clumping in order to achieve particles within the nano range. Lower TiO₂ concentrations (50µg/ml) showed absorption of caffeine following 24h to be $17.4 \pm 5.6\mu\text{g}/\text{cm}^2$ with water alone and $15.2 \pm 5.3\mu\text{g}/\text{cm}^2$ with 50µg/ml TiO₂ plus caffeine (Figure 132, Figure 133 and Table 14). Absorption through the human skin after 24h appeared to be similar for control and test suspensions. A significant difference was however seen in TiO₂ distribution across the SC (tape strips 3-10). The mean value for caffeine in water absorption was $0.669 \pm 0.078\mu\text{g}/\text{cm}^2$ compared to $1.121 \pm 0.27\mu\text{g}/\text{cm}^2$ with caffeine plus 50µg/ml TiO₂ in water (Figure 132). Significantly more caffeine was found in the deeper epidermal layers of the TiO₂ (50µg/ml) dosed skin compared to the control group. Photoactivation of TiO₂ (1mg/ml) using UVA

showed no significant effects on the level of caffeine absorption through human skin when compared to the non-photo activated samples (Figure 134, Figure 135 and Table 15).

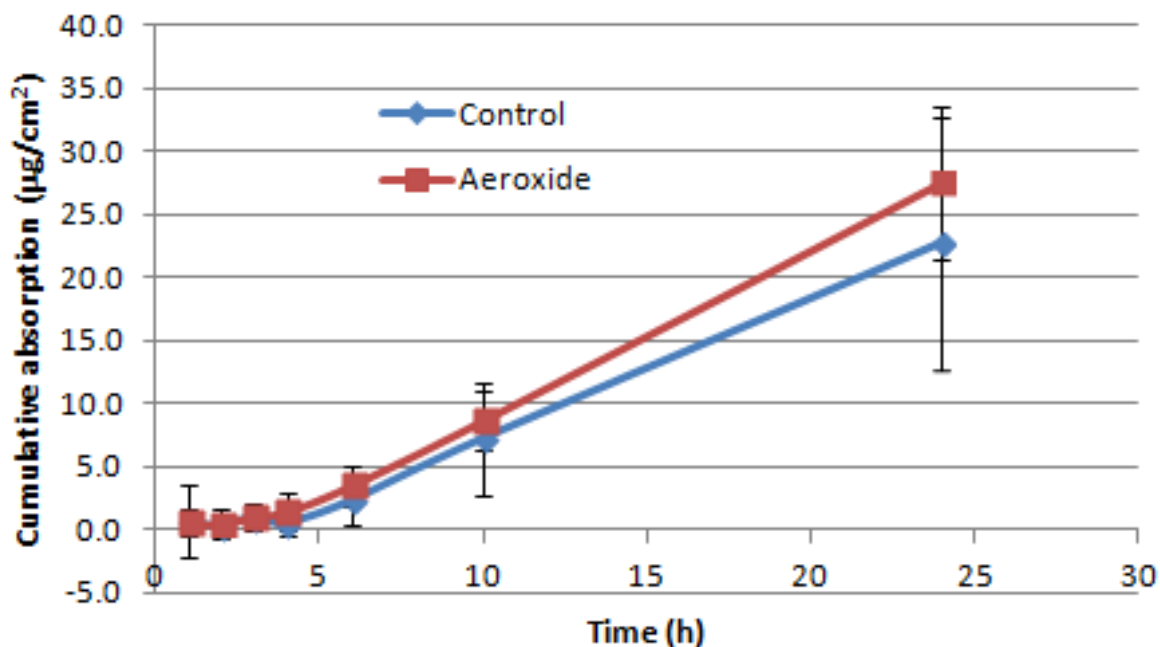


Figure 130: Cumulative absorption of radiolabelled caffeine through human skin plus or minus 5mg/ml TiO₂
 The mean value and standard deviation of 5 control (10mg/ml caffeine only) and 5 test (10mg/ml caffeine plus aeroxide at 5mg/ml) replicates are shown. Samples were taken from a single donor and the distribution of caffeine assessed after 0, 1, 2, 3, 4, 6, 10 and 24h exposure when applied to human skin as an infinite dose of 2911.3µg/cm². The Shapiro-Wilk test was used to assess data for normal distribution, once normality of data was confirmed a T-test was carried out to identify potential significance in differences between the two experimental conditions.

Caffeine retrieval (%)	
Control	TiO ₂ (aeroxide)
93.5	98.5
96.9	98.8
92.8	85.1
99.7	94.7
99.8	98.0

Table 13: Showing the total level of caffeine retrieval from each Franz-cells (radiolabelled caffeine plus or minus TiO₂ (5mg/ml))

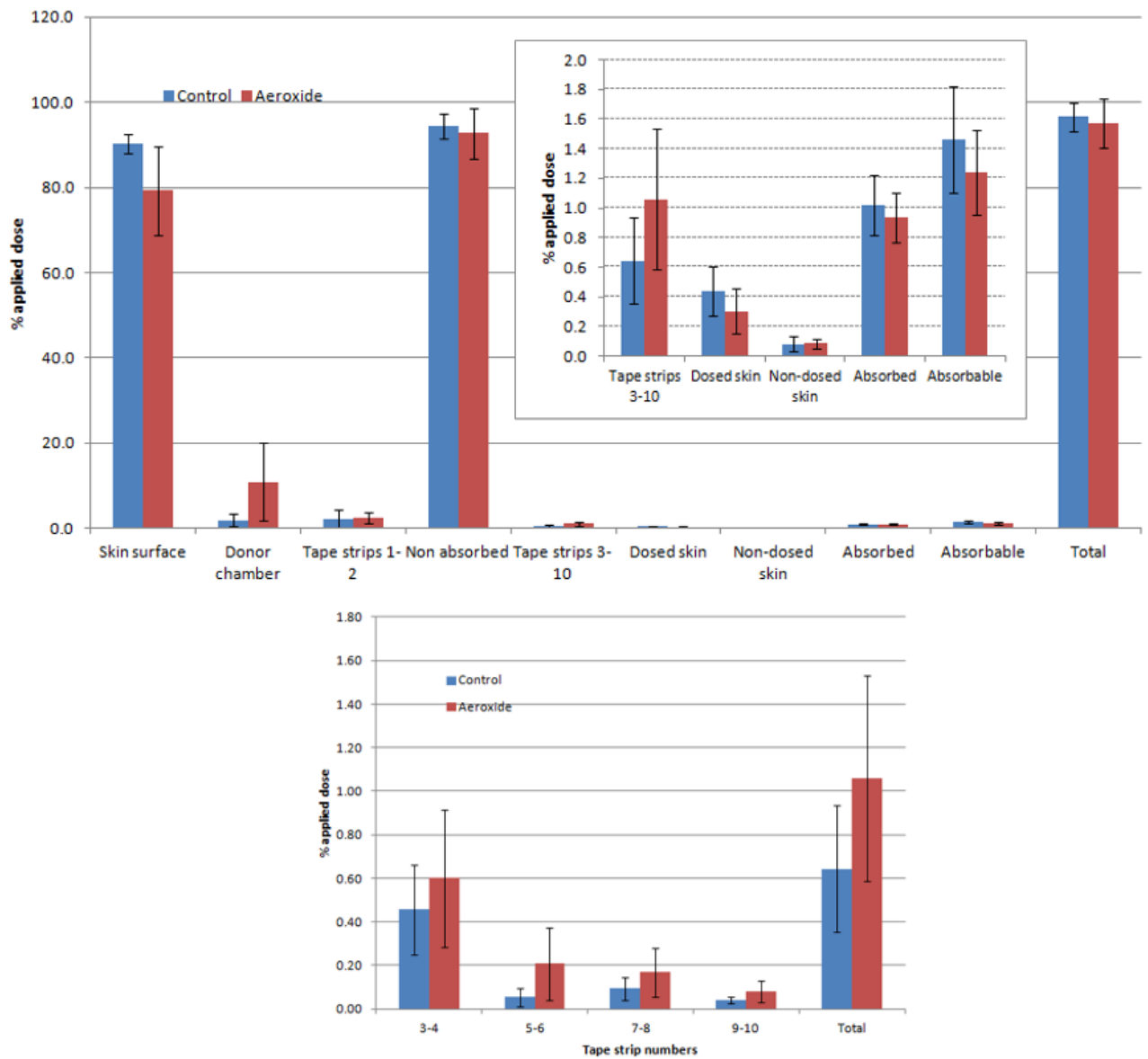


Figure 131: Mass balance showing the distribution of radiolabelled caffeine through human skin plus or minus 5mg/ml TiO₂

Data shows the mean value and standard deviation of 5 control (10mg/ml caffeine only) and 5 test (10mg/ml caffeine plus aeroxide at 5mg/ml) replicate samples taken from a single donor. The distribution of caffeine was assessed after a 24h exposure period. The blue bars represent caffeine only (10mg/ml in water). Red bars represent caffeine (10mg/ml in water) plus aeroxide (5mg/ml in water) values displayed are the mean ± SEM. Data for the tape strips classed within the absorbed dose is shown separately below.

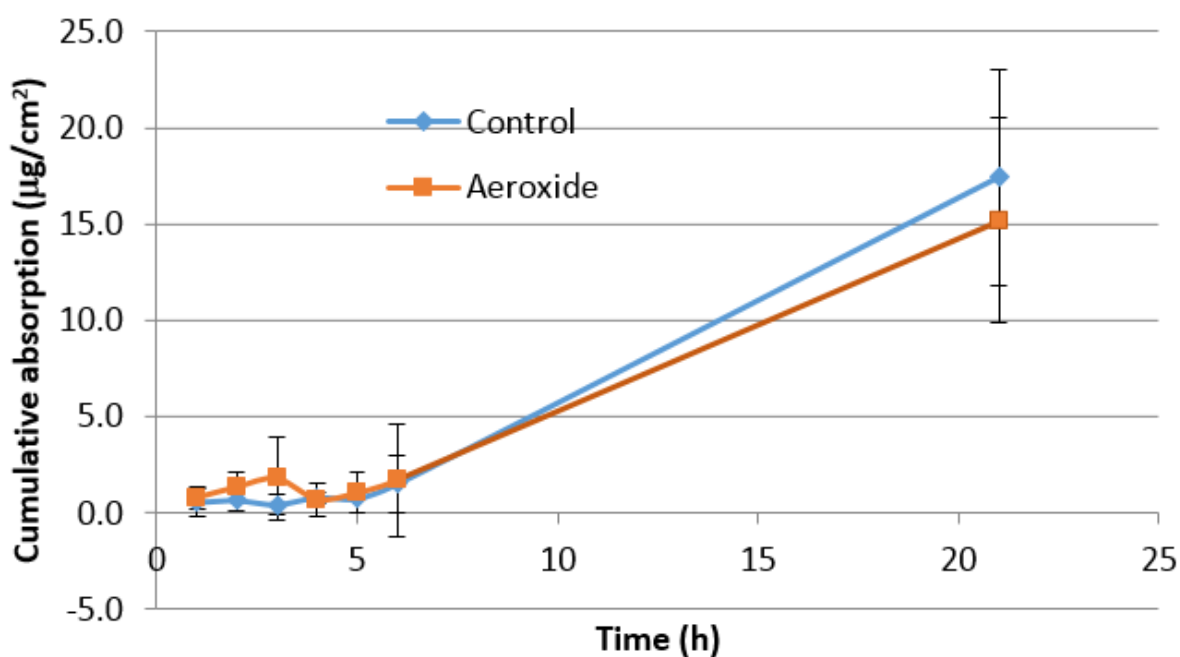


Figure 132: Cumulative absorption of radiolabelled caffeine through human skin plus or minus 50µg/ml TiO₂
 The mean value and standard deviation of 5 control (10mg/ml caffeine only) and 5 test (10mg/ml caffeine plus aeroxide at 50µg/ml) replicate are shown. Samples were taken from a single donor and the distribution of caffeine assessed after 0, 1, 2, 3, 4, 6, 10 and 24h exposure when applied to human skin as an infinite dose of 2911.3µg/cm². The Shapiro-Wilk test was used to assess data for normal distribution, once normality of data was confirmed a T-test was carried out to identify potential significance in differences between the two experimental conditions.

Caffeine retrieval (%)	
Control	TiO ₂ (aeroxide)
93.5	98.5
96.9	98.8
92.8	85.1
99.7	94.7
99.8	98

Table 14: Showing the total level of caffeine retrieval from each Franz-cells (radiolabelled caffeine plus or minus TiO₂ (50µg/ml))

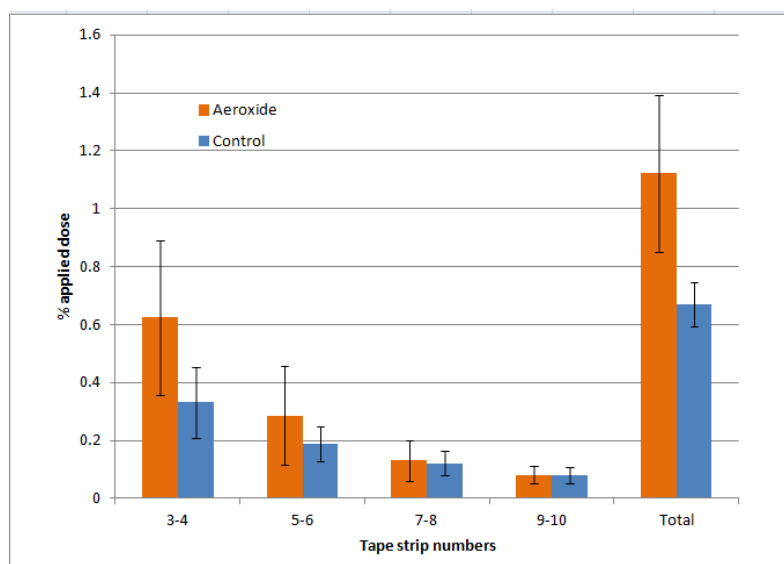
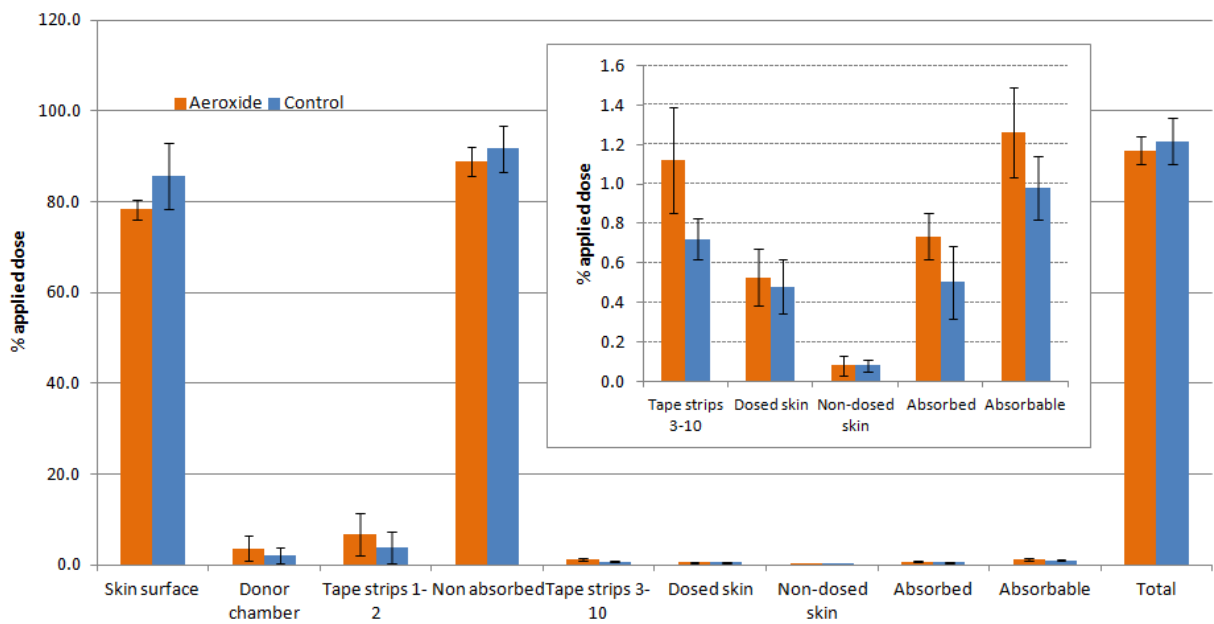


Figure 133: Mass balance showing the distribution of radiolabelled caffeine through human skin plus or minus 50µg/ml TiO₂

Data shows the mean value and standard deviation of 5 control (10mg/ml caffeine only) and 5 test (10mg/ml caffeine plus aeroxide at 50µg/ml) replicate samples taken from a single donor. The distribution of caffeine was assessed after a 24h exposure period. The blue bars represent caffeine only (10mg/ml in water). Red bars represent caffeine (10mg/ml in water) plus aeroxide (50µg/ml in water) values displayed are the mean ± SEM. Data for the tape strips classed within the absorbed dose is shown separately below.

1mg/ml TiO₂ +/- UVA Caffeine absorption 10mg/ml

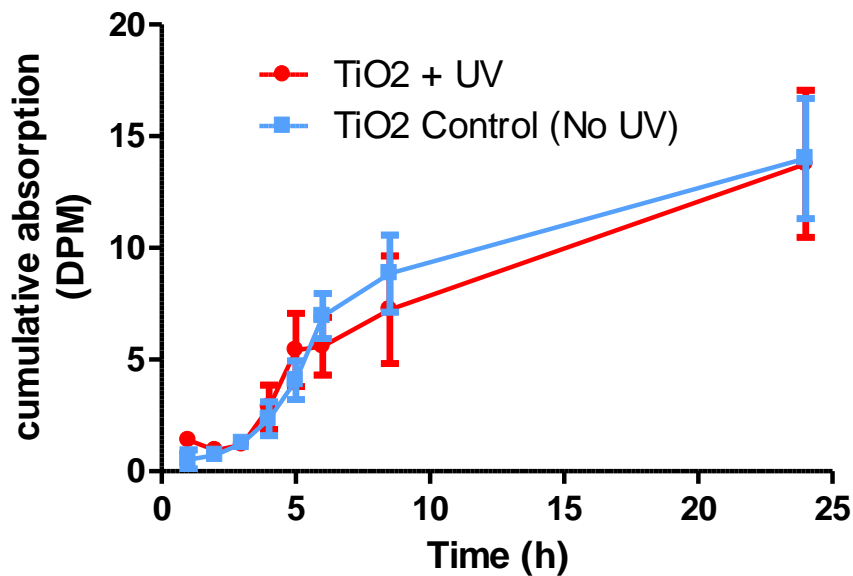


Figure 134: Cumulative absorption of radiolabelled caffeine through human skin exposed to 1mg/ml TiO₂ plus or minus UVA

The mean value and standard deviation of 4 control (10mg/ml caffeine plus TiO₂ at 1mg/ml) and 4 test (10mg/ml caffeine plus TiO₂ at 1mg/ml plus UVA) replicates are shown. Samples were taken from a single donor and the distribution of caffeine assessed after 0, 1, 2, 3, 4, 6, 10 and 24h exposure when applied to human skin as an infinite dose of 2911.3µg/cm². The Shapiro-Wilk test was used to assess data for normal distribution, once normality of data was confirmed a T-test was carried out to identify potential significance in differences between the two experimental conditions.

Caffeine retrieval (%)	
TiO ₂	TiO ₂ plus UV
95.5	87.5
93.7	84.2
90.4	86.1
90.8	84.5

Table 15: Showing the total level of caffeine retrieval from each Franz-cells (radiolabelled caffeine plus 1mg/ml TiO₂ (plus or minus UVA))

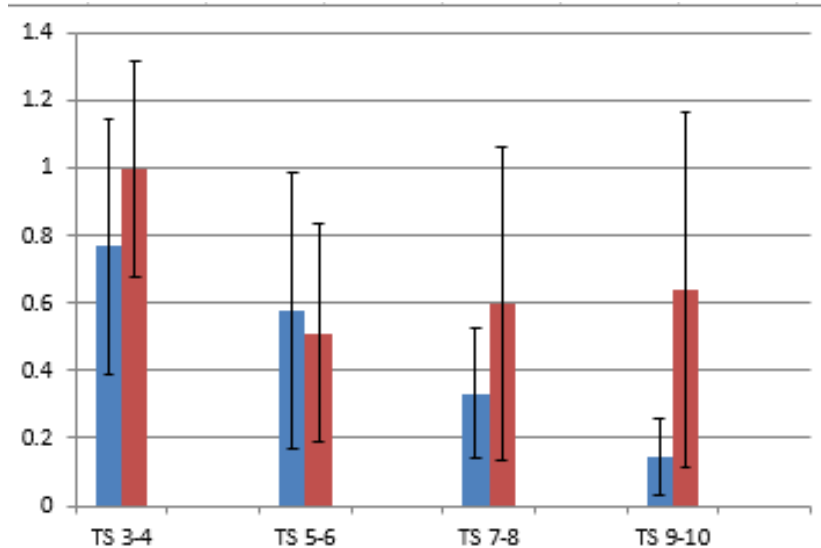
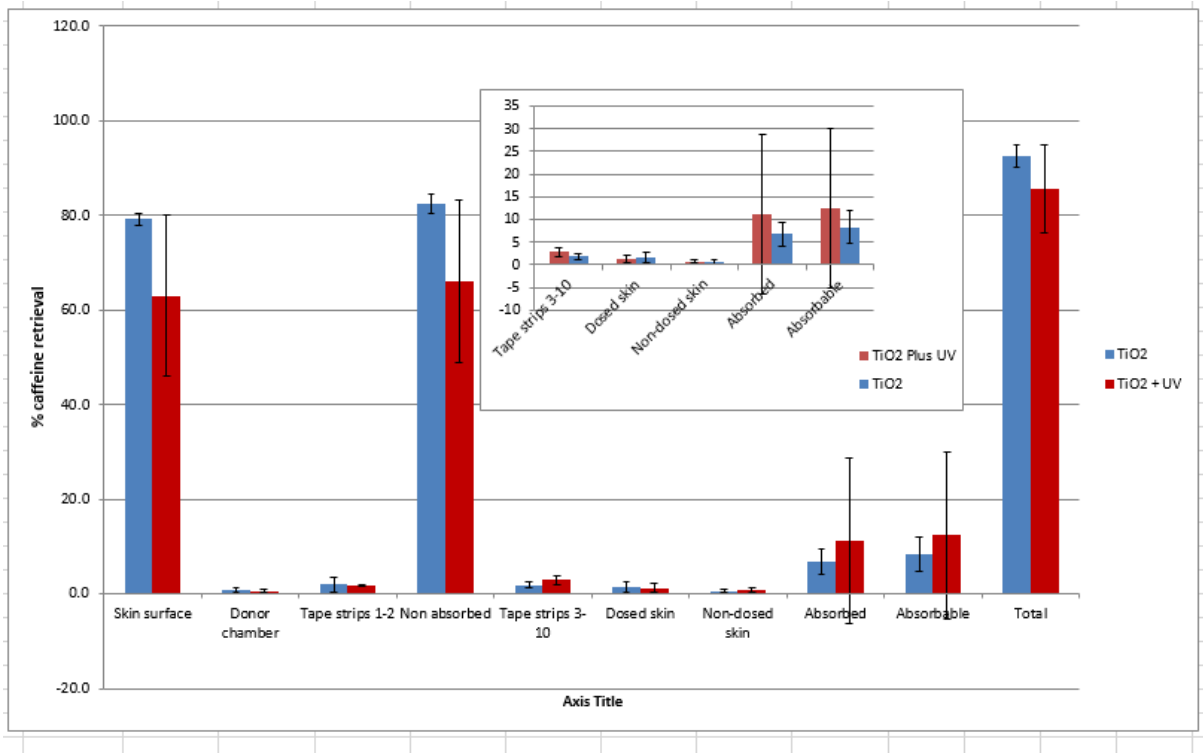


Figure 135: Mass balance showing the distribution of radiolabelled caffeine through human skin when exposed to 1mg/ml TiO₂ plus or minus 1mg/ml TiO₂

Data shows the mean value and standard deviation of 4 control (10mg/ml caffeine plus TiO₂ at 1mg/ml) and 4 test (10mg/ml caffeine plus TiO₂ at 1mg/ml plus UVA) replicate samples taken from a single donor. The distribution of caffeine was assessed after a 24 h exposure period. The blue bars represent caffeine plus TiO₂. Red bars represent caffeine plus TiO₂ plus UVA. Values displayed are the mean ± SEM. Data for the tape strips classed within the absorbed dose is shown separately below.

5.9.2 Temperature and irradiance of the Cleo performance lamp

The rate of compound absorption through a membrane is known to be effected by temperature changes. The temperature under the UV lamp (Cleo performance + glass) was therefore monitored over time with the first reading being taken after 5 min from the lamp being switched on (Figure 136). UV readings taken over time appeared to be constant as shown in Figure 136.

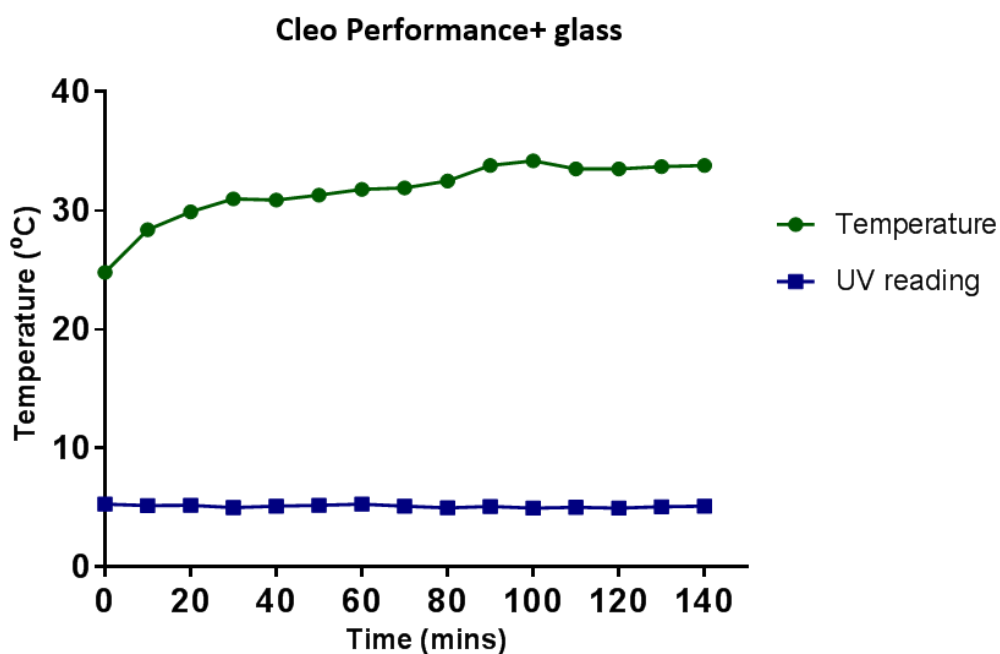


Figure 136: Temperature and irradiance readings of Cleo performance+ glass lamp over time

5.9.3 Ambient light measurement

The ambient light conditions in the lab were measured as shown in Figure 137

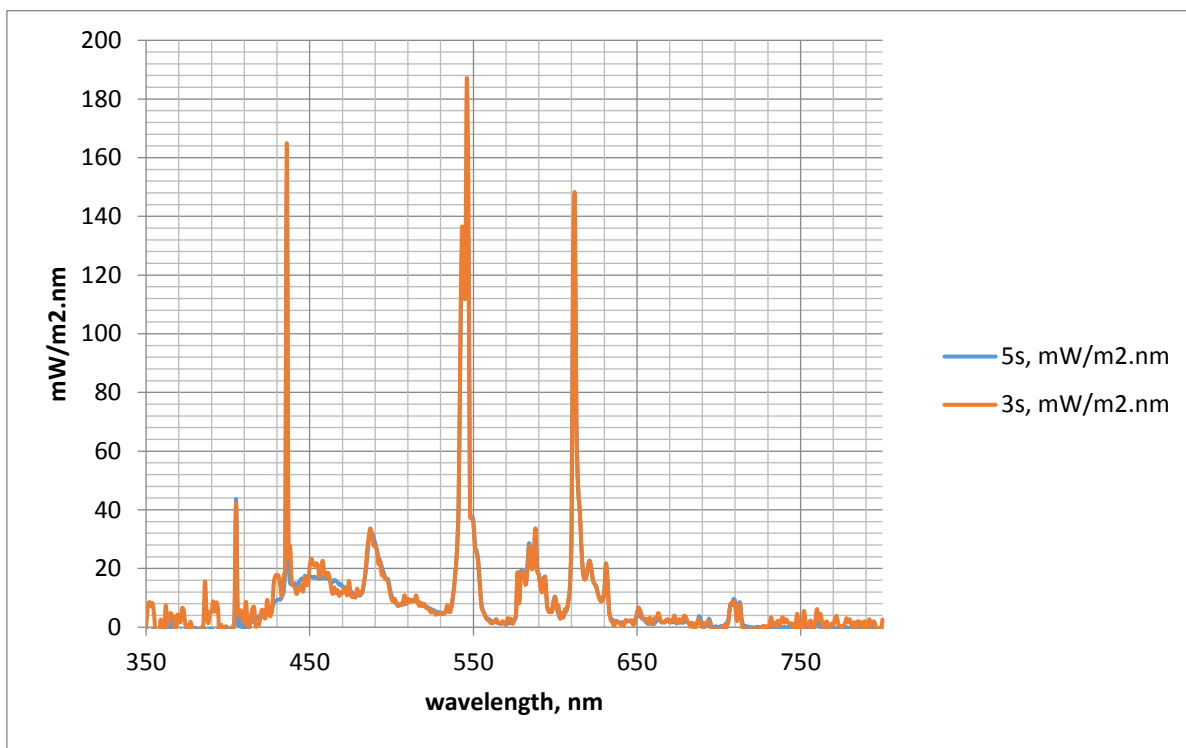


Figure 137: Ambient light measurements

Readings were taken with the probe at the same approximate position as the skin within the diffusion cells. The signal in the UV region was due to noise and is not thought to be genuine. Taking the area under the curve between 400- 750 nm this gives a total irradiance of 4227 mW/m². An average of two readings were taken.

5.9.4 The CutaFlex™ cell model for dermal absorption studies

Skin flexion has been theorised to assist the translocation of nanoparticles across the stratum corneum (Crosera et al., 2009). Current in vitro methods used to study dermal absorption involve the exclusive use of immobile skin within diffusion cells. A novel skin-flexing diffusion cell system “CutaFlex™” has therefore been developed at PHE and the University of Hertfordshire to incorporate reproducible skin flexing. The work involved the development and characterisation of the CutaFlex™ model which is able to simultaneously flex the skin whilst performing dermal absorption measurements. The “CutaFlex™” diffusion cells are made of an inert plastic polytetrafluoroethylene (PTFE) and the expanding bladder from latex (Figure

138). The diffusion cell is based upon the OECD-compliant Franz-type static diffusion cell and as such can accommodate various preparations of skin, several magnetic stir bars and provides close contact between the skin and receptor phase. The CutaFlex™ also incorporates a jacketed chamber, which is connected through the diffusion manifold to a heated recirculating pump, allowing for a consistent skin temperature to be maintained. Findings from the previous study were reported as follows;

"The results demonstrated that skin flexing did not alter skin barrier function and that the CutaFlex™ system was in general agreement with historical measurements of skin permeability. Furthermore, controlled chemical or physical damage to the stratum corneum was not exacerbated by skin flexing. Skin flexion did not facilitate the dermal absorption of a range of nanoparticles (quantum dots). However, differences in the partitioning of nanoparticles into the stratum corneum were observed (independent of the degree of flexing), with greater amounts of negatively charged nanoparticles found in the superficial layers of the stratum corneum in comparison with positive or neutral nanoparticles. Flexing had a modest effect on the performance of a skin barrier cream which was limited to low dose applications; an effect tentatively ascribed to flexion-induced movement of cream to previously untreated areas" (Viegas, 2014).

Work carried out previously has utilised porcine skin however no work has been done on human skin using the CutaFlex model. The TiO₂ compound in nano form which has also been suggested to influence absorption through skin has not been previously assessed using this model. The initial aims of this section were to investigate the CutaFlex model further in collaboration with PHE. Equipment was setup at PHE labs and assessed initially using a synthetic membrane and porcine skin. The experimental conditions used for flexing (section 5.7.2) were setup as described previously as such conditions were found to be optimal (Viegas, 2014).

The flexing system works by air being introduced through the latex bladder via a peristaltic pump controlled using programmable computer software (Figure 139). The increase in air leads to an expansion of the latex bladder which displaces the receptor fluid within the air-

tight diffusion cell. Displacement of receptor fluid results in stretching of the skin upwards away from the diffusion cell. This was measured to be approximately 3mm. When air is removed from the diffusion cell, vertical displacement of the skin occurs in the opposite (concave) direction with an approximate displacement of 3mm.

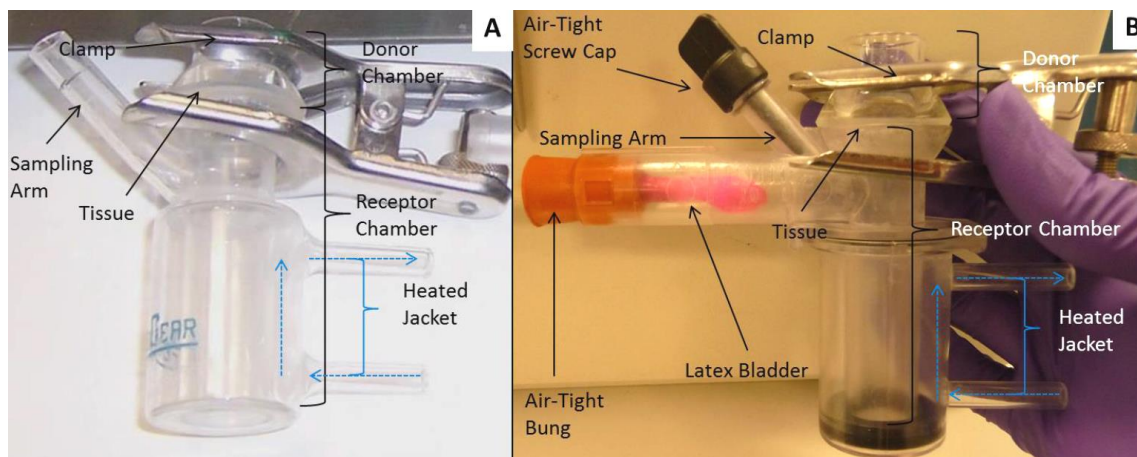


Figure 138: In vitro diffusion cells used for percutaneous absorption studies - Franz-Type and CutaFlex™

The Franz-type (A) static diffusion cell is comprised of a donor chamber (where the compound under study is applied), receptor chamber (collection of compound that passes through the membrane), skin section (clamped between the donor and receptor chambers), sampling arm for removing aliquots of the receptor fluid and the heated jacket to keep the skin at a constant temperature. The CutaFlex™ (B) flexing diffusion cell consists of a latex bladder attached to an air-tight bung which is connected to a peristaltic pump, an air-tight screw cap seals the sampling arm of which receptor fluid samples are taken, a donor chamber, skin sample, receptor chamber and a heated jacket (Viegas, 2014).

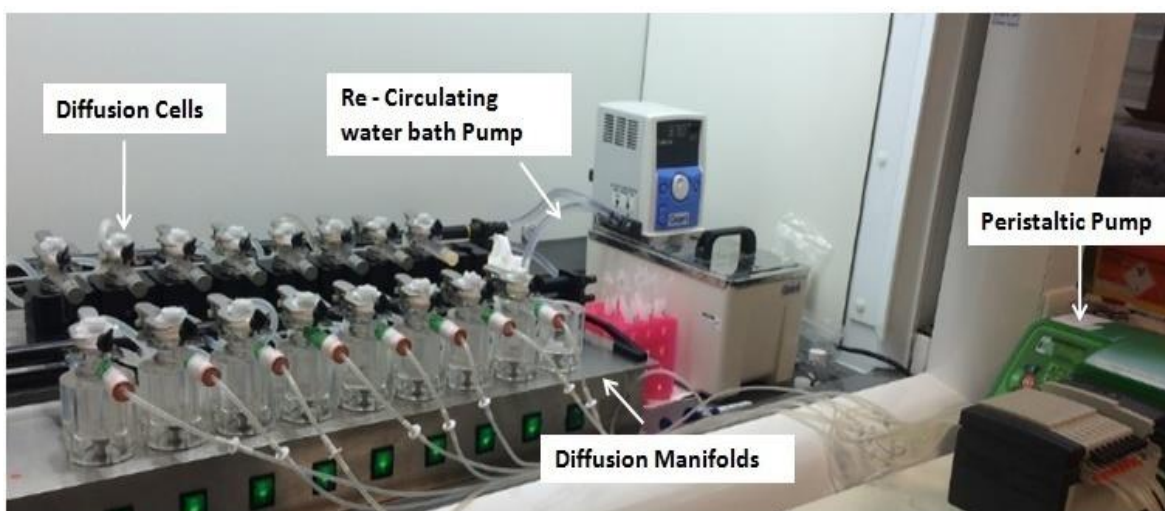


Figure 139: Diffusion Cell experimental setup

The peristaltic pump is operated through the use of computer software, this inflates the latex bladder in the CutaFlex™ cells. Both Franz-type and CutaFlex™ cells were placed in metal chambers within the diffusion manifolds on top of stir blocks, this ensured constant mixing of the receptor fluid contents. The re-circulating heated pump was connected to the diffusion cells via the diffusion manifold this maintained a constant temperature of the skin within the cells.

The CutaFlex model allows skin samples to be flexed through the use of a peristaltic pump which alters the pressure in the receiver chamber. An artificial membrane was initially used to optimise the flexing motion of the Franz-Type cells. Dermatomed pig skin was later used to assess the effect of flexing on dermal absorption. In order to minimise any potential experimental variables the static Franz cells (Figure 140, Figure 141 and Table 16) and the CutaFlex cells (Figure 142, Figure 143 and Table 17) were setup at the same time both with and without the application of TiO₂ alongside caffeine. Four experimental conditions were carried out simultaneously with the conditions being flexed skin plus or minus TiO₂ and static skin plus or minus TiO₂. The data obtained using porcine skin showed lower than optimal levels of caffeine retrieval, further optimisation experiments were later carried out whereby sufficient levels of caffeine retrieval were achieved (Figure 144, Figure 145 and Table 18). The initial lack of radiolabelled caffeine retrieval may be attributed to the Cutaflex design as the top of the receiver chamber has an inward curvature present allowing for a proportion of the dose to become trapped. This factor was taken into consideration by including further wash steps in the mass balance during the optimisation procedure. Porcine skin was also left for a longer period of time (5 days) in the scintillation fluid prior to the analysis step.

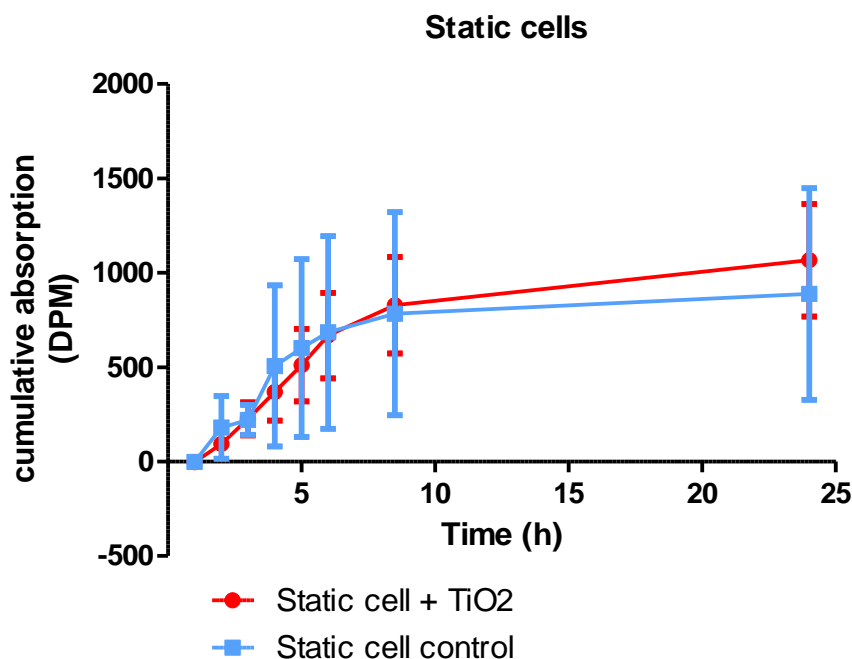


Figure 140: Cumulative absorption of radiolabelled caffeine through porcine skin under static conditions plus or minus TiO₂ (5mg/ml)

The mean value and standard deviation of 5 controls (10mg/ml caffeine only) and 5 test (10mg/ml caffeine plus aeroxide at 5mg/ml) replicates are shown. Samples were taken from a single donor and the distribution of caffeine assessed after 0, 1, 2, 3, 4, 6, 8 and 24h exposure when applied to porcine skin as an infinite dose of 2911.3µg/cm². The Shapiro-Wilk test was used to assess data for normal distribution, once normality of data was confirmed a T-test was carried out to identify potential significance in differences between the two experimental conditions.

Caffeine retrieval (%)	
Static + TiO ₂	Control static
40.7	30.8
20.2	18.4
11.8	46.2
22.0	54.4
40.7	30.8

Table 16: Showing the total level of caffeine retrieval from the static Franz cells (radiolabelled caffeine plus or minus TiO₂ (5mg/ml))

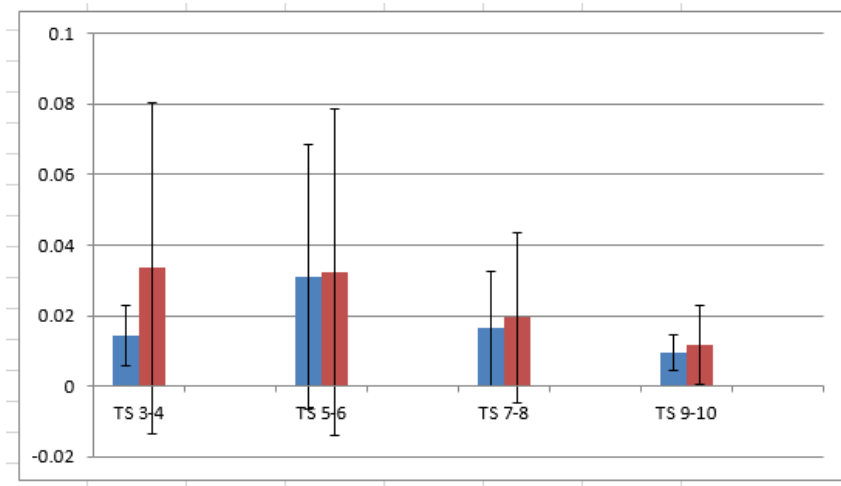
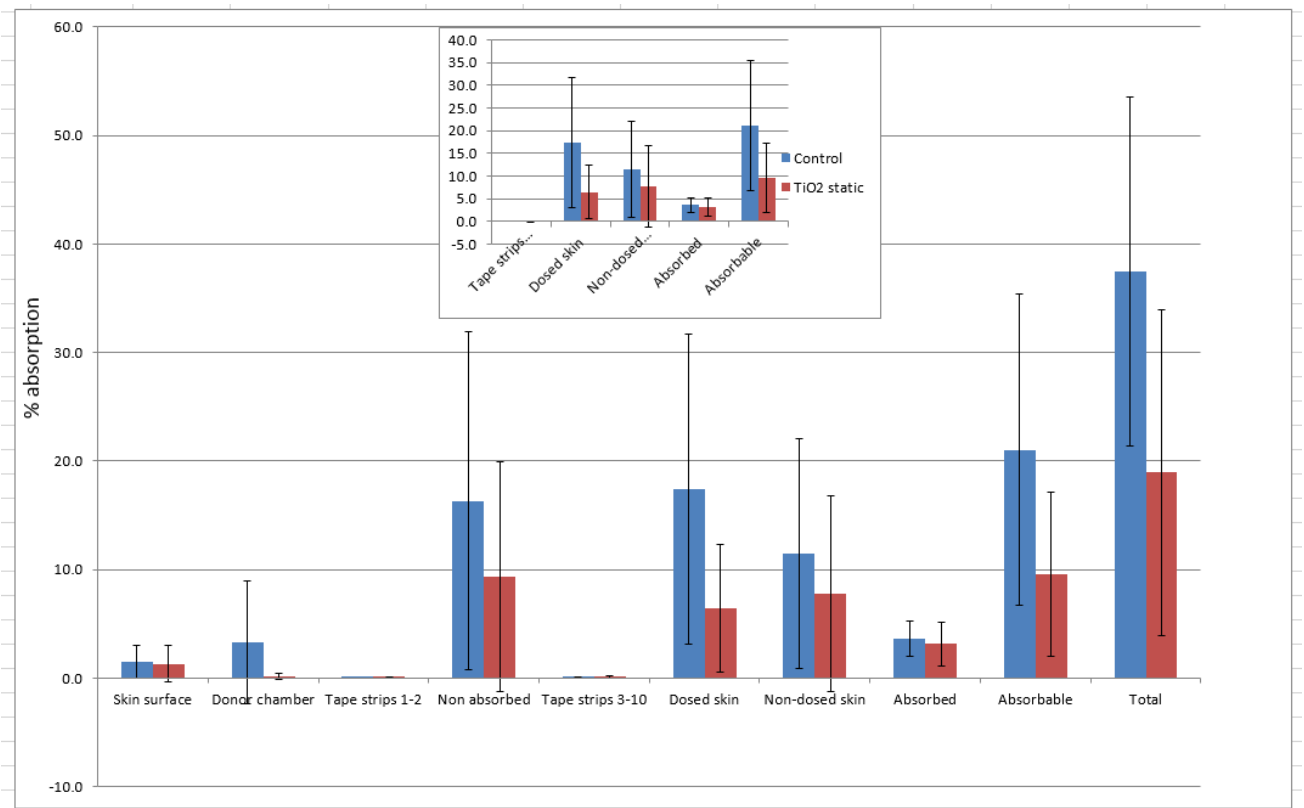


Figure 141: Mass balance showing the distribution of radiolabelled caffeine through porcine skin plus or minus TiO₂ (5mg/ml) - Static cells

Data shows the mean value and standard deviation of 5 control (10mg/ml caffeine only) and 5 test (10mg/ml caffeine plus aerioxide at 5mg/ml) replicate samples taken from a single donor. The distribution of caffeine was assessed after a 24h exposure period. The blue bars represent caffeine only (10mg/ml in water). Red bars represent caffeine (10mg/ml in water) plus aerioxide (5mg/ml in water). The values displayed are the mean \pm SEM. Data for the tape strips is shown separately below

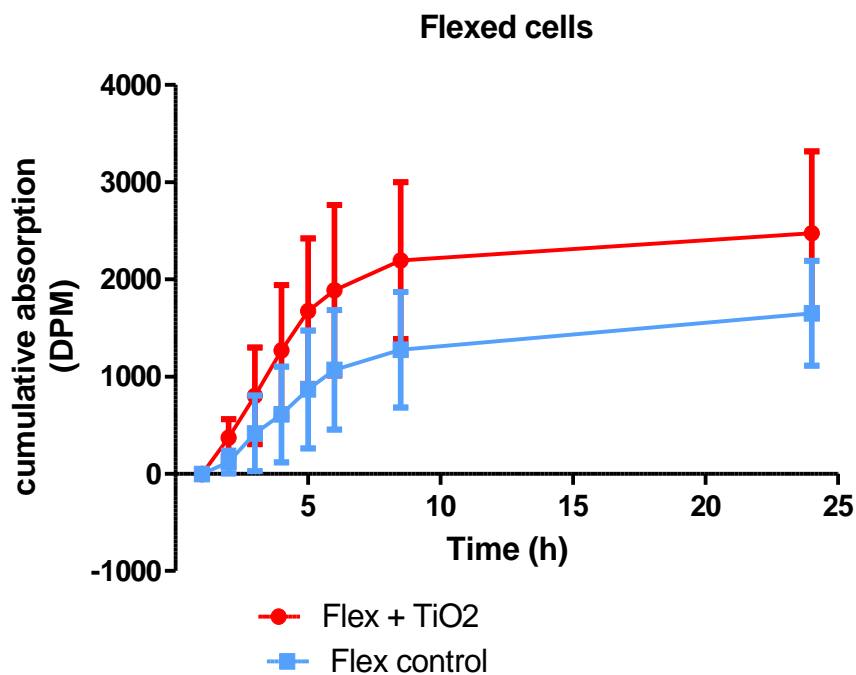


Figure 142: Cumulative absorption of radiolabelled caffeine through porcine skin under flexed conditions plus or minus TiO₂ (5mg/ml)

The mean value and standard deviation of 5 controls (10mg/ml caffeine only) and 5 test (10mg/ml caffeine plus aeroxide at 5mg/ml) replicates are shown. Samples were taken from a single donor and the distribution of caffeine assessed after 0, 1, 2, 3, 4, 6, 8 and 24h exposure when applied to porcine skin as an infinite dose of 2911.3µg/cm². The Shapiro-Wilk test was used to assess data for normal distribution, once normality of data was confirmed a T-test was carried out to identify potential significance in differences between the two experimental conditions.

Caffeine retrieval (%)	
Static + TiO ₂	Control static
31.6	53.3
25.6	37.5
38.8	15.9
45.4	33.8

Table 17: Showing the total level of caffeine retrieval from static Franz cells (radiolabelled caffeine plus or minus TiO₂ (5mg/ml))

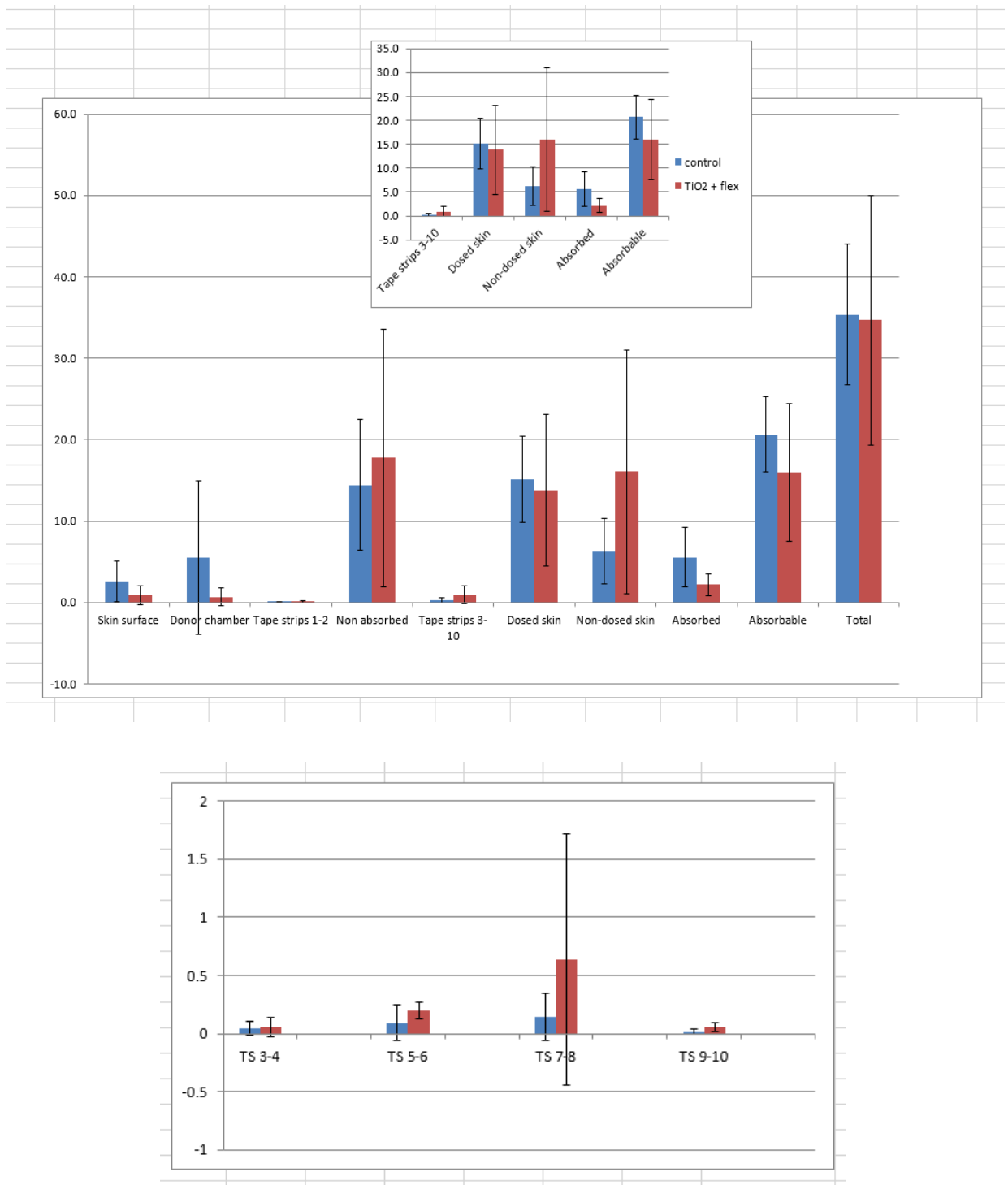


Figure 143: Mass balance showing the distribution of radiolabelled caffeine through porcine skin plus or minus 5mg/ml TiO₂ - Flexed cells

Data shows the mean value and standard deviation of 5 control (10mg/ml caffeine only) and 5 test (10mg/ml caffeine plus aeroxide at 5mg/ml) replicate samples taken from a single donor. The distribution of caffeine was assessed after a 24 h exposure period. The blue bars represent caffeine only (10mg/ml in water). Red bars represent caffeine (10mg/ml in water) plus aeroxide (5mg/ml in water). The values displayed are the mean \pm SEM. Data for the tape strips is shown separately below

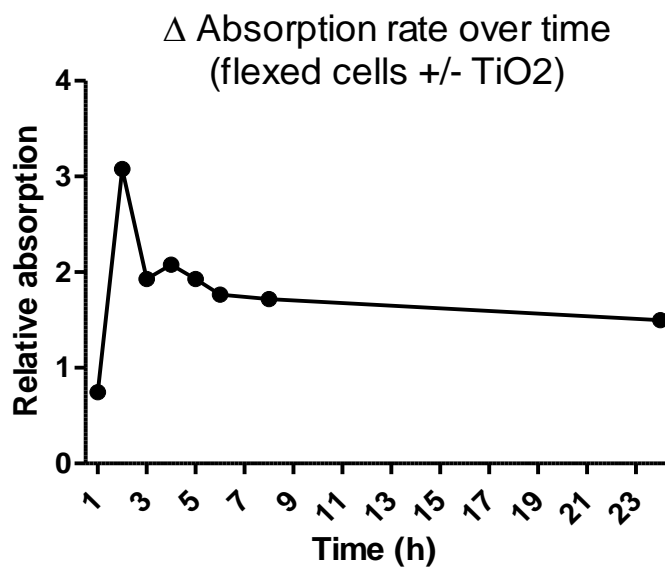
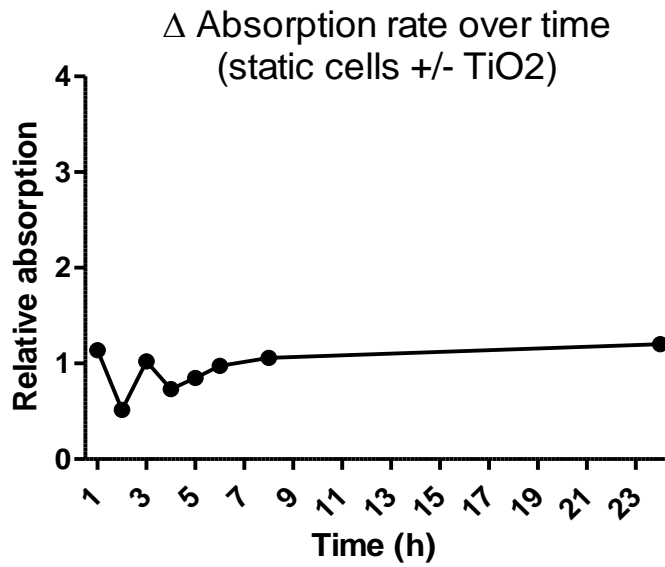


Figure 144: Absorption rate over time

The average of the values at each time point were taken for the control and TiO₂ treated cells. The average value for the TiO₂ treated cells was then divided by the average value for control at that time point. The graph represents the change in absorption rate relative to the time point control.

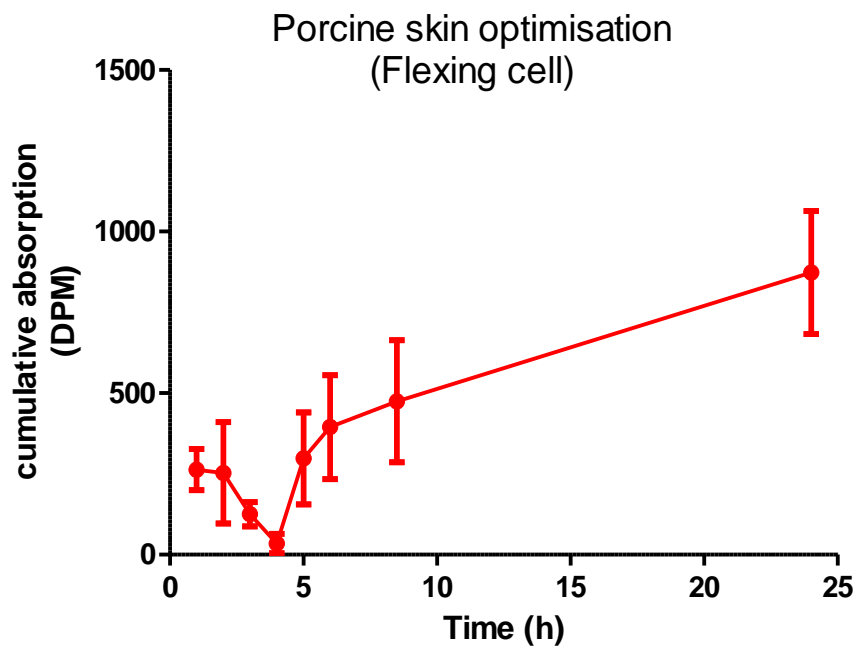


Figure 145: Cumulative absorption of radiolabelled caffeine through porcine skin in the CutaFlex cell model
 The mean value and standard deviation of 4 samples dosed with caffeine (10mg/ml) is shown. Samples were taken from a single donor and the distribution of caffeine assessed after 0, 1, 2, 3, 4, 6, 8 and 24 h exposure when applied to porcine skin as an infinite dose of 2911.3 μ g/cm²

Caffeine retrieval (%)
78
82
60.9
88.1

Table 18: Showing the total level of radiolabelled caffeine retrieval from each Franz cell

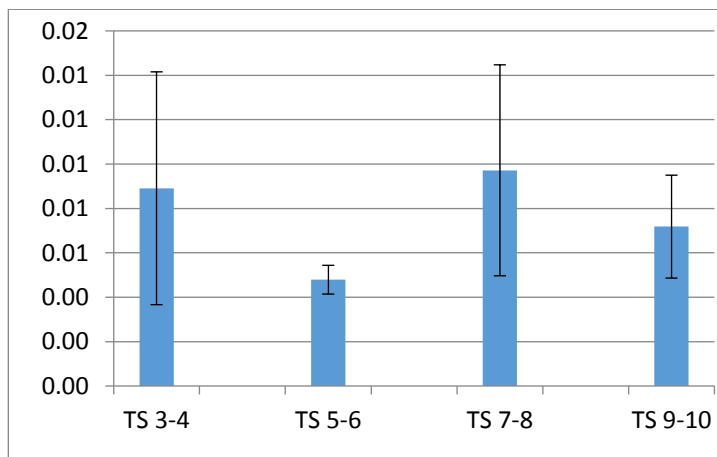
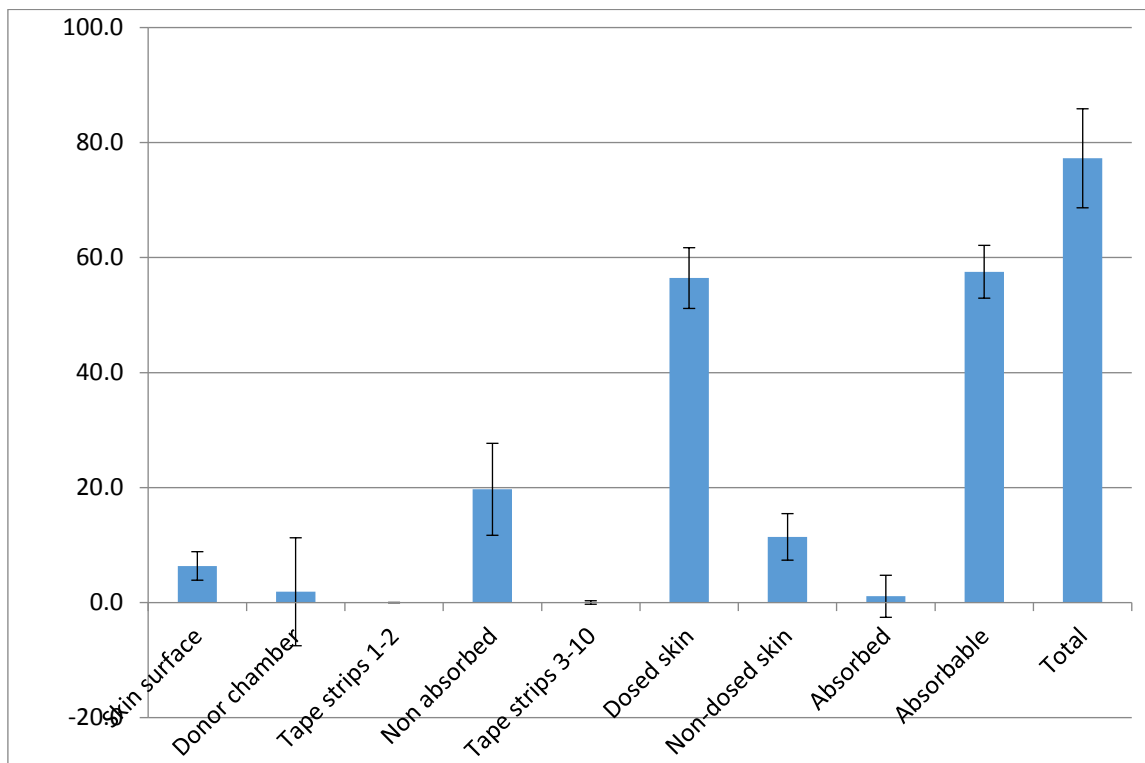


Figure 146: Mass balance showing the distribution of radiolabelled caffeine through porcine skin in the presence of TiO₂ (5mg/ml)

Data shows the mean value and standard deviation of 4 control replicate samples taken from a single donor. The distribution of caffeine was assessed after a 24 h exposure period. Values are displayed as the mean \pm SEM. Data for the tape strips is shown separately below.

Static Franz-Type (plus heated magnetic stirrer)	Cutaflex (plus heated jackets and magnetic stirrer)	
Pros	<ul style="list-style-type: none"> Receiver media can be loaded with ease No water leakage occurs from the heated magnetic stirrer Donor and receiver chambers are designed with a solid glass surface (less chance of damage) Shorter distance between the skin and the bottom of the diffusion cell makes it easier to stir the receiver media with only one magnetic stirrer being required Experiments do not need to be carried out in a confined area such as a fume hood to account for water leakage 	<ul style="list-style-type: none"> Jacket system creates an even distribution of heat across the cell Effects of skin flexion on absorption levels can be assessed
Cons	<ul style="list-style-type: none"> Heat loss would have to be accounted for when assessing final temperature of the receiver fluid Cell design does not allow for skin flexing to be assessed 	<ul style="list-style-type: none"> Difficult to retrieve caffeine dose fully due to objects in flexing port such as the latex bladder Leakage in the water pump system restricts the experiment to a controlled area Due to the large volume of the receiver chamber two magnetic stirrers are required for efficient stirring Donor and receiver chamber skin loading regions have ridges which may punch through and damage the skin sample when pressure is applied
Further Details	<ul style="list-style-type: none"> Receiver chamber volume is smaller 	<ul style="list-style-type: none"> Larger receiver chamber volume Latex bladder used must be small enough to allow for air to be displaced without too much resistance from the surrounding area

Table 19: Outlining the key difference observed between the static Franz cell and CutaFlex cell model

5.10 Discussion

5.10.1 TiO₂ is not absorbed beyond the skins superficial layer

The majority of reports suggest that nanosize TiO₂ particles do not bypass the skin beyond the first two layers of the SC (SCCP, 2013). It has however been suggested that this may be due to limitations in the methodologies used during the studies or potentially due to the experimental design (SCCP, 2013). Prasad et al., 2013 suggested that the potential dermal exposure to nano TiO₂ from sunscreens may be up to a dose of 75 mg/cm² under the current regulations (Prasad et al., 2012). TiO₂ exposure often occurs under conditions where the skin barrier function is impaired for example sunburnt, micro-injured or 'soaked' skin (Kiss et al., 2008). Furthermore, it has been hypothesized that the rubbing-in of sunscreen formulations containing nano TiO₂ agglomerates may act to disperse these agglomerates further (McCall, 2011). Given the surface area of skin and the recommended regular use of sunscreens, even trace amounts bypassing the skin may become significant over time. The toxicological concerns regarding the use of nano TiO₂ in topical sunscreen formulations are only applicable providing that the TiO₂ reaches the viable cells within the skin (SCCP, 2007b;SCCP, 2013).

Mavon et al., determined the distribution of TiO₂ particles (20 nm) within human skin both in vitro and in vivo. Tape stripping was used to determine the dermal penetration of TiO₂ 5h following the direct topical application to human skin or to human skin explants. The majority of the TiO₂ was found in the stratum corneum, with minimal levels within the epidermis both in the in vitro and in vivo investigation (Mavon et al., 2007). Similarly, Schulz et al., determined the influence of particle size, coating and shape on TiO₂ skin penetration. A number of TiO₂ containing sunscreen formulations were tested that had different particle surface characteristics. Formulations were topically applied to human skin at a concentration of 4 mg/cm, for 6 h, and skin biopsies later taken. All particle types assessed were solely located on the outermost surface of the stratum corneum, and did not penetrate deeper to reach subcutaneous, epidermal or dermal layers (Schulz et al., 2002).

TiO₂ nanoparticle suspensions in synthetic sweat solution were applied on Franz cells for 24 h using intact and needle-abraded human skin. Following a 24 h exposure period, no TiO₂ was detected in the receiver chamber solution of both intact and damaged skin. TiO₂ was reported

in the epidermal layer after 24h whilst in the dermal layer, the concentration was below the limit of detection (Johnston et al., 2009). In a different approach, Kiss et al., evaluated the barrier function of skin, within human foreskin grafts transplanted onto severe immunodeficient mice. A commercially available TiO₂ microparticulate containing sunscreen was administered at a concentration of 2 mg/cm² via an occlusive bandage to skin grafts for a 24h duration. The penetration of TiO₂ was later determined within the skin biopsies. TiO₂ particles did not penetrate through the stratum corneum of the human skin graft transplants. The stratum corneum was therefore deemed to be an adequate, effective barrier against TiO₂ permeation through intact human skin. However, the authors noted that TiO₂ exposure is likely to occur when skin barrier functions may be impaired (Kiss et al., 2008). It has been suggested that hair follicles can also act as a long term storage of nanoparticles (Lademann et al., 2011). Most investigations using animal models have also shown that TiO₂ nanoparticles remain on the outermost layer of skin, however some researchers have demonstrated that TiO₂ can bypass into the deeper skin layers via the hair follicles (Bennett et al., 2012).

A study on minipigs found no effect on the absorption of TiO₂ through skin from sunscreen formulations. It was noted that nanopartilces with sizes >10nm in diameter have the potential to accumulate in hair follicles (Sadrieh et al., 2010a). Polymeric nanoparticles have been shown to be preferentially located in “skin furrows” and around hair follicles not penetrating beyond the superficial SC layer (Wu et al., 2009).

Wu et al., investigated the effect of the long term application of TiO₂ on the skin of hairless mouse as well as pig ear skin. After the exposure of TiO₂ nanoparticles to isolated porcine skin for 24 h, no TiO₂ could be detected beyond the stratum corneum. Interestingly, when studied in vivo, quite different results were obtained. After topical application on pig ear skin for 30 days, TiO₂ nanoparticles (4nm and 60 nm) were able to bypass the SC. According to the authors particles were found located in the deeper layers of the epidermis. Furthermore, after 60 days dermal exposure in hairless mice, nano TiO₂ particles were seen to be absorbed through the skin, reach different tissues and induce diverse pathological lesions in several major organs (Wu et al., 2009). Notably, the P25 (21 nm) TiO₂ nanomaterial showed a wider tissue distribution, and could even be found in the brain without inducing any pathological changes. Among all of the organs examined, the skin and liver were found to display the most severe pathological changes (Wu et al., 2009). Although Wu and co-workers showed TiO₂ transport

through the stratum corneum in live pigs, similar to other researchers, they did not observe TiO₂ penetration into the deeper layers of the isolated skin sections (Sadrieh et al., 2010b; Lademann et al., 1999; Gamer et al., 2006).

Miquel-Jeanjean et al., simulated a worst case scenario for the topical application of sunscreen which may act to promote TiO₂ nanoparticle absorption through the skin. The experiments involved mimicking skin with a pre-existing impaired barrier function. TiO₂ nanoparticles were included in sunscreen formulation and assessed on intact, damaged, irradiated, and damaged/irradiated pig skin. Cutaneous penetration and localization of TiO₂ after a 24h sunscreen application was investigated quantitatively using inductively coupled plasma-mass spectrometry, and qualitatively using transmission electron microscopy. TiO₂ nanoparticles were found to remain in the uppermost layers of the SC, whether in intact skin or in compromised and/or skin exposed to solar radiation. This study suggested that compromised or compromised sunburnt skin does not exhibit greater susceptibility to cutaneous absorption of TiO₂ nanoparticles such as TiO₂ in vitro, as the absorption of TiO₂ nanoparticles into the epidermis was found to be minimal (Miquel-Jeanjean et al., 2012).

In a study comparing TiO₂ dermal absorption in healthy and psoriatic skin biopsies using scanning transmission ion microscopy, Rutherford backscattering spectrometry and particle induced X-ray emission, Pinheiro et al., reported that the permeation profile of TiO₂ was similar in normal and psoriatic skin despite the labile structure of the SC in psoriatic skin. In normal skin, the nanoparticles seemed to be retained in the outermost layers, TiO₂ permeation in psoriatic skin reached deeper regions of the SC when compared to healthy skin however, in no case did nanoparticles reach the living layers of the granulosum or spinosum strata (Pinheiro et al., 2007).

5.10.2 TiO₂ is suspected to act as a dermal absorption enhancer however this was not been found to be the case in human skin

In order to enhance the level of permeation through skin, both a surface charge-driven adhesion and an oxidative disorganization of the SC lipids is required. It has been suggested that the ability of TiO₂ to lead to the perturbation of skin barrier function can theoretically be modulated depending on the TiO₂ surface charge (coating) and oxidative potential (crystalline

phase). The enhancer effect of nano TiO₂ may then be increased or decreased depending on the required effect (Cai et al., 2016).

Turci et al., carried out studies on ex vivo porcine skin whereby different crystalline forms of TiO₂ (anatase, rutile and rutilite/anatase mixture) were assessed for the level of adhesion to skin. TiO₂ was found to bind to skin and promote the structural rearrangement of the lipid bilayer in the stratum corneum. The positively charged anatase and anatase/ rutile mixture were found to bind to the skin, this was not the case for the negatively charged rutile TiO₂ crystalline form. A low amount of UVA (<1mW/m²) was found to be sufficient to photoactivate the ROS production in nano-TiO₂ and induce oxidative damage to the skin. Following on from this finding the authors suggest that rutile form TiO₂ should be used in cosmetics (Turci et al., 2013).

Nano TiO₂ has been reported to cross the first two layers of the SC and have the ability to generate free radicals, even under low levels of UV. Such occurrences have the potential to disrupt the skin barrier function and modulate the levels of transdermal compound permeation (Cai et al., 2016). Peira et al., used amphotericin as a marker compound in two different media (10% (V/V) DMSO in water and oil in water emulsion), in the presence of three differently coated TiO₂ to assess the influence of TiO₂ (5mg/ml) on the level of compound permeation through porcine skin (Peira et al., 2014). The uncoated (aeroxide P25), but not the two coated TiO₂ compounds showed dermal enhancer properties, with a fourfold increase in the level of amphotericin flux being observed in the presence of uncoated TiO₂. Only the positively-charged, uncoated TiO₂ strongly adhered to and altered the SC structure (Peira et al., 2014). The media used in the donor chamber (DMSO) may have enhanced the level of drug penetration through the skin and contributed to the outcome seen however the authors mention that a 60% DMSO concentration is required before an effect on skin barrier function is seen (Anigbogu et al., 1995).

The OECD guideline recommends the use of one of three commonly used reference compounds for absorption studies, those being benzoic acid, caffeine and testosterone (Van Gele et al., 2011). Molecules which may interfere with the absorption kinetics were avoided in the study carried out in this chapter to minimise the possibility of masking the effects of TiO₂ on skin. Water was used as the vector for caffeine in the donor chamber along with a

physiological medium (PBS) in the acceptor chamber. No other molecules that may have interfered with the skin barrier function were used other than TiO₂. This is made possible as caffeine is water soluble whereas other compounds such as amphotericin require DMSO for solubilisation (Faustino et al., 2015).

Numerous studies have used porcine skin as it is thought to share similar permeation properties with human skin (Miquel-Jeanjean et al., 2012). It is also worth mentioning that although porcine skin has close resemblance to human skin they are physiologically different due to the increased hair follicle density (Barbero and Frascch, 2009). The stratum corneum is also double the thickness of that found in human skin (Bennett et al., 2012) which makes the use of human skin more relevant and the "gold standard" for toxicological studies.

The study carried out in this chapter shows that uncoated TiO₂ (5mg/ml) does not have a significant effect on the enhancement of radiolabelled caffeine absorption through human skin compared to control samples under ambient light conditions. Based on findings from section I, suspensions were dispersed in water to minimise the level of TiO₂ settling on skin. Further assessments were carried out using a much lower level of TiO₂ (50µg/ml) and 1mg/nm under ambient light conditions. This was done in order to minimise the level of aggregation in suspension and achieve a more nano size formulation. No significant effects on the overall perturbation of the skin barrier function were observed.

It was hypothesised that these findings may be due to uncoated TiO₂ being physically inert under ambient light conditions (Cai et al., 1992). Photoinduced disaggregation has the potential to increase nanoparticle transport in vivo. Absorption of light provides enough energy to partially disaggregate TiO₂ in aqueous media, releasing small particles from larger aggregates (Bennett et al., 2012). In the context of sunscreens, formulations are usually applied prior to the skin being exposed to the sun. UV has also been found in other studies to increase the dermal penetration of organic UV filters (Duracher et al., 2009).

The effect of TiO₂ photoactivation was assessed through dosing with UVA following the application of the TiO₂ formulations on to skin. A TiO₂ concentration of 1mg/ml was chosen for this experiment as this concentration of TiO₂ was found to be stable in water during the 72h sedimentation experiments. The addition of UVA (2 SED) did not lead to any significant

enhancement in the absorption of radiolabelled caffeine through the skin. Albeit caffeine retrieval was below the amount in some of the samples from TiO₂ plus UV data.

5.10.3 Skin flexion

Skin flexion has been previously shown to influence the level of absorption through human skin for example Tinkle et al., have shown size dependent penetration of 0.5-4mm BeO spherical particles through the stratum corneum into the epidermis of flexed human skin (Tinkle et al., 2003). Previous in vitro skin flexing devices have been documented in the literature. The systems described however were not present within a diffusion cell when investigating the potential for nanoparticle absorption through the skin (Rouse et al., 2006; Zhang and Monteiro-Riviere, 2008).

One potential disadvantage of the current CutaFlex™ design is the latex bladder, which may potentially absorb or adsorb penetrants and thus artificially reduce penetrant concentration in the receptor chamber fluid. Previous work carried out on the model has shown that the cumulative amount of penetrant in the receptor chambers was consistently less than Franz cells, suggesting that loss of penetrant may have occurred (Viegas, 2014). Caffeine retrieval in the CutaFlex model was optimised to an acceptable retrieval level in further experiments carried out. The CutaFlex model mimics the dynamic nature of skin through flexing and may therefore provide a better in vitro representation model of skin during absorption studies (Monteiro-Riviere and Riviere, 2009; Zhang and Monteiro-Riviere, 2008; Larese et al., 2009).

5.11 Summary of main findings:

- TiO₂ plus or minus UV was not seen to have an effect on the level of absorption of marker compound C14 radiolabelled caffeine through human skin compared to non-dosed skin and skin dosed with TiO₂ only.
- Further work may be required to assess skin flexion effects on the disruption of human skin barrier function. Further work is also required to assess the influence of TiO₂ on the disruption of skin barrier function when skin is flexed.

Chapter 6 – Final Discussion

6.1 Main Conclusions

6.1.1 Components of solar light act synergistically to produce the level of biomarkers of damage observed, perhaps suggesting that sunscreens should incorporate further UVA protection

One aim of the project was to investigate the contribution of UV, IR and VIS on the level of biomarkers of cellular damage induction (ROS generation, mtDNA and nDNA damage) in skin cells. Solar UV alone was found to have moderate effects on ROS generation therefore suggesting a role for IR and VIS. The level of ROS which was generated following the application of UV, VIS or IR and combinations did not correspond to the levels detected when complete solar light was applied. The findings suggest that all components of solar light act synergistically to result in the levels of biomarkers which were detected. Data for the mtDNA and nDNA damage were in agreement with the ROS-Glo data. To my knowledge this finding has not been previously reported in the literature.

A second aim was to compare the response of dermal and epidermal cells to solar light, both in primary culture and in cell lines. Fibroblast cells appeared to be more sensitive to longer wavelengths of solar light when compared to keratinocyte cells. This has been previously demonstrated in the lab whereby fibroblast cells were found to be more responsive to the longer wavelengths (Latimer et al., 2015), work carried out in this thesis reiterates these findings. HDFn cells were also primed with either IR or UV and the cellular stress response was assessed. No differences in response were observed in terms of a change in ROS generation following such exposures, despite other reports suggesting that there may be (Kimeswenger et al., 2016; Jantschitsch et al., 2009). Perhaps further work such as assessing the level of nDNA damage induced and the capacity for DNA repair is required. The level of apoptosis may also be investigated in order to establish whether priming cells with either UV or IR effects these mechanisms.

As previously mentioned, the different skin cell types used were donor matched and the various solar light doses were assessed at similar times on cells of the same passage number. This further ensured that any differences observed between the various solar light doses were not due to experimental error or donor variability. Viability assays were carried out to identify any potential cytotoxic effects of the doses which were assessed, therefore ensuring that sublethal doses were applied. The radiation sources used for dosing experiments were calibrated under the expertise of the Regional Medical Physics Department and where possible, confounding factors such as heating effects were assessed.

Commercially available sunscreens are designed to filter the majority of the UVB and a proportion of the UVA component (Aldahan et al., 2015). In Chapter 4 the solar light blocking abilities of sunscreens were mimicked by using either the glass or plastic filter. These filters provide a 100% block in UVB whilst removing 51% and 89% of the UVA transmission respectively. Although no sunscreen claims to block UVB by 100%. SPF 50 for example is able to block 99% of the UVB (Latha et al., 2013), therefore for the purpose of this study the filters served well as a proof of concept investigation. The findings showed that dosing cells with 49% UVA alongside the IR and VIS components was sufficient as it led to the synergistic effects seen in terms of ROS generation. Reducing the UVA component even further (11%) did not appear to induce synergistic effects. This suggests that the presence of a small percentage of UVA in this case being 11%, alongside the IR and VIS component, is not sufficient to induce synergy. To my knowledge such findings have not been previously reported within literature. With reference to sunscreen formulations this data suggests that perhaps protection against the UVA component should be further increased. Currently UVA protection is recommended to be at least one third of the UVB component (Wang et al., 2008). Such responses were not however seen in mtDNA damage, as presence of the glass or plastic filter during solar light dosing did not induce significantly greater damage levels compared to the other dosing conditions which were assessed. Synergy was not observed in terms of mtDNA damage. This is perhaps due to the removal of the UVB component which would otherwise have a role in the direct damage of DNA (Sinha and Häder, 2002; Brugè et al., 2014). A higher dose of solar light may be used in future experiments to assess the effect, alternatively a different biomarker for assessing damage may be used such as MMP protein and/or mRNA expression levels.

Work carried out in this chapter demonstrated that the individual components of solar radiation and components in combination have minimal effects on both ROS and mtDNA. Evidence from other studies has been contradictory, in particular studies involving IR, with some reports finding damaging effects whilst others have not (Diffey and Cadars, 2016). The effects of IR damage are reported to be dose dependent, doses assessed in this study demonstrate minimal levels of ROS and mtDNA damage as a result of IR (Holick, 2016).

Although the use of primary and cell line cultures in monolayer is an established method for the understanding of mechanisms at a subcellular level, obvious limitations exist. The skin structure is highly complex and responses seen in skin as a whole organ may be different to those seen in monolayer (Marionnet et al., 2006). Future work may involve using these findings as a platform to assess the effect of solar light on skin equivalents or perhaps using human skin biopsies for further investigations. Secondary effects of ROS generation, and downstream signalling pathways may be assessed such as the expression of MMPs and the induction of apoptosis at different time points following solar light dosing (Dupont et al., 2013). It is difficult to generalise the level of exposure to solar light as this varies from one individual to another and is further complicated by the multiple factors which influence the final dose received (Diffey, 2016). Doses of up to 7.5 SED (equivalent to approximately 7h in the Mediterranean sun at noon during the summer months) were used in HDFn and HaCat cells as a proof of concept to illustrate that the effects seen are consistent across higher doses.

6.1.2 Sunscreens provide protection against solar light therefore reducing the risk of DNA damage, this finding is also relevant during exposure to suberythemal doses

The level of mtDNA damage caused over time due to intermittent or an equivalent single large dose of solar light exposure was assessed. The results obtained in HDFn cells indicate that mtDNA damage accumulates over time with intermittent exposures to equal the damage produced from a single large dose. The ability of sunscreens to provide protection against intermittent and single doses was also investigated. Sunscreens (SPF15 and 30) applied at 2mg/cm² were seen to provide protection against the solar light induced mtDNA damage. These findings were also relevant to suberythemal exposures as DNA damage may occur prior to erythema being noticed in skin (Birch-Machin et al., 2013a). With repeated exposures, particularly during sun filled holidays, photoadaptation can develop due to tanning and

hyperplasia. This in turn may increase the threshold for visible signs of erythema in skin (Pissavini and Diffey, 2013) therefore potentially encouraging the sunscreen user to stay in the sun for a longer period of time. The mtDNA genome can cope with high levels of damage due to factors such as the large numbers found within cells and their ability to undergo compensatory effects (Birch-Machin and Swalwell, 2010). nDNA also has mechanisms of damage repair however repeated exposures over time increase the risk of skin cancer development due to the increased levels of mutation accumulation (Ichihashi et al., 2003).

Discrepancies were highlighted between the 1 and 11kb QPCR template when investigating multiple dosing conditions perhaps as a result of the nature of the assay. The 11kb fragment template was found to be more reliable in identifying the mtDNA damage levels when a single large dose was applied. This may be due to a wider area of the mitochondrial genome being covered therefore increasing the chance for damage detection (Kleinle et al., 1997). The 1kb fragment template on the other hand did not detect a large amount of damage with the single large dose exposure relative to the multiple intermittent doses. The 1kb template only covers the D-Loop region (Rothfuss et al., 2010). With multiple irradiations the chances of damaging the D-loop region becomes greater as multiple hits are received. The 1kb template therefore may not be suitable for use in experiments comparing exposures to multiple and single solar light doses. The experiments carried out as expected highlight the greater sensitivity of the 11kb assay. However the 1kb has the advantage of being more cost effective with a shorter run time. The 1kb assay is also more suitable for the detection of large amounts of damage where the 11kb assay may not be feasible for this purpose (Bowman and Birch-Machin, 2015).

Similar experiments may be repeated in keratinocyte cells to assess whether they respond differently to fibroblasts regarding the damage accumulation from intermittent and single large dose exposures. Further regions of the mitochondrial genome may also be investigated for mutation hotspots. The protective effect of sunscreen use can be assessed in 3D skin equivalents to gain an understanding of the simultaneous effects of solar light on fibroblast and keratinocyte cells. Alternatively human skin samples may be used for this purpose.

6.1.3 TiO₂ exhibits interference properties and instability in suspension albeit, toxicity in HDFn cells was seen under the conditions assessed with relevant controls in place

The initial aim of project involving the study of TiO₂ was to identify areas from the published research which required further investigations. There are currently no specified methods for the toxicological analysis of nanomaterials although in the case of TiO₂ it is known to have interference properties (Ong et al., 2014). Initial experiments were performed to optimise and characterise TiO₂ dispersion and stability within suspension. TiO₂ was most stable in water, with suspensions becoming unstable under physiologically relevant conditions as demonstrated by the data obtained from the settling assays. Following on from this finding the exposure time versus settling rate of TiO₂ could be taken in to consideration during experimentation as the aim was to create and maintain stable suspensions with particle sizes within a "nano range". Sonication was not seen to aid stability however the addition of DMEM increased stability. Suspensions created in the lab were found to provide both acellular and cellular protection. TiO₂ protection against IR was also demonstrated although this appeared to be lower than the UV protection offered at equivalent doses.

The TiO₂ dispersions made were used to investigate a range of cytotoxic endpoints including cell viability, ROS generation and genotoxicity. TiO₂ was seen to interfere in the cell viability assays (MTS and RT-Glo) possibly due to interactions with light (Ong et al., 2014). Internalisation has also been suggested to influence the toxicological outcome of compounds in cells. Further investigations are required to establish with greater certainty whether TiO₂ is internalised in fibroblast and keratinocyte cells. Photoactivated TiO₂ induced ROS generation in both HDFn and HaCat cells and had the ability to induce cytotoxicity without the influence of solar light. The ROS-Glo assay appeared to be more sensitive at detecting ROS. During the experiments carried out relevant controls were included to identify possible interference effects due to the TiO₂ compound.

6.1.4 No perturbation in human skin barrier function was seen as a result of exposure to TiO₂

TiO₂ plus or minus UV was not seen to have an effect on the level of absorption of marker compound (1-methyl ¹⁴C radiolabeled caffeine) through human skin compared to the non-dosed control skin. The negative absorption data suggests that TiO₂ does not lead to skin barrier disruption following application under the influence of ambient light and UV. This suggests that the use of nanoparticulate TiO₂ within sunscreens should not in theory enhance the dermal absorption of other compounds within the formulation. So far there has been sparse evidence in support of the harmful effects of TiO₂ on human skin. The effect of skin flexion on dermal absorption levels was assessed through investigations involving the use of the Cutaflex absorption model. Dermal absorption studies incorporating skin flexion are theorised to provide a more representative model of the in vivo situation (Monteiro-Riviere and Riviere, 2009). Human skin is considered to be the best model for absorption studies and was therefore used for investigations involving TiO₂ (Godin and Touitou, 2007).

The TiO₂ compound investigated during the study was uncoated therefore allowing for a maximal response in surface reactivity to be achieved. This simulates a worst case scenario therefore any interference effects are more likely to be detected. Studies involving the Franz cells require an acceptable retrieval of radioactive compound in the mass balance therefore some experiments were eliminated due to this factor. This was particularly the case with the CutaFlex model as the scaffold design required further considerations to prevent the loss of the caffeine compound during experimentation. This factor was taken into consideration during optimisation procedures. Further work may be required to assess skin flexing effects on the disruption of skin barrier function. Although cosmetic products are intended for use on intact skin, consumers are known to apply products to non-healthy skin regions (Miquel-Jeanjean et al., 2012). In particular sunscreens are most often applied to skin which is already physiologically compromised such as sunburnt skin, dry skin patches, or skin which has been abraded or compromised by environmental factors such as sand and water (SCCP, 2013). Absorption experiments may be carried out to simulate skin abrasion or sunburn prior to the application of TiO₂ formulations. Future work may also involve assessing the effect of agglomeration of TiO₂ when it contact with the skin surface as this has not been investigated previously. Future studies are required to determine the effects of repeated, short-term

exposures to TiO₂ nanoparticles. Although sunscreens are usually removed within 24h they are often reapplied (SCCP, 2013).

6.2 Implications of the study in the wider field

The overall aim of the thesis was to investigate the impact of solar radiation and sunscreen exposures on the skin and barrier function with the core interest being public health. Solar radiation exposure is an inevitable part of everyday life, understanding the effects on the body, in particular skin (the first point of contact to the outside world) is of great importance.

6.2.1 Solar exposure

There has been a lot of interest regarding the effects of solar exposure particularly on vitamin D production as well as the more recent emerging evidence on the beneficial effects of sunlight (Holick, 2011). There are ongoing debates concerning the amount of solar exposure necessary to achieve the relevant amounts of vitamin D required. Access to sun filled holiday destinations exposes individuals to prolonged sunshine and in some cases sunburn may be induced. This is particularly concerning in younger children who have more vulnerable skin (Bearer, 1995). Attitude towards solar exposure and protective strategies is therefore crucial. Although sunlight is beneficial, in excess it can lead to damaging effects on skin.

Skin is the largest organ which primarily functions to encase and protect the internal structures of the body. The ability of skin to provide protection is of great importance as substantial disruption to the skins barrier function can influence the internal health of the body and in severe cases may be fatal for example as in the case of harlequin ichtheyosis (Gupta et al., 2008). As well as the functionality of skin the aesthetic appearance is also of great social importance and in some cases this may influence the amount of time spent in the sun. The use of sunscreens is recommended by the majority of dermatologists with formulations being shown to reduce the level of damage in skin over time (Stanton et al., 2004). Use of sunscreens as a strategy for reducing the risk of skin cancer development however has been suggested to be a controversial area. Misuse of sunscreens such as overestimating the protective ability, not applying enough product, missing areas of the body

or not reapplying at the recommended frequency may therefore expose the consumer to excessive amounts of sunlight (Autier et al., 2007).

Even with relatively mild sunburn a vast number of changes in the skins physiology and structure can be induced which in turn can influence the barrier function. For example, within the first few hours prostaglandin synthesis can be observed. Prostaglandins target the E-cadherin regulating receptors such that within hours E-cadherin levels are significantly decreased. Expression of tight junction related proteins (ZO-1, claudin-1 and occludin) are also known to be disrupted following UVB exposure (Yuki et al., 2011). These proteins are important when considering compound absorption through UV exposed skin, as they promote intercellular adhesions. Loosening of these adhesions allows for the corresponding cellular proliferative response to quickly replenish differentiating epidermal cells that form a thickened stratum corneum layer. While the UV repair process initiates, exogenous compounds may encounter loosened intercellular adhesions causing an outside-in defect that could favour absorption. Alternatively, one can imagine that the accelerated keratinocyte proliferation and differentiation response enhances the net migration of cells to the skin surface which may help prevent compound translocation. The competing processes of loosened intercellular junctions, oxidative damage, and the hyperplasia response of the epidermis following exposure to a damaging UV dose, all provide potential mechanisms to impact the disruption of the skins barrier (Hung et al., 2015).

6.2.2 Protection against solar exposure

A further question is whether existing sunscreens are sufficient in providing protection against solar radiation. Since 2006 newer emerging formulations have offered protection against IR, however the scientific evidence behind this is not yet clear, as inconsistencies in the detection of deleterious effects as a result of IR exposure have been reported (Barolet et al., 2016a). IR for example has been demonstrated to have beneficial effects in terms of wound healing and promoting fibroblast migration. Other papers have expressed concerns over IR and photoageing with some studies suggesting that the interaction of UV with IR for instance, may promote the survival of damaged cells and contribute to the development of skin cancers

(Kimeswenger et al., 2016). Claims that are in support of IR protection are mainly based on an anti-ageing motive (Dupont et al., 2013). This is important for the cosmetic world as combating skin photoageing is a major target. In terms of public health the main concern would be skin cancer development in particular melanoma which in some cases can be fatal. Non-melanoma skin cancers, many of which have been associated with over exposure to solar radiation, also place a burden on both patient health and the health care services (Carli et al., 2003). Public awareness campaigns have been raised over the years as lifestyle choices can help to reduce the risk of skin cancer. This includes for example the banning of sun bed use for consumers below the age of 18 within the UK (Pawlak et al., 2012). A select group of the population are intolerant to solar radiation and require protection not only against UV but also IR and in some cases VIS. This includes conditions such as solar urticaria, patients may therefore be advised to use reflectant sunscreens which also offer some protection against VIS (Faurshou and Wulf, 2008). Understanding the interactions of solar light is also important, as phototherapy is used widely within dermatology and other medical fields as well as for health and wellbeing purposes.

Phototherapy is used for the treatment of a wide range of conditions. Blue VIS (400-410nm, BLU-U, TruBlu,) and red VIS (630-635nm, Aktelite) are the two specific wavelengths that have been used with photodynamic therapy in the treatment of actinic keratoses (pre-cancers), certain types of superficial skin cancers, acne, skin infections, hidradenitis suppurativa, psoriasis, vascular lesions as well as in skin rejuvenation and hair removal. Low level light therapy (LLLT, ex. BBL, Lumiere Spa, Omnilux, Synergie ELITE, Zeron) exploits red VIS lasers (630nm-800nm) for a variety of skin conditions including dermatitis, fat reduction, hair growth, wound healing, pain relief and skin rejuvenation. IR has been used in the treatment of muscle and joint pain (AdvancedDermatology, 2017). For the skin, there are over-the-counter and industry devices for acne, anti-aging, nail fungus, scars, stretch marks and wrinkles. IR is also used for skin contouring and tightening purposes through the numerous devices available commercially this includes devices such as SkinTyte II and Solera Titan (AdvancedDermatology, 2017).

Due to the perceived undesirable effects of sunscreen formulations such as the reapplication process and their aesthetic feel and appearance, alternative sun protective strategies have

been under development such as for example the "BioAstin" oral pill (Koch et al., 2016). The BioAstin product formulation contains a mixture of ingredients including a chemical extracted from algae known as astaxanthin. This has been found to protect the skin against UV exposure and therefore sunburn. Such interventions have the advantage of acting on the body as a whole and not being washed off following exposure to water. Albeit manufacturers advise that such products should be used alongside sunscreen formulations in order to provide further protection (Capelli and Cysewski, 2012).

6.2.3 Use of nano technology in sunscreen formulations

So far publications on nano TiO₂ have been in support of its safety as nano TiO₂ has often been reported as being unable to bypass the skin barrier. It has however been argued that in the past, examples such as in the case of asbestos, CFC's DDT, and PCBs have been of concern and action must therefore be taken to respond quickly to avoid repeating the same mistakes when it comes to nanomaterials (Gee, 2008;Albrecht et al., 2006). It is essential to take into consideration the effect of nanomaterials on workers, the general public and the environment. Construction workers may be exposed to TiO₂ for example through cement, paint and primers as well as the general public through use of sunscreens and other cosmetic products via the dermal route. Workers exposed to TiO₂ nanoparticles in cement dust and paints most likely wash this from their skin within 24h. Likewise, sunscreens, lotions and cosmetics are usually washed from the skin within a day (Jacobs et al., 2010b). However, dermal exposure to TiO₂ nanoparticles in personal care products may be repetitive with many people receiving subsequent exposures on a daily basis (SCCS 2013).

In 2008 TiO₂ nanoparticles came in to attention when they were suspected to be one of the main factors causing premature weathering of pre-painted steel roof sheets that had been handled by workers using sunscreen on their hands. This has also been reported to cause the deterioration of surface coatings and paints on cars and other products. The anatase crystalline form of TiO₂ present in the sunscreens was found to be the cause of the significant problems with "Bluescope steel Colorbond roofing". This finding raised concerns regarding the consumer safety of TiO₂ use on human skin (Sales, 2013). Numerous studies have been undertaken to investigate the potential toxicity of TiO₂ use in sunscreens. Large scale

collaborative projects involving a number of countries have been carried out, most notably the European Nanoderm project. Similarly to other studies, a conclusion was reached that TiO₂ does not cause a threat to health when applied topically (Shi et al., 2013).

A large proportion of the population across Europe are atopic with an estimated 10–20% occurrence amongst children (Nutten, 2015). It has also been estimated that 2-7% of the European population have psoriasis (Raychaudhuri and Farber, 2001). Often these conditions are characterised by an impairment in the skin barrier function. There are currently only a few published studies on the potential absorption of nanomaterials through impaired (Senzui et al., 2010;Monteiro-Riviere et al., 2011) or sunburnt human skin (Monteiro-Riviere et al., 2011). If the integrity of the skin barrier is breached either by mechanical, physical, or chemical damage, the disruption of the rate-limiting SC barrier could potentiate the bioavailability of chemicals as well as nanoparticles. Studies in healthy and psoriatic skin showed that TiO₂ penetrated more deeply in the psoriatic skin relative to normal skin due to the disorganised stratum corneum however no TiO₂ reached the cells within the viable epidermal layer (Pineiro et al., 2007). The effect of TiO₂ on human skin under skin flexion has not previously been investigated although this may be more representative of the real life exposure scenario.

Active ingredients used in sunscreens have been widely studied. There have been concerns in the past over chemical compounds such as oxybenzone crossing the skin barrier and leading to allergies as well as other effects such as hormonal disruption. There are currently 28 active ingredients, both chemical and physical filters, approved within the EU (Sambandan and Ratner, 2011). TiO₂ however is a desirable compound due to its apparent inert nature, ability to act instantly following application, and ability to provide a wide spectrum protection (Jacobs et al., 2010a).

In order for TiO₂ to exhibit systemic effects it must first enter the body. In the case of sunscreens this can theoretically either occur via dermal absorption or through inhalation following the use of spray formulations. Nevertheless a number of studies have investigated the systemic effects of TiO₂ as well as other nano materials both in vitro and in vivo. In an ex-vivo human placental perfusion model, nanosized fluorescently labelled polystyrene beads (up

to 500 nm in size) were seen to cross the placental barrier (Wick et al., 2010). One study carried out on mice found that TiO₂ nanoparticles were able to translocate across the brain of prenatally exposed mice. Nano TiO₂ in the anatase form administered subcutaneously to pregnant ICR mice, were found to be transferred to and affected the genital and cranial nerve systems of the offspring (Takeda et al., 2009).

TiO₂ has been evaluated as a Group 2B carcinogen whereby it is possibly carcinogenic to humans according to the World Health Organisation (WHO)/International Agency for Research on Cancer (IARC, 2010), based on two-year animal aerosol inhalation studies (Mohr et al., 2006). Pulmonary exposure to TiO₂ promotes lung carcinogenesis in rats, and the promotion effect is possibly associated with TiO₂ burdened alveolar macrophage derived macrophage inflammatory protein 1 alpha (MIP1a), which acts as a growth factor to stimulate the proliferation of human lung adenocarcinoma cells (A549) in vitro (Xu et al., 2010). According to the SCCP report the evidence for the TiO₂ carcinogenic properties in humans is not yet clear, however as a safety precaution nano size TiO₂ is not recommended for use in spray form (SCCP, 2013).

The use of animal models for the testing of finished cosmetic products is banned within Europe since September 2004. A ban on testing ingredients or combinations of ingredients on animals has been in place since March 2009 (European Commission, 2017). Such regulations emphasise the need for the development of alternative strategies of in vitro testing able to yield both reliable and reproducible results (Abd et al., 2016).

The SPF is an index which has been globally adopted and is currently displayed on the labels of all sunscreen products. Over the years different methods of testing have coexisted (Lodén et al., 2011; Lionetti and Rigano, 1994). Currently, in 2017, there are only two standard methods for the determination of the SPF those being, the ISO 24444:2010 (now under revision) and the US FDA 2011. This test is carried out on subjects with photo-type I, II or III skin according to the Fitzpatrick classification system. The UVA protection factor and the critical wavelength in vitro testing was issued by Colipa in 2007. Two subsequent revisions on the methodology followed in 2009 and in 2011, after which the Colipa method was

substituted by the ISO 24443:2012 method (Lionetti and Rigano, 2017). Variations in the UVA test methodologies however exist internationally (Fourtanier et al., 2012). Sunscreen formulations are regulated differently around the world both in terms of testing criteria and the active ingredients permissible for use in marketed personal care products (Aldahan et al., 2015). Efficient, up to date formulations suitable for international marketing are a real challenge for formulators to achieve. The stability and performance of the formulations over the shelf life of the product and the consumer health all areas for consideration (Lionetti and Rigano, 2017).

The work presented within this thesis explores some of the key debates regarding the effectiveness of current sunscreen formulations. Experiments carried out in chapter 3 identified the action of complete solar light as behaving in a polychromatic manner to induce the biomarkers of damage detected. This novel finding may be explored further in future work, and may be used to inform the development of newer generation sunscreens able to provide more efficient protection. The work presented also investigated the effects of the TiO₂ compound which has been speculated to be a sunscreen active of concern. Assessments carried out on human skin did not identify any positive influence of TiO₂ on the disruption of the skin barrier function, therefore further adding to the body of evidence in support for the safety of its use. This work provides a platform for future studies involving the use of methodologies for understanding the potential toxicity profile of nano TiO₂ and similar nanoparticulate compounds.

Chapter 7 - References

- Abd, E., Yousef, S.A., Pastore, M.N., Telaprolu, K., Mohammed, Y.H., Namjoshi, S., Grice, J.E. and Roberts, M.S. (2016) 'Skin models for the testing of transdermal drugs', *Clinical Pharmacology : Advances and Applications*, 8, pp. 163-176.
- Abel, J. and Haarmann-Stemmann, T. 391 (2010) 'An introduction to the molecular basics of aryl hydrocarbon receptor biology' *Biological Chemistry*. p. 1235 11. Available at: <https://www.degruyter.com/view/j/bchm.2010.391.issue-11/bc.2010.128/bc.2010.128.xml> (Accessed: 07/07/2017).
- Advanced Dermatology (2017) *Light and Energy-Based Therapies*. Available at: <https://www.advancedderm.com/conditions-treatment/medical-dermatology/light-based-therapies.aspx> (Accessed: 03/07/2017).
- Akhalaya, M.Y., Maksimov, G.V., Rubin, A.B., Lademann, J. and Darvin, M.E. (2014) 'Molecular action mechanisms of solar infrared radiation and heat on human skin', *Ageing Research Reviews*, 16, pp. 1-11.
- Albrecht, M.A., Evans, C.W. and Raston, C.L. (2006) 'Green chemistry and the health implications of nanoparticles', *Green Chemistry*, 8(5), pp. 417-432.
- Aldahan, A.S., Shah, V.V., Mlacker, S. and Nouri, K. (2015) 'The history of sunscreen', *JAMA Dermatology*, 151(12), pp. 1316-1316.
- Alfadda, A.A. and Sallam, R.M. (2012) 'Reactive Oxygen Species in Health and Disease', *Journal of Biomedicine and Biotechnology*, 2012, p. 14.
- Anigbogu, A.N., Williams, A.C., Barry, B.W. and Edwards, H.G. (1995) 'Fourier transform Raman spectroscopy of interactions between the penetration enhancer dimethyl sulfoxide and human stratum corneum', *International Journal of Pharmaceutics*, 125(2), pp. 265-282.
- Applegate, L.A., Noël, A., Vile, G., Frenk, E. and Tyrrell, R.M. (1995) 'Two genes contribute to different extents to the heme oxygenase enzyme activity measured in cultured human skin fibroblasts and keratinocytes: implications for protection against oxidant stress', *Photochemistry and Photobiology*, 61(3), pp. 285-291.
- Arora, S., Rajwade, J.M. and Paknikar, K.M. (2012) 'Nanotoxicology and in vitro studies: the need of the hour', *Toxicology and Applied Pharmacology*, 258(2), pp. 151-165.
- Asuri, P., Bale, S.S., Karajanagi, S.S. and Kane, R.S. (2006) 'The protein–nanomaterial interface', *Current Opinion in Biotechnology*, 17(6), pp. 562-568.
- Auffan, M., Rose, J., Bottero, J.-Y., Lowry, G.V., Jolivet, J.-P. and Wiesner, M.R. (2009) 'Towards a definition of inorganic nanoparticles from an environmental, health and safety perspective', *Nat Nano*, 4(10), pp. 634-641.
- Autier, P., Boniol, M. and Doré, J.F. (2007) 'Sunscreen use and increased duration of intentional sun exposure: still a burning issue', *International journal of cancer*, 121(1), pp. 1-5.

Baer, D.R., Gaspar, D.J., Nachimuthu, P., Techane, S.D. and Castner, D.G. (2010) 'Application of surface chemical analysis tools for characterization of nanoparticles', *Analytical and bioanalytical chemistry*, 396(3), pp. 983-1002.

Barbero, A.M. and Frasch, H.F. (2009) 'Pig and guinea pig skin as surrogates for human in vitro penetration studies: a quantitative review', *Toxicology in Vitro*, 23(1), pp. 1-13.

Bargoil, S.C. and Erdman, L.K. (1993) 'Safe tan An oxymoron', *Cancer Nursing*, 16(2), pp. 139-144.

Barolet, D., Christiaens, F. and Hamblin, M.R. (2016) 'Infrared and Skin: Friend or Foe', *Journal of photochemistry and photobiology. B, Biology*, 155, pp. 78-85.

Baron, E.D. and Suggs, A.K. (2014) 'Introduction to Photobiology', *Dermatologic Clinics*, 32(3), pp. 255-266.

Bartosova, L. and Bajgar, J. (2012) 'Transdermal drug delivery in vitro using diffusion cells', *Current medicinal chemistry*, 19(27), pp. 4671-4677.

Bashir, M.M., Sharma, M.R. and Werth, V.P. (2009) 'UVB and proinflammatory cytokines synergistically activate TNF-alpha production in keratinocytes through enhanced gene transcription', *J Invest Dermatol*, 129(4), pp. 994-1001.

Bearer, C.F. (1995) 'Environmental health hazards: how children are different from adults', *The Future of Children*, pp. 11-26.

Bennett, S.W., Zhou, D., Mielke, R. and Keller, A.A. (2012) 'Photoinduced disaggregation of TiO₂ nanoparticles enables transdermal penetration', *PLoS One*, 7(11), p. e48719.

Berneburg, M., Plettenberg, H., Medve-König, K., Pfahlberg, A., Gers-Barlag, H., Gefeller, O. and Krutmann, J. (2004) 'Induction of the Photoaging-Associated Mitochondrial Common Deletion In Vivo in Normal Human Skin', *Journal of Investigative Dermatology*, 122(5), pp. 1277-1283.

Berneburg, M., Grether-Beck, S., Kurten, V., Ruzicka, T., Briviba, K., Sies, H., and Krutmann J. (1999) "Singlet Oxygen Mediates the UVA-induced Generation of the Photoaging-associated Mitochondrial Common Deletion" *The Journal of Biological Chemistry*, 274 (22), pp. 15345–15349.

Bharadwaj, S., Garg, V.K., Sharma, P., Bansal, M. and Kumar, N. (2011) 'Recent advancement in transdermal drug delivery system', *Int. J. of Pharma Professional's Research*, 2(1), pp. 6-9.

Bharath, A.K. and Turner, R.J. (2009) *Impact of climate change on skin cancer*. The Royal Society of Medicine. Available at: <http://www.ncbi.nlm.nih.gov/pmc/articles/PMC2697050/> (Accessed 08/06/2017)

Bhattacharya, K., Davoren, M., Boertz, J., Schins, R.P., Hoffmann, E. and Dopp, E. (2009) 'Titanium dioxide nanoparticles induce oxidative stress and DNA-adduct formation but not DNA-breakage in human lung cells', *Particle and Fibre Toxicology*, 6(1), p. 17.

Birch-Machin, Russell, E.V. and Latimer, J.A. (2013) *Mitochondrial DNA damage as a biomarker for ultraviolet radiation exposure and oxidative stress*. Blackwell Publishing Ltd [Online]. Available at: <http://dx.doi.org/10.1111/bjd.12207>. (Accessed 13/05/17)

Birch-Machin, M.A. (2006) 'The role of mitochondria in ageing and carcinogenesis', *Clinical and Experimental Dermatology*, 31(4), pp. 548-552.

Birch-Machin, M.A., Russell, E.V. and Latimer, J.A. (2013) 'Mitochondrial DNA damage as a biomarker for ultraviolet radiation exposure and oxidative stress', *British Journal of Dermatology*, 169, pp. 9-14.

Birch-Machin, M.A. and Swalwell, H. (2010) 'How mitochondria record the effects of UV exposure and oxidative stress using human skin as a model tissue', *Mutagenesis*, 25(2), pp. 101-107.

Birch-machin, M.A., Tindall, M., Turner, R., Haldane, F. and Rees, J.L. (1998) 'Mitochondrial DNA Deletions in Human Skin Reflect Photo- Rather Than Chronologic Aging', *Journal of Investigative Dermatology*, 110(2), pp. 149-152.

Birch-Machin, M.A. and Wilkinson, S.C. (2008) *Skin Photobiology*. John Wiley & Sons, Ltd [Online]. Available at: <http://dx.doi.org/10.1002/9780470773093.ch3>. (Accessed 20/07/2017)

Bjørås, M., Luna, L., Johnsen, B., Hoff, E., Haug, T., Rognes, T. and Seeberg, E. (1997) 'Opposite base-dependent reactions of a human base excision repair enzyme on DNA containing 7, 8-dihydro-8-oxoguanine and abasic sites', *The EMBO journal*, 16(20), pp. 6314-6322.

Boiteux, S. and Radicella, J.P. (1999) 'Base excision repair of 8-hydroxyguanine protects DNA from endogenous oxidative stress', *Biochimie*, 81(1), pp. 59-67.

Bolzinger, M.A., Briançon, S., Pelletier, J. and Chevalier, Y. (2012) 'Penetration of drugs through skin, a complex rate-controlling membrane', *Current Opinion in Colloid & Interface Science*, 17(3), pp. 156-165.

Bos, J.D. and Meinardi, M.M.H.M. (2000) 'The 500 Dalton rule for the skin penetration of chemical compounds and drugs', *Experimental Dermatology*, 9(3), pp. 165-169.

Boukamp, P., P.R.T., Breitkreutz, D., Hornung, J., Markham, A. and Fusenig, a.N.E. (1988) 'Normal keratinization in a spontaneously immortalized aneuploid human keratinocyte cell line', *The Journal of Cell Biology*, 106(3), pp. 761-771.

Boulton, S., Anderson, A., Swalwell, H., Henderson, J.R., Manning, P. and Birch-Machin, M.A. (2011) 'Implications of using the fluorescent probes, dihydrorhodamine 123 and 2',7'-

dichlorodihydrofluorescein diacetate, for the detection of UVA-induced reactive oxygen species', *Free Radical Research*, 45(2), pp. 115-122.

Bouwstra, J.A. and Ponc, M. (2006) 'The skin barrier in healthy and diseased state', *Biochimica et Biophysica Acta (BBA) - Biomembranes*, 1758(12), pp. 2080-2095.

Bowman, A. and Birch-Machin, M.A. (2015) 'Mitochondrial DNA as a Biosensor of UV Exposure in Human Skin', in Weissig, V. and Edeas, M. (eds.) *Mitochondrial Medicine: Volume II, Manipulating Mitochondrial Function*. New York, NY: Springer New York, pp. 379-388.

Bronaugh, R.L. and Stewart, R.F. (1985) 'Methods for in vitro percutaneous absorption studies IV: The flow-through diffusion cell', *Journal of pharmaceutical sciences*, 74(1), pp. 64-67.

Browning, C.L., The, T., Mason, M.D. and Wise Sr, J.P. (2014) 'Titanium Dioxide Nanoparticles are not Cytotoxic or Clastogenic in Human Skin Cells', *Journal of environmental & analytical toxicology*, 4(6).

Brugè, F., Tiano, L., Astolfi, P., Emanuelli, M. and Damiani, E. (2014) 'Prevention of UVA-Induced Oxidative Damage in Human Dermal Fibroblasts by New UV Filters, Assessed Using a Novel In Vitro Experimental System', *PLOS ONE*, 9(1), p. e83401.

Burke, K.E. (2011) 'Photoprotection of the Skin with Vitamins C and E: Antioxidants and Synergies', in Pappas, A. (ed.) *Nutrition and Skin: Lessons for Anti-Aging, Beauty and Healthy Skin*. New York, NY: Springer New York, pp. 43-58.

Burnett, M.E. and Wang, S.Q. (2011) 'Current sunscreen controversies: a critical review', *Photodermatology, Photoimmunology & Photomedicine*, 27(2), pp. 58-67.

Bustin, S.A. (2010) 'Why the need for qPCR publication guidelines?—The case for MIQE', *Methods*, 50(4), pp. 217-226.

Cai, R., Kubota, Y., Shuin, T., Sakai, H., Hashimoto, K. and Fujishima, A. (1992) 'Induction of cytotoxicity by photoexcited TiO₂ particles', *Cancer research*, 52(8), pp. 2346-2348.

Cai, X., Woods, A., Mesquida, P. and Jones, S. (2016) 'Assessing the Potential for Drug-Nanoparticle Surface Interactions To Improve Drug Penetration into the Skin', *Molecular pharmaceuticals*, 13(4), pp. 1375-1384.

Calles, C., Schneider, M., Macaluso, F., Benesova, T., Krutmann, J. and Schroeder, P. (2010) 'Infrared A Radiation Influences the Skin Fibroblast Transcriptome: Mechanisms and Consequences', *Journal of Investigative Dermatology*, 130(6), pp. 1524-1536.

CancerResearch UK (2017) Available at:<http://www.cancerresearchuk.org/about-cancer/causes-of-cancer/sun-uv-and-cancer> (Accessed: 28/07/2017)

Capelli, B. and Cysewski, G. (2012) 'Natural Astaxanthin', *The world's best kept health secret*. Cyanotech Corporation, Kailua-Kina, 188.

Carli, P., De Giorgi, V., Giannotti, B., Seidenari, S., Pellacani, G., Peris, K., Piccolo, D., Rubegni, P. and Andreassi, L. (2003) 'Skin cancer day in Italy: method of referral to open access clinics and tumor prevalence in the examined population', *EJD*, 13(1), pp. 76-79.

Casey, A., Herzog, E., Lyng, F.M., Byrne, H.J., Chambers, G. and Davoren, M. (2008) 'Single walled carbon nanotubes induce indirect cytotoxicity by medium depletion in A549 lung cells', *Toxicology Letters*, 179(2), pp. 78-84.

CHEM101-Introductory Chemistry (2017) 'Electromagnetic Radiation ', *PENNSSTATE Eberly College of Science*. Available from: https://online.science.psu.edu/chem101_sp1/node/11822 (Accessed: 15/07/2017)

Chen, M., Liu, X. and Fahr, A. (2011) 'Skin penetration and deposition of carboxyfluorescein and temoporfin from different lipid vesicular systems: in vitro study with finite and infinite dosage application', *International journal of pharmaceuticals*, 408(1), pp. 223-234.

Chilcott, R.P. (2008) 'Cutaneous Anatomy and Function', in *Principles and Practice of Skin Toxicology*. John Wiley & Sons, Ltd, pp. 1-16.

Chinnery, P. and Schon, E. (2003) 'Mitochondria', *Journal of Neurology, Neurosurgery, and Psychiatry*, 74(9), pp. 1188-1199.

Cho, S., Lee, M.J., Kim, M.S., Lee, S., Kim, Y.K., Lee, D.H., Lee, C.W., Cho, K.H. and Chung, J.H. (2008) 'Infrared plus visible light and heat from natural sunlight participate in the expression of MMPs and type I procollagen as well as infiltration of inflammatory cell in human skin in vivo', *Journal of dermatological science*, 50(2), pp. 123-133.

Cho, S., Shin, M.H., Kim, Y.K., Seo, J.-E., Lee, Y.M., Park, C.-H. and Chung, J.H. (2009) 'Effects of Infrared Radiation and Heat on Human Skin Aging in vivo', *Journal of Investigative Dermatology Symposium Proceedings*, 14(1), pp. 15-19.

Christiano, L.J. and Fitzgerald, T.J. (2003) 'The Band Pass Filter*', *International Economic Review*, 44(2), pp. 435-465.

Council, N.R. (2000) *Strategies to Protect the Health of Deployed US Forces: Force Protection and Decontamination*. National Academies Press.

Available from: <https://www.nap.edu/catalog/9717/strategies-to-protect-the-health-of-deployed-us-forces-force> (Accessed 12/08/2017)

Crosera, M., Bovenzi, M., Maina, G., Adami, G., Zanette, C., Florio, C. and Larese, F.F. (2009) 'Nanoparticle dermal absorption and toxicity: a review of the literature', *International archives of occupational and environmental health*, 82(9), pp. 1043-1055.

Crosera, M., Prodi, A., Mauro, M., Pelin, M., Florio, C., Bellomo, F., Adami, G., Apostoli, P., De Palma, G., Bovenzi, M., Campanini, M. and Filon, F. (2015) 'Titanium Dioxide Nanoparticle Penetration into the Skin and Effects on HaCaT Cells', *International Journal of Environmental Research and Public Health*, 12(8), p. 9282.

Danno, K., Mori, N., Toda, K.i., Kobayashi, T. and Utani, A. (2001) 'Near-infrared irradiation stimulates cutaneous wound repair: laboratory experiments on possible mechanisms', *Photodermatology, photoimmunology & photomedicine*, 17(6), pp. 261-265.

de Gruijl, F.R. (2000) '[33] Photocarcinogenesis: UVA vs UVB', *Methods in Enzymology*, 319, pp. 359-366.

Derjaguin, B. and Landau, L. (1941) 'The theory of stability of highly charged lyophobic sols and coalescence of highly charged particles in electrolyte solutions', *Acta Physicochim. URSS*, 14(633-52), p. 58.

Dhawan, A. and Sharma, V. (2010) 'Toxicity assessment of nanomaterials: methods and challenges', *Analytical and bioanalytical chemistry*, 398(2), pp. 589-605.

Di Virgilio, A., Reigosa, M., Arnal, P. and De Mele, M.F.L. (2010) 'Comparative study of the cytotoxic and genotoxic effects of titanium oxide and aluminium oxide nanoparticles in Chinese hamster ovary (CHO-K1) cells', *Journal of Hazardous Materials*, 177(1), pp. 711-718.

Diffey, B. (2016) 'New sunscreens and the precautionary principle', *JAMA Dermatology*, 152(5), pp. 511-512.

Diffey, B. and Cadars, B. (2016) 'An appraisal of the need for infrared radiation protection in sunscreens', *Photochemical & Photobiological Sciences*, 15(3), pp. 361-364.

Diffey, B.L. (2002) 'Sources and measurement of ultraviolet radiation', *Methods*, 28(1), pp. 4-13.

Diffey, B.L. (2004) 'The future incidence of cutaneous melanoma within the U.K.', *British Journal of Dermatology*, 151(4), pp. 868-872.

Diffey, B.L. (2011) 'The impact of topical photoprotectants intended for daily use on lifetime ultraviolet exposure', *Journal of Cosmetic Dermatology*, 10(3), pp. 245-250.

Diffey, B.L. and Farr, P.M. (1991) 'Tanning with UVB or UVA: An appraisal of risks', *Journal of Photochemistry and Photobiology B: Biology*, 8(2), p. 219.

Diffey, B.L., Jansén, C.T., Urbach, F. and Wulf, H.C. (1997) 'The standard erythema dose: a new photobiological concept', *Photodermatology, Photoimmunology & Photomedicine*, 13(1-2), pp. 64-66.

DiSomma, J. and Brion, G.M. (1999) 'Sunblock composition suitable for sensitive skin areas'. Google Patents. Available from: Di Somma, J. and Brion, G.M. (1999) 'Sunblock composition suitable for sensitive skin areas'. Google Patents. (Accessed: 12/08/2017)

Doak, S., Griffiths, S., Manshian, B., Singh, N., Williams, P., Brown, A. and Jenkins, G. (2009) 'Confounding experimental considerations in nanogenotoxicology', *Mutagenesis*, 24(4), pp. 285-293.

Dorland (2007) 'Dorland's Medical Dictionary for Health Consumers'.

available at: <http://medical-dictionary.thefreedictionary.com/epidermis>
(Accessed: 12/08/2017)

Dorser-Medicines (2015) *Advisory Group* Available at:
<http://www.dorsetccg.nhs.uk/Downloads/aboutus/medicinesmanagement/Other%20Guidelines/Commissioning%20Statement%20Dundee%20sunscreen%20Jan%2015.pdf>.
(Accessed: 17/06/2017)

Dranka, B.P., Benavides, G.A., Diers, A.R., Giordano, S., Zelickson, B.R., Reily, C., Zou, L., Chatham, J.C., Hill, B.G., Zhang, J., Landar, A. and Darley-Usmar, V.M. (2011) 'Assessing bioenergetic function in response to oxidative stress by metabolic profiling', *Free Radical Biology and Medicine*, 51(9), pp. 1621-1635.

Dunford, R., Salinaro, A., Cai, L., Serpone, N., Horikoshi, S., Hidaka, H. and Knowland, J. (1997) 'Chemical oxidation and DNA damage catalysed by inorganic sunscreen ingredients', *FEBS letters*, 418(1-2), pp. 87-90.

Dupont, E., Gomez, J. and Bilodeau, D. (2013) 'Beyond UV radiation: A skin under challenge', *International Journal of Cosmetic Science*, 35(3), pp. 224-232.

Duracher, L., Blasco, L., Abdel Jaoued, A., Vian, L. and Marti-Mestres, G. (2009) 'Irradiation of skin and contrasting effects on absorption of hydrophilic and lipophilic compounds', *Photochemistry and photobiology*, 85(6), pp. 1459-1467.

Durham, S., Krishnan, K., Betts, J. and Birch-Machin, M. (2003) 'Mitochondrial DNA damage in non-melanoma skin cancer', *British Journal of Cancer*, 88(1), p. 90.

Ebeling, P.R. (2014) 'Vitamin D and bone health: Epidemiologic studies', *BoneKEy Rep*, 3.
Eirheim, H.U., Bundgaard, C. and Nielsen, H.M. (2004) 'Evaluation of different toxicity assays applied to proliferating cells and to stratified epithelium in relation to permeability enhancement with glycocholate', *Toxicology in vitro*, 18(5), pp. 649-657.

El-Boury, S., Couteau, C., Boulande, L., Papis, E. and Coiffard, L. (2007) 'Effect of the combination of organic and inorganic filters on the Sun Protection Factor (SPF) determined by in vitro method', *International journal of pharmaceuticals*, 340(1), pp. 1-5.

Elena Peira a, Francesco Turci b,c,* , Ingrid Corazzari b,c, Daniela Chirio a, and Luigi Battaglia a, B.F.b., c, Marina Gallarate (2014) 'The influence of surface charge and photo-reactivity on skin-permeation enhancer property of nano-TiO₂ in ex vivo pig skin model under indoor light', *International Journal of Pharmaceutics*, 467, pp. 90-99.

Eshaghian, A., Vleugels, R.A., Canter, J.A., McDonald, M.A., Stasko, T. and Sligh, J.E. (2006) 'Mitochondrial DNA Deletions Serve as Biomarkers of Aging in the Skin, but Are Typically Absent in Nonmelanoma Skin Cancers', *Journal of Investigative Dermatology*, 126(2), pp. 336-344.

EU Cosmetics Legislation (2017) *European Commission*.
Available at: https://ec.europa.eu/growth/sectors/cosmetics/legislation_en

(Accessed 15/07/2017)

European Commission (2013) *European Commission Animal testing - Targeted Stakeholder Consultation - 2013 Implementation Date Marketing Ban Cosmetics Directive*.

Available at:

<http://ec.europa.eu/DocsRoom/documents/13145/attachments/1/translations>.

(Accessed: 15/07/2017).

European Commission (2017) *Ban on animal testing*

Available at: https://ec.europa.eu/growth/sectors/cosmetics/animal-testing_en

(Accessed: 04/08/17).

Evans, S.O., Jameson, M.B., Cursons, R., Peters, L.M., Bird, S. and Jacobson, G.M. (2016) 'Development of a qPCR method to measure mitochondrial and genomic DNA damage with application to chemotherapy-induced DNA damage and cryopreserved cells', *Biology*, 5(4), p. 39.

Fairbairn, D.W., Olive, P.L. and O'Neill, K.L. (1995) 'The comet assay: a comprehensive review', *Mutation Research/Reviews in Genetic Toxicology*, 339(1), pp. 37-59.

Fakin, D., Kleinschek, K.S. and Ojstr²ek, A. (2015) 'The Role of TiO₂ Nanoparticles on the UV Protection Ability and Hydrophilicity of Polyamide Fabrics', *Acta Phys Pol A*, 127(4), pp. 943-946.

Falck, G., Lindberg, H., Suhonen, S., Vippola, M., Vanhala, E., Catalan, J., Savolainen, K. and Norppa, H. (2009) 'Genotoxic effects of nanosized and fine TiO₂', *Human & experimental toxicology*, 28(6-7), pp. 339-352.

Falck, G.C., Lindberg, H.K., Suhonen, S., Vippola, M., Vanhala, E., Catalan, J., Savolainen, K. and Norppa, H. (2009) 'Genotoxic effects of nanosized and fine TiO₂', *Hum Exp Toxicol*, 28.

Faure, B., Salazar-Alvarez, G., Ahniyaz, A., Villaluenga, I., Berriozabal, G., De Miguel, Y.R. and Bergström, L. (2013) 'Dispersion and surface functionalization of oxide nanoparticles for transparent photocatalytic and UV-protecting coatings and sunscreens', *Science and technology of advanced materials*, 14(2), p. 023001.

Faurschou, A. and Wulf, H.C. (2008) 'Synergistic effect of broad-spectrum sunscreens and antihistamines in the control of idiopathic solar urticaria', *Archives of dermatology*, 144(6), pp. 765-769.

Faustino, C., Serafim, C., Ferreira, I., Pinheiro, L. and Calado, A. (2015) 'Solubilization power of an amino acid-based gemini surfactant towards the hydrophobic drug amphotericin B', *Colloids and Surfaces A: Physicochemical and Engineering Aspects*, 480, pp. 426-432.

Forman, A.B., Roenigk, H.H., Jr, Caro, W.A. and Magid, M.L. (1989) 'Long-term follow-up of skin cancer in the puva-48 cooperative study', *Archives of Dermatology*, 125(4), pp. 515-519.

Fourtanier, A., Moyal, D. and Seite, S. (2012) 'UVA filters in sun-protection products: regulatory and biological aspects', *Photochemical & Photobiological Sciences*, 11(1), pp. 81-89.

Francesco Turci, E.P., Ingrid Corazzari, Ivana Fenoglio, Michele Trotta, and Bice Fubini (2013) 'Crystalline Phase Modulates the Potency of Nanometric TiO₂ to Adhere to and Perturb the Stratum Corneum of Porcine Skin under Indoor Light', *Chem. Res. Toxicol.*, 26, p. 1579–1590.

Frank, S., Menezes, S., Coster, L.D., Oster, M., Dubertret, L. and Coulomb, B. (2006) 'Infrared radiation induces the p53 signaling pathway: role in infrared prevention of ultraviolet B toxicity', *Experimental dermatology*, 15(2), pp. 130-137.

Frank, S., Oliver, L., Lebreton-De Coster, C., Moreau, C., Lecabelle, M.-T., Michel, L., Vallette, F.M., Dubertret, L. and Coulomb, B. (2004) 'Infrared Radiation Affects the Mitochondrial Pathway of Apoptosis in Human Fibroblasts', *Journal of Investigative Dermatology*, 123(5), pp. 823-831.

Franken, N., Rodermond, H., Stap, J., Haveman, J. and van Bree, C. (2006) 'Clonogenic assay of cells in vitro. Nature Protoc 2006; 1: 2315-9; PMID: 17406473'.

Frelon, S., Douki, T., Ravanat, J.-L., Pouget, J.-P., Tornabene, C. and Cadet, J. (2000) 'High-performance liquid chromatography– tandem mass spectrometry measurement of radiation-induced base damage to isolated and cellular DNA', *Chemical research in toxicology*, 13(10), pp. 1002-1010.

Frijhoff, J., Winyard, P.G., Zarkovic, N., Davies, S.S., Stocker, R., Cheng, D., Knight, A.R., Taylor, E.L., Oettrich, J., Ruskovska, T., Gasparovic, A.C., Cuadrado, A., Weber, D., Poulsen,

H.E., Grune, T., Schmidt, H.H.H.W. and Ghezzi, P. (2015) 'Clinical Relevance of Biomarkers of Oxidative Stress', *Antioxidants & Redox Signaling*, 23(14), pp. 1144-1170.

Gamer, A., Leibold, E.v. and Van Ravenzwaay, B. (2006) 'The in vitro absorption of microfine zinc oxide and titanium dioxide through porcine skin', *Toxicology in vitro*, 20(3), pp. 301-307.

Gao, X., Wang, Y., Peng, S., Yue, B., Fan, C., Chen, W. and Li, X. (2015) 'Comparative toxicities of bismuth oxybromide and titanium dioxide exposure on human skin keratinocyte cells', *Chemosphere*, 135, pp. 83-93.

Gawkrodger, D.J., & Ardern-Jones, M. R. (2012) 'Dermatology: an illustrated colour text', *Edinburgh, Churchill Livingstone Elsevier*.

Gee, D. (2008) 'Establishing evidence for early action: the prevention of reproductive and developmental harm', *Basic & clinical pharmacology & toxicology*, 102(2), pp. 257-266.

Gerloff, K., Albrecht, C., Boots, A.W., Förster, I. and Schins, R.P. (2009) 'Cytotoxicity and oxidative DNA damage by nanoparticles in human intestinal Caco-2 cells', *Nanotoxicology*, 3(4), pp. 355-364.

Gilbert, E., Pirot, F., Bertholle, V., Roussel, L., Falson, F. and Padois, K. (2013) 'Commonly used UV filter toxicity on biological functions: review of last decade studies', *International Journal of Cosmetic Science*, 35(3), pp. 208-219.

Godin, B. and Touitou, E. (2007) 'Transdermal skin delivery: predictions for humans from in vivo, ex vivo and animal models', *Advanced drug delivery reviews*, 59(11), pp. 1152-1161.

Gonzalez, V.C., Beheregaray, A.C.M., Peres, B.M., Sallis, E.S.V., Varela Junior, A.S. and Trindade, G.S. (2015) 'Histopathological Analysis of UVB and IR Interaction in Rat Skin', *Photochemistry and Photobiology*, 91(4), pp. 895-900.

Grether-Beck, S., Marini, A., Jaenicke, T. and Krutmann, J. (2015) 'Effective Photoprotection of Human Skin against Infrared A Radiation by Topically Applied Antioxidants: Results from a Vehicle Controlled, Double-Blind, Randomized Study', *Photochemistry and photobiology*, 91(1), pp. 248-250.

Gulson, B., McCall, M.J., Bowman, D.M. and Pinheiro, T. (2015) 'A review of critical factors for assessing the dermal absorption of metal oxide nanoparticles from sunscreens applied to humans, and a research strategy to address current deficiencies', *Archives of Toxicology*, 89(11), pp. 1909-1930.

Gummer, C., Hinz, R. and Maibach, H. (1987) 'The skin penetration cell: a design update', *International journal of pharmaceuticals*, 40(1-2), pp. 101-104.

Gupta, J., Grube, E., Ericksen, M.B., Stevenson, M.D., Lucky, A.W., Sheth, A.P., Assa'ad, A.H. and Hershey, G.K.K. (2008) 'Intrinsically defective skin barrier function in children with atopic dermatitis correlates with disease severity', *Journal of Allergy and Clinical Immunology*, 121(3), pp. 725-730. e2.

Gurr, J.R., Wang, A.S., Chen, C.H. and Jan, K.Y. (2005) 'Ultrafine titanium dioxide particles in the absence of photoactivation can induce oxidative damage to human bronchial epithelial cells', *Toxicology*, 213.

Halamoda-Kenzaoui, B., Ceridono, M., Urban, P., Bogni, A., Ponti, J., Gioria, S. and Kinsner-Ovaskainen, A. (2017) 'The agglomeration state of nanoparticles can influence the mechanism of their cellular internalisation', *J Nanobiotechnology*, 15(1), p. 48.

Han, X., Gelein, R., Corson, N., Wade-Mercer, P., Jiang, J., Biswas, P., Finkelstein, J.N., Elder, A. and Oberdörster, G. (2011) 'Validation of an LDH assay for assessing nanoparticle toxicity', *Toxicology*, 287(1), pp. 99-104.

Harbottle, A., Krishnan, K.J. and Birch-Machin, M.A. (2004) 'Implications of using the ND1 gene as a control region for real-time PCR analysis of mitochondrial DNA deletions in human skin', *The Journal of investigative dermatology*, 122(6), pp. 1518-1521.

Harman, D. (1956) 'Aging: A Theory Based on Free Radical and Radiation Chemistry', *Journal of Gerontology*, 11(3), pp. 298-300.

Hedderman, T.G., Keogh, S.M., Chambers, G. and Byrne, H.J. (2004) 'Solubilization of SWNTs with Organic Dye Molecules', *The Journal of Physical Chemistry B*, 108(49), pp. 18860-18865.

Helleday, T., Lo, J., van Gent, D.C. and Engelward, B.P. (2007) 'DNA double-strand break repair: From mechanistic understanding to cancer treatment', *DNA Repair*, 6(7), pp. 923-935.

HighSchoolNanoScience (2017). Available at:
<http://highschoolnanoscience.cnsi.ucla.edu/publicview/images/biotoxicityBG2.gif>.
(Accessed 08/07/2017)

Hoffmann, G. (2009) 'Water-filtered infrared-A (wIRA) in acute and chronic wounds', *GMS Krankenhaushygiene Interdisziplinär*, 4(2), p. Doc12.

Hoh, A. and Maier, K. (1993) 'Comparative Cytotoxicity Test with Human Keratinocytes, HaCaT Cells, and Skin Fibroblasts to Investigate Skin-Irritating Substances', *Cell and Tissue Culture Models in Dermatological Research* pp 341-347

Bereiter-Hahn, J., Hevert, F. and Holzmann, H. (eds.) *Cell and Tissue Culture Models in Dermatological Research*. Berlin, Heidelberg: Springer Berlin Heidelberg, pp. 341-347.

Holder, A.L., Goth-Goldstein, R., Lucas, D. and Koshland, C.P. (2012) 'Particle-Induced Artifacts in the MTT and LDH Viability Assays', *Chemical Research in Toxicology*, 25(9), pp. 1885-1892.

Holick, M.F. (2011) 'Vitamin D deficiency in 2010: health benefits of vitamin D and sunlight: a D-bate', *Nature Reviews Endocrinology*, 7(2), pp. 73-75.

Holick, M.F. (2016) 'Biological Effects of Sunlight, Ultraviolet Radiation, Visible Light, Infrared Radiation and Vitamin D for Health', *Anticancer Res*, 36(3), pp. 1345-56.

Holzer, A.M. and Elmet, C.A. (2010) 'The Other End of the Rainbow: Infrared and Skin', *The Journal of investigative dermatology*, 130(6), pp. 1496-1499.

Hongbo Shi, R.M., Vincent Castranova and Jinshun Zhao (2013) 'Titanium dioxide nanoparticles: a review of current toxicological data', *Particle and Fibre Toxicology*, 10(15).

Hönigsmann, H. (2012) *History of phototherapy in dermatology. Photochemical & Photobiological Science.*, 12, pp. 16-21

Hornig-Do, H.-T., von Kleist-Retzow, J.-C., Lanz, K., Wickenhauser, C., Kudin, A.P., Kunz, W.S., Wiesner, R.J. and Schauen, M. (2007) 'Human epidermal keratinocytes accumulate superoxide due to low activity of Mn-SOD, leading to mitochondrial functional impairment', *Journal of Investigative Dermatology*, 127(5), pp. 1084-1093.

Hudson, L., Bowman, A., Rashdan, E. and Birch-Machin, M.A. (2016) 'Mitochondrial damage and ageing using skin as a model organ', *Maturitas*, 93, pp. 34-40.

Huncharek, M. and Kupelnick, B. (2002) 'Use of Topical Sunscreens and the Risk of Malignant Melanoma: A Meta-Analysis of 9067 Patients From 11 Case–Control Studies', *American Journal of Public Health*, 92(7), pp. 1173-1177.

Hung, C.-F., Chen, W.-Y., Aljuffali, I.A., Lin, Y.-K., Shih, H.-C. and Fang, J.-Y. (2015) 'Skin aging modulates percutaneous drug absorption: the impact of ultraviolet irradiation and ovariectomy', *Age*, 37(2), p. 21.

Hunter, S.E., Jung, D., Di Giulio, R.T. and Meyer, J.N. (2010) 'The QPCR assay for analysis of mitochondrial DNA damage, repair, and relative copy number', *Methods*, 51(4), pp. 444-451.

Hussain, S., Thomassen, L.C., Ferecatu, I., Borot, M.-C., Andreau, K., Martens, J.A., Fleury, J., Baeza-Squiban, A., Marano, F. and Boland, S. (2010) 'Carbon black and titanium dioxide nanoparticles elicit distinct apoptotic pathways in bronchial epithelial cells', *Particle and fibre toxicology*, 7(1), p. 10.

Ichihashi, M., Ueda, M., Budiyanto, A., Bito, T., Oka, M., Fukunaga, M., Tsuru, K. and Horikawa, T. (2003) 'UV-induced skin damage', *Toxicology*, 189(1), pp. 21-39.

Ilves, M., Palomäki, J., Vippola, M., Lehto, M., Savolainen, K., Savinko, T. and Alenius, H. (2014) 'Topically applied ZnO nanoparticles suppress allergen induced skin inflammation but induce vigorous IgE production in the atopic dermatitis mouse model', *Particle and Fibre Toxicology*, 11(1), p. 38.

J. Moan D. Brune, R.H., B.R.R. Persson and R. Pääkkönen. (2001) 'Visible light and UV radiation. In: Radiation at home, outdoors and in the workplace. Eds. ', *Scandinavian Science Publisher, Oslo*, , pp. 69-85.

Jacobs, J.F., Poel, I.v.d. and Osseweijer, P. (2010) 'Sunscreens with Titanium Dioxide (TiO₂) Nano-Particles: A Societal Experiment', *Nanoethics*, 4, pp. 103-113.

Jacobs, J.F., van de Poel, I. and Osseweijer, P. (2010) 'Sunscreens with Titanium Dioxide (TiO₂) Nano-Particles: A Societal Experiment', *Nanoethics*, 4(2), pp. 103-113.

Jaeger, A., Weiss, D.G., Jonas, L. and Kriehuber, R. (2012) 'Oxidative stress-induced cytotoxic and genotoxic effects of nano-sized titanium dioxide particles in human HaCaT keratinocytes', *Toxicology*, 296.

Janjua, N.R., Kongshoj, B., Andersson, A.M. and Wulf, H.C. (2008) 'Sunscreens in human plasma and urine after repeated whole-body topical application', *Journal of the European Academy of Dermatology and Venereology*, 22(4), pp. 456-461.

Jantschitsch, C., Majewski, S., Maeda, A., Schwarz, T. and Schwarz, A. (2009) 'Infrared Radiation Confers Resistance to UV-Induced Apoptosis Via Reduction of DNA Damage and Upregulation of Antiapoptotic Proteins', *Journal of Investigative Dermatology*, 129(5), pp. 1271-1279.

Jantschitsch, C., Weichenthal, M., Maeda, A., Proksch, E., Schwarz, T. and Schwarz, A. (2011) 'Infrared radiation does not enhance the frequency of ultraviolet radiation-induced skin tumors, but their growth behaviour in mice', *Experimental dermatology*, 20(4), pp. 346-350.

Jatana, S. and DeLouise, L.A. (2014) 'Understanding engineered nanomaterial skin interactions and the modulatory effects of ultraviolet radiation skin exposure', *Wiley Interdisciplinary Reviews: Nanomedicine and Nanobiotechnology*, 6(1), pp. 61-79.

Ji, Z., Xue Jin, Saji George, Tian Xia, Huan Meng, Xiang Wang, Elizabeth Suarez, Haiyuan Zhang, Eric M.V. Hoek, Hilary Godwin, André E. Nel and Zink, J.I. (2010) 'Dispersion and Stability Optimization of TiO₂ Nanoparticles in Cell Culture Media', *Environ. Sci. Technol.*, 44, pp. 7309–7314.

Jin, C.-Y., Zhu, B.-S., Wang, X.-F. and Lu, Q.-H. (2008) 'Cytotoxicity of titanium dioxide nanoparticles in mouse fibroblast cells', *Chemical research in toxicology*, 21(9), pp. 1871-1877.

Johnston, H.J., Hutchison, G.R., Christensen, F.M., Peters, S., Hankin, S. and Stone, V. (2009) 'Identification of the mechanisms that drive the toxicity of TiO₂ particulates: the contribution of physicochemical characteristics', *Particle and fibre toxicology*, 6(1), p. 33.

Jugan, M.-L., Barillet, S., Simon-Deckers, A., Herlin-Boime, N., Sauvaigo, S., Douki, T. and Carriere, M. (2012) 'Titanium dioxide nanoparticles exhibit genotoxicity and impair DNA repair activity in A549 cells', *Nanotoxicology*, 6(5), pp. 501-513.

Kane, R.S. and Stroock, A.D. (2007) 'Nanobiotechnology: Protein-Nanomaterial Interactions', *Biotechnology Progress*, 23(2), pp. 316-319.

Kang, S.J., Kim, B.M., Lee, Y.J. and Chung, H.W. (2008) 'Titanium dioxide nanoparticles trigger p53-mediated damage response in peripheral blood lymphocytes', *Environ Mol Mutagen*, 49.

Karlsson, H.L., Cronholm, P., Gustafsson, J. and Moller, L. (2008) 'Copper oxide nanoparticles are highly toxic: a comparison between metal oxide nanoparticles and carbon nanotubes', *Chemical research in toxicology*, 21(9), pp. 1726-1732.

Karu, T.I. (2008) 'Mitochondrial Signaling in Mammalian Cells Activated by Red and Near-IR Radiation', *Photochemistry and Photobiology*, 84(5), pp. 1091-1099.

Kaur, G. and Dufour, J.M. (2012) 'Cell lines: Valuable tools or useless artifacts', *Spermatogenesis*, 2(1), pp. 1-5.

Kielbassa, C., Roza, L. and Epe, B. (1997) 'Wavelength dependence of oxidative DNA damage induced by UV and visible light', *Carcinogenesis*, 18(4), pp. 811-6.

Kim, H.H., Lee, M.J., Lee, S.R., Kim, K.H., Cho, K.H., Eun, H.C. and Chung, J.H. (2005) 'Augmentation of UV-induced skin wrinkling by infrared irradiation in hairless mice', *Mechanisms of Ageing and Development*, 126(11), pp. 1170-1177.

Kim, M.-S., Kim, Y.K., Cho, K.H. and Chung, J.H. (2006) 'Regulation of type I procollagen and MMP-1 expression after single or repeated exposure to infrared radiation in human skin', *Mechanisms of ageing and development*, 127(12), pp. 875-882.

Kimeswenger, S., Schwarz, A., Födinger, D., Müller, S., Pehamberger, H., Schwarz, T. and Jantschitsch, C. (2016) 'Infrared A radiation promotes survival of human melanocytes carrying ultraviolet radiation-induced DNA damage', *Experimental dermatology*, 25(6), pp. 447-452.

Kiss, B., Bíró, T., Czifra, G., Tóth, B.I., Kertész, Z., Szikszai, Z., Kiss, Á.Z., Juhász, I., Zouboulis, C.C. and Hunyadi, J. (2008) 'Investigation of micronized titanium dioxide penetration in human skin xenografts and its effect on cellular functions of human skin-derived cells', *Experimental dermatology*, 17(8), pp. 659-667.

Kleesz, P., Darlenski, R. and Fluhr, J.W. (2012) 'Full-Body Skin Mapping for Six Biophysical Parameters: Baseline Values at 16 Anatomical Sites in 125 Human Subjects', *Skin Pharmacology and Physiology*, 25(1), pp. 25-33.

Kleinle, S., Wiesmann, U., Superti-Furga, A., Krahenbuhl, S., Boltshauser, E., Reichen, J. and Liechti-Gallati, S. (1997) 'Detection and characterization of mitochondrial DNA rearrangements in Pearson and Kearns-Sayre syndromes by long PCR', *Hum Genet*, 100(5-6), pp. 643-50.

Kligman, A.M. (1969) 'Early destructive effect of sunlight on human skin', *JAMA*, 210(13), pp. 2377-2380.

Kligman, L.H. (1982) 'Intensification of ultraviolet-induced dermal damage by infrared radiation', *Archives of Dermatological Research*, 272(3), pp. 229-238.

Koch, H., Wittern, K.-P. and Bergemann, J. (2001) 'In Human Keratinocytes the Common Deletion Reflects Donor Variabilities Rather Than Chronologic Aging and can be Induced by Ultraviolet A Irradiation', *Journal of Investigative Dermatology*, 117(4), pp. 892-897.

Koch, S., Pettigrew, S., Strickland, M., Slevin, T. and Minto, C. (2016) 'Sunscreen increasingly overshadows alternative sun-protection strategies', *Journal of Cancer Education*, pp. 1-4.

Kochevar IE, T.C., Krutmann J. (2008) 'Fundamentals of cutaneous photobiology and photoimmunology. ', in *In: Wolff K, Goldsmith LA, Katz S, et al. (Eds.). Fitzpatrick's Dermatology in General Medicine 7th edn. McGraw-Hill:New York.*

Kohl, E., Steinbauer, J., Landthaler, M. and Szeimies, R.M. (2011) 'Skin ageing', *Journal of the European Academy of Dermatology and Venereology*, 25(8), pp. 873-884.

Krasnikov, I., Popov, A., Seteikin, A. and Myllylä, R. (2011) 'Influence of titanium dioxide nanoparticles on skin surface temperature at sunlight irradiation', *Biomedical Optics Express*, 2(12), pp. 3278-3283.

Krause, M., Klit, A., Blomberg Jensen, M., Sjøborg, T., Frederiksen, H., Schlumpf, M., Lichtensteiger, W., Skakkebaek, N.E. and Drzewiecki, K.T. (2012) 'Sunscreens: are they beneficial for health? An overview of endocrine disrupting properties of UV-filters', *International Journal of Andrology*, 35(3), pp. 424-436.

Krishnan, K.J. and Birch-Machin, M.A. (2006) 'The Incidence of Both Tandem Duplications and the Common Deletion in mtDNA from Three Distinct Categories of Sun-Exposed Human Skin

and in Prolonged Culture of Fibroblasts', *Journal of Investigative Dermatology*, 126(2), pp. 408-415.

Krishnan, K.J., Harbottle, A. and Birch-Machin, M.A. (2004) 'The Use of a 3895 bp Mitochondrial DNA Deletion as a Marker for Sunlight Exposure in Human Skin', *Journal of Investigative Dermatology*, 123(6), pp. 1020-1024.

Kvam, E. and Tyrrell, R.M. (1997) 'Induction of oxidative DNA base damage in human skin cells by UV and near visible radiation', *Carcinogenesis*, 18(12), pp. 2379-2384.

L. Bartosova, a.J.B. (2012) 'Transdermal Drug Delivery In Vitro Using Diffusion Cells', *Current Medicinal Chemistry*, 19, pp. 4671-4677.

Labban, N., Al-Otaibi, H., Alayed, A., Alshankiti, K. and Al-Enizy, M.A. (2017) 'Assessment of the influence of gender and skin color on the preference of tooth shade in Saudi population', *The Saudi Dental Journal*, 29(3), pp. 102-110.

Lademann, J., Richter, H., Schanzer, S., Knorr, F., Meinke, M., Sterry, W. and Patzelt, A. (2011) 'Penetration and storage of particles in human skin: perspectives and safety aspects', *European Journal of Pharmaceutics and Biopharmaceutics*, 77(3), pp. 465-468.

Lademann, J., Weigmann, H.-J., Rickmeyer, C., Barthelmes, H., Schaefer, H., Mueller, G. and Sterry, W. (1999) 'Penetration of titanium dioxide microparticles in a sunscreen formulation into the horny layer and the follicular orifice', *Skin Pharmacology and Physiology*, 12(5), pp. 247-256.

Lane, M.E. (2013) 'Skin penetration enhancers', *International Journal of Pharmaceutics*, 447(1), pp. 12-21.

Larese, F.F., D'Agostin, F., Crosera, M., Adami, G., Renzi, N., Bovenzi, M. and Maina, G. (2009) 'Human skin penetration of silver nanoparticles through intact and damaged skin', *Toxicology*, 255(1), pp. 33-37.

Larese Filon, F., Mauro, M., Adami, G., Bovenzi, M. and Crosera, M. (2015) 'Nanoparticles skin absorption: New aspects for a safety profile evaluation', *Regulatory Toxicology and Pharmacology*, 72(2), pp. 310-322.

Latha, M.S., Martis, J., Shobha, V., Sham Shinde, R., Bangera, S., Krishnankutty, B., Bellary, S., Varughese, S., Rao, P. and Naveen Kumar, B.R. (2013) 'Sunscreening Agents: A Review', *The Journal of Clinical and Aesthetic Dermatology*, 6(1), pp. 16-26.

Latimer, J.A., Lloyd, J.J., Diffey, B.L., Matts, P.J. and Birch-Machin, M.A. (2015) 'Determination of the action spectrum of UVR-induced mitochondrial DNA damage in human skin cells', *Journal of Investigative Dermatology*, 135(10), pp. 2512-2518.

Lehmann, P. and Schwarz, T. (2011) 'Photodermatoses: Diagnosis and Treatment', *Deutsches Ärzteblatt International*, 108(9), pp. 135-141.

Lewinski, N., Colvin, V. and Drezek, R. (2008) 'Cytotoxicity of nanoparticles', *small*, 4(1), pp. 26-49.

- Liebel, F., Kaur, S., Ruvolo, E., Kollias, N. and Southall, M.D. (2012) 'Irradiation of Skin with Visible Light Induces Reactive Oxygen Species and Matrix-Degrading Enzymes', *Journal of Investigative Dermatology*, 132(7), pp. 1901-1907.
- Liesa, M., Borda-d'Água, B., Medina-Gómez, G., Lelliott, C.J., Paz, J.C., Rojo, M., Palacín, M., Vidal-Puig, A. and Zorzano, A. (2008) 'Mitochondrial Fusion Is Increased by the Nuclear Coactivator PGC-1 β ', *PLOS ONE*, 3(10), p. e3613.
- Limbach, L.K., Li, Y., Grass, R.N., Brunner, T.J., Hintermann, M.A., Muller, M., Gunther, D. and Stark, W.J. (2005) 'Oxide nanoparticle uptake in human lung fibroblasts: effects of particle size, agglomeration, and diffusion at low concentrations', *Environmental science & technology*, 39(23), pp. 9370-9376.
- Liochev, S.I. (2013) 'Reactive oxygen species and the free radical theory of aging', *Free Radical Biology and Medicine*, 60, pp. 1-4.
- Lionetti, N. and Rigano, L. (2017) 'The New Sunscreens among Formulation Strategy, Stability Issues, Changing Norms, Safety and Efficacy Evaluations', *Cosmetics*, 4(2), p. 15.
- Lodén, M., Beitner, H., Gonzalez, H., Edström, D.W., Åkerström, U., Austad, J., Buraczewska-Norin, I., Matsson, M. and Wulf, H.C. (2011) 'Sunscreen use: controversies, challenges and regulatory aspects', *British Journal of Dermatology*, 165(2), pp. 255-262.
- Losquadro, W.D. (2017) 'Anatomy of the Skin and the Pathogenesis of Nonmelanoma Skin Cancer', *Facial Plastic Surgery Clinics of North America*, 25(3), pp. 283-289.
- MacCormack, T.J., Clark, R.J., Dang, M.K.M., Ma, G., Kelly, J.A., Veinot, J.G.C. and Goss, G.G. (2012) 'Inhibition of enzyme activity by nanomaterials: Potential mechanisms and implications for nanotoxicity testing', *Nanotoxicology*, 6(5), pp. 514-525.
- MacNeil, S. (2007) 'Progress and opportunities for tissue-engineered skin', *Nature*, 445(7130), pp. 874-880.
- Maddodi, N., Jayanthi, A. and Setaluri, V. (2012) 'Shining Light on Skin Pigmentation: The Darker and the Brighter Side of Effects of UV Radiation', *Photochemistry and Photobiology*, 88(5), pp. 1075-1082.
- Madison, K.C. (2003) 'Barrier Function of the Skin: [ldquo]La Raison d'Être[rdquo] of the Epidermis', *J Investig Dermatol*, 121(2), pp. 231-241.
- Magdolenova, Z., Bilaničová, D., Pojana, G., Fjellsbø, L.M., Hudecova, A., Hasplova, K., Marcomini, A. and Dusinska, M. (2012) 'Impact of agglomeration and different dispersions of titanium dioxide nanoparticles on the human related in vitro cytotoxicity and genotoxicity', *Journal of Environmental Monitoring*, 14(2), pp. 455-464.
- Mahmoud, B.H., Ruvolo, E., Hexsel, C.L., Liu, Y., Owen, M.R., Kollias, N., Lim, H.W. and Hamzavi, I.H. (2010) 'Impact of Long-Wavelength UVA and Visible Light on Melanocompetent Skin', *Journal of Investigative Dermatology*, 130(8), pp. 2092-2097.

Maibach, H.I., Feldmann, R.J., Milby, T.H. and Serat, W.F. (1971) 'Regional Variation in Percutaneous Penetration in Man', *Archives of Environmental Health: An International Journal*, 23(3), pp. 208-211.

Marionnet, C., Pierrard, C., Vioux-Chagnoleau, C., Sok, J., Asselineau, D. and Bernerd, F. (2006) 'Interactions between fibroblasts and keratinocytes in morphogenesis of dermal epidermal junction in a model of reconstructed skin', *Journal of investigative dermatology*, 126(5), pp. 971-979.

Marks, R., Foley, P.A., Jolley, D., Knight, K.R., Harrison, J. and Thompson, S.C. (1995) 'The effect of regular sunscreen use on vitamin d levels in an australian population: Results of a randomized controlled trial', *Archives of Dermatology*, 131(4), pp. 415-421.

Marzulli, F.N. (1962) *Barriers to Skin Penetration**From the U.S. Army Chemical Research and Development Laboratories Army Chemical Center, Maryland* [Online]. Available at: <http://www.sciencedirect.com/science/article/pii/S0022202X15497660>. (Accessed 13/05/2017)

Maslin, D.L. (2014) 'Do sunscreens protect us?', *International Journal of Dermatology*, 53(11), pp. 1319-1323.

Maslov, A.Y., Ganapathi, S., Westerhof, M., Quispe-Tintaya, W., White, R.R., Van Houten, B., Reiling, E., Dollé, M.E., Steeg, H. and Hasty, P. (2013) 'DNA damage in normally and prematurely aged mice', *Aging cell*, 12(3), pp. 467-477.

Matsumura, Y. and Ananthaswamy, H.N. (2004) 'Toxic effects of ultraviolet radiation on the skin', *Toxicology and Applied Pharmacology*, 195(3), pp. 298-308.

Matteo Crosera, M.B., Giovanni Maina, , Gianpiero Adami, C.Z., Chiara Florio, and Larese, F.F. (2009) 'Nanoparticle dermal absorption and toxicity: a review of the literature', *Int Arch Occup Environ Health*, 82, pp. 1043-1055.

Mavon, A., Miquel, C., Lejeune, O., Payre, B. and Moretto, P. (2007) 'In vitro percutaneous absorption and in vivo stratum corneum distribution of an organic and a mineral sunscreen', *Skin pharmacology and physiology*, 20(1), pp. 10-20.

McCall, M.J. (2011) 'Environmental, health and safety issues: nanoparticles in the real world', *Nature nanotechnology*, 6(10), pp. 613-614.

Meinke, M.C., Haag, S.F., Schanzer, S., Groth, N., Gersonde, I. and Lademann, J. (2011) 'Radical protection by sunscreens in the infrared spectral range', *Photochemistry and photobiology*, 87(2), pp. 452-456.

Meinke, M.C., Syring, F., Schanzer, S., Haag, S.F., Graf, R., Loch, M., Gersonde, I., Groth, N., Pflücker, F. and Lademann, J. (2013) 'Radical Protection by Differently Composed Creams in the UV/VIS and IR Spectral Ranges', *Photochemistry and Photobiology*, 89(5), pp. 1079-1084.

Meißner T., Oelschlägel K. and A., P. (2014) 'Dispersion of nanomaterials used in toxicological studies: a comparison of sonication approaches demonstrated on TiO₂ P25', *J Nanopart Res*, 16(2228), pp. 1-13.

Melnikova, V.O. and Ananthaswamy, H.N. (2005) 'Cellular and molecular events leading to the development of skin cancer', *Mutation Research/Fundamental and Molecular Mechanisms of Mutagenesis*, 571(1–2), pp. 91-106.

Michaels, A.S., Chandrasekaran, S.K. and Shaw, J.E. (1975) 'Drug permeation through human skin: Theory and in vitro experimental measurement', *AIChE Journal*, 21(5), pp. 985-996.

Miquel-Jeanjean, C., Crepel, F., Raufast, V., Payre, B., Datas, L., Bessou-Touya, S. and Duplan, H. (2012) 'Penetration Study of Formulated Nanosized Titanium Dioxide in Models of Damaged and Sun-Irradiated Skins', *Photochem Photobiol*, 88.

Miquel-Jeanjean, C., Crépel, F., Raufast, V., Payre, B., Datas, L., Bessou-Touya, S. and Duplan, H. (2012) 'Penetration Study of Formulated Nanosized Titanium Dioxide in Models of Damaged and Sun-Irradiated Skins', *Photochemistry and photobiology*, 88(6), pp. 1513-1521.

Mohr, U., Ernst, H., Roller, M. and Pott, F. (2006) 'Pulmonary tumor types induced in Wistar rats of the so-called "19-dust study"', *Experimental and Toxicologic Pathology*, 58(1), pp. 13-20.

Monteiro-Riviere, N., Wiench, K., Landsiedel, R., Schulte, S., Inman, A. and Riviere, J. (2011) 'Safety evaluation of sunscreen formulations containing titanium dioxide and zinc oxide nanoparticles in UVB sunburned skin: an in vitro and in vivo study', *Toxicological Sciences*, 123(1), pp. 264-280.

Monteiro-Riviere, N.A., Inman, A.O. and Zhang, L.W. (2009) 'Limitations and relative utility of screening assays to assess engineered nanoparticle toxicity in a human cell line', *Toxicology and Applied Pharmacology*, 234(2), pp. 222-235.

Monteiro-Riviere, N.A. and Riviere, J.E. (2009) 'Interaction of nanomaterials with skin: Aspects of absorption and biodistribution'. Taylor & Francis. *Nanotoxicology*, 3, (3), pp 188- 193.

Moore, C.A., Wilkinson, S.C., Blain, P.G., Dunn, M., Aust, G.A. and Williams, F.M. (2014) 'Percutaneous absorption and distribution of organophosphates (chlorpyrifos and dichlorvos) following dermal exposure and decontamination scenarios using in vitro human skin model', *Toxicology Letters*, 229(1), pp. 66-72.

Moser, K., Kriwet, K., Naik, A., Kalia, Y.N. and Guy, R.H. (2001) 'Passive skin penetration enhancement and its quantification in vitro', *European Journal of Pharmaceutics and Biopharmaceutics*, 52(2), pp. 103-112.

Moss, G.P., Gullick, D.R. and Wilkinson, S.C. (2015) 'Methods for the Measurement of Percutaneous Absorption', in *Predictive Methods in Percutaneous Absorption*. Springer, pp. 25-42.

Naidoo, K. and Birch-Machin, M. (2017) 'Oxidative Stress and Ageing: The Influence of Environmental Pollution, Sunlight and Diet on Skin', *Cosmetics*, 4(1), p. 4.

Nanoderm (2007) *Quality of Skin as a Barrier to ultra-fine Particles - Final Report*
Available at: https://www.nanoportal-bw.de/pb/site/nanoportal-bw/get/documents_E806223784/nanoportalbw/Objekte/pdf/Linkliste%20%20Dokumente/Nanoderm_2007FinalReport.pdf (Accessed: 03/08/17).

Nash, J.F., Tanner, P.R. and Matts, P.J. (2006) 'Ultraviolet A Radiation: Testing and Labeling for Sunscreen Products', *Dermatologic Clinics*, 24(1), pp. 63-74.

Ness, A.R., Frankel, S.J., Gunnell, D.J. and Smith, G.D. (1999) 'Are we really dying for a tan?', *BMJ*, 319(7202), pp. 114-116.

Newport 'Solar Simulators'. Available at: <https://www.newport.com/c/solar-simulators>
(Accessed: 06/05/17)

Newsholme, P., Rebelato, E., Abdulkader, F., Krause, M., Carpinelli, A. and Curi, R. (2012) 'Reactive oxygen and nitrogen species generation, antioxidant defenses, and β -cell function: a critical role for amino acids', *Journal of Endocrinology*, 214(1), pp. 11-20.

Nohynek, G.J., Lademann, J., Ribaud, C. and Roberts, M.S. (2007) 'Grey Goo on the Skin? Nanotechnology, Cosmetic and Sunscreen Safety', *Critical Reviews in Toxicology*, 37(3), pp. 251-277.

Nutten, S. (2015) 'Atopic Dermatitis: Global Epidemiology and Risk Factors', *Annals of Nutrition and Metabolism*, 66(suppl 1)(Suppl. 1), pp. 8-16.

Öschlager, V., Schrader, A. and Hockertz, S. (2009) 'Comparison of Primary Human Fibroblasts and Keratinocytes with Immortalized Cell Lines Regarding their Sensitivity to Sodium Dodecyl Sulfate in a Neutral Red Uptake Cytotoxicity Assay', *Arzneimittelforschung*, 59(03), pp. 146-152.

Ong, K.J., MacCormack, T.J., Clark, R.J., Ede, J.D., Ortega, V.A., Felix, L.C., Dang, M.K.M., Ma, G., Fenniri, H., Veinot, J.G.C. and Goss, G.G. (2014) 'Widespread Nanoparticle-Assay Interference: Implications for Nanotoxicity Testing', *PLoS ONE*, 9(3), p. e90650.

P Tucci, G.P., M Agostini, D Dinsdale, I Iavicoli, K Cain, A Finazzi-Agro', G Melino and A Willis (2013) 'Metabolic effects of TiO₂ nanoparticles, a common component of sunscreens and cosmetics, on human keratinocytes', *Cell Death and Disease*, 4.

Pacia, M., Warszynski, P. and Macyk, W. (2014) 'UV and visible light active aqueous titanium dioxide colloids stabilized by surfactants', *Dalton Transactions*, 43(33), pp. 12480-12485.

Pan, Z., Lee, W., Slutsky, L., Clark, R.A., Pernodet, N. and Rafailovich, M.H. (2009) 'Adverse effects of titanium dioxide nanoparticles on human dermal fibroblasts and how to protect cells', *Small*, 5(4), pp. 511-520.

Park, C.-H., Lee, M.J., Ahn, J., Kim, S., Kim, H.H., Kim, K.H., Eun, H.C. and Chung, J.H. (2004) 'Heat Shock-Induced Matrix Metalloproteinase (MMP)-1 and MMP-3 Are Mediated through ERK and JNK Activation and via an Autocrine Interleukin-6 Loop', *Journal of Investigative Dermatology*, 123(6), pp. 1012-1019.

Park, S., Lee, Y.K., Jung, M., Kim, K.H., Chung, N., Ahn, E.-K., Lim, Y. and Lee, K.-H. (2007) 'Cellular toxicity of various inhalable metal nanoparticles on human alveolar epithelial cells', *Inhalation toxicology*, 19(sup1), pp. 59-65.

Parr, R.L., Dakubo, G.D., Crandall, K.A., Maki, J., Reguly, B., Aguirre, A., Wittcock, R., Robinson, K., Alexander, J.S., Birch-Machin, M.A., Abdel-Malak, M., Froberg, M.K., Diamandis, E.P. and

Thayer, R.E. (2006) 'Somatic Mitochondrial DNA Mutations in Prostate Cancer and Normal Appearing Adjacent Glands in Comparison to Age-Matched Prostate Samples without Malignant Histology', *The Journal of Molecular Diagnostics*, 8(3), pp. 312-319.

Parrish, J.A. and Jaenicke, K.F. (1981) 'Action Spectrum for Phototherapy of Psoriasis', *Journal of Investigative Dermatology*, 76(5), pp. 359-362.

Passos, J.F., Saretzki, G., Ahmed, S., Nelson, G., Richter, T., Peters, H., Wappler, I., Birket, M.J., Harold, G., Schaeuble, K., Birch-Machin, M.A., Kirkwood, T.B.L. and von Zglinicki, T. (2007) 'Mitochondrial Dysfunction Accounts for the Stochastic Heterogeneity in Telomere-Dependent Senescence', *PLoS Biology*, 5(5), p. e110.

Patlevič, P., Vašková, J., Švorc, P., Vaško, L. and Švorc, P. (2016) 'Reactive oxygen species and antioxidant defense in human gastrointestinal diseases', *Integrative Medicine Research*, 5(4), pp. 250-258.

Pawlak, M.T., Bui, M., Amir, M., Burkhardt, D.L., Chen, A.K. and Dellavalle, R.P. (2012) 'Legislation restricting access to indoor tanning throughout the world', *Archives of dermatology*, 148(9), pp. 1006-1012.

Peira, E., Turci, F., Corazzari, I., Chirio, D., Battaglia, L., Fubini, B. and Gallarate, M. (2014) 'The influence of surface charge and photo-reactivity on skin-permeation enhancer property of nano-TiO₂ in ex vivo pig skin model under indoor light', *International Journal of Pharmaceutics*, 467(1–2), pp. 90-99.

Penta, J.S., Johnson, F.M., Wachsman, J.T. and Copeland, W.C. (2001) 'Mitochondrial DNA in human malignancy', *Mutat Res*, 488(2), pp. 119-33.

Pérez, V.I., Buffenstein, R., Masamsetti, V., Leonard, S., Salmon, A.B., Mele, J., Andziak, B., Yang, T., Edrey, Y., Friguet, B., Ward, W., Richardson, A. and Chaudhuri, A. (2009) 'Protein stability and resistance to oxidative stress are determinants of longevity in the longest-living rodent, the naked mole-rat', *Proceedings of the National Academy of Sciences*, 106(9), pp. 3059-3064.

Petersen, E.J., Henry, T.B., Zhao, J., MacCuspie, R.I., Kirschling, T.L., Dobrovolskaia, M.A., Hackley, V., Xing, B. and White, J.C. (2014) 'Identification and avoidance of potential artifacts

and misinterpretations in nanomaterial ecotoxicity measurements', *Environ. Sci. Technol.*, 48(8), pp. 4226-4246.

Petit-Frère, C., Capulas, E., Lyon, D.A., Norbury, C.J., Lowe, J.E., Clingen, P.H., Riballo, E., Green, M.H.L. and Arlett, C.F. (2000) 'Apoptosis and cytokine release induced by ionizing or ultraviolet B radiation in primary and immortalized human keratinocytes', *Carcinogenesis*, 21(6), pp. 1087-1095.

Phillips, T.J., Bhawan, J., Yaar, M., Bello, Y., LoPiccolo, D. and Nash, J.F. (2000) 'Effect of daily versus intermittent sunscreen application on solar simulated UV radiation-induced skin response in humans', *Journal of the American Academy of Dermatology*, 43(4), pp. 610-618.

Piazena, H., Pittermann, W., Müller, W., Jung, K., Kelleher, D.K., Herrling, T., Meffert, P., Uebelhack, R. and Kietzmann, M. (2014) 'Effects of water-filtered infrared-A and of heat on cell death, inflammation, antioxidative potential and of free radical formation in viable skin – First results', *Journal of Photochemistry and Photobiology B: Biology*, 138, pp. 347-354.

Picton, O. (2013) 'The complexities of complexion: a cultural geography of skin colour and beauty products', *Geography*, 98, p. 85.

Pinheiro, T., Pallon, J., Alves, L., Veríssimo, A., Filipe, P., Silva, J. and Silva, R. (2007) 'The influence of corneocyte structure on the interpretation of permeation profiles of nanoparticles across skin', *Nuclear Instruments and Methods in Physics Research Section B: Beam Interactions with Materials and Atoms*, 260(1), pp. 119-123.

Pissavini, M. and Diffey, B. (2013) 'The likelihood of sunburn in sunscreen users is disproportionate to the SPF', *Photodermatology, photoimmunology & photomedicine*, 29(3), pp. 111-115.

Pittayapruerk, P., Meephansan, J., Prapapan, O., Komine, M. and Ohtsuki, M. (2016) 'Role of Matrix Metalloproteinases in Photoaging and Photocarcinogenesis', *International Journal of Molecular Sciences*, 17(6), p. 868.

Polefka, T.G., Meyer, T.A., Agin, P.P. and Bianchini, R.J. (2012) 'Effects of Solar Radiation on the Skin', *Journal of Cosmetic Dermatology*, 11(2), pp. 134-143.

Prasad, R.Y., Chastain, P.D., Nikolaishvili-Feinberg, N., Smeester, L., Kaufmann, W.K. and Fry, R.C. (2012) 'Titanium dioxide nanoparticles activate the ATM-Chk2 DNA damage response in human dermal fibroblasts', *Nanotoxicology*, 7(6), pp. 1111-1119.

Prasad, R.Y., Chastain, P.D., Nikolaishvili-Feinberg, N., Smeester, L., Kaufmann, W.K. and Fry, R.C. (2013) 'Titanium dioxide nanoparticles activate the ATM-Chk2 DNA damage response in human dermal fibroblasts', *Nanotoxicology*, 7(6), pp. 1111-1119.

Proksch, E., Brandner, J.M. and Jensen, J.-M. (2008) 'The skin: an indispensable barrier', *Experimental Dermatology*, 17(12), pp. 1063-1072.

Promega (2016) 'Technical Manual ROS-Glo™ H2O2 Assay'. Available at: <https://www.newport.com/c/solar-simulators>

(Accessed: 25/07/2017)

Rajapakse, K., Drobne, D., Kastelec, D. and Marinsek-Logar, R. (2013) 'Experimental evidence of false-positive Comet test results due to TiO₂ particle–assay interactions', *Nanotoxicology*, 7(5), pp. 1043-1051.

Rajapakse, K., Drobne, D., Valant, J., Vodovnik, M., Levart, A. and Marinsek-Logar, R. (2012) 'Acclimation of *Tetrahymena thermophila* to bulk and nano-TiO₂ particles by changes in membrane fatty acids saturation', *Journal of hazardous materials*, 221, pp. 199-205.

Randhawa, M., Seo, I., Liebel, F., Southall, M.D., Kollias, N. and Ruvolo, E. (2015) 'Visible Light Induces Melanogenesis in Human Skin through a Photoadaptive Response', *PLOS ONE*, 10(6), p. e0130949.

Rastogi, R.P., Richa, Kumar, A., Tyagi, M.B. and Sinha, R.P. (2010) 'Molecular Mechanisms of Ultraviolet Radiation-Induced DNA Damage and Repair', *Journal of Nucleic Acids*,

Ray, A.J., Turner, R., Nikaido, O., Rees, J.L. and Birch-Machin, M.A. (2000) 'The Spectrum of Mitochondrial DNA Deletions is a Ubiquitous Marker of Ultraviolet Radiation Exposure in Human Skin', *Journal of Investigative Dermatology*, 115(4), pp. 674-679.

Raychaudhuri, S. and Farber, E. (2001) 'The prevalence of psoriasis in the world', *Journal of the European Academy of Dermatology and Venereology*, 15(1), pp. 16-17.

Reeves, J.F., Davies, S.J., Dodd, N.J. and Jha, A.N. (2008) 'Hydroxyl radicals (OH) are associated with titanium dioxide (TiO₂) nanoparticle-induced cytotoxicity and oxidative DNA damage in fish cells', *Mutation Research/Fundamental and Molecular Mechanisms of Mutagenesis*, 640(1), pp. 113-122.

Rinnerthaler, M., Bischof, J., Streubel, M.K., Trost, A. and Richter, K. (2015) 'Oxidative Stress in Aging Human Skin', *Biomolecules*, 5(2), pp. 545-589.

Robert, C., Bonnet, M., Marques, S., Numa, M. and Doucet, O. (2015) 'Low to moderate doses of infrared A irradiation impair extracellular matrix homeostasis of the skin and contribute to skin photodamage', *Skin pharmacology and physiology*, 28(4), pp. 196-204.

Rodrigues, A.M., Sniehotta, F.F., Birch-Machin, M.A. and Araujo-Soares, V. (2017) 'Aware, motivated and striving for a 'safe tan': an exploratory mixed-method study of sun-protection during holidays', *Health Psychology and Behavioral Medicine*, 5(1), pp. 276-298.

Rodríguez, E., Valbuena, M.C., Rey, M. and Porrás de Quintana, L. (2006) 'Causal agents of photoallergic contact dermatitis diagnosed in the national institute of dermatology of Colombia', *Photodermatology, Photoimmunology & Photomedicine*, 22(4), pp. 189-192.

Rothfuss, O., Gasser, T. and Patenge, N. (2010) 'Analysis of differential DNA damage in the mitochondrial genome employing a semi-long run real-time PCR approach', *Nucleic Acids Research*, 38(4), pp. e24-e24.

Rouse, J.G., Yang, J., Ryman-Rasmussen, J.P., Barron, A.R. and Monteiro-Riviere, N.A. (2006) 'Effects of Mechanical Flexion on the Penetration of Fullerene Amino Acid-Derivatized Peptide Nanoparticles through Skin', *Nano Letters*, 7(1), pp. 155-160.

Sadrieh, N., Wokovich, A.M., Gopee, N.V., Zheng, J., Haines, D., Parmiter, D., Siitonen, P.H., Cozart, C.R., Patri, A.K. and McNeil, S.E. (2010) 'Lack of significant dermal penetration of titanium dioxide from sunscreen formulations containing nano- and submicron-size TiO₂ particles', *Toxicol Sci*, 115.

Sales, L. (2013) 'Testing reveals potentially dangerous free radical producing ingredients in sunscreen and cosmetics', *Chain Reaction*, (117), p. 17.

Sambandan, D.R. and Ratner, D. (2011) 'Sunscreens: an overview and update', *Journal of the American Academy of Dermatology*, 64(4), pp. 748-758.

Saqib, Q., Al-Khedhairi, A.A., Siddiqui, M.A., Abou-Tarboush, F.M., Azam, A. and Musarrat, J. (2012) 'Titanium dioxide nanoparticles induced cytotoxicity, oxidative stress and DNA damage in human amnion epithelial (WISH) cells', *Toxicol In Vitro*, 26.

Saqib Q, A.-K.A., Siddiqui MA, Abou-Tarboush FM, Azam A, Musarrat J. (2012) 'Titanium dioxide nanoparticles induced cytotoxicity, oxidative stress and DNA damage in human amnion epithelial (WISH) cells.', 26, pp. 351–361.

Sathya, T., Vardhini, N. and Balakrishnamurthy, P. (2010) 'REVOLUTION OF 'NANO' IN IN-VITRO GENETIC TOXICOLOGY', *Journal of Cell and Tissue Research*, 10(3), p. 2389.

SCCNFP (2000) 'OPINION OF THE SCIENTIFIC COMMITTEE ON COSMETIC PRODUCTS AND NON-FOOD PRODUCTS INTENDED FOR CONSUMERS CONCERNING TITANIUM DIOXIDE Available at: http://ec.europa.eu/health/ph_risk/committees/sccp/documents/out135_en.pdf (Accessed 27/07/2017)

SCCP, S.C.o.C.S. (2007) 'Opinion on Titanium Dioxide (Nano form)', *European Commisision Available at:* https://ec.europa.eu/health/ph_risk/committees/04_sccp/docs/sccp_o_099.pdf Accessed (26/07/2017)

SCCP, S.C.o.C.S. (2013) 'Opinion on Titanium Dioxide (Nano form)', *European Commisision Available at:* https://ec.europa.eu/health/scientific_committees/consumer_safety/docs/sccs_o_136.pdf Accessed (26/07/2017)

Schalka, S. and Reis, V.M.S.d. (2011) 'Fator de proteção solar: significado e controvérsias', *Anais Brasileiros de Dermatologia*, 86, pp. 507-515.

Schaefer, H., & Redelmeier, T. E. (1996) 'Skin barrier: principles of percutaneous absorption. *Basel, Karger.*

Scheffler, I.E. (2007) 'Structure and Morphology. Integration into the Cell', in *Mitochondria*. John Wiley & Sons, Inc., pp. 18-59.

Schieke, S.M., Schroeder, P. and Krutmann, J. (2003) 'Cutaneous effects of infrared radiation: from clinical observations to molecular response mechanisms', *Photodermatology, Photoimmunology & Photomedicine*, 19(5), pp. 228-234.

Schmook, F.P., Meingassner, J.G. and Billich, A. (2001) 'Comparison of human skin or epidermis models with human and animal skin in in-vitro percutaneous absorption', *International journal of pharmaceutics*, 215(1), pp. 51-56.

Schroeder, P., Calles, C., Benesova, T., Macaluso, F. and Krutmann, J. (2010) 'Photoprotection beyond Ultraviolet Radiation – Effective Sun Protection Has to Include Protection against Infrared A Radiation-Induced Skin Damage', *Skin Pharmacology and Physiology*, 23(1), pp. 15-17.

Schroeder, P., Haendeler, J. and Krutmann, J. (2008) 'The role of near infrared radiation in photoaging of the skin', *Experimental Gerontology*, 43(7), pp. 629-632.

Schroeder, P. and Krutmann, J. (2017) 'Infrared A-Induced Skin Aging', in Farage, M.A., Miller, K.W. and Maibach, H.I. (eds.) *Textbook of Aging Skin*. Berlin, Heidelberg: Springer Berlin Heidelberg, pp. 695-700.

Schroeder, P., Pohl, C., Calles, C., Marks, C., Wild, S. and Krutmann, J. (2007) 'Cellular response to infrared radiation involves retrograde mitochondrial signaling', *Free Radical Biology and Medicine*, 43(1), pp. 128-135.

Schulz, J., Hohenberg, H., Pflücker, F., Gärtner, E., Will, T., Pfeiffer, S., Wepf, R., Wendel, V., Gers-Barlag, H. and Wittern, K.-P. (2002) 'Distribution of sunscreens on skin', *Advanced drug delivery reviews*, 54, pp. S157-S163.

Selim Uzunoglu, B.K., Harika Atmaca, Asli Kisim, Canfeza Sezgin, Bulent Karabulut, and Uslu, a.R. (2010) 'Comparison of XTT and Alamar blue assays in the assessment of the viability of various human cancer cell lines by AT-101 (-/- gossypol)', 20, 8, pp. 482–486.

Senzui, M., Tamura, T., Miura, K., Ikarashi, Y., Watanabe, Y. and Fujii, M. (2010) 'Study on penetration of titanium dioxide (TiO₂) nanoparticles into intact and damaged skin in vitro', *The Journal of toxicological sciences*, 35(1), pp. 107-113.

Seo, M.-D., Kang, T.J., Lee, C.H., Lee, A.-Y. and Noh, M. (2012) 'HaCaT Keratinocytes and Primary Epidermal Keratinocytes Have Different Transcriptional Profiles of Cornified Envelope-Associated Genes to T Helper Cell Cytokines', *Biomolecules & Therapeutics*, 20(2), pp. 171-176.

Serpone, N. (2006) 'Is the band gap of pristine TiO₂ narrowed by anion-and cation-doping of titanium dioxide in second-generation photocatalysts?'. ACS Publications.

Serpone, N., Dondi, D. and Albini, A. (2007) *Inorganic and organic UV filters: Their role and efficacy in sunscreens and sun care product*. *Inorganica Chimica Acta*, 360 (3), pp. 794-802.

Serrano, M.-A., Cañada, J. and Moreno, J.C. (2012) 'Solar UV exposure of children in a summer school in Valencia, Spain', *International Journal of Biometeorology*, 56(2), pp. 371-377.

Setyawati, M.I., Khoo, P.K.S., Eng, B.H., Xiong, S., Zhao, X., Das, G.K., Tan, T.T.Y., Loo, J.S.C., Leong, D.T. and Ng, K.W. (2013) 'Cytotoxic and genotoxic characterization of titanium dioxide, gadolinium oxide, and poly (lactic-co-glycolic acid) nanoparticles in human fibroblasts', *Journal of Biomedical Materials Research Part A*, 101(3), pp. 633-640.

Shadel GS, C.D. (1997) 'Mitochondrial DNA maintenance in vertebrates. ', *Annu Rev Biochem* 66: 409–435.

Sherratt, M.J., Bayley, C.P., Reilly, S.M., Gibbs, N.K., Griffiths, C.E.M. and Watson, R.E.B. (2010) 'Low-dose ultraviolet radiation selectively degrades chromophore-rich extracellular matrix components', *The Journal of Pathology*, 222(1), pp. 32-40.

Shi, H., Magaye, R., Castranova, V. and Zhao, J. (2013) 'Titanium dioxide nanoparticles: a review of current toxicological data', *Particle and Fibre Toxicology*, 10(1), p. 15.

Shokolenko, I., Venediktova, N., Bochkareva, A., Wilson, G.L. and Alexeyev, M.F. (2009) 'Oxidative stress induces degradation of mitochondrial DNA', *Nucleic Acids Research*, 37(8), pp. 2539-2548.

Shukla, R.K., Kumar, A., Pandey, A.K., Singh, S.S. and Dhawan, A. (2011) 'Titanium dioxide nanoparticles induce oxidative stress-mediated apoptosis in human keratinocyte cells', *Journal of biomedical nanotechnology*, 7(1), pp. 100-101.

Shukla, R.K., Sharma, V., Pandey, A.K., Singh, S., Sultana, S. and Dhawan, A. (2011) 'ROS-mediated genotoxicity induced by titanium dioxide nanoparticles in human epidermal cells', *Toxicology in Vitro*, 25(1), pp. 231-241.

Simões, M.C.F., Sousa, J.J.S. and Pais, A.A.C.C. (2015) 'Skin cancer and new treatment perspectives: A review', *Cancer Letters*, 357(1), pp. 8-42.

Simon-Deckers, A., Gouget, B., Mayne-L'Hermite, M., Herlin-Boime, N., Reynaud, C. and Carriere, M. (2008) 'In vitro investigation of oxide nanoparticle and carbon nanotube toxicity and intracellular accumulation in A549 human pneumocytes', *Toxicology*, 253(1), pp. 137-146.

Singh, N.P., McCoy, M.T., Tice, R.R. and Schneider, E.L. (1988) 'A simple technique for quantitation of low levels of DNA damage in individual cells', *Exp Cell Res*, 175(1), pp. 184-91.

Sinha, R.P. and Häder, D.-P. (2002) 'UV-induced DNA damage and repair: a review', *Photochemical & Photobiological Sciences*, 1(4), pp. 225-236.

SkinCancerFoundation (2016). Available at: <http://www.skincancer.org/prevention/sun-protection/sunscreen> (Accessed 25/07/2017).

Sklar, L.R., Almutawa, F., Lim, H.W. and Hamzavi, I. (2013) 'Effects of ultraviolet radiation, visible light, and infrared radiation on erythema and pigmentation: a review', *Photochemical & Photobiological Sciences*, 12(1), pp. 54-64.

Skocaj, M., Filipic, M., Petkovic, J. and Novak, S. (2011) 'Titanium dioxide in our everyday life; is it safe?', *Radiology and Oncology*, 45(4), pp. 227-247.

Smijs, T.G. and Pavel, S. (2011) 'Titanium dioxide and zinc oxide nanoparticles in sunscreens: focus on their safety and effectiveness', *Nanotechnology, science and applications*, 4, p. 95.

Smith, C.C., O'donovan, M.R. and Martin, E.A. (2006) 'hOGG1 recognizes oxidative damage using the comet assay with greater specificity than FPG or ENDOIII', *Mutagenesis*, 21(3), pp. 185-190.

Stankovich, S. (2007) 'Synthesis of graphene-based nanosheets via chemical reduction of exfoliated graphite oxide. Carbon'. pp. 1558-1564.

Stanton, W.R., Janda, M., Baade, P.D. and Anderson, P. (2004) 'Primary prevention of skin cancer: a review of sun protection in Australia and internationally', *Health promotion international*, 19(3), pp. 369-378.

Stone, V., Johnston, H. and Schins, R.P. (2009) 'Development of in vitro systems for nanotoxicology: methodological considerations', *Critical reviews in toxicology*, 39(7), pp. 613-626.

Stueker, O., Ortega, V.A., Goss, G.G. and Stepanova, M. (2014) 'Understanding Interactions of Functionalized Nanoparticles with Proteins: A Case Study on Lactate Dehydrogenase', *Small*, 10(10), pp. 2006-2021.

Suzuki, H., Toyooka, T. and Ibuki, Y. (2007) 'Simple and easy method to evaluate uptake potential of nanoparticles in mammalian cells using a flow cytometric light scatter analysis', *Environmental science & technology*, 41(8), pp. 3018-3024.

Swalwell, H., Latimer, J., Haywood, R.M. and Birch-Machin, M.A. (2012) 'Investigating the role of melanin in UVA/UVB- and hydrogen peroxide-induced cellular and mitochondrial ROS production and mitochondrial DNA damage in human melanoma cells', *Free Radical Biology and Medicine*, 52(3), pp. 626-634.

Takeda, K., Suzuki, K., Ishihara, A., Kubo-Irie, M., Fujimoto, R., Tabata, M., Oshio, S., Nihei, Y., Ihara, T. and Sugamata, M. (2009) 'Nanoparticles Transferred from Pregnant Mice to Their Offspring Can Damage the Genital and Cranial Nerve Systems', *J Heal Sci*, 55.

Tanaka, Y. (2012) *Impact of near-infrared radiation in dermatology*.

Available at: <http://www.cnki.com.cn/Article/CJFDTotol-PFZZ201203003.htm>

(Accessed: 09/08/2017)

Tanaka, Y. and Gale, L. (2015) *Protection from Near-Infrared to Prevent Skin Damage*.

Teegarden, J.G., Hinderliter, P.M., Orr, G., Thrall, B.D. and Pounds, J.G. (2007) 'Particokinetics in vitro: dosimetry considerations for in vitro nanoparticle toxicity assessments', *Toxicol Sci*, 95(2), pp. 300-12.

Teo, B.S.X., Basri, M., Zakaria, M.R.S., Salleh, A.B., Rahman, R.N.Z.R.A. and Rahman, M.B.A. (2010) 'A potential tocopherol acetate loaded palm oil esters-in-water nanoemulsions for nanocosmeceuticals', *Journal of Nanobiotechnology*, 8(1), p. 4.

Tetz, L.M., Kamau, P.W., Cheng, A.A., Meeker, J.D. and Loch-Carusio, R. (2013) 'Troubleshooting the dichlorofluorescein assay to avoid artifacts in measurement of toxicant-stimulated cellular production of reactive oxidant species', *Journal of pharmacological and toxicological methods*, 67(2), pp. 56-60.

Theogaraj, E., Riley, S., Hughes, L., Maier, M. and Kirkland, D. (2007) 'An investigation of the photo-clastogenic potential of ultrafine titanium dioxide particles', *Mutation Research/Genetic Toxicology and Environmental Mutagenesis*, 634(1), pp. 205-219.

Tinkle, S.S., Antonini, J.M., Rich, B.A., Roberts, J.R., Salmen, R., DePree, K. and Adkins, E.J. (2003) 'Skin as a route of exposure and sensitization in chronic beryllium disease', *Environmental health perspectives*, 111(9), p. 1202.

Traynor, M.J., Wilkinson, S.C. and Williams, F.M. (2008) 'Metabolism of butoxyethanol in excised human skin in vitro', *Toxicology letters*, 177(3), pp. 151-155.

Trifunovic, A. and Larsson, N.G. (2008) 'Mitochondrial dysfunction as a cause of ageing', *Journal of Internal Medicine*, 263(2), pp. 167-178.

Trouiller, B., Reliene, R., Westbrook, A., Solaimani, P. and Schiestl, R.H. (2009) 'Titanium dioxide nanoparticles induce DNA damage and genetic instability in vivo in mice', *Cancer research*, 69(22), pp. 8784-8789.

Tucci, P., Porta, G., Agostini, M., Dinsdale, D., Iavicoli, I., Cain, K., Finazzi-Agró, A., Melino, G. and Willis, A. (2013) 'Metabolic effects of TiO₂ nanoparticles, a common component of sunscreens and cosmetics, on human keratinocytes', *Cell Death & Disease*, 4(3), p. e549.

Turci, F., Peira, E., Corazzari, I., Fenoglio, I., Trotta, M. and Fubini, B. (2013) 'Crystalline phase modulates the potency of nanometric TiO₂ to adhere to and perturb the stratum corneum of porcine skin under indoor light', *Chemical research in toxicology*, 26(10), pp. 1579-1590.

Turrens, J.F. (2003) 'Mitochondrial formation of reactive oxygen species', *The Journal of Physiology*, 552(2), pp. 335-344.

Utrillas, M.P., Martínez-Lozano, J.A., Esteve, A.R., Serrano, D. and Marín, M.J. (2012) 'UV Index experimental values on vertical surfaces', *International Journal of Climatology*, 32(13), pp. 2066-2072.

Vaddi, H., Ho, P. and Chan, S. (2002) 'Terpenes in propylene glycol as skin-penetration enhancers: Permeation and partition of haloperidol, fourier transform infrared spectroscopy, and differential scanning calorimetry', *Journal of pharmaceutical sciences*, 91(7), pp. 1639-1651.

- Vamanu, C.I., Cimpan, M.R., Høi, P.J., Sørnes, S., Lie, S.A. and Gjerdet, N.R. (2008) 'Induction of cell death by TiO₂ nanoparticles: studies on a human monoblastoid cell line', *Toxicology in Vitro*, 22(7), pp. 1689-1696.
- Van Gele, M., Geusens, B., Brochez, L., Speeckaert, R. and Lambert, J. (2011) 'Three-dimensional skin models as tools for transdermal drug delivery: challenges and limitations', *Expert opinion on drug delivery*, 8(6), pp. 705-720.
- Vanicek, K., Frei, T., Litynska, Z. and Schmalwieser, A. (2000) 'UV-Index for the Public', *Publication of the European Communities, Brussels, Belgium*.
- Venegas, V., Wang, J., Dimmock, D. and Wong, L.J. (2011) 'Real-time quantitative PCR analysis of mitochondrial DNA content', *Current protocols in human genetics*, pp. 19.7. 1-19.7. 12.
- Vevers, W.F. and Jha, A.N. (2008) 'Genotoxic and cytotoxic potential of titanium dioxide (TiO₂) nanoparticles on fish cells in vitro', *Ecotoxicology*, 17(5), pp. 410-420.
- Videira, I.F.d.S., Moura, D.F.L. and Magina, S. (2013) 'Mechanisms regulating melanogenesis()', *Anais brasileiros de dermatologia*, 88(1), pp. 76-83.
- Viegas, V.A. (2014) *Characterisation of a Novel Flexing Diffusion Cell (CutaFlex™) for Assessing Dermal Exposure to Nanoparticles* [Online]. Available at: <http://hdl.handle.net/2299/14838> (Accessed: 30/07/2017).
- Virkutyte, J., Jegatheesan, V. and Varma, R.S. (2012) 'Visible light activated TiO₂/microcrystalline cellulose nanocatalyst to destroy organic contaminants in water', *Bioresour Technol*, 113, pp. 288-93.
- Wahie, S., Lloyd, J.J. and Farr, P.M. (2007) 'Sunscreen ingredients and labelling: a survey of products available in the UK', *Clinical and Experimental Dermatology*, 32(4), pp. 359-364.
- Wan, M.T. and Lin, J.Y. (2014) 'Current evidence and applications of photodynamic therapy in dermatology', *Clinical, Cosmetic and Investigational Dermatology*, 7, pp. 145-163.
- Wan, R., Mo, Y., Feng, L., Chien, S., Tollerud, D.J. and Zhang, Q. (2012) 'DNA damage caused by metal nanoparticles: involvement of oxidative stress and activation of ATM', *Chemical research in toxicology*, 25(7), pp. 1402-1411.
- Wang, G., Wang, H., Ling, Y., Tang, Y., Yang, X., Fitzmorris, R.C., Wang, C., Zhang, J.Z. and Li, Y. (2011) 'Hydrogen-Treated TiO₂ Nanowire Arrays for Photoelectrochemical Water Splitting', *Nano Letters*, 11(7), pp. 3026-3033.
- Wang, J.J., Sanderson, B.J. and Wang, H. (2007) 'Cyto- and genotoxicity of ultrafine TiO₂ particles in cultured human lymphoblastoid cells', *Mutat Res*, 628.
- Wang, P., Henning, S.M. and Heber, D. (2010) 'Limitations of MTT and MTS-Based Assays for Measurement of Antiproliferative Activity of Green Tea Polyphenols', *PLoS ONE*, 5(4), p. e10202.

- Wang, S.Q., Stanfield, J.W. and Osterwalder, U. (2008) 'In vitro assessments of UVA protection by popular sunscreens available in the United States', *Journal of the American Academy of Dermatology*, 59(6), pp. 934-942.
- Wang, S.Q. and Tooley, I.R. (2011) 'Photoprotection in the Era of Nanotechnology', *Seminars in Cutaneous Medicine and Surgery*, 30(4), pp. 210-213.
- Warheit, D.B., Hoke, R.A., Finlay, C., Donner, E.M., Reed, K.L. and Sayes, C.M. (2007) 'Development of a base set of toxicity tests using ultrafine TiO₂ particles as a component of nanoparticle risk management', *Toxicology letters*, 171(3), pp. 99-110.
- Weir, A., Westerhoff, P., Fabricius, L., Hristovski, K. and von Goetz, N. (2012) 'Titanium Dioxide Nanoparticles in Food and Personal Care Products', *Environmental Science & Technology*, 46(4), pp. 2242-2250.
- Wick, P., Malek, A., Manser, P., Meili, D., Maeder-Althaus, X., Diener, L., Diener, P.A., Zisch, A., Krug, H.F. and von Mandach, U. (2010) 'Barrier capacity of human placenta for nanosized materials', *Environ Health Perspect*, 118.
- Widodo, N., Shah, N., Priyandoko, D., Ishii, T., Kaul, S.C. and Wadhwa, R. (2009) 'Deceleration of senescence in normal human fibroblasts by withanone extracted from ashwagandha leaves', *Journals of Gerontology Series A: Biomedical Sciences and Medical Sciences*, 64(10), pp. 1031-1038.
- Wilkinson, S.C. (2008) 'Biochemistry of the Skin', in *Principles and Practice of Skin Toxicology*. John Wiley & Sons, Ltd, pp. 17-49.
- Wills, J.W., Hondow, N., Thomas, A.D., Chapman, K.E., Fish, D., Maffei, T.G., Penny, M.W., Brown, R.A., Jenkins, G.J., Brown, A.P., White, P.A. and Doak, S.H. (2016) 'Genetic toxicity assessment of engineered nanoparticles using a 3D in vitro skin model (EpiDerm)', *Part Fibre Toxicol*, 13(1), p. 50.
- Wokovich, A., Tyner, K., Doub, W., Sadrieh, N. and Buhse, L.F. (2009) 'Particle size determination of sunscreens formulated with various forms of titanium dioxide', *Drug development and industrial pharmacy*, 35(10), pp. 1180-1189.
- Wong, T. and Orton, D. (2011) 'Sunscreen allergy and its investigation', *Clinics in Dermatology*, 29(3), pp. 306-310.
- Woodruff, R.S., Li, Y., Yan, J., Bishop, M., Jones, M.Y., Watanabe, F., Biris, A.S., Rice, P., Zhou, T. and Chen, T. (2012) 'Genotoxicity evaluation of titanium dioxide nanoparticles using the Ames test and Comet assay', *J Appl Toxicol*, 32.
- Wu, J., Liu, W., Xue, C., Zhou, S., Lan, F., Bi, L., Xu, H., Yang, X. and Zeng, F.-D. (2009) 'Toxicity and penetration of TiO₂ nanoparticles in hairless mice and porcine skin after subchronic dermal exposure', *Toxicology letters*, 191(1), pp. 1-8.

Wulf, H.C., Heydenreich, J. and Philipsen, P.A. (2010) 'Variables in full-body ultraviolet B treatment of skin diseases', *Photodermatology, Photoimmunology & Photomedicine*, 26(3), pp. 165-169.

Xia, T., Kovochich, M., Brant, J., Hotze, M., Sempf, J., Oberley, T., Sioutas, C., Yeh, J.I., Wiesner, M.R. and Nel, A.E. (2006) 'Comparison of the abilities of ambient and manufactured nanoparticles to induce cellular toxicity according to an oxidative stress paradigm', *Nano letters*, 6(8), pp. 1794-1807.

Xu, A., Chai, Y., Nohmi, T. and Hei, T.K. (2009) 'Genotoxic responses to titanium dioxide nanoparticles and fullerene in gpt delta transgenic MEF cells', *Particle and Fibre Toxicology*, 6(1), p. 3.

Xu, J., Futakuchi, M., Iigo, M., Fukamachi, K., Alexander, D.B., Shimizu, H., Sakai, Y., Tamano, S., Furukawa, F., Uchino, T., Tokunaga, H., Nishimura, T., Hirose, A., Kanno, J. and Tsuda, H. (2010) 'Involvement of macrophage inflammatory protein 1 α (MIP1 α) in promotion of rat lung and mammary carcinogenic activity of nanoscale titanium dioxide particles administered by intra-pulmonary spraying', *Carcinogenesis*, 31(5), pp. 927-935.

Yanti, Madriena and Ali, S. (2017) 'Cosmeceutical Effects of Galactomannan Fraction from *Arenga pinnata* Fruits In vitro', *Pharmacognosy Research*, 9(1), pp. 39-45.

Yarosh, D.B., O'Connor, A., Alas, L., Potten, C. and Wolf, P. (1999) 'Photoprotection by Topical DNA Repair Enzymes: Molecular Correlates of Clinical Studies', *Photochemistry and Photobiology*, 69(2), pp. 136-140.

Yoshiura, Y., Izumi, H., Oyabu, T., Hashiba, M., Kambara, T., Mizuguchi, Y., Lee, B.W., Okada, T., Tomonaga, T. and Myojo, T. (2015) 'Pulmonary toxicity of well-dispersed titanium dioxide nanoparticles following intratracheal instillation', *Journal of Nanoparticle Research*, 17(6), p. 241.

Yuan, Y., Ding, J., Xu, J., Deng, J. and Guo, J. (2010) 'TiO₂ nanoparticles co-doped with silver and nitrogen for antibacterial application', *J Nanosci Nanotechnol*, 10.

Yuki, T., Hachiya, A., Kusaka, A., Sriwiriyanont, P., Visscher, M.O., Morita, K., Muto, M., Miyachi, Y., Sugiyama, Y. and Inoue, S. (2011) 'Characterization of tight junctions and their disruption by UVB in human epidermis and cultured keratinocytes', *Journal of Investigative Dermatology*, 131(3), pp. 744-752.

Zhang, L. and Monteiro-Riviere, N. (2008) 'Assessment of quantum dot penetration into intact, tape-stripped, abraded and flexed rat skin', *Skin pharmacology and physiology*, 21(3), pp. 166-180.

Zhang, L. and Monteiro-Riviere, N. (2008) 'Assessment of quantum dot penetration into intact, tape-stripped, abraded and flexed rat skin', *Skin pharmacology and physiology*, 21(3), pp. 166-180.

Zhao, J., Bowman, L., Zhang, X., Vallyathan, V., Young, S.-H., Castranova, V. and Ding, M. (2009) 'Titanium dioxide (TiO₂) nanoparticles induce JB6 cell apoptosis through activation of the

caspase-8/Bid and mitochondrial pathways', *Journal of Toxicology and Environmental Health, Part A*, 72(19), pp. 1141-1149.

Zijno, A., De Angelis, I., De Berardis, B., Andreoli, C., Russo, M.T., Pietraforte, D., Scorza, G., Degan, P., Ponti, J. and Rossi, F. (2015) 'Different mechanisms are involved in oxidative DNA damage and genotoxicity induction by ZnO and TiO₂ nanoparticles in human colon carcinoma cells', *Toxicology in Vitro*, 29(7), pp. 1503-1512.

Appendix

Beyond UV Protection

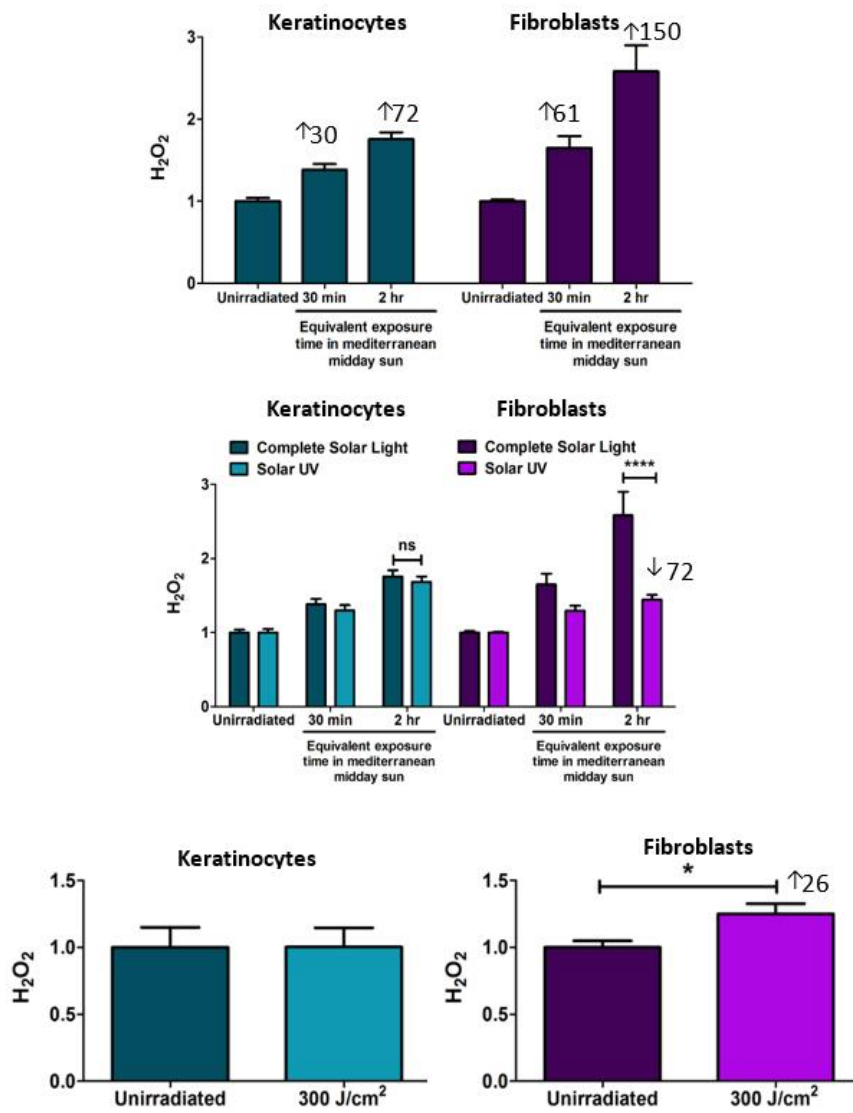
In-Cosmetics, Paris, 2016

Ian R Tooley, Bhaven Chavan, Robert Sayer,
Mark A Birch-Machin & Laura Hudson
Croda Europe Ltd & Newcastle University

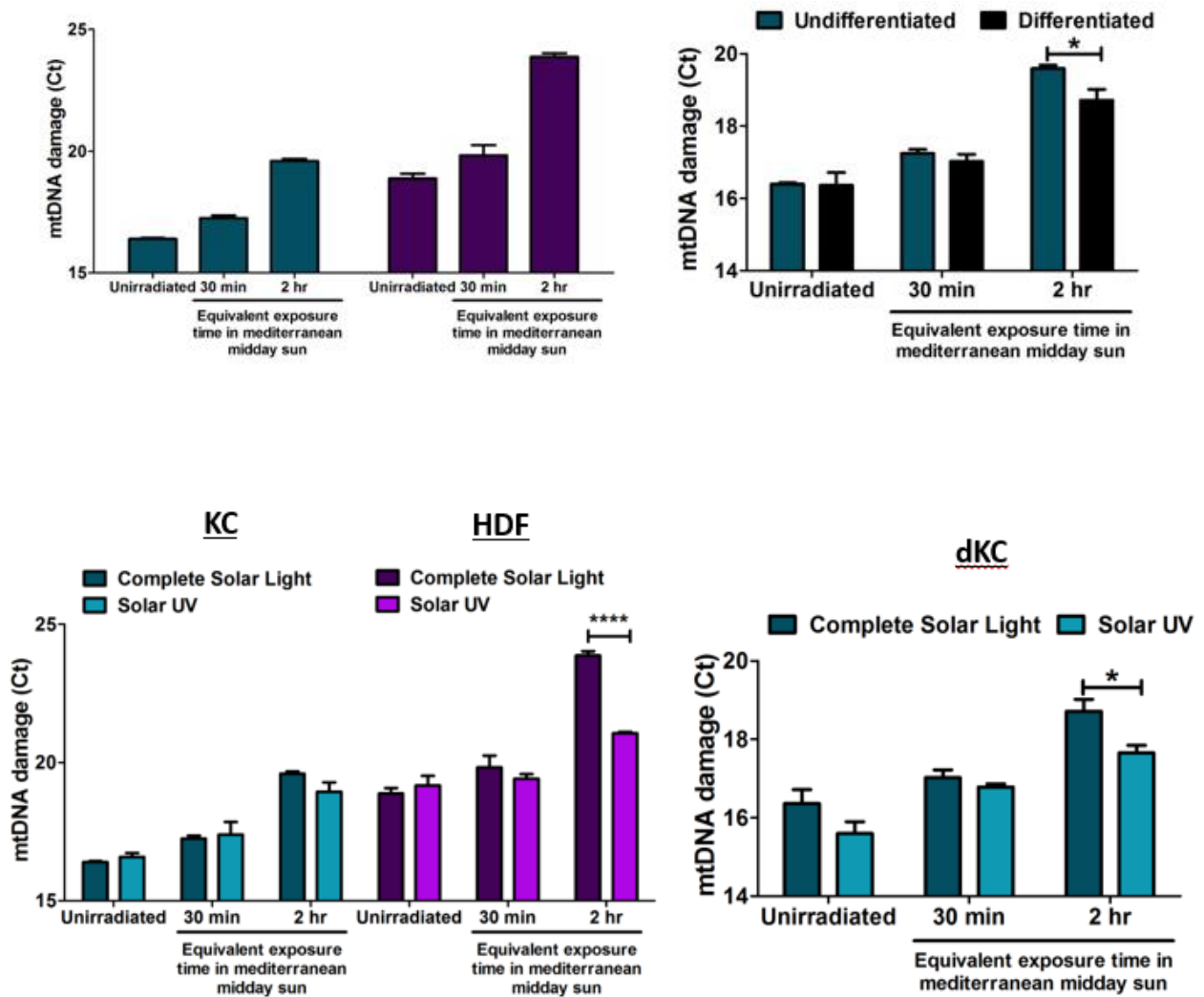
Innovation you can build on™

CRODA

Appendix Figure 1

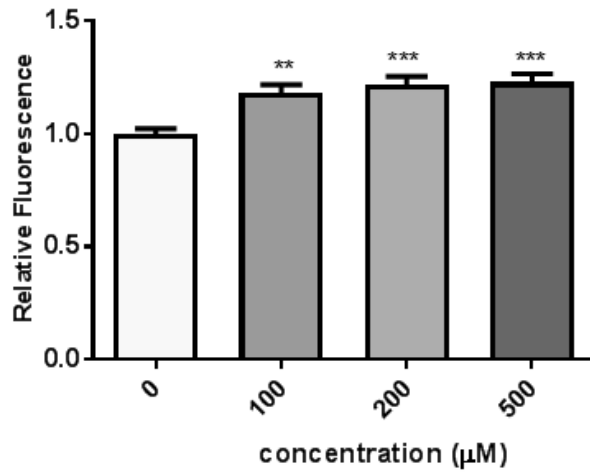


Appendix Figure 1.1: Solar light induced ROS and the contribution of IR/VIS in keratinocytes and fibroblasts. Cells were dosed with either solar UV or complete solar light and the resulting level of ROS in the form of H₂O₂ was assessed using the ROS-Glo method (level of H₂O₂ generation is equivalent to the relative luminescence). Percentage fold changes are displayed on the graph. An unpaired T test using Welch's correction was applied to assess statistical significance ****P<0.0001 (error bars represent the SEM) N=3, N=3 respectively.

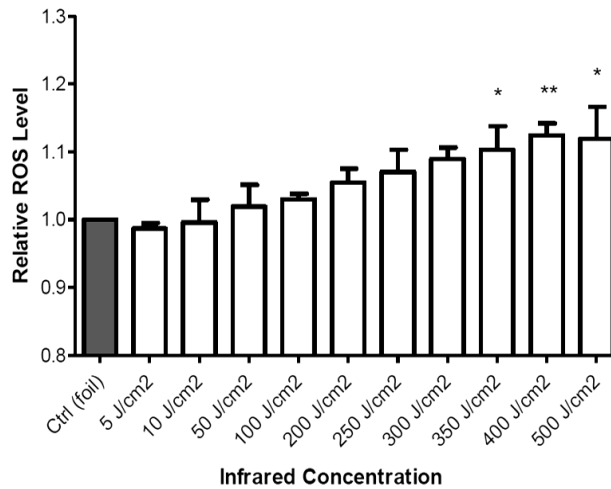


Appendix Figure 1.2: Solar light induced mtDNA damage and the contribution of IR/VIS in keratinocytes and fibroblasts.

Cells were dosed with either solar UV or complete solar light and the resulting level of mtDNA damage was assessed using QPCR analysis. CT values are displayed as relative to the unirradiated (control) cells. An unpaired T test using Welch's correction was applied to assess statistical significance ****P<0.0001 (error bars represent the SEM) N=3, N=3 respectively.



Appendix Figure 2: ROS generation in HaCat cells following exposure to H₂O₂ using the DCFDA method. Statistical analysis was assessed using a one-way ANOVA with Dunnett's correction to compare treated columns to the 0 control (error bars shown represent the SEM) ***P < 0.0001, N=2



Appendix Figure 3: ROS generation in HDFn cells following exposure to IR detected using the ROS-Glo method. Statistical analysis was assessed using a one-way ANOVA with Dunnett's correction to compare treated columns to the 0 control (foil) (error bars shown represent the SEM) *P < 0.05 ** P < 0.001, N=3

Sample	Age	Sex	Race	Anatomical site
S991F	60	Male	Caucasian	Foreskin
S993F	48	Male	Caucasian	Foreskin
S990F	66	Male	Caucasian	Foreskin
S1001F	49	Male	Caucasian	Foreskin
S1009F	50	Male	Caucasian	Foreskin
S1013F	51	Male	Caucasian	Foreskin
S1026F	Data not available	Male	Caucasian	Foreskin
S1054F	27	Male	Caucasian	Foreskin
S1057F	49	Male	Caucasian	Foreskin
S1058F	59	Male	Caucasian	Foreskin
S1073F	64	Male	Caucasian	Foreskin
S1074F	35	Male	Caucasian	Foreskin
S1075F	19	Male	Caucasian	Foreskin
S1137F	33	Male	Caucasian	Foreskin
S1139F	18	Male	Caucasian	Foreskin
S1140F	21	Male	Caucasian	Foreskin

Appendix Table 1: Donor information for the human skin keratinocyte and fibroblast samples.

The sample names, as well as the age, sex, race, and anatomical site of each donor, are given for the keratinocyte and fibroblast cell samples.

Cell Name	Cell Type	Disease	Age	Sex	Anatomical Site
HDFn	Fibroblast	Normal	Neonatal	Male	Foreskin
HaCaT	Keratinocyte	Distant periphery of a Melanoma	62 years old	Male	Back

Appendix Table 2: Details on the cell lines used.

The cell type and disease status of each cell line is given, as well as information regarding the age and sex of the donor, and the anatomical site from which the sample was taken. Both cell lines were derived from humans.

Publications:

Hudson L, Bowman A, Rashdan E, Birch-Machin MA. (2016) mitochondrial damage and ageing using skin as a model organ. *Maturita*, 93, pp. 34-40.

Rashdan E, Wilkinson S, Birch-Machin M-A, 2015. The effect of nanoparticulate titanium dioxide on perturbation of skin barrier function. Conference: 94th Annual Meeting of the British-Association-of-Dermatologists, Volume: 172

Poster Presentations:

Rashdan, E., Wilkinson, S., Birch-Machin, M.A (2017) "Sunscreens and the effects of solar radiation exposure on human skin", Gordon Research Conference – Redox Biology in Disease and Translational Medicine, Lucca, Italy

Rashdan, E., Wilkinson, S., Birch-Machin, M.A (2017) "Sunscreens and the effects of solar radiation exposure on human skin", Stratified Medicine Research Day, Newcastle

Rashdan, E., Wilkinson, S., Birch-Machin, M.A (2017) "Sunscreens and the effects of solar radiation exposure on human skin", Understanding the Harmful Effects of Chemicals on our Health and Ecosystem, Newcastle

Rashdan, E., Wilkinson, S., Birch-Machin, M.A (2017) "Sunscreens and the effects of solar radiation exposure on human skin", MRC Proximity to Discovery theme week Dermatology/Rheumatology, Newcastle

Rashdan, E., Wilkinson, S., Birch-Machin, M.A (2016) "The effect of nanoparticulate titanium dioxide on perturbation of skin barrier function", MRC Proximity to Discovery theme week Dermatology/Rheumatology, Newcastle

Rashdan, E., Wilkinson, S., Birch-Machin, M.A (2016) "The effect of nanoparticulate titanium dioxide on perturbation of skin barrier function", North East Postgraduate Conference, Newcastle

Rashdan, E., Wilkinson, S., Birch-Machin, M.A (2016) "The effect of nanoparticulate titanium dioxide on perturbation of skin barrier function", PHE PhD Student Day, Oxfordshire

Rashdan, E., Wilkinson, S., Birch-Machin, M.A (2015) "The effect of nanoparticulate titanium dioxide on perturbation of skin barrier function", British Society of Investigative Dermatology (BSID), Southampton

Oral Presentations:

Rashdan, E., Wilkinson, S., Birch-Machin, M.A (2017) "Sunscreens and the effects of solar radiation exposure on human skin", Skin Metabolism meeting, Sunderland University

Rashdan, E., Wilkinson, S., Birch-Machin, M.A (2017) "Sunscreens and the effects of solar radiation exposure on human skin", Institute of Cellular Medicine Directors Day, Newcastle University

Rashdan, E., Wilkinson, S., Birch-Machin, M.A (2017) "Sunscreens and the effects of solar radiation exposure on human skin", PHE Research and Applied Epidemiology Scientific Conference, University of Warwick

Rashdan, E., Wilkinson, S., Birch-Machin, M.A (2017) "The skin and barrier function in radiation and chemical exposures" Research in progress meeting, Royal Victoria Infirmary Hospital, Newcastle

Rashdan, E., Wilkinson, S., Birch-Machin, M.A (2016) "The skin and barrier function in radiation and chemical exposures" Research in progress meeting, Royal Victoria Infirmary Hospital, Newcastle

Rashdan, E., Wilkinson, S., Birch-Machin, M.A (2016) "The skin and barrier function in radiation and chemical exposures" PHE- Centre for Radiation, Chemical and Environmental Hazards, Seminar guest speaker, Didcot

Rashdan, E., Wilkinson, S., Birch-Machin, M.A (2016) "Sunscreens and the effects of solar radiation exposure on human skin", North East Postgraduate Conference, Newcastle